Modélisation mathématique et simulation numérique du transport mucociliaire

Chabane Meziane

université PARIS-SACLAY

Modélisation mathématique et simulation numérique du transport mucociliaire

Mathematical modeling and numerical simulation of mucus flow in bronchi

Thèse de doctorat de l'université Paris-Saclay

École doctorale n° 574, mathématique Hadamard (EDMH)
Spécialité de doctorat: mathématiques appliquées
Graduate School: Mathématiques. Référent: Faculté des sciences d'Orsay

Thèse préparée dans l'unité de recherche **Laboratoire de mathématiques d'Orsay** (Université Paris-Saclay, CNRS) sous la direction de **Astrid DECOENE**, professeure, la co-direction de **Sébastien MARTIN**, professeur

Thèse soutenue à Paris-Saclay le 25 novembre 2024, par

Chabane MEZIANE

Composition du jury

Membres du jury avec voix délibérative

Olivier LAFITTE Professeur, Université Sorbonne Paris Nord	Président & rapporteur
Vitaly VOLPERT Directeur de recherche, CNRS, Institut Camille Jordan Lyon	Rapporteur & examinateur
Filipa CAETANO Maîtresse de conférences, IMO, Paris Saclay	Examinatrice
Benjamin MAUROY Directeur de recherche, CNRS, Université de Nice	Examinateur
Clément MOREAU Chargé de recherche, CNRS, LS2N Nantes	Examinateur

THESE DE DOCTORAT

NNT : 2024UPASM042

université PARIS-SACLAY | ÉCOLE DOCTORALE de mathématiques Hadamard (EDMH)

Titre: Modélisation mathématique et simulation numérique du transport mucociliaire
Mots clés: Théorie des corps fins, cil, Problème de Stokes, glandes submucosales.

Résumé: Le transport de fluide biologique par le mouvement des cils est un phénomène naturel qu'on retrouve chez presque tous les êtres vivants. Le but de cette thèse est la modélisation et la simulation numérique de la clairance mucociliaire, faisant intervenir l'action des cils sur le fluide visqueux (composé de mucus et du liquide périciliaire), modélisé par des équations de Stokes. Le modèle fait intervenir aussi la sécrétion du mucus par les cellules sécrétrices, présentes au niveau de l'épithélium bronchique. Le premier chapitre traite de la modélisation 3D de l'écoulement du fluide sous l'action des cils, dont la contribution est modélisée par une courbe 1D représentant la ligne centrale du cil. Le problème résultant est un problème de Stokes singulier et non-local. Dans le chapitre 2 nous avons étudié, dans un modèle d'arbre bronchique symétrique dyadique, les épaisseurs de la couche mucus à l'équilibre, résultant de la sécrétion du mucus par l'épithélium, et de l'évacuation du mucus par les cils d'autre part. Enfin dans le chapitre 3, nous avons étudié l'influence de l'écoulement d'air à travers la lumière bronchique sur l'efficacité de la clairance mucociliaire, et ce, dans un régime de respiration normale, fort, puis extrême.

Title: Mathematical modeling and numerical simulation of mucus flow in bronchi
Keywords: Slender body theory, cilium, Stokes problem, submucosal glands.

Abstract: The transport of biological fluid by the movement of cilia is a natural phenomenon found in almost all living beings. The aim of this thesis is the modeling and numerical simulation of mucociliary clearance, involving the action of cilia on the viscous fluid (composed of mucus and PCL), modeled by Stokes equations. As well as the secretion of mucus by the submucosal glands and the goblet cells, present in the bronchial epithelium. The first chapter deals with the 3D modeling of the fluid flow under the action of the cilia, the contribution of which is modeled by a 1D curve representing the central line of the cilium. The resulting problem is a singular and non-local Stokes problem. In Chapter 2, we studied in a model of a symmetrical dyadic bronchial tree, the thickness of the mucus layer at equilibrium, resulting from the secretion of mucus by the epithelium on the one hand, and from the evacuation of mucus through the cilia on the other hand. Finally, in Chapter 3, we studied the influence of airflow through the bronchial lumen on the efficiency of mucociliary clearance, and this, by considering a normal, strong, and extreme breathing regime.


cnrs

Remerciements

Premièrement, je tient à exprimer mes profonds remerciements envers mes encadrants, Astrid Decoene, Sébastien Martin et Benjamin Mauroy. Merci d'avoir accepté de m'encadrer malgré ma situation d'handicap, et mes notes quelque peu discutable. J'ai énormément appris à vos côtés, et je suis très reconnaissant pour l'attention que vous m'aviez accorder, ainsi que l'ensemble du temps que vous m'aviez consacrer. Votre curiosité scientifique et connaissances en science resteront une source d'inspiration pour moi.

Mes remerciements vont également à Marcela Szopos, pour ses recommandations pertinentes qui ont enrichi la qualité de ce travail de recherche. Je souhaite également exprimer ma reconnaissance envers tous les membres du jury pour avoir accepté d'évaluer ce travail.

Je tiens également à remercier sincèrement MAP5 ainsi que le LMO, pour avoir mis à ma disposition les ressources nécessaires à la réalisation de cette thèse. Pendant cette thèse, j'ai eu la chance de travailler dans un environnement particulièrement chaleureux et bienveillant. Je suis également reconnaissant envers le CNRS, pour son soutien financier qui a facilité la réalisation de ce projet, ainsi que le financement de la prolongation de ma thèse. Cette thèse n'aurait pas été possible sans le soutient de l'école doctorale Jacques Hadamard, c'est pourquoi je tiens à remercier Stéphane Nonnenmacher pour l'ensemble de ses conseils.

Un grand merci vont à mes collègues doctorant.e.s, post-doctorant.e.s ainsi que les enseignant.e.s chercheur.e.s du MAP5 qui ont partagé avec moi cette aventure intellectuelle et humaine, pour leur soutien moral et leur amitié précieuse. Merci à tous les doctorants du MAP5, ancien et actuelle, les parties de Tarot partagés avec vous ont été très agréables. Merci à mes collègues de bureau: Safa, Yen, Florian, Antoine Monod, Apolline L., Adrien Chevallier, Charlie, Clémence, Lucie, Élisa et Arielle, ainsi qu'à la stagiaire Paulina Petoukha. Nos discussion et rigolades resteront parmi les meilleurs souvenirs du laboratoire. Les remerciements vont aussi au autres collègues doctorants : Ousmane, Julianna, Pierre Louis, Remi Laumont, Remi Boutin, Antoine Salmona, Anton, Herb, Loïc, Eloi, Ivan, Zoé, Sonia, Mehdi, Mariem, Diala, Beatriz, Bianca, Yassine, Adélie, Alexander, Sinda. Merci pour cette ambiance amicale et chaleureuse et pour tous ces bons moments passés ensemble. Enfin, une pensée toute particulière pour mes co-bureau d'Orsay avec qui j'ai eu la chance de partager quelques peu de moments avec eux malgré ma très faible présence au laboratoire.

Mes remerciements vont également à ma famille et mes ami.e.s, pour leur soutien indéfectible, leur encouragement constant et leur compréhension tout au long de cette période intense.

Contents

Introduction

Le poumon est un appareil respiratoire indispensable à la survie chez les mammifères. Plusieurs phénomènes régissent le poumon, et les principaux sont les échanges gazeux au niveau des alvéoles. L'air inspiré chargé d'oxygène est transporté à travers les bronches vers les alvéoles. Par ailleurs, l'air qui s'écoule peut contenir des impuretés (bactéries par exemple) potentiellement nocives pour l'organisme. Cependant, les bronches pulmonaires sont tapissées par un fluide visqueux dans lequel les bactéries sont emprisonnées, ce fluide constitue alors une barrière protectrice. Les bronches pulmonaires sont aussi tapissées des cils qui, par leurs mouvements synchronisés, conduisent à une circulation de la couche du fluide. Ce processus appelé transport mucociliaire permet alors l'évacuation des impuretés inspirées à l'extérieur de l'appareil respiratoire: c'est la clairance mucociliaire. L'efficacité du transport est principalement basée sur l'interaction entre les cils et le fluide environnant. Mais mieux comprendre l'ensemble des paramètres impliqués dans le système, ainsi que le mouvement du cil et ses caractéristiques est indispensable pour l'étude de cas pathologiques, tels que la mucoviscidose. La thèse porte sur la simulation du mouvement de cils dans un fluide visqueux. Dans un premier temps, on considère un modèle de l'écoulement dans une boite en 3D. Et dans un deuxième temps, ce modèle est réduit à une seule dimension qui nous servira à étudier l'évolution du volume du fluide sur tout l'arbre bronchique idéalisé. On obtient ainsi une étude précise de la clairance mucociliaire. Nos simulations numériques prennent en compte des mécanismes situés à l'échelle microscopique, à savoir celles des cils, et macroscopique, à savoir celles des bronches. L'objectif de la thèse est de contribuer à la conception d'une hiérarchie de modèles (3D et 1D), permettant de comprendre l'influence des différents paramètres physiologiques sur l'efficacité du transport mucociliaire dans les bronches pulmonaires.

0.1 Contexte

Les parois bronchiques sont constituées d'un tissu qui s'appelle l'épithélium (ou la couche épithéliale). Il est constitué de cellules emboîtées dites ciliées, ainsi que des glandes submucosales. Ces dernières secrètent un fluide visqueux dont le rôle est double :

- il capture les impuretés inhalées et les fait remonter le long des bronches, puis le long de la trachée, d'où elles basculent dans l'œsophage et sont éliminées dans l'estomac.
- il protège la paroi des bronches des agents pathogènes (particules de pollution, bactéries, etc.)

Ce fluide visqueux a ainsi un rôle de film protecteur, et il est composé de deux couches superposées:

- la couche périciliaire (PCL, pour periciliary layer en anglais), dont laquelle les cils battent, et de viscosité semblable à celle de l'eau [26].

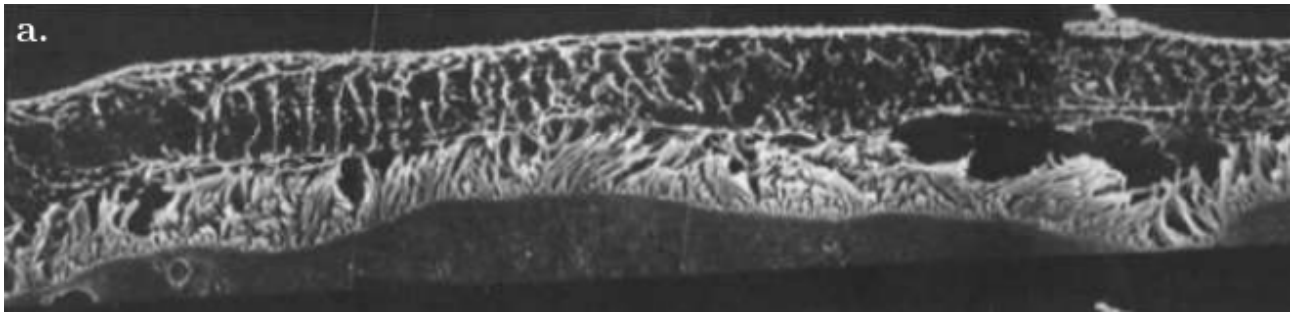

Figure 1 – Section d'une forêt de cils obtenu grâce un microscope électronique [64].

- le mucus, plus visqueux que la PCL, est composé d'eau et de lipides, ainsi que de mucines (protéine de haut poids moléculaire) [34, 9, 39].

Ces deux fluides forment une barrière protectrice de quelques micromètres d'épaisseur. Les impuretés piégées dans le mucus sont transportées hors de l'appareil respiratoire grâce à des cils baignant essentiellement dans la couche périciliaire (Figure 1), et dont le battement permet la propulsion du mucus vers le haut de la trachée. Ce mécanisme est appelé clairance mucociliaire (ou transport mucociliaire). Un autre mécanisme entrant en jeu dans le transport mucociliaire est l'échange ionique entre l'épithélium et la paroi bronchique grâce à une protéine appelé CFRT (pour Cystic Fibrosis Transmembrane conductance Regulator). Le rôle final de cette protéine est de diminuer la viscosité du mucus présent dans la paroi et ainsi faciliter son évacuation.

0.2 Position du problème

Une des grandes difficultés dans l'étude du transport mucociliaire est le manque de données expérimentales. La structure complexe de l'arbre bronchique rend impossible les mesures in vivo à partir de la sixième génération. Par ailleurs, très peu de données ont été renseignées sur le taux de production du mucus ainsi que les épaisseurs de la couche de mucus en chaque génération de bronche. C'est pourquoi il serait intéressant de développer un outil numérique donnant accès à des mesures, par exemple de vitesses difficilement obtenables via l'expérience.

Une autre difficulté provient des différentes échelles de longueur qu'on doit considérer : moléculaire, ciliaire, etc. La figure (2) illustre les différentes échelles mises en jeu. Enfin, la complexité structurelle du transport mucociliaire rend son étude mathématique difficile. Beaucoup de paramètres sont à prendre en compte :

- le fluide nappant la paroi des bronches n'est pas homogène, il est composé de deux fluides de viscosités très différentes (le mucus est 1000 fois plus visqueux que la couche périciliaire [39]), et donc la dynamique de l'interface entre ces deux fluides peut faire l'objet d'une étude approfondie.

- les cils sont très fins, et très petits par rapport au grandeurs de la bronche donc difficiles à prendre en compte numériquement, et la fréquence de battement est élevée.

- l'influence de l'air inspiré ou expiré sur le mucus. Dans un régime d'inspiration/expiration l'écoulement d'air est considéré incompressible (du fait que le nombre de Mach est inférieur à 0.3 puisque la vitesse de l'air au niveau de la trachée varie au alentour de $1\ m.s^{-1}$ au repos).

- l'évaporation/absorption de l'eau contenue dans le mucus par l'épithélium tend à modifier sa viscosité (notamment au niveau de la trachée [34]), le fluide devient ainsi de plus en plus visqueux au fur et à mesure qu'on s'approche de la trachée.

La simulation du transport mucociliaire est un enjeu important: cela nous aidera à mieux comprendre certaines pathologies respiratoires, et aussi, donner une estimation de certains paramètres, par exemple: le taux de production de mucus, qui jusqu'à là est très difficile à quantifier. La complexité du processus, dont une liste non exhaustive des difficultés est donnée ci-dessus, rend le modèle à la fois très riche mais aussi très compliqué à simuler. Dès lors, la compréhension du processus requiert une combinaison de différentes méthodes qui incluent la modélisation mathématique, l'analyse des données résultantes et le calcul scientifique. Dans cette thèse on abordera principalement deux approches : la première est la simulation directe en 3D du mouvement d'un très grand nombre de cils immergés dans un bifluide, ce qui permet une analyse de la vitesse de l'écoulement du bifluide dû au mouvement des cils. La deuxième partie, concerne un modèle 1D qui dérive du modèle 3D: il nous permettra d'étudier l'évolution en temps de l'épaisseur de la couche de mucus en chaque génération d'un arbre bronchique idéalisé à 17 générations, en fonction des différents paramètres physiologiques présents dans le poumon tels que :

- la densité des cils, la hauteur des cils ainsi que leur épaisseur dans chaque génération.
- la fréquence de battement des cils peut varier d'une génération à l'autre [26].
- le taux de production du mucus. Quelques travaux [34, 77] ont mentionné la quantité de mucus produit dans les bronches pulmonaires.

Les modélisations présentées dans les chapitres suivants sont guidées par la volonté de limiter les coûts de calculs, qui peuvent vite devenir exorbitants, tout en essayant de faire le minimum d'hypothèses possible.

0.3 État de l'art

0.3.1 Au niveau d'un échantillon d'une paroi bronchique

De nombreux travaux se sont intéressés à la modélisation et la simulation numérique de cils interagissant avec un fluide visqueux. L'un des premiers modèles est celui de Barton et Raynor [3], ils considèrent un modèle idéalisé de battement de cils dans un mucus ayant des propriétés newtoniennes. La viscosité est plus petite au niveau de la couche des cils et augmente jusqu'à atteindre son maximum au niveau de l'interface air/mucus, dû au fait que le flux d'air tend à déshydrater le mucus. La contrainte de cisaillement moyenne a l'interface PCL/mucus est connue et elle remplace la force dûe au mouvement des cils, et enfin, l'influence de l'air sur le mucus n'est pas prise en compte. Les auteurs ont pu ainsi estimer la vitesse moyenne au niveau de la couche mucus aux alentours de $6.6mm/min$.

Plus tard, Ross [61] a développé un modèle de transport en utilisant une approche d'enveloppe dans laquelle l'interface mucus-cils est représentée comme un "tapis" ondulé imperméable. L'auteur a utilisé un système bifluide; de plus, il considère le mucus comme un fluide viscoélastique et la couche périciliaire comme un fluide newtonien sans modéliser le mouvement des cils. Les forces gravitationnelles et d'inerties sont négligées. En utilisant ce modèle pour la couche périciliaire et le

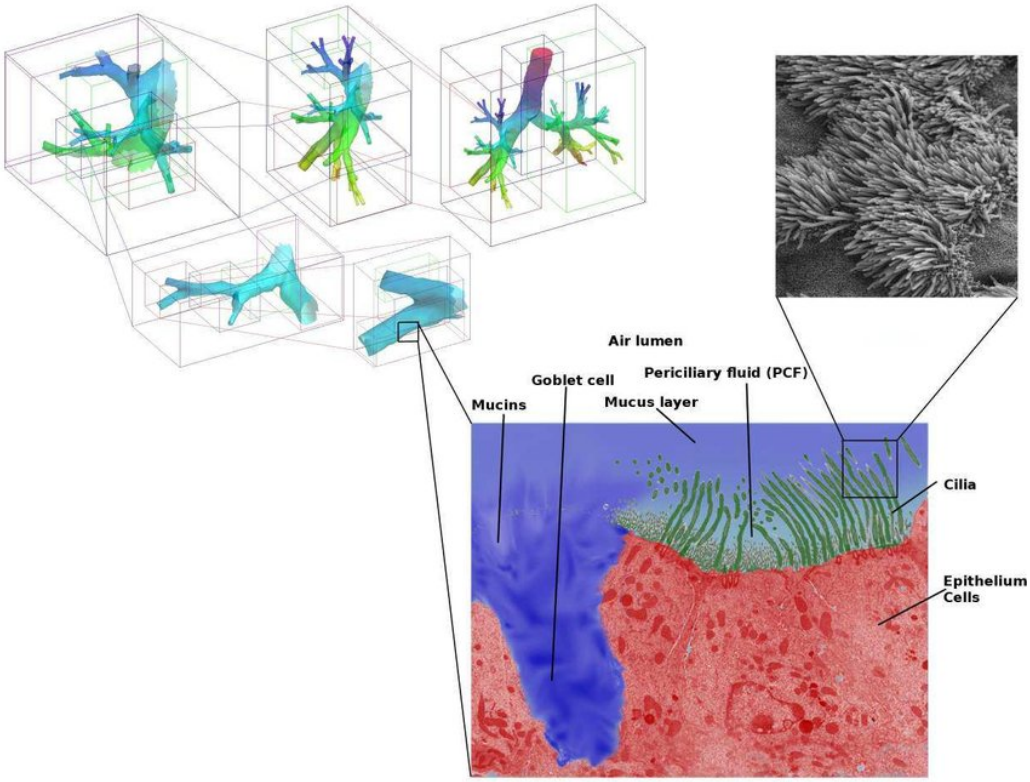

Figure 2 – Vue schématique multi-échelles des poumons humain, de la trachée et les premières générations de bronches ($\approx$ 1cm) jusqu'aux cellules épithéliales (≈ 5 μm), image à partir de [17].

mucus, il a pu calculer la vitesse moyenne de l'écoulement du mucus, les trajectoires des particules propulsées, ainsi que les débits de mucus et le profil de l'interface air/mucus.

D'autres travaux sur la modélisation et la simulation numérique de cils ont été réalisés, parmi eux, Fulford et Blake [26]. Les auteurs étudient le transport mucociliaire dans les bronches pulmonaires, c'est-à-dire l'interaction entre les cils bronchiques et le fluide environnant. Ils arrivent ainsi, à l'aide d'un modèle réduit, à évaluer la vitesse de l'écoulement du fluide visqueux au niveau des cils. À partir d'observations expérimentales [64], ils proposent une paramétrisation du battements des cils sous la forme d'une série de Fourier tronquée dont les coefficients sont obtenus par la méthode des moindres carrés. Les cils sont modélisés par des filaments en une dimension dont la distribution de forces est approchée en utilisant la "résistive force theory" et les effets sur le bifluide sont étudiés numériquement en considérant une forêt de cils battant dans le fluide.

Lacouture [38] a utilisé la même paramétrisation des cils bronchiques que celle de Fulford and Blake [26], en considérant une distribution de forces ponctuelles le long des cils, dont l'intensité est obtenue explicitement par la "slender body theory". Dans ce travail, l'objectif est de modéliser le mouvement d'un bifluide soumis à des forces ponctuelles. Pour cela, un problème de Stokes est résolu de façon directe à l'aide de la méthode de soustraction, puis par une méthode numérique de type éléments finis. L'analyse numérique du problème singulier considéré est menée par des estimations d'erreurs locales, et des résultats de convergence locale quasi-optimale sont obtenus. Des conditions au bords de type bi-periodique sur les cotés du domaine sont prises en compte, cela permet de simuler le transport mucociliaire numériquement en considérant une forêt d'une centaine de cils parmi une infinité (du moins grande quantité) de cils.

Dans [17, 18], le cil est modélisé par une structure en 3D dont les déplacements le long de l'axe

central vérifient une équation d'advection unidimensionnelle. Le mouvement ainsi obtenu est proche de la paramétrisation de Fulford et Blake [26] au sens où le mouvement est séparé en deux phases, une phase active et une phase retour. Le fluide entourant les cils est modélisé par un fluide newtonien à faible nombre de Reynolds dont la viscosité est variable et dépend de la concentration des mucines présentes dans le fluide, qui vérifie une équation de convection-diffusion. La condition de continuité des vitesses entre les cils et le fluide est prise en compte par pénalisation dans les équations de Stokes et la résolution numérique de ce problème est réalisée par des méthodes utilisant un solveur FFT. Deux méthodes ont été introduites pour la résolution de leurs équations, une méthode dite lagrangienne, et une autre méthode basée sur une grille. Ces méthodes permettent une étude détaillée de l'influence des différents paramètres du modèle sur l'efficacité du transport du fluide par les battements des cils.

Dans chacun des articles cités jusque là, le mouvement d'une forêt de cils est imposé, et l'action du fluide sur les cils est négligé. C'est d'ailleurs la même démarche qui est considérée dans cette thèse.

Dans [22], l'auteur a étudié un modèle a énergie imposée pour la déformation d'un cil en 3D plongé dans un fluide visqueux avec un modèle dit d'élasticité active, l'action du fluide sur le cil est cette fois-ci bien prise en compte, et le problème résultant est un modèle d'interaction fluide structure complet. L'auteur a pu étudier l'influence du mouvement bien établi d'un cil, puis deux cils avec différents jeux de donnés tels que la viscosité et la distance entre les deux cils. L'auteur a aussi pris en compte l'interaction entre 2 cils.

0.3.2 Au niveau d'un arbre bronchique

Un modèle de clairance mucociliaire a été développé dans le travail de Mauroy et al [48]. Dans un arbre bronchique humain rigide idéalisé (de type Weibel), les auteurs ont étudié l'interaction entre la géométrie de l'arbre, les propriétés physiques du mucus et l'amplitude du débit d'air. Le mucus est considéré comme un fluide non-newtonien de Bingham qui est déplacé vers le haut de l'arbre grâce à son interaction avec le flux d'air et le mouvement des cils. L'air est considéré comme un fluide newtonien de viscosité 1000 fois plus petite que la viscosité de l'eau, et l'action des cils est représentée par une condition sur la vitesse au niveau de la paroi bronchique. Un système d'EDO porté sur chaque génération et basé sur la conservation du volume du mucus a été développé afin de déterminer l'épaisseur de la couche de mucus en chaque génération et à chaque instant.

Certains auteurs [58, 34, 75, 13, 11] se sont intéressés aux mécanismes d'absorption et d'évaporation de l'eau contenue dans le mucus, ainsi qu'à la sécrétion du mucus par l'épithélium. Mauroy et al [34] ont proposé un modèle pour étudier les mécanismes contrôlant le volume de mucus dans la région bronchique des poumons d'un adulte humain en bonne santé. Les mécanismes cités sont : le transport mucociliaire, l'évaporation de l'eau contenue dans le mucus (qui se produit généralement au niveau des générations proximales), l'absorption de l'eau par l'épithélium, ainsi qu'une sécrétion du mucus au niveau des glandes submucosales.

Un autre modèle de clairance mucociliaire a été développé par Kurbatova et al [37]. Les auteurs se basent sur le modèle de Smith et al [70]. Le mouvement des cils est obtenu en utilisant une paramétrisation établie par Fulford et Blake [26]. Kurbatova et al considèrent le fluide tapissant les parois bronchiques comme un fluide à trois couches: la couche PCL supposée newtonienne, où les cils battent, la couche de traction, où les cils pénètrent la couche de mucus, modélisée par un fluide viscoélastique de Maxwell, et enfin la couche de mucus au-dessus de la région de traction. L'influence de l'air est négligée. Comme dans Mauroy et al [48], le modèle d'arbre bronchique considéré est de type Weibel. Par la suite, à l'aide des équations de conservation de la masse, les auteurs étudient

la dynamique de la couche de mucus. Par ailleurs, les auteurs ont pris en compte le taux de mucus produit dans les glandes submucosales, en utilisant les valeurs renseignées dans Waldron [77]. En se basant sur des données expérimentales, les auteurs ont pu étudier un cadre pathologique qui est la mucoviscidose.

0.4 Nouveaux modèles développés dans la thèse

Durant la thèse, nous avons développé des modèles mathématiques de clairance mucociliaire prenant en compte à la fois l'influence des cils bronchiques et celle de l'air. Comme précisé précédemment, dans un premier temps nous considérons un modèle 3D pour le transport mucociliaire dans une boite représentant un bout de bronche (Figure 7). Ce modèle permet d'obtenir la distribution de la vitesse de l'écoulement dans la PCL et la couche de mucus. Dans un deuxième temps, on réduit le modèle 3D pour se ramener à un modèle 1D, permettant de calculer la vitesse moyenne de l'écoulement du mucus. Par la suite, le modèle 1D nous servira à étudier l'évolution du volume du mucus dans un arbre bronchique idéalisé.

Pour cela, nous avons eu recours à divers modèles développés par certains auteurs cités dans la section précédente.

0.4.1 Modèle pour le fluide

Le liquide périciliaire est essentiellement composé d'eau et donc le plus souvent considéré comme newtonien [26, 18, 17, 19]. En revanche, pour le mucus, les modèles sont différents selon les auteurs: du modèle newtonien [26, 18, 17], au modèle viscoélastique [70, 61, 19], et même un fluide de Bingham [48]. Comme dans [26, 18, 17], le liquide périciliaire ainsi que le mucus (plus visqueux) seront considérés comme un fluide newtonien, bien que ce dernier contient une certaine quantité de mucines [39], et ces dernières rendent le fluide non-newtonien [19]. L'ensemble est modélisé par un modèle bifluide dont l'interface entre les deux fluides reste plane et invariante dû aux effets de tension superficielle [26, 71].

Soit $\mathbf{u}$ et p respectivement la vitesse et la pression du fluide, les équations gouvernant un fluide newtonien de masse volumique ρ et de viscosité μ, soumis a des forces extérieurs $\mathbf{f}_{ext}$ sont:

$$\begin{aligned} \rho(\frac{\partial \mathbf{u}}{\partial t} + \mathbf{u}\cdot\nabla\mathbf{u}) - \mu\Delta\mathbf{u} + \nabla p &= \mathbf{f}_{ext}, \\ \nabla\cdot\mathbf{u} &= 0, \end{aligned} \tag{1}$$

auxquelles il convient d'ajouter des conditions aux limites et initiales appropriées. On peut adimensionner les équations de Navier-Stokes en utilisant les longueurs caractéristique U et L, on peut considérer les quantités sans dimension $\tilde{\mathbf{u}}$, $\tilde{p}$, $\tilde{t}$ et $\tilde{\mathbf{f}}_{ext}$ qu'on définit

$$\tilde{\mathbf{u}} = \frac{1}{U}\mathbf{u}, \quad \tilde{p} = \frac{L^2}{\mu U}p, \quad \tilde{t} = \frac{U}{L}t, \quad \tilde{\mathbf{f}}_{ext} = \frac{t}{\rho U}\mathbf{f}_{ext},$$

et le nombre de Reynolds

$$Re = \frac{\rho U L}{\mu}.$$

On obtient alors les équations adimensionnées:

$$\begin{aligned} Re(\frac{\partial \tilde{\mathbf{u}}}{\partial \tilde{t}} + \tilde{\mathbf{u}}\cdot\tilde{\nabla}\tilde{\mathbf{u}}) - \tilde{\Delta}\tilde{\mathbf{u}} + \tilde{\nabla}\tilde{p} &= \tilde{\mathbf{f}}_{ext}, \\ \tilde{\nabla}\cdot\tilde{\mathbf{u}} &= 0 \end{aligned} \tag{2}$$

Le nombre de Reynolds est une quantité sans dimension qui mesure le rapport entre les forces d'inerties et les forces visqueuses qui sont présentes dans l'écoulement. Un faible nombre de Reynolds ($Re < 1$ par exemple) correspond donc à un régime où les effets visqueux du fluide dominent les effets inertiels. La longueur caractéristique dans le cas du transport mucociliaire est le micromètre et la vitesse ($\sim 100\mu$m.s^{-1}), de sorte que le nombre de Reynolds soit de l'ordre de 10^{-6} (le cil étant de longueur $L = 6\ \mu m$ et de vitesse de battement U de l'ordre de $10^2 \mu m s^{-1}$), rendant ainsi les termes inertiels négligeables dans les équations de Navier-Stokes. On considère donc les équations de Stokes

$$\begin{cases} -\tilde{\Delta}\tilde{\mathbf{u}} + \tilde{\nabla}\tilde{p} &= \tilde{\mathbf{f}}_{ext}, \\ \tilde{\nabla}\cdot\tilde{\mathbf{u}} &= 0. \end{cases} \tag{3}$$

0.4.2 Modèlisation de l'interaction du cil avec le fluide

Dans cette thèse on considère un modèle faiblement couplé (c'est-à-dire qu'on tient compte uniquement de l'action des cils sur le fluide) pour simuler en 3D l'écoulement du fluide dû à l'action d'une forêt de cils. La faisabilité des calculs, autrement dit éviter des coûts numériques exorbitants, constitue une motivation majeure dans le choix du modèle pour le cil. Un modèle faiblement couplé serait:

- on distingue un domaine fluide d'un domaine structuré modélisé en 3D et qui représente le cil. On impose par la suite des conditions de continuité des vitesses sur la frontière de chaque cil. On note $\mathbf{u}_{cil}$ la vitesse du mouvement du cil (donnée). Le modèle s'écrit alors, soit $(\mathbf{u}, p)$ solution du problème de Stokes:

$$\begin{cases} -\Delta\mathbf{u} + \nabla p &= 0, \\ \nabla\cdot\mathbf{u} &= 0, \\ \mathbf{u} &= \mathbf{u}_{cil}, \quad \text{à la frontière du cil.} \end{cases} \tag{4}$$

  La vitesse $\mathbf{u}_{cil}$ ainsi que la position du cil sont obtenues soit par résolution des équation mécaniques, ou bien en les imposant analytiquement en chaque temps.

Dans ce modèle, on construit un maillage 3D pour la structure représentant le cil. Par contre, si une simulation de l'écoulement dûe au mouvement de quelques cils en 3D est envisageable, il devient compliqué de simuler une forêt à plusieurs centaines de cils en raison de la structure fine du cil.

0.4.3 Paramétrisation du cil

Comme mentionné précédemment, le cil est représenté par une courbe 1D à laquelle on associe une distribution linéique de forces, portée par l'axe central du cil. Mais avant de définir la distribution de la force le long du cil, nous devons choisir une paramétrisation du cil. La paramétrisation que nous avons choisie a été établie par Fulford et Blake [26]. Le mouvement du cil étant périodique, les auteurs ont utilisé une décomposition en série de Fourier du battement du cil à partir d'images récoltées par Sanderson et Sleigh [64] suivant différents instants à pas de temps égaux. Plus précisément, à chaque instant t, le cil est représenté par une courbe:

$$s \mapsto \boldsymbol{\xi}(s, t)$$

où $s \in [0, L]$ est la longueur d'arc depuis la base du cil, L représente la longueur du cil et f est la fréquence de battement du cil. Le mouvement du cil est divisé en deux phases, une phase active (où

le cil propulse le fluide) et une phase de retour (figure 3)): ce mouvement irreversible en temps est nécessaire dans un fluide de Stokes pour faire avancer le mucus, puisque l'une des caractéristiques des équations de Stokes est qu'elles sont réversibles en temps, ce qui résulte de leur instantanéité et de leur linéarité. Cela signifie qu'un flagelle dans un fluide de Stokes doit briser la symétrie de son mouvement pour avancer. C'est ce que stipule le fameux théorème de la coquille Saint-Jacques introduit par Purcell [60].

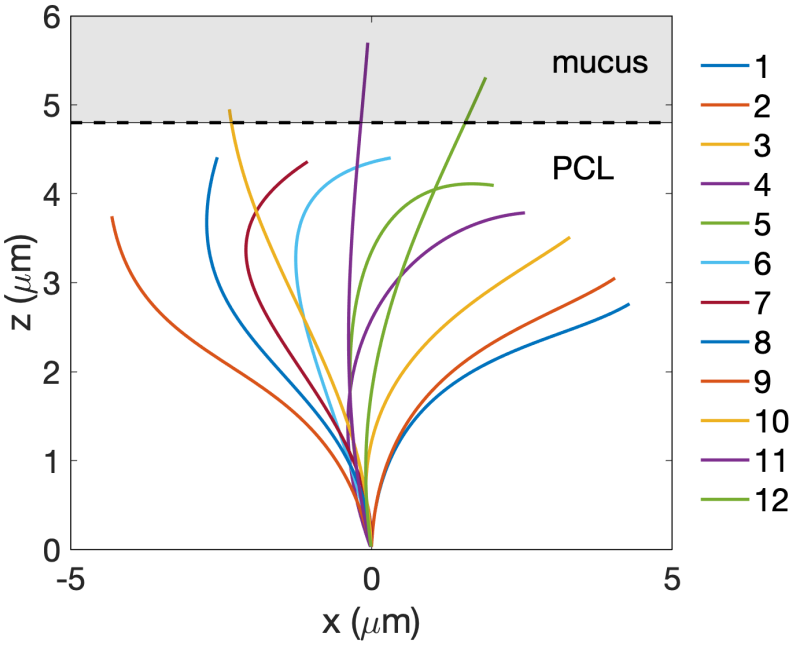

Figure 3 – Mouvement d'un cil pendant une période battement, établie selon la description faite par Sanderson et Sleigh [64], (de 1 à 8) représente à la phase retour et la phase active de (9 à 12).

0.4.4 Paramétrisation de la forêt de cils

Une paramétrisation d'une forêt de cils est établie dans [64]. Elle dépend essentiellement de deux paramètres : l_0 qui est l'espacement entre chaque cil, ainsi que λ la longueur d'onde métachronale qui résulte du mouvement périodique et déphasé en temps entre chaque cil suivant l'axe x. Le mouvement reste le même suivant y. Notre modèle de forêt de cils est caractérisé par une forêt à $n_x n_y$ cils, avec n_x (respectivement n_y) le nombre de cils dans la direction x (respectivement la direction y). Le cil (i, j), où $i \in [[1, n_x]]$ et $j \in [[1, n_y]]$, est paramétrisé par la courbe:

$$\boldsymbol{\xi}^{(i,j)}(s,t) = il_0\overrightarrow{\boldsymbol{e}_x} + jl_0\overrightarrow{\boldsymbol{e}_y} + \boldsymbol{\xi}(s, \frac{il_0}{f\lambda} + t).$$

Dans notre modèle, on supposera que le cil évolue uniquement dans le plan (x, z).

0.4.5 Distribution de la force le long du cil

Étant donneé la paramétrisation du mouvement du cil, on lui associe par la suite la force exercée sur le fluide dûe à ce mouvement. Pour cela on utilise la "Slender Body Theory", basée sur un développement asymptotique quand le ratio ϵ entre l'épaisseur et la longueur du corps tend vers 0. Cox [20] a

établi une expression approchée explicite entre la vitesse de battement du cil et la force résultante: si

$$s \mapsto \boldsymbol{\xi}(s,t)$$

est une paramétrisation de la position du cil à l'instant t en coordonnés curvilignes, l'expression de la force au point s est

$$\mathbf{f}(s,t) = \frac{2\pi\mu}{\ln(\frac{L}{r})}\left(2\mathbb{I}_3 \frac{\partial_s\boldsymbol{\xi}(s,t)\otimes\partial_s\boldsymbol{\xi}(s,t)}{|\partial_s\boldsymbol{\xi}(s,t)|^2}\right)(\partial_t\boldsymbol{\xi}(s,t) - \mathbf{u}_{bg}\boldsymbol{\xi}(s,t)) + O\left(\frac{1}{(\ln(L/r))^2}\right), \tag{5}$$

où r l'épaisseur du cil et $\mathbf{u}_{bg}$ est la vitesse du fluide dit background: pour une forêt de cils donnée la vitesse $\mathbf{u}_{bg}(\boldsymbol{\xi})$ en tout point du cil $\boldsymbol{\xi}$ représente la vitesse de l'écoulement du fluide en l'absence de ce cil. Cette expression de la force a été établie en utilisant deux approches:

la première consiste à établir un développement asymptotique de la vitesse de l'écoulement au voisinage du corps fin qui est supposé un cylindre de longueur L qui tend vers l'infini et d'épaisseur r constante.

la deuxième consiste à établir un développement asymptotique de la vitesse de l'écoulement loin du corps fin, vu comme un cylindre d'épaisseur r qui tend vers 0 et de longueur L constante. Comme dans Fulford et Blake [26], on approche $\mathbf{u}_{bg}$ par la vitesse moyenne du fluide; notre problème de Stokes devient ainsi non local.

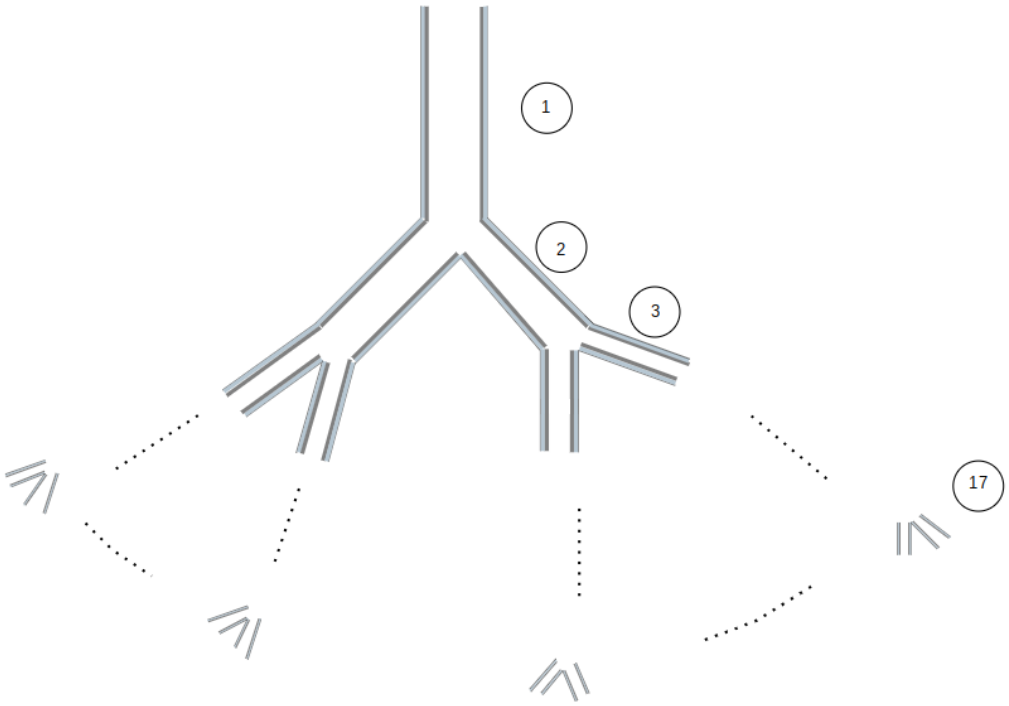

Figure 4 – Schéma d'arbre dyadique, la zone colorée en gris clair représente la couche PCL, et la zone foncée représente la couche de mucus.

0.4.6 Modèle pour l'air

Dans le chapitre 3 de cette thèse, on étudiera l'influence de l'écoulement d'air sur le mucus dans un modèle d'arbre bronchique à 17 générations. L'écoulement d'air est newtonien et incompress-

ible, néanmoins il serait très coûteux d'étudier l'écoulement d'un tri-fluide (air, mucus et PCL) dans une géométrie de bronches pulmonaires à plusieurs générations, même si la géométrie est idéalisée. Pour cela, nous l'approchons par un écoulement laminaire de Poiseuille: la vitesse de l'air est ainsi axisymétrique en chaque génération de bronche qui, elle, est représentée par un cylindre de longueur et rayon de sa section différent suivant chaque génération. Une remarque est que cette approximation néglige les effets inertiels, bien qu'ils ne sont pas négligeables dans les générations proximales.

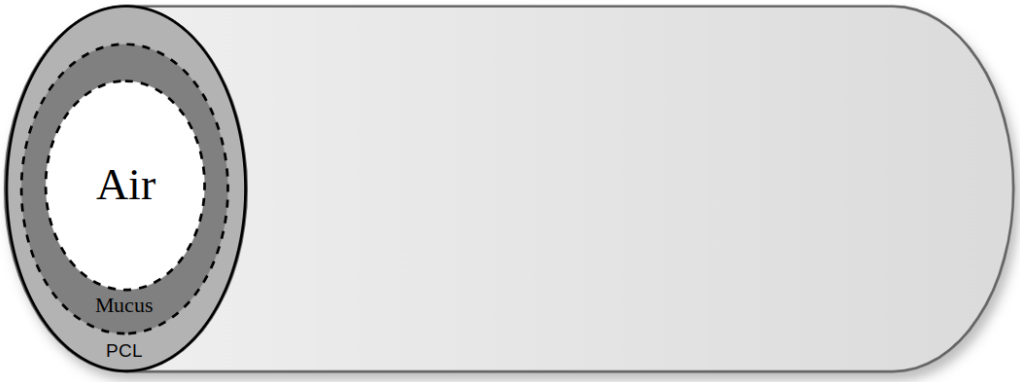

Figure 5 – Schema représentant une bronche tapissée de mucus.

Dans notre modèle la paroi du cylindre qui représente une bronche est tapissée par du mucus. Ce dernier est mis en mouvement par les cils, et l'action de l'écoulement de l'air sur le mucus est prise en compte grâce au différentiel de pression entre l'entrée et la sortie de la bronche, et de la contrainte de cisaillement au niveau de l'interface air/mucus. Par ailleurs, l'action du mucus sur l'air est négligeable.

0.4.7 Conditions aux bords

Pour compléter notre modèle, nous allons considérer des conditions aux bords. Dans le premier chapitre, le domaine 3D de calcul est un parallélépipède rectangle dont le bord inférieur représente la paroi des bronches (ou l'épithélium), et le bord supérieur l'interface entre le mucus et l'air. On suppose que le bi-fluide adhère à la paroi des bronches, donc on y impose une condition d'adhérence. Comme dans certains travaux menés sur le sujet ([26, 71]), on impose que la partie supérieure du mucus (interface air/mucus) reste plane, de même pour l'interface mucus/PCL ([26, 71]). Cette dernière condition modélise l'influence de la tension superficielle entre les deux fluides. On intègre ainsi les effets de cette tension au modèle par une contrainte sur la composante normale de la vitesse nulle au niveau de l'interface PCL/mucus. On néglige les effets de l'air sur le mucus, on a ainsi une condition de glissement, et la composante normale de la vitesse nulle. À l'échelle des cils, la longueur dans la direction x du domaine du fluide est restreint à la longueur de l'onde métachronale, c'est-à-dire $L_x = 30\mu$m. Dans la direction z, sa hauteur $L_z = 10\mu$m représente l'épaisseur de la couche de mucus+PCL, et dans la direction y la longueur du domaine est $L_y = 4.8\mu$m. Comme la distance entre chaque cil est de 0.3μm, on a ainsi une centaine de cils suivant la longueur de notre domaine. Sur les côtés du domaine, les conditions aux bords considérées sont les conditions bipériodiques en la vitesse. De cette façon, on prend en compte le battement des cils à l'extérieur de la boîte. Les conditions aux bords considérées sont illustrées par la Figure (7) et (3.21).

Dans le deuxième chapitre, le domaine 3D de calcul est un cylindre troué. La paroi du cylindre représente la paroi d'une bronche pulmonaire. Les conditions au bords sont les mêmes que celles établies durant le premier chapitre, sauf que l'influence de l'air sur le bifluide est prise en compte à travers une condition de frottement. On a ainsi une contrainte qui s'ajoute à notre modèle au niveau de l'interface air/mucus.

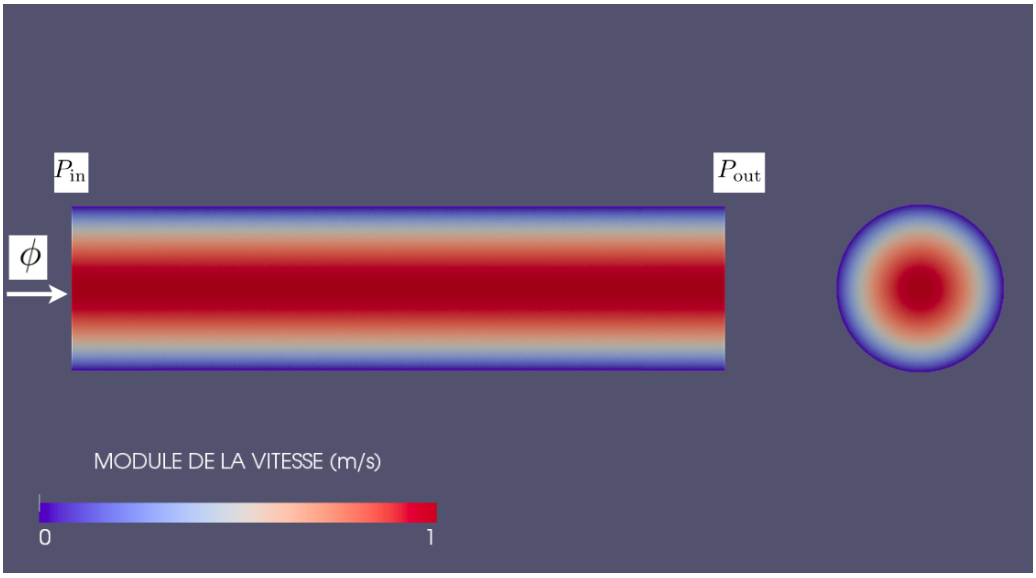

Figure 6 – Schéma de l'écoulement de Poiseuille obtenu dans [45] modifié. ϕ est le debit de l'écoulement, P_{in} et P_{out} sont respectivement la pression a l'entrée et la sortie du cylindre.

0.5 Résumé de la thèse

0.5.1 Chapitre 1 : Un modèle 3D du transport mucociliaire

L'objectif dans ce modèle est de décrire l'effet sur le fluide environnant du mouvement de plusieurs cils qui battent suivant une direction donnée de sorte à évacuer le mucus des bronches. Les choix de modélisation décrits précédemment aboutissent à l'étude d'un problème mathématique singulier et non local. Pour le caractère non-local du problème, la difficulté réside dans la résolution numérique; en effet, dans notre travail, la résolution numérique se fait par la méthode des éléments finis. Pour un problème non-local, la matrice de rigidité qu'on obtient n'est pas creuse et donc très chère à inverser, cela motive alors l'élaboration d'une méthode de résolution adaptée.

Le modèle 3D considéré consiste à trouver le couple $(\mathbf{u}, p, \gamma)$, où $\mathbf{u}$ est la vitesse, p la pression et γ est la tension superficielle, solution du problème singulier et non local suivant:

$$\begin{cases} -\mathrm{div}(\mu\nabla\mathbf{u}) + \nabla p + \gamma\mathbf{e}_z\delta_{\Gamma_*} = \sum_{i,j}\mathbf{f}_{ij}[\mathbf{u}]\,\delta_{\Gamma_{ij}} & \text{dans } \Omega, \\ \mathrm{div}(\mathbf{u}) = 0 & \text{dans } \Omega, \\ [(\mu\nabla\mathbf{u} - p\mathbb{I})\cdot\mathbf{n}]\cdot\mathbf{t} = 0 & \text{dans } \Gamma_\uparrow, \\ \mathbf{u}\cdot\mathbf{n} = 0 & \text{dans } \Gamma_\uparrow \cup \Gamma_*, \\ \mathbf{u} = 0 & \text{dans } \Gamma_\downarrow. \end{cases} \tag{6}$$

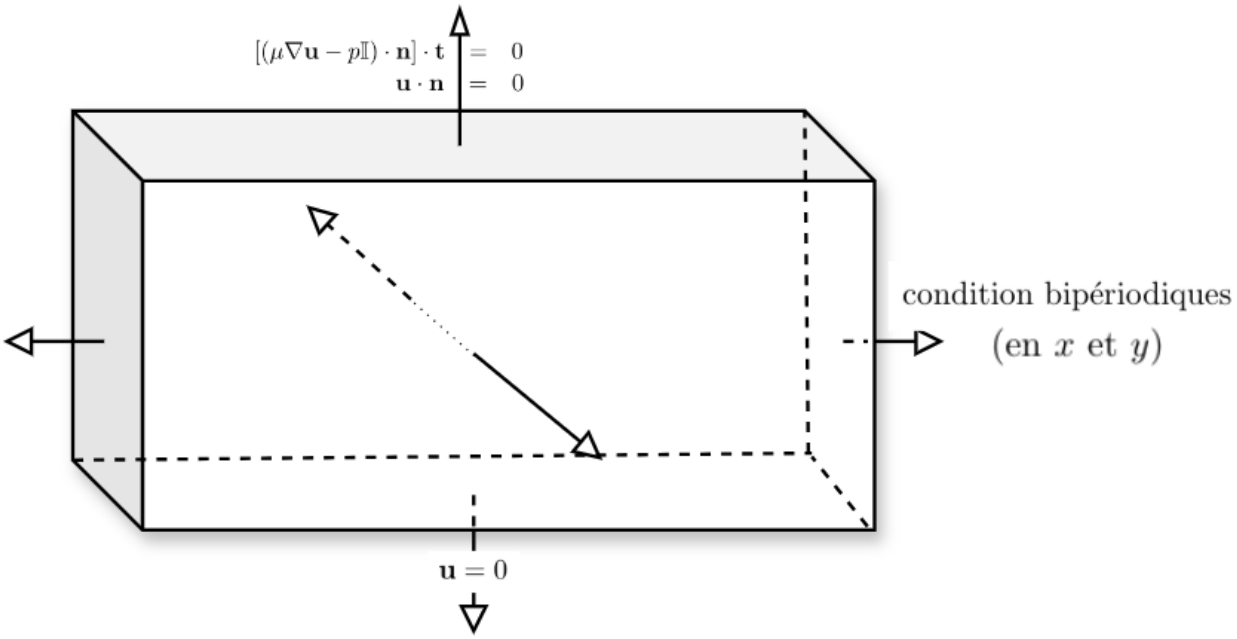

Figure 7 – Conditions aux bords associé au modèle 3D.

Le domaine fluide noté Ω est divisé en deux couches: la couche PCL, de viscosité μ_1 , occupe le sous domaine $\{z < H\}$; la couche mucus, de viscosité $\mu_2 > \mu_1$ occupe le sous domaine $\{z > H\}$. Γ_{ij} représente la courbe 1D décrivant la ligne centrale du (i, j)-ème cil, et $\mathbf{f}_{ij}[\mathbf{u}](\cdot, t)$ est la distribution de la force exercée par le (i, j)-ème cil au temps t sur le bifluide. L'expression de la force ainsi que la paramétrisation du cil sont celles explicitées précédemment. Comme mentionné auparavant l'interface PCL/mucus est plane et n'évolue pas dans le temps, dû aux effets de la tension superficielle. Du point de vue mathématique, cette contrainte est imposée par dualité: pour cela, on introduit la tension superficielle γ (inconnue) agissant au niveau de l'interface, et qui représente un multiplicateur de Lagrange pour la contrainte $\mathbf{u} \cdot \mathbf{n} = 0$ sur Γ_* . Ici $\mathbf{n}$ est le vecteur unité sortant, $\mathbf{t}$ le vecteur unité tangentiel à l'interface.

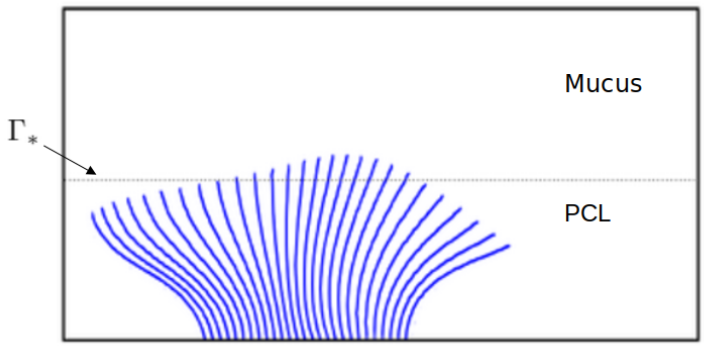

Figure 8 – Échantillon d'une forêt de cil plongée dans un bifluide.

Dans la partie suivante nous introduisons et étudions la formulation faible du problème pseudo stationnaire associé. Le terme $\delta_{\Gamma_{ij}}$ est singulier, en effet $\delta_{\Gamma_{ij}} \in (W^{1,r^*}(\Omega))'$ avec $r^* > 2$. Introduisons

l'espace fonctionnel suivant

$\mathcal{V}_{r^*} := \{\mathbf{v} = (v_x, v_y, v_z) \in (W^{1,r^*}(\Omega))^3,\ \mathbf{v}_{|\Gamma_\downarrow} = 0 \text{ dans } (L^{r^*}(\Gamma_\downarrow))^3,\ v_{z|\Gamma_\uparrow} = 0 \text{ dans } L^{r^*}(\Gamma_\uparrow),\ v_{z|\Gamma_*} = 0 \text{ dans } L^{r^*}(\Gamma_*)\}$.

Soit $r = \frac{r^*}{1-r^*}$ alors $1 \leq r < 2$. La formulation variationnelle s'écrit

$$\left\{ \begin{array}{l} \text{trouver } \mathbf{u} \in \mathcal{V}_r, p \in L^r_0(\Omega) \text{ tel que} \\ \begin{array}{rcll} a(\mathbf{u},\mathbf{v}) + nl(\mathbf{u},\mathbf{v}) - b(p,\mathbf{v}) & = & \ell(\mathbf{v}), & \forall \mathbf{v} \in \mathcal{V}_{r^*}, \\ b(q,\mathbf{u}) & = & 0, & \forall q \in L^{r^*}_0(\Omega). \end{array} \end{array} \right. \tag{7}$$

En écrivant la décomposition suivante

$$\hat{\mathbf{f}}_{ij}[\mathbf{u}](s,t) = \hat{\mathbf{f}}^0_{ij}(s,t) - \overline{u_x}^{x,y}(\xi_z^{(ij)}(s,t))\, \hat{\mathbf{m}}^{(ij)}(s,t),$$

les formes bilinéaires sont ainsi données

$$\begin{array}{rcl} a(\mathbf{u},\mathbf{v}) & := & \displaystyle\int_\Omega \mu \nabla \mathbf{u} \cdot \nabla \mathbf{v}\, d\mathbf{x}, \\ nl(\mathbf{u},\mathbf{v}) & := & \displaystyle\sum_{i,j} \int_0^L \overline{u_x}^{x,y}(\xi_z^{(ij)}(s))\, \hat{\mathbf{m}}^{(ij)}(s) \cdot \mathbf{v}(\boldsymbol{\xi}^{(ij)}(s))\, |\partial_s \boldsymbol{\xi}^{(ij)}(s)|\, \mathrm{d}s, \\ b(p,\mathbf{v}) & := & \displaystyle\int_\Omega p\, \mathrm{div}(\mathbf{v})\, d\mathbf{x}, \end{array} \tag{8}$$

et la forme linéaire

$$\ell(\mathbf{v}) := \sum_{i,j} \int_0^L \hat{\mathbf{f}}^0_{ij}(s) \cdot \mathbf{v}(\boldsymbol{\xi}^{(ij)}(s))\, |\partial_s \boldsymbol{\xi}^{(ij)}(s)|\, \mathrm{d}s, \tag{9}$$

sous l'hypothèse mentionnée précédemment que la vitesse du fluide background est approchée

$$\mathbf{u}_{\mathrm{bg}}(x,y,z) = \begin{pmatrix} \overline{u_x}^{x,y}(z) \\ 0 \\ 0 \end{pmatrix},$$

avec

$$\mathbf{f}(\boldsymbol{\xi}(s,t);t) = \hat{\mathbf{f}}(s,t).$$

Pour des raisons purement numériques, au niveau de l'implémentation de notre formulation variationnelle, nous approchons l'intégrale définie dans (9) via une formule de quadrature, typiquement de type point milieu.

Par la suite, on moyenne les équations 3D suivant x et y, en tirant profit du caractère bipériodique de $\mathbf{u}$ et p. On obtient alors une EDO sur la première composante de la vitesse moyenne $\overline{u_x}^{x,y}$, que l'on résout numériquement. La solution numérique de cette EDO peut alors être injectée dans le modèle 3D. On obtient ainsi un problème de Stokes singulier sans terme non-local, dont on sait montrer qu'il est bien posé et que l'on sait résoudre numériquement. L'EDO obtenue s'écrit

$$\left\{ \begin{array}{rcll} -\partial_z(\mu \partial_z \overline{u_x}^{x,y}) & = & \displaystyle\sum_{i,j} \overline{f_{ij,x}[\overline{u_x}^{x,y}]\delta_\Gamma}^{x,y} & \text{dans } \mathcal{D}'(0,L_z), \\ \overline{u_x}^{x,y}(0) & = & 0, & \\ \partial_z \overline{u_x}^{x,y}(L_z) & = & 0. & \end{array} \right. \tag{10}$$

Un remarque importante est le fait que la solution $\overline{u_x}^{x,y}$ admet une meilleure régularité que la vitesse définie dans le modèle 3D puisque $\overline{u_x}^{x,y}$ est dans $H^1(0,L_z)$. La formulation faible associée au

problème (10) est: Soit l'espace $V = \{v \in H^1(0, L_z),\ v(0) = 0\}$, alors on cherche $\overline{u_x}^{x,y}(\cdot, t) \in V$ telle que $\forall v \in V$:

$$\begin{aligned}
&\int_0^{L_z} \mu(z)\, \partial_z \overline{u_x}^{x,y}(z,t) \cdot \partial_z v(z)\, \mathrm{d}z \\
&\qquad + \frac{1}{L_x L_y} \sum_{i,j} \int_0^L \hat{m}_{xx}^{(ij)}(s,t)\, \overline{u_x}^{x,y}(\xi_z^{(ij)}(s,t);t)\, v(\xi_z^{(ij)}(s,t))\, |\partial_s \boldsymbol{\xi}^{(ij)}(s,t)|\, \mathrm{d}s \\
&\qquad = \frac{1}{L_x L_y} \sum_{i,j} \int_0^L \left(\hat{m}_{xx}^{(ij)} \hat{u}_{\text{cil.},x}^{(ij)} + \hat{m}_{xz}^{(ij)} \hat{u}_{\text{cil.},z}^{(ij)} \right)(s,t)\, v(\xi_z^{(ij)}(s,t))\, |\partial_s \boldsymbol{\xi}^{(ij)}(s,t)|\, \mathrm{d}s.
\end{aligned} \tag{11}$$

Par ailleurs, la formulation variationnelle (1.5) du problème réduit 1D peut être dérivée de la formulation variationnelle (1.3) du problème 3D: il suffit de considérer une fonction test $v \in \mathcal{D}(\Omega)$ qui ne dépend pas de x et de y. On démontrera par la suite l'existence et l'unicité de la solution pour chacun des problèmes 1D et 3D. Pour le problème 1D, c'est la résultante du théorème de Lax Milgram dans l'espace $H^1(\Omega)$, et pour le modèle 3D, un théorème de Lax Milgram généralisé qu'on applique aux espaces de Sobolev $\mathcal{W}_{r^*} := \{\mathbf{v} = (v_x, v_y, v_z) \in \mathcal{V}_{r^*},\ \mathrm{div}(\mathbf{v}) = 0\}$.

Dans ce chapitre, on a proposé un modèle pour le transport mucociliaire, on a pu ainsi étudier précisément l'action des battements des cils sur l'écoulement du mucus, cela grâce à des résultats numériques générés en trois dimensions. Dans la figure (9) on observe un écoulement très perturbé au niveau de la couche PCL, dû à la présence des cils dont leur mouvement est divisé en deux phases (phase active, phase retour). Mais au niveau de la couche de mucus, on observe un écoulement à vitesse quasiment constante, de l'ordre de 333μm.

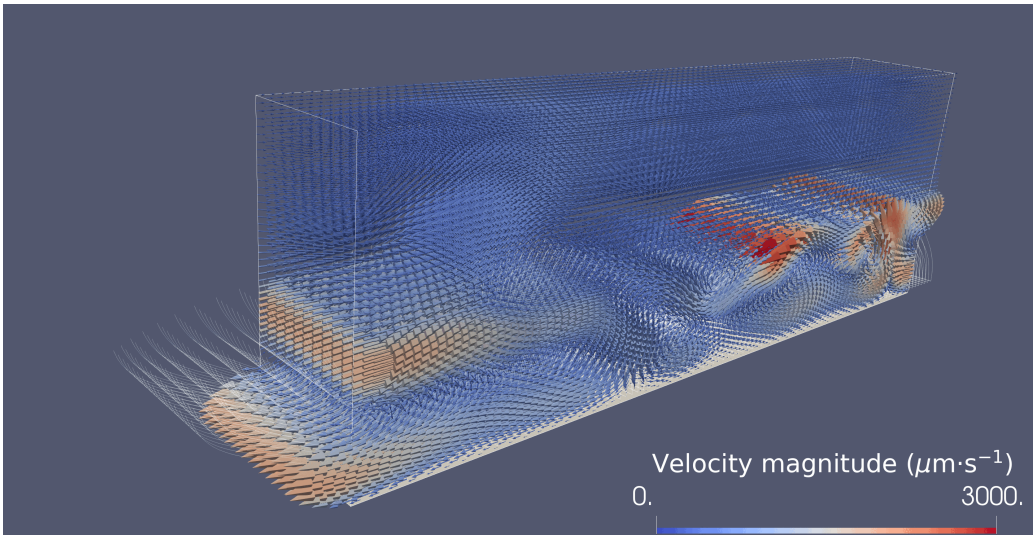

Figure 9 – Distribution de la vitesse obtenue sous l'action d'une forêt de cils dans un bifluide (MUCUS+PCL), les données sont fournies dans le premier chapitre.

Par la suite, nous souhaiterons appliquer ce modèle à un arbre bronchique pour étudier l'évolution en temps de la couche de mucus.

0.5.2 Chapitre 2: Estimation du taux de sécrétion dans un arbre bronchique

Dans ce chapitre, nous avons développé un modèle pour la clairance mucociliaire à l'échelle d'un arbre dyadique symétrique à 17 génération, où la distribution de l'épaisseur de la couche mucus est

la même dans chaque bronche d'une même génération. Ce modèle permet de calculer l'évolution en temps du volume du mucus présent dans les bronches pulmonaires, en prenant en compte à la fois le battement des cils et l'écoulement de l'air à travers la lumière bronchique. Pour ce faire nous allons considérer les 2 modèles d'arbre bronchique suivants:

- le modèle de Weibel, un modèle très utilisé notamment dans Mauroy et al[48], qui suppose un rapport homothétique entre chaque longueur l_i^b et rayon r_i^b d'une bronche appartenant à la i-ème génération.
- le modèle dit morphométrique, basé sur des données expérimentales [73, 74].

On considère tout d'abord un modèle 3D qui est le même que celui défini dans le chapitre 1, sauf que le domaine considéré est un cylindre troué noté Ω_i

$$\Omega_i = \{(r,\theta,z),\ \ 0 \le \theta \le 2\pi,\ 0 \le z \le l_i^b,\ r_i^a \le r \le r_i^b\},$$

où i représente l'indice de la génération. De plus une nouvelle contrainte (plus précisément de cisaillement) se rajoute à notre problème dûe à l'écoulement d'air au niveau de l'interface air/mucus. En se plaçant dans un système de coordonnées cylindriques, on écrit la vitesse $\mathbf{u}(r,\theta,z,t) = u_r(r,\theta,z,t)\mathbf{e}_r + u_\theta(r,\theta,z,t)\mathbf{e}_\theta + u_z(r,\theta,z,t)\mathbf{e}_z$. Le problème s'écrit:

$$\begin{cases} -\frac{1}{r}\frac{\partial}{\partial r}(r\mu\frac{\partial u_r}{\partial r}) - \mu(\frac{1}{r^2}\frac{\partial^2 u_r}{\partial\theta^2} + \frac{\partial^2 u_r}{\partial z^2} - \frac{u_r}{r^2} + \frac{2}{r^2}\frac{\partial u_\theta}{\partial\theta}) + \frac{\partial p}{\partial r} + \gamma\delta_{\Gamma_i^m} = \sum_{j=1}^M f_r^j \delta_{\Gamma_i(t)} & \text{dans } \Omega_i, \\ -\frac{1}{r}\frac{\partial}{\partial r}(r\mu\frac{\partial u_\theta}{\partial r}) - \mu(\frac{1}{r^2}\frac{\partial^2 u_\theta}{\partial\theta^2} + \frac{\partial^2 u_\theta}{\partial z^2} - \frac{u_\theta}{r^2} + \frac{2}{r^2}\frac{\partial u_r}{\partial\theta}) + \frac{\partial p}{\partial\theta} = 0 & \text{dans } \Omega_i, \\ -\frac{1}{r}\frac{\partial}{\partial r}(r\mu\frac{\partial u_z}{\partial r}) - \mu(\frac{1}{r^2}\frac{\partial^2 u_z}{\partial\theta^2} + \frac{\partial^2 u_z}{\partial z^2}) + \frac{\partial p}{\partial z} = \sum_{j=1}^M f_z^j \delta_{\Gamma_j(t)} & \text{dans } \Omega_i, \\ \frac{1}{r}\frac{\partial(ru_r)}{\partial r} + \frac{1}{r}\frac{\partial u_\theta}{\partial\theta} + \frac{\partial u_z}{\partial z} = 0 & \text{dans } \Omega_i. \end{cases} \tag{12}$$

avec les conditions aux bords:

$$\begin{cases} \sigma_{r\theta} = \mu(\frac{1}{r}\frac{\partial u_r}{\partial\theta} + \frac{\partial u_\theta}{\partial r} - \frac{u_\theta}{r}) = \sigma_{r\theta|\text{air}} & \text{sur } \Gamma_i^{\text{a}}, \\ \sigma_{rz} = \mu(\frac{1}{r}\frac{\partial u_r}{\partial z} + \frac{\partial u_z}{\partial r}) = \sigma_{rz|\text{air}} & \text{sur } \Gamma_i^{\text{a}}, \\ u_r = 0 & \text{sur } \Gamma_i^{\text{a}}, \\ u_r = u_\theta = u_z = 0 & \text{sur } \Gamma_i^{\text{b}}. \end{cases} \tag{13}$$

σ_{air} est le tenseur des contraintes associé à l'écoulement d'air, μ est la viscosité du bifluide

$$\mu(r) = \begin{cases} \mu_{\text{m}} & r_i^m \le r \le r_i^a, \\ \mu_{\text{PCL}} & 0 \le r < r_i^m. \end{cases}$$

Le bord $\Gamma_i^{\text{b}} := \{r = r_i^b\}$ représente la paroi bronchique, le bord $\Gamma_i^{\text{m}} := \{r = r_i^m\}$ représente l'interface mucus/PCL et $\Gamma_i^{\text{a}} := \{r = r_i^a\}$ représente l'interface séparant le mucus de l'air. La paramétrisation du cil et la force exercée par le cil s'écrira en coordonnées cylindriques: pour tout $s \in [0, L]$, $t > 0$

$$\begin{aligned} \boldsymbol{\xi}(s,t) &= \xi_r(s,t)\mathbf{e}_r + \xi_z(s,t)\mathbf{e}_z, \\ \mathbf{f}(s,t) &= f_r(s,t)\mathbf{e}_r + f_z(s,t)\mathbf{e}_z. \end{aligned} \tag{14}$$

En moyennant nos équations (2.6) en la i-ème génération on obtient:

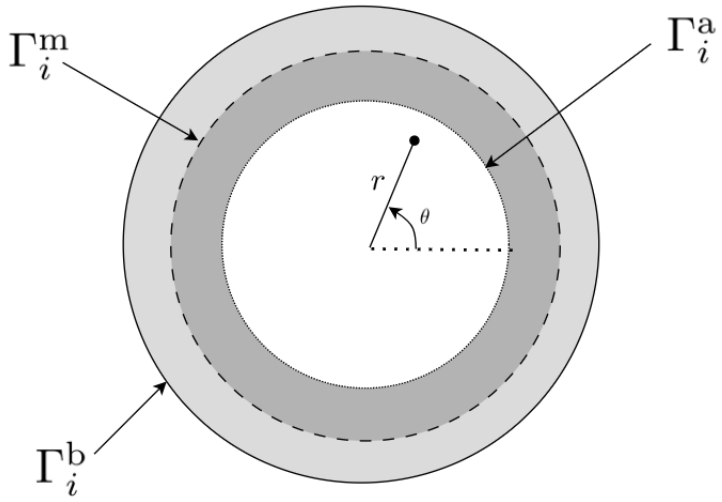

Figure 10 – Ensemble des bords considérés dans le modèle 1D pour une bronche de la i-ème génération.

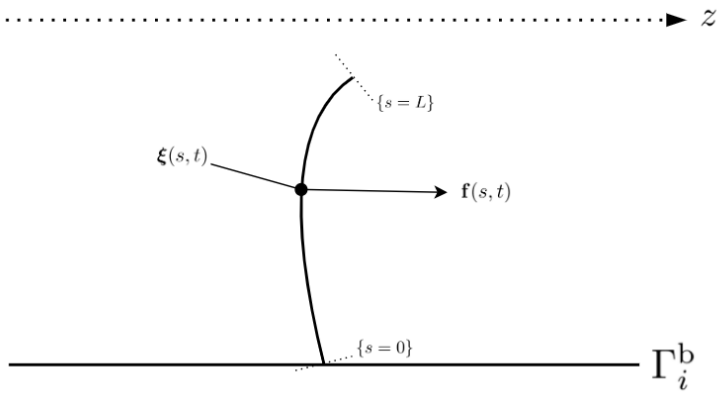

Figure 11 – Schéma représentant la ligne centrale du cil modélisé par une courbe en coordonnées curvilignes.

$$\begin{cases} -\frac{1}{r}\frac{\mathrm{d}}{\mathrm{d}r}(r\mu\frac{\mathrm{d}\overline{u_z}^{\theta,z}}{\mathrm{d}r}) + \frac{P_{\mathrm{out},i}-P_{\mathrm{in},i}}{l_i^b} &= \sum_{j=1}^{M} \overline{f_z^j}^{\theta,z}\delta_{\Gamma_j(t)} & \text{dans } (r_i^a, r_i^b), \\ \mu\frac{\mathrm{d}}{\mathrm{d}r}\overline{u}_z^{\theta,z} &= \mu_{air}\frac{\mathrm{d}}{\mathrm{d}r}u_{\mathrm{air}} & \text{sur } \{r = r_i^a\}, \\ \overline{u}_z^{\theta,z} &= 0 & \text{sur } \{r = r_i^b\}. \end{cases} \tag{15}$$

$P_{\mathrm{in},i} - P_{\mathrm{out},i}$ est la différence de pression de l'air entre l'entrée et la sortie de la bronche de la i-ème génération (Figure 12). On considère un écoulement d'air de type Poiseuille, donc :

$$\begin{aligned} P_{\mathrm{in},i} - P_{\mathrm{out},i} &= \frac{8\mu_{\mathrm{air}} l_b^i}{\pi (r_i^a)^4}\phi_i^{\mathrm{air}}, \\ \frac{d}{dr}u_{\mathrm{air}}(r) &= \frac{-4\mu_{air}}{\pi r_{a,i}^3}\phi_i^{\mathrm{air}}. \end{aligned} \tag{16}$$

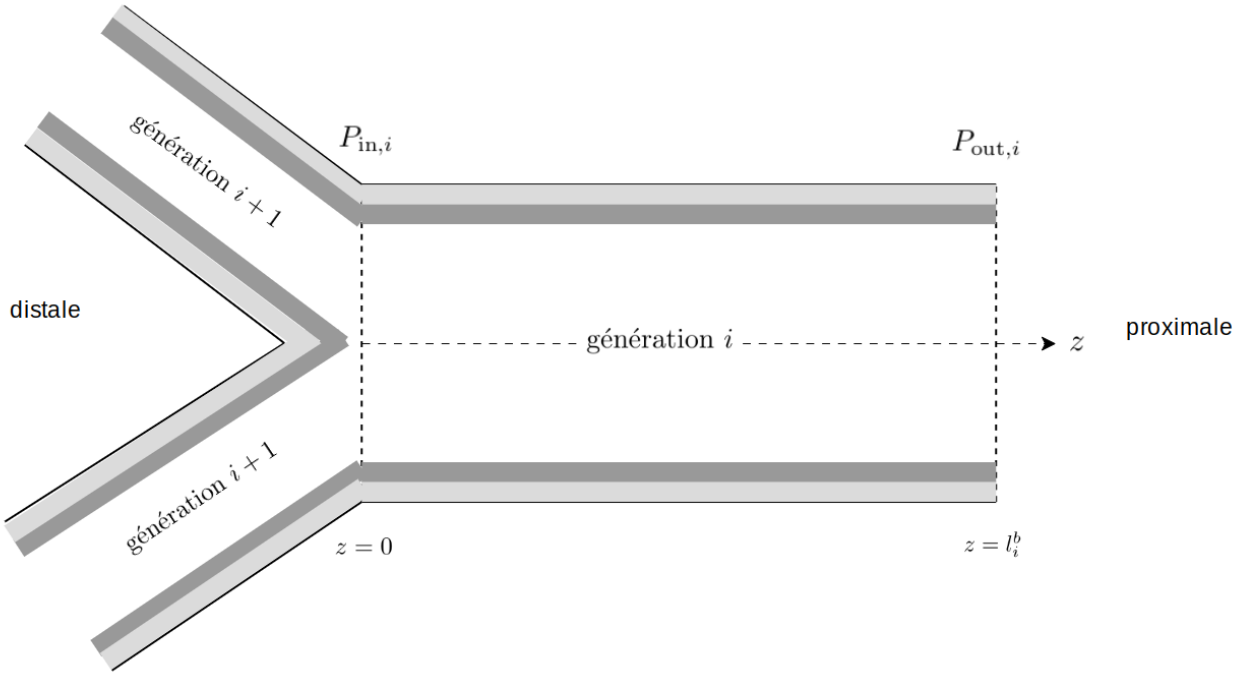

Figure 12 – Schéma d'une bronche de la i-ème génération avec une bifurcation.

μ_{air} est la viscosité de l'air, ϕ_i^{air} est le débit d'air à l'entrée de la bronche de la i-ème génération:

$$\phi_i^{\mathrm{air}} = \frac{\Phi_{\mathrm{air}}}{2^{i-1}},$$

Φ_{air} est le débit d'air à la trachée ($\Phi_{\mathrm{mouth}}^{\mathrm{air}} < 0$ à l'inspiration et $\Phi_{\mathrm{mouth}}^{\mathrm{air}} > 0$ à l'expiration). Soit l'espace fonctionnel $V = \{v \in H^1(r_i^a, r_i^b),\ v(r_i^b) = 0\}$, on cherche $u \in V$ telle que $\forall v \in V$

$$
\begin{aligned}
&\int_{r_i^a}^{r_i^b} r\mu(r)\,\frac{du}{dr}(r)\,\frac{dv}{dr}(r)\,\mathrm{d}r \\
&\qquad + \frac{1}{2\pi L_z}\sum_j \int_0^L \xi_r^{(j)}(s,t))\,\hat{m}_{zz}^{(j)}(s,t)\,u(\xi_r^{(j)}(s,t))\,v(\xi_r^{(j)}(s,t))\,|\partial_s \boldsymbol{\xi}^{(j)}(s,t)|\,\mathrm{d}s \\
&\qquad = \frac{1}{2\pi L_z}\sum_j \int_0^L \xi_r^{(j)}(s,t))\left(\hat{m}_{zz}^{(j)}\hat{u}_{\mathsf{cil.},z}^{(j)} + \hat{m}_{zr}^{(j)}\hat{u}_{\mathsf{cil.},r}^{(j)}\right)(s,t)\,v(\xi_r^{(j)}(s,t))\,|\partial_s \boldsymbol{\xi}^{(j)}(s,t)|\,\mathrm{d}s \\
&\qquad + \int_{r_i^a}^{r_i^b} r\,f_1\,v(r)\,dr + r_i^a\,f_2\,v(r_i^a).
\end{aligned}
\tag{17}
$$

Les termes f_1 et f_2 s'écrivent :

$$
f_1 = \frac{8\mu_{\mathrm{air}}\Phi_{\mathrm{mouth}}^{\mathrm{air}}}{2^{i-1}\pi(r_i^a)^4}, \quad f_2 := \frac{\mu_{\mathrm{air}}}{\mu_{\mathrm{m}}}\frac{du_{\mathrm{air}}}{dr}(r_i^a)
$$

et représentent l'influence de l'air sur l'écoulement du bifluide. Le terme f_1 agit sur tout le domaine fluide (mucus+PCL) et le terme f_2 vient de la contrainte de cisaillement agissant uniquement au niveau de l'interface $\{r = r_i^a\}$. Après avoir décrit la dynamique du mucus en chaque génération, on décrit l'évolution de la distribution de l'épaisseur de la couche mucus sur tout l'arbre bronchique. En utilisant l'équation de la conservation de la masse, notre modèle est ainsi régi par un système d'EDO portant sur le rayon r_i^a de chaque génération:

$$
\frac{dr_i^a}{dt}(t) = \frac{Q_i(U_i; r_i^a(t)) - 2Q_{i+1}(U_{i+1}; r_{i+1}^a(t)) - \phi_i}{2\pi l_i^b r_i^a(t)}, \qquad i \in \{1,..,N\}, \tag{18}
$$

avec une condition initiale $r_i^a(0)$ donnée. On note U_i la vitesse moyenne solution de l'EDO (2.10) au niveau de la i-ème génération, N est le nombre de générations (ici $N = 17$). $Q_i(U_i; r_i^a(t))$ est le débit d'écoulement du mucus à la i-ème génération, à l'instant t. A noter que la production du mucus se fait uniquement de la génération 1 à $N = 17$ [51, 76], par conséquent le débit au niveau de la génération N est nul ($Q_{N+1} = 0$). Aussi, le modèle (2.1) prend en compte le phénomène de sécrétion du mucus par l'épithélium, mais aussi d'éventuelles phénomènes d'absorption et d'évaporation, grâce au terme source ϕ_i en chaque génération i. Mais on abrège en définissant $(\phi_i)_{i\in\{1,..,N\}}$ le débit de sécrétion par l'épithélium. Une estimation des taux $(\phi_i)_{i\in\{1,..,N\}}$ est mentionnée dans les travaux de Kurbatova et al [37], les auteurs s'accordent sur le fait que la production journalière totale du mucus est de $100 - 150$ ml comme mentionné dans Waldron [77], les taux $(\phi_i)_{i\in\{1,..,N\}}$ sont alors ajustés pour obtenir cette production totale. De plus en tenant compte du fait que le nombre de glandes submucosales décroît de la trachée à la dernière génération, les auteurs considèrent une distribution des taux $(\phi_i)_{i\in\{0,..,16\}}$ affine et décroissante suivant qu'on avance dans les générations. Durant la thèse, on estime les taux de sécrétion du mucus par l'épithélium dans la section (2) en considérant les états d'équilibres du système (2.1).

Comme précisé dans la partie contexte, le taux de production est très difficile à estimer. On simplifiera notre système (2.1) en normalisant le taux ϕ_i en chaque génération i par rapport a la surface de la bronche ($\phi_i = 2\pi\, r_i^b\, l_i^b, \tilde{\phi}$ et $\tilde{\phi}$ constant), et on suppose que la sécrétion est homogène en chaque unité de surface de la paroi bronchique.

On note $\{r_i^{a\star}\}_{i\in\{1,\cdots,N\}}$ l'état d'équilibre du système (2.1), qui est solution du système :

$$
Q_i(u_i; r_i^{a\star}) - 2Q_{i+1}(u_{i+1}; r_{i+1}^{a\star}) - 2\pi\, r_i^b\, l_i^b, \tilde{\phi} = 0 \qquad i \in \{1,..,N\}. \tag{19}
$$

Dans le cas ou $\Phi^{\text{air}}_{\text{mouth}} = 0$, le système (2.14) donne une relation explicite entre le taux de sécrétion normalisé $\tilde{\phi}$ et l'état d'équilibre $\{r_i^{a\star}\}_{i\in\{1,\cdots,N\}}$. Deux choix s'offrent a nous:

- On connaît au moins une des valeurs $r_{i_0}^{a\star}$ en une génération i_0: on peut alors calculer la valeur du taux de sécrétion $\tilde{\phi}$ correspondant.

- On connaît la valeur de $\tilde{\phi}$ ou même le taux de production du mucus par jour, on obtient alors directement les états d'équilibre $r_i^{a\star}$ suivant chaque génération.

Les ordres de grandeurs de l'épaisseur de la couche de mucus trouvés ans la littérature sont de $10 - 30$ μm au niveau de la trachée [1] et décroît jusqu'à $2 - 5$ μm au niveau des générations les plus distales [1]. Dans un premier temps, on fixera l'épaisseur de la couche de mucus à l'équilibre à $r_0^m - r_0^{a\star} := 10\mu$m à la trachée. Dans cette configuration, et pour $\Phi^{\text{air}}_{\text{mouth}} = 0$, on obtient $\tilde{\phi} = 5.779\cdot 10^{-4}$ avec le modèle d'arbre de type Weibel et $\tilde{\phi} = 4.772\cdot 10^{-4}$ avec le modèle morphométrique. La distribution des épaisseurs de la couche de mucus à l'équilibre est illustrée dans la Figure (13) et dans le tableau 1. On observe des ordres de grandeurs de $10^{-2} - 10^{-3}\mu$m au niveau des six dernières générations pour les épaisseurs des couches de mucus.

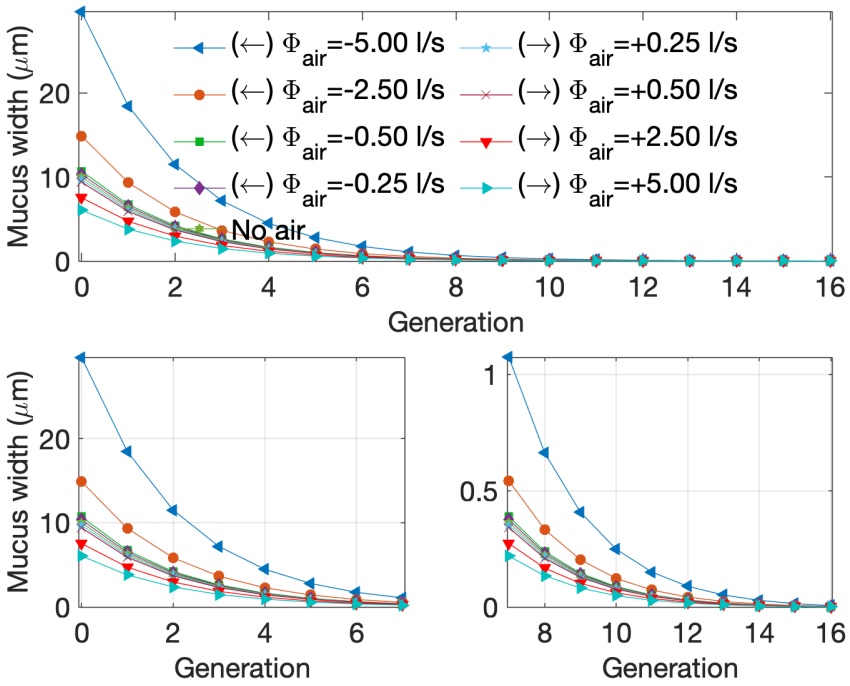

Figure 13 – Distribution des épaisseurs de la couche de mucus $\delta_i := r_i^m - r_i^{a\star}$ à l'équilibre pour divers débit d'air imposés à la trachée ($\leftarrow$ pour l'inspiration, $\rightarrow$ pour l'expiration). Le modèle d'arbre bronchique considéré et de type Weibel.

Jusqu'à présent nous avons étudié le système (2.1) avec des débits d'air constant en temps, dans le chapitre 3 nous considérerons des débits d'air respiratoires périodiques en temps.

génération	Weibel	morphométrique
1	10	10
2	6.2674	7.28018
3	3.92303	5.31051
4	2.45155	3.927
5	1.52874	2.43618
6	0.950667	1.55997
7	0.589063	0.969799
8	0.363288	0.585908
9	0.222655	0.358408
10	0.135327	0.21315
11	0.0813154	0.123432
12	0.0480846	0.0712316
13	0.0277805	0.0388491
14	0.0154892	0.0207802
15	0.00814234	0.0100785
16	0.003828	0.00588769
17	0.0013588	0.00195532

Table 1 – Épaisseur de la couche de mucus à l'état d'équilibre en μm en chaque génération pour une fréquence de battement des cils à 15Hz.

0.5.3 Chapitre 3: Dynamique du transport mucociliaire dans un arbre bronchique

Dans ce chapitre, nous étudions l'évolution en temps long des épaisseurs de la couche de mucus soumises à des débits respiratoires (inspiration puis expiration). Nous considérons deux types de débits respiratoires: le premier est sinusoïdal; ce modèle est très utilisé notamment dans [34, 48, 47]. Le deuxième modèle, dans une perspective d'obtenir des débits d'air plus réaliste, découle d'une équation modélisant la dynamique du volume pulmonaire due à une pression P_{ext} exercée par le diaphragme et éventuellement les muscles de l'abdomen. On considère uniquement l'arbre de type morphométrique. On se donne $T > 0$ représentant une période respiratoire et $t \mapsto \Phi^{\text{air}}_{\text{mouth}}(t)$ le débit d'air imposé au niveau de la trachée $T-$périodique. Le problème périodique s'écrit alors:

Trouver $r_0^a = (r_{1,0}^a, ..., r_{N,0}^a)$ telle que le solution unique de

$$(\mathrm{O}_i) \begin{cases} \dfrac{\mathrm{d}r_i^a(t)}{\mathrm{d}t} & = \dfrac{Q_i(U_i; r_i^a(t)) - 2Q_{i+1}(U_{i+1}; r_{i+1}^a(t))}{2\pi \ell_i^b r_i^a(t)} - \tilde{\phi}\dfrac{r_i^b}{r_i^a(t)},\ t \in (0,T),\ i \in \{1,..N\} \\ r_i^a(0) & = r_{i,0}^a,\ i \in \{1,..N\}, \end{cases} \tag{20}$$

satisfait $r_i^a(T) = r_i^a(0)$ pour tout $i \in \{1,..N\}$. Pour rappel, $Q_{N+1} = 0$ et U_i est la vitesse moyenne de l'écoulement du mucus dû à l'influence de l'air et au mouvements des cils. Dans le cas où $\Phi^{\text{air}}_{\text{mouth}}$ est nulle la solution de (20) est simplement

$$r_i^a(T) = r_i^a(0) = r_i^{a\star},$$

où $\{r_i^{a\star}\}_{i\in\{1,\cdots,N\}}$ est l'état équilibre calculé dans le deuxième chapitre. Dans le cas où l'influence de l'air est prise en compte grâce à un débit d'air périodique imposé à la trachée, pour résoudre (20)

nous avons utilisé la méthode du point fixe. Aussi, deux choix s'offrent à nous pour la discrétisation de notre système (20): schéma explicite et semi-implicite. Le schéma semi-implicite offre une meilleure stabilité en temps que le schéma explicite, mais le temps de calcul numérique est le même. La figure (14) illustre l'évolution de l'épaisseur de la couche de mucus solution $t \mapsto \delta_{17}(t) = r_{17}^b - r_{17}^a(t)$ où $t \mapsto r_{17}^a(t)$ satisfait le problème (O_{17}) du système (20). Le débit respiratoire (inspiration puis expiration) considéré est celui obtenu grâce à une équation modélisant la dynamique du volume pulmonaire. On observe qu'à l'inspiration l'épaisseur de la couche de mucus augmente, et qu'à l'expiration l'épaisseur tend à diminuer. De plus, l'amplitude de la courbe représentant l'évolution en temps de l'épaisseur de la couche de mucus augmente en augmentant l'intensité du débit d'air imposé à la trachée. Par ailleurs, dans une période de temps, on observe que l'épaisseur de la couche de mucus oscille autour de l'épaisseur de la couche à l'état d'équilibre. Mais pour autant, on ne peut pas démontrer que la moyenne en temps $\int_0^T \delta_{17}(t)dt$ soit égale à l'épaisseur δ_{17} à l'équilibre.

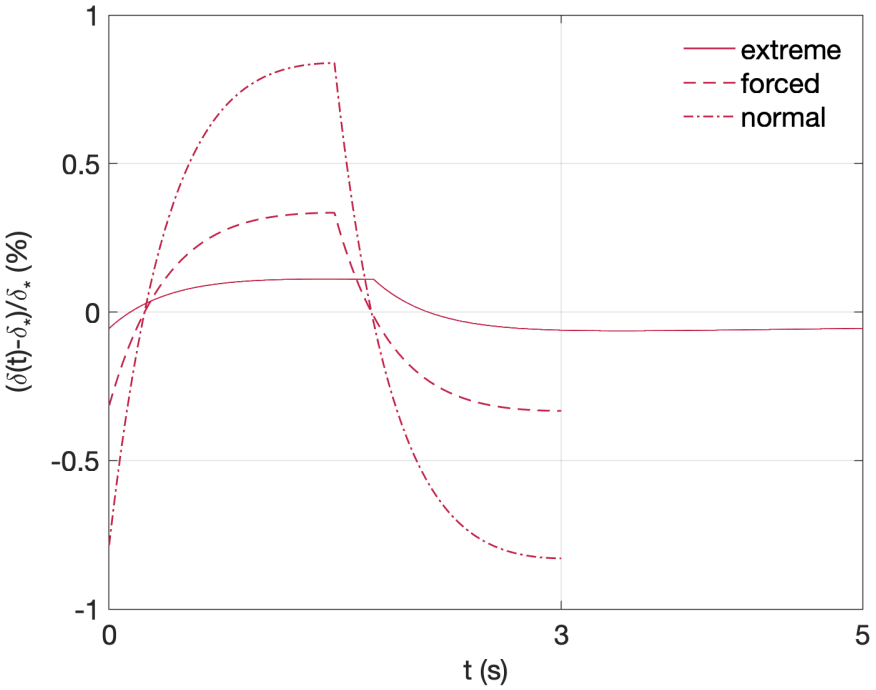

Figure 14 – Évolution de l'épaisseur de la couche de mucus $t \mapsto \delta_{17}(t) = r_{17}^b - r_{17}^a(t)$ à la dernière génération suivant différent régimes respiratoires : respiration *normal* ($\Phi_{\max}^{\text{air}} \sim 1.00\,\mathrm{L}\cdot\mathrm{s}^{-1}$) avec une période de respiration de 5 seconde, respiration *forcée* ($\Phi_{\max}^{\text{air}} \sim 4.00\,\mathrm{L}\cdot\mathrm{s}^{-1}$) et respiration *extrême* ($\Phi_{\max}^{\text{air}} \sim 10.00\,\mathrm{L}\cdot\mathrm{s}^{-1}$) avec une période de respiration de 3 seconde. δ_* représente l'épaisseur de la couche de mucus à l'équilibre.

Chapter 1

3D simulation of active thin structures in a viscous fluid and application to mucociliary transport

Tiré de l'article "3D simulation of active thin structures in a viscous fluid and application to mucociliary transport" publié dans Mathematical Modelling of Natural Phenomena

We propose a hierarchy of mathematical models for the numerical simulation of active thin structures in a viscous fluid and its application to mucociliary clearance. Our aim is to simulate large forests of cilia and analyze the collective dynamics arising in the flow, as well as their impact on the efficiency of the mucus transport. In a 3D model we describe the cilia individually and study their joint actions on the fluid. The model is built upon a 3D Stokes problem with singular source terms that represent the action of the 1D cilia on the fluid, including the influence of the background flow (making the problem nonlocal). Surface tension between the periciliary layer and the mucus is taken into account. From the 3D model we also derive a 1D space averaged model, describing the dynamics of the mean velocity of the mucus that is propelled by the cilia, hence allowing lower computational costs and still providing useful characterization of the efficiency of the transport. Mathematical properties of the models (existence and uniqueness of solutions in suitable functional spaces) are analyzed. Numerical simulations highlight the influence of critical parameters on the efficiency of the mucociliary transport in the case of dense forests of cilia.

Introduction

The present work deals with the mathematical modeling and the numerical simulation of active thin structures in a viscous fluid and its application to mucociliary clearance. The human lung is protected against dehydration and inhaled particles, like dust or allergens, by a thin liquid layer lining the interior of the airways. This airway surface liquid is a bilayer composed of mucus, a visco-elastic fluid secreted by the respiratory epithelium [39], and a thin fluid layer known as the periciliary liquid [36], commonly called PCL. Preserving the lung from inhaled impurities is necessary, since they could obstruct the bronchi and limit the exchange area for oxygen and carbon dioxide. Mucus traps aspirated particles and is then itself evacuated from the lung by the action of numerous cilia lining the lung bronchi. Other factors that help drain mucus in the bronchial tree are cough and forced breathing [4]. Under

pathological conditions, mucus characteristics and mucociliary clearance efficiency can be altered. For example, due to a modification of the viscosity of the mucus or a degradation of cilia, ciliary motion can become ineffective, inducing mucus stasis that often leads to infections.

Active research has been devoted to the study of the motion of bronchial cilia since the pioneering work by Lucas [43]. Cilia are very slender structures whose length is about $6\ \mu$m and radius is $0.1\,\mu\mathrm{m}$, and they are fixed on the epithelial cells in the bronchi. They beat in the periciliary layer, where viscosity is much lower than in the mucus, at an average frequency of 15 Hz depending on the characteristics of the environment. A detailed description of the mechanism of motility has been given by Gibbons in [28] and more recently in [52, 55, 59]. Each beat of a cilium can be divided into two phases, a recovery stroke and an effective stroke, during which the motion is not symmetric under time reversal. In fact, since mucus and PCL are viscous fluids at the scale of a cilium, a reversible movement of the cilium would not permit the mucus to be transported [60]. According to Sanderson and Dirksen [63], the effective stroke is two or three times faster than the recovery stroke, and cilia may penetrate the overlying mucus during the faster phase. Cilia that propel mucus coordinate into a metachronal wave, which wavelength is of the order of a hundred of cilia, that is around $30\,\mu\mathrm{m}$, and that propagates in the opposite direction of mucus transport. It is believed that coordination of the beating into a metachronal wave arises during the recovery stroke and is due to hydrodynamic interactions between the cilia [12]. Changes in the viscosity of the medium, in the length or in the spacing of the cilia may therefore have a deep influence on the characteristics of the metachronal wave.

The complexity of the process is high (high amount of cilia, three layers if we consider air that is driven in the bronchus, several interfaces, several scales, etc) and only a few data are available. Although a wide variety of works can be found in the literature about mucociliary clearance, the numerical simulation remains at present time a challenge.

Some authors have developed models in which the action of cilia is represented via a prescribed velocity at the bottom of the mucus layer, like for instance in [24], where a numerical investigation of the interaction between respiratory mucus motion and air circulation is presented. Using the same approach, Mitran proposes in [54] a multiscale model to study the effect of airflow shear forces, as exerted by tidal breathing and cough, upon clearance, and Mauroy and coauthors investigate in [48] the role of the geometry of the airway tree on clearance. These works present interesting multiscale approaches of the process but they do not allow to investigate details of the role of ciliary motion.

Other authors use a continuum representation of the airway surface liquid as a traction layer, with a continuous distribution of forces. In [71], for instance, Smith and coauthors replace the forest of cilia by an active porous medium in which the cilia are modeled by a volumic resistive force directly dependent on the local velocity of the cilia. They consider a three-layer fluid in dimension 2: a Maxwell fluid for the mucus, a Newtonian fluid for the periciliary layer and a layer of transition. Kurbatova and coauthors use the same model in [37] in order to estimate mucociliary velocity in different generations of the lung, adding influx terms from previous generations and production of mucus. In [19] Choudhury and coauthors replace the forest of cilia by a Navier-slip boundary condition derived in [10] which allows for a continuum description of the mucus film (considered as viscolelastic, not purely viscous).

A very different approach consists in representing the cilia individually, either by prescribing their beating or by modeling in some way their internal activity. Several authors have worked on models for the internal activity of cilia, in order for instance to investigate the emergence of ciliary metachronism [30, 31, 29, 23, 22]. In [23] for instance, Dillon and coauthors used a discrete representation of the internal structures of cilia and a curvature control mechanism for their activity, and solved the interaction of these structures with the fluid (PCL and mucus) in 2D using the immersed boundary

method. Sedaghat and coauthors use hybrid finite difference-lattice Boltzmann-method combined with immersed boundary method, in 2D, to investigate the additional effect of viscoelasticity in 2D [67] and in 3D [66]. Mitran [53] proposed the most complete model for the internal mechanism of bronchial cilia, with a detailed description of the internal microtubule structures in 3D using thin-wall beams and spring elements to model nexin links. Activity was modelled through a forces scenario exerted between adjacent microtubules. The fluid-structure interaction was solved using finite elements for the structure and finite volumes for fluid. He simulated the configuration of up to 256 cilia in a row, bringing evidence for a hydrodynamic origin to observed ciliary synchronization. However, the computational effort is such that no parametric study could be made. Recent works have proposed models based on a sliding regulation mechanism for dynein activity proposed in [57]. Cilia movement is modeled with 1D elastic equations and the fluid-structure problem is solved using the slender body theory. These works have allowed to reproduce typical spontaneous oscillations observed in cilia [44] as well as synchronization resulting from hydrodynamical interactions [14, 15].

Nevertheless, how the internal ciliary engine affects the ciliary beat form is still not completely understood, and its modelling induces heavy additional computational effort. That is why many works focus on the flow fields produced by cilia with given beat pattern and frequency. Due to their slenderness, the action of individual cilia can be represented by a centerline distribution of forces, following the slender body theory (see for instance [20], or for a rigorous asymptotic analysis [56]). This idea was initially developed in studies such as Liron and Mochon [42] and Fulford and Blake [25], and then further developed in other works [30]. The distribution of point forces is derived from the prescribed beat pattern either using an asymptotic formula, as in [25], or by prescribing the velocity at the surface of each cilium as in [42] and [70], leading to the resolution of an integral equation. The different works based on this idea can be distinguished by the way the force distribution is computed, but also by the use of particular singular solutions adapted to the conditions at the boundaries of the domain. They have obtained estimates of the mean field velocity in both the periciliary layer and the mucous layer (both liquids being assumed to have Newtonian fluid properties), but the profiles are time- and space-averaged. Besides, no penetration of the cilia into the mucus layer is taken into account. They show that the mean field velocity is very small in the lower part of the periciliary layer and increases very quickly close to the mucus layer. In [41] the authors used a similar model in 2D allowing to investigate non-averaged velocity profiles both in the PCL and in the mucus; a parametric study was made, showing the impact of changing the viscosity ratio or the length of cilia. In particular, they show that the velocity of mucus decreases when its viscosity increases, what they explain via the fact that viscous forces between the mucus and the PCL increase. In [16] cilia are also modeled by thin structures whose deformations are prescribed. However the computations are 3-dimensional and the numerical method is different : the equality of the fluid and solid velocities on the fluid-structure interface is imposed with the immersed boundary method. In addition, the action of the fluid on the structure is partially taken into account, modeled by a damping term that changes the intensity of the velocity of the structures. The authors investigate synchronization of cilia through hydrodynamic interactions, but the velocity profiles inside the layers are not analyzed.

Some works consider a 3-dimensional representation of each cilium with prescribed movement. Chatelin and coauthors [17], for instance, proposed a 3-dimensional model where the viscosity is the solution of a convection-diffusion equation of mucin proteins. The movement of the cilia is prescribed and the effects of the cilia on the fluid are treated by an efficient fictitious domain method. However the amount of cilia in simulations remains limited, due to the high computational cost induced by the representation of the structure's thickness. In [46], the authors modeled in two-dimension the viscosity as the solution of a reaction-advection-diffusion equation depending on the temperature,

but the model for the flow is very simplified. To the best of our knowledge, in the other works which consider a variable viscosity, the viscosity is defined constant by part.

This work focuses on a model that allows to efficiently simulate a large amount of active thin structures and perform a parametric study to investigate the impact of different parameters on mucus velocity. The complexity of the phenomenon leads us to consider several restrictive assumptions. On the one hand, we have chosen to work in the case of a prescribed movement of the structures, in the asymptotic limit of infinite slenderness: we thus represent the slender bodies as 1D curves immersed in a 3D viscous flow. The action of the structures on the fluid is represented through a Dirac distribution of forces along the 1D curve. Retroaction of the fluid on the structures is not taken into account. On the other hand, although mucus is a viscoelastic fluid, its relaxation time is long with respect to the cilia beating cycle. It is thus reasonable to model it as a Newtonian viscous fluid. And since both mucus and the PCL are viscous at the scale of the cilia, we solve the Stokes equations in both layers. The significant difference in viscosity is taken into account through a bi-fluid model with a fixed and flat interface, consistently to experimental observations. The presence of air above the mucus layer is taken into account through a boundary condition, airways are not represented in our simulations. A bottom-up approach is developped: i) at the cilia individual scale, we use equations of motion for 3D Stokes flow to which we associate the cilia individually and solve the action of each of them on the fluid. ii) at an averaged scale, we derive a 1D model that describes how the ciliary activity governs the mean axial velocity of the fluid (which is directly related to the efficiency of the mucociliary transport), with a computational cost that is considerably lowered. A rigorous mathematical framework is presented for both problems, including well-posedness in suitable functional spaces. Additionally, we use a finite element method to solve both problems: the method is still well-defined in the presence of the singular source term and the rigorous error analysis has been performed in [7] (the FEM is still proven to be converging, with a convergence rate that is locally slowed down). The models and numerical methods allow us to simulate the action of very large forests of cilia on the flow, and investigate the impact of some parameters on the mucociliary efficiency. They can contribute to a better understanding of mechanisms involved in mucociliary clearance, in the perspective of analyzing the collective dynamics arising in the flow, as well as their impact on the efficiency of the mucus transport.

This paper is organized as follows: in section 1 we describe the model developed for the fluid-cilia interaction, and in section 2 we discuss the mathematical properties of the resulting equations, i.e. a nonlocal Stokes system with a singular right-hand side. Section 3 is devoted to the numerical method developed in order to retrieve the optimal order of the finite element method applied to these equations. The last section concerns the application of this model to the simulation of the mucociliary transport and the presentation of numerical results in a reference configuration along with an investigation of critical parameters for the mucociliary efficiency.

1.1 Three-dimensional modelling

We are interested in modelling the interaction of active cilia with a viscous flow in the context of mucociliary transport. Bronchial cilia are attached to the bronchial walls and immersed in a bilayer composed of a first thin liquid layer called the periciliary liquid (PCL), adjacent to the walls, and a second layer composed of mucus (see Figure 1.1). They essentially beat inside the PCL, but eventually penetrate the mucus layer during a short part of their periodic movement. At the top of the bilayer, mucus is in contact with the air flowing inside the bronchi. Since the aim of this work is to simulate dense suspensions of active cilia, we are concerned with limiting the computational cost related to the problem, while trying to keep assumptions minimal.

An essential feature of our problem is that cilia are slender bodies that beat very quickly in the viscous fluid. In the case of bronchial cilia, the ratio between their cross-sectional radius and their length is $\frac{r}{L} \sim \frac{0.1}{6}$, and their beating frequency is about $f = 15$ Hz. Representing each cilium as a three-dimensional body immersed in the fluid domain involves a considerable computational effort to represent the fluid-body interface. An option in order to reduce this cost can be to use a fictitious domain approach (see for instance [17]). However, we have chosen to take advantage of the geometry of the structure and work in the asymptotic of infinite slenderness, that is when the ratio between the thickness and the length of the structure $\epsilon = \frac{r}{L}$ vanishes. Keeping the force exerted by each section of the body constant when ϵ vanishes allows to conserve the action of the cilium on the fluid, while the velocity of the fluid becomes infinite at the centerline of the slender body. Our model thus consists of the Stokes equations governing the dynamics of a viscous fluid, with in the source term a line distribution of forces along a 1D curve representing the thin structures. For an analysis of the convergence of the solution to the full problem, that means with a volumic distribution of the hydrodynamic force on the 3D structure, to the solution of the asymptotic model when ϵ vanishes, we refer the reader to [38].

As for the activity of the cilia, a complete model would consist in a mechanical model for the structure coupled to the fluid equations, so that both the action of the structure on the fluid and the retroaction of the fluid on the structure are taken into account. However, modeling the mechanics of active thin structures like the bronchial cilia for instance is a difficult task, since the underlying internal dynamics are not well understood. Besides, since the solution of the Stokes problem with a line Dirac distribution is singular, our model does not allow to compute the velocity of the structure in a straightforward way in order to retrieve its movement. That is why in this work, we do not address the problem of the construction of the mechanical model, and we consider that the movement of each cilium is given. The resulting model is therefore "one-way", in the sense that it only aims at reproducing the effects of the active structures on the fluid and neglects the retroaction of the fluid on the structures.

On the other hand, experiments show that the PCL-mucus interface does not evolve in time, presumably due to surface tension. We will take into account surface tension and enforce the interface to be constant in time. In addition we will assume both the PCL-mucus and the mucus-air interfaces to be at all times parallel to the bronchial walls.

Parametrization of a cilium and of a forest of cilia

We use the parametrization established by Fulford and Blake in [26], based on the Fourier series decomposition of the beat of one cilium of cultured rabbit tracheal epithelium described in [64]. The authors also proposed an extension of the parametrization to the movement of a whole forest of cilia, via two parameters that represent respectively the distance between two cilia and the wavelength of the metachronal wave. It is based on the assumption that the metachronal wave propagates in the direction of the cilia beat, although experiments show that some activity is also propagated in the transversal direction. However this approximation is classical and experiments [27] show that increasing viscosity causes the metachronal wave to become more and more orthoplectic (*i.e.* in the direction of mucociliary transport). In the simulations presented in this paper, this assumption has also been made, but the model allows to prescribe a metachronal wave with arbitrary direction.

Let us start with the parametrization of the movement of a single cilium. A cilium is assumed to evolve in a $(x - z)$ plane: at each time t the cilium is represented by the truncated Fourier series of

the parametric curve

$$\boldsymbol{\xi}^{2D}(s,t) = \begin{pmatrix} \xi_x^{2D}(s,t) \\ \xi_z^{2D}(s,t) \end{pmatrix} = L\left[\frac{1}{2}\mathbf{a}_0(s) + \sum_{n=1}^{6} \mathbf{a}_n(s)\cos(2n\pi ft) + \mathbf{b}_n(s)\sin(2n\pi ft)\right],$$

where $s \in [0,1]$ measures arclength from the base of the cilium, L and f are respectively the length and the beat frequency of the cilium. The Fourier coefficients $\mathbf{a}_n$, $\mathbf{b}_n$ are vector quantities, which are approximated by the following 3-degree polynomial functions

$$\mathbf{a}_n(s) = \sum_{k=1}^{3} \mathbf{a}_{n,k} s^k \text{ and } \mathbf{b}_n(s) = \sum_{k=1}^{3} \mathbf{b}_{n,k} s^k$$

where $\mathbf{a}_{n,k}$ and $\mathbf{b}_{n,k}$ are constant vectors of $\mathbb{R}^2$, given in Table 1.1.

$\mathbf{a}_{n,k}$

	$n=0$	$n=1$	$n=2$	$n=3$	$n=4$	$n=5$	$n=6$
$k=1$	-0.449	0.130	-0.169	0.063	-0.050	-0.040	-0.068
	2.076	-0.003	0.054	0.007	0.026	0.022	0.010
$k=2$	-0.072	-1.502	0.260	-0.123	0.011	-0.009	0.196
	-1.074	-0.230	-0.305	-0.180	-0.069	0.001	-0.080
$k=3$	0.658	0.793	-0.251	0.049	0.009	0.023	-0.111
	0.381	0.331	0.193	0.082	0.029	0.002	0.048

$\mathbf{b}_{n,k}$

	$n=1$	$n=2$	$n=3$	$n=4$	$n=5$	$n=6$
$k=1$	-0.030	-0.093	0.037	0.062	0.016	-0.065
	0.080	-0.044	-0.017	0.052	0.007	0.051
$k=2$	1.285	-0.036	-0.244	-0.093	-0.137	0.095
	-0.298	0.513	0.004	-0.222	0.035	-0.128
$k=3$	-1.034	0.050	0.143	0.043	0.098	-0.054
	0.210	-0.367	0.009	0.120	-0.024	0.102

Table 1.1 – Fourier-least squares coefficients for the cilia beat pattern. The upper and lower numbers in each entry correspond to the x and z components respectively, the y component is always zero.

Figure 1.1 shows the beat of a cilium obtained using this parametrization and allows to observe a good correspondance with the description made by Sanderson and Sleigh in [64]. Let us note that the cilium crosses the interface between the mucus and the peryciliary layer (PCL) only during the effective stroke and not during the recovery stroke. This feature is known to be important in order to guarantee an efficient mucus transport.

The extension to a 3D setting is natural: assume that the cilium evolves in the $(x-z)$ plane at $y = y^{(0)}$, we define

$$\boldsymbol{\xi}(s,t) = \begin{pmatrix} \xi_x^{2D}(s,t) \\ y^{(0)} \\ \xi_z^{2D}(s,t) \end{pmatrix}.$$

The parametrisation of a whole forest of cilia given in [26] depends on two important parameters : the space ℓ_0 between two cilia (in each direction) and the wavelength λ of the metachronal wave.

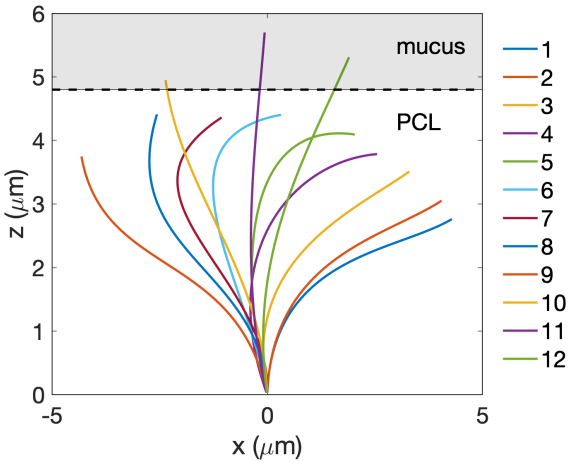

Figure 1.1 – Traces of a cilium during one period of its beat with a PCL-mucus interface at $z = 4.8\,\mu\mathrm{m}$. Description made by Sanderson and Sleigh [64, 26].

More precisely, in order to model a forest of $n_x \times n_y$ cilia, with n_x (respectively n_y) the number of cilia in the direction x (respectively the direction y), the cilium (i, j), where $i \in [\![1, n_x]\!]$ and $j \in [\![1, n_y]\!]$, is parametrized by the curve

$$\boldsymbol{\xi}^{(ij)}(s,t) = i\ell_x^0 \mathbf{e}_x + j\ell_y^0 \mathbf{e}_y + \boldsymbol{\xi}\left(s, \frac{i\ell_x^0}{f\lambda} + t\right),$$

where $s \in [0, 1]$. Let us note the phase shift $\varphi_i = i\ell_x^0/f\lambda$ in x (and only in x, as there is no phase shift not in y) which the metachronal wave comes from. We have drawn in Figure 1.2 a section of the forest in the direction x. The propagation of the metachronal wave (to the left on the picture) is in the opposite direction of mucus transport (to the right). Figure 1.3 shows a forest in 3D as we model it in the simulations, with values of the cilia spacings ℓ_x^0 and ℓ_y^0 that have been voluntarily increased for the sake of clarity.

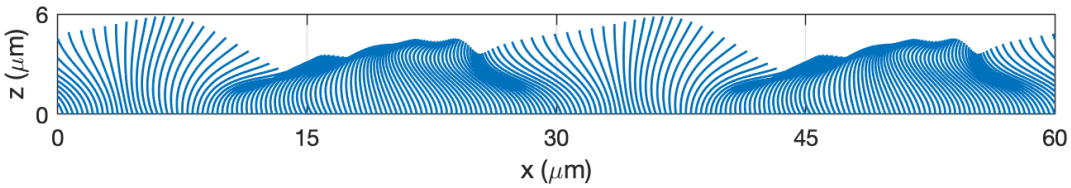

Figure 1.2 – Parametrization of a dense forest of cilia: section of a forest with the parametrization established by Fulford and Blake [26] over two metachronal waves length.

Distribution of the forces exerted by the cilia on the fluid: the slender body theory

Since we work with a given movement of the cilia, defined by the parametrization introduced previously, we need to deduce the distribution of forces induced by this movement on the fluid. For that purpose, we use the so-called slender-body theory, based on asymptotic expansions when the ratio ϵ between the thickness and the length of the body vanishes. Cox [20] established an asymptotic

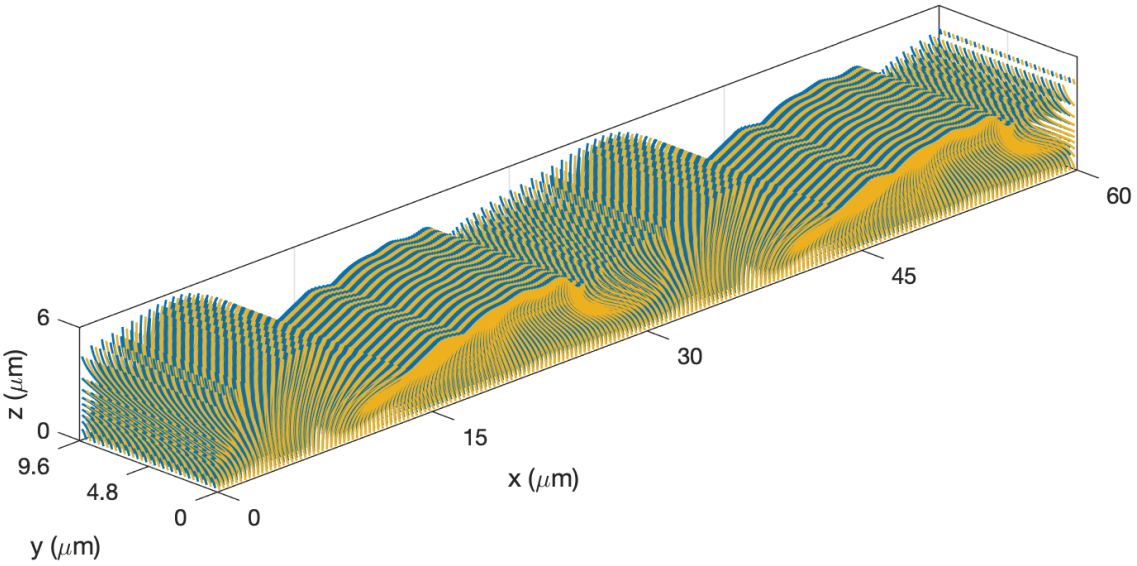

Figure 1.3 – Dense forest of cilia with the parametrization established by Fulford and Blake [26] over two metachronal waves length. Ciliary spacing is $0.3\,\mu\mathrm{m}$ in both axial and azimuthal directions (hence 200×32 cilia are represented here).

expansion of the force at each point of the slender-body. If

$$s \mapsto \boldsymbol{\xi}(s,t)$$

is a parametrization of the position of the body at time t in curvilinear coordinates, the expression of the force at the point of curvilinear abscissa s is

$$\hat{\mathbf{f}}(s,t) := \frac{2\pi\mu}{\ln(L/r)} \left(2\mathbb{I}_3 - \frac{\partial_s\boldsymbol{\xi}(s,t) \otimes \partial_s\boldsymbol{\xi}(s,t)}{\|\partial_s\boldsymbol{\xi}(s,t)\|^2} \right) \left(\hat{\mathbf{u}}_{\text{cil.}}(s,t) - \mathbf{u}_{\text{bg}} \right) + O\left(\frac{1}{(\ln(L/r))^2} \right),$$

where $\hat{\mathbf{u}}_{\text{cil.}}(s,t) := \partial_t\boldsymbol{\xi}(s,t)$ denotes the local velocity of the slender body at curvilinear abscissa s and time t, and $\mathbf{u}_{\text{bg}}$ denotes the background flow (*i.e.* the velocity of the fluid in the absence of the structure). This relation has been established in [20] by confronting two different approaches:

1. the inner expansion consists in studying the fluid velocity near the slender body, which is thus seen as an infinite cylinder. The corresponding regime is L tends to infinity while a remains constant.
2. the outer expansion considers the flow far from the slender body seen as a zero-thickness body, which corresponds to the regime a goes to zero while L remains constant.

We apply the slender body theory as presented previously to compute the distribution of forces applied by each cilium on the fluid, and for the sake of more simple notations, we define

$$\hat{\mathbb{M}}(s,t) := \frac{2\pi\mu}{\ln(L/r)} \left(2\mathbb{I}_3 - \frac{\partial_s\boldsymbol{\xi}(s,t) \otimes \partial_s\boldsymbol{\xi}(s,t)}{\|\partial_s\boldsymbol{\xi}(s,t)\|^2} \right),$$

so that the slender body theory at main order relates the hydrodynamical force exerted by a single cilium to the ciliary dynamics by

$$\hat{\mathbf{f}}(s,t) = \hat{\mathbb{M}}(s,t) \cdot \left(\hat{\mathbf{u}}_{\text{cil.}}(s,t) - \hat{\mathbf{u}}_{\text{bg}}(s,t) \right), \tag{1.1}$$

Remark 1. *In the presence of several cilia, the background flow $\mathbf{u}_{bg}$ takes into account the disturbance flow caused by adjacent cilia. The term involving the background flow then models how the collective dynamics due to all cilia damps/increases the action of each cilium over the fluid.*

Remark 2. *In order to fix ideas, it may be convenient to change the curvilinear coordinates into the 3D coordinates describing the cilia. Therefore we may use the following change of variables:*

$$\mathbf{f}(\boldsymbol{\xi}(s,t);t) = \hat{\mathbf{f}}(s,t).$$

Remark 3. *It is worthwhile noticing that assumptions on the cilia patterns (which evolve in the $(x-z)$ plane) lead to some simplifications: in particular $\partial_s \xi_y = 0$ so that*

$$\partial_s \boldsymbol{\xi} \otimes \partial_s \boldsymbol{\xi} = \begin{pmatrix} |\partial_s \xi_x|^2 & 0 & \partial_s \xi_x \partial_s \xi_z \\ 0 & 0 & 0 \\ \partial_s \xi_x \partial_s \xi_z & 0 & |\partial_s \xi_z|^2 \end{pmatrix}.$$

As a consequence, if we assume that $\hat{u}_{\mathrm{bg},y} = 0$ (which is a reasonable assumption, that will be discussed in Assumption 1) and since $\hat{u}_{\mathrm{cil.},y} = \partial_t \xi_y = 0$, the second component of the force field is null, namely

$$\hat{f}_y(s,t) = 0.$$

Fundamental equations in 3D

We consider $(\mathbf{e}_x, \mathbf{e}_y, \mathbf{e}_z)$ an orthonormal basis in $\mathbb{R}^3$ and a domain $\Omega \subset \mathbb{R}^3$ defined as

$$\Omega = \{\mathbf{x} = (x,y,z) \in \mathbb{R}^3, x/L_x \in \mathbb{T},\ y/L_y \in \mathbb{T}, z \in (0, L_z)\}.$$

In order to capture the main phenomenological aspects, we set $L_x = \lambda$ corresponding to the length of the metachronal wave: this ensures the periodicity of the ciliary beat patterns in Ω. Moreover as the cilia evolve in the $(x-z)$ plane, most phenomena in the y direction can be neglected. Thus the domain is L_x-periodic in x, L_y-periodic in y and we denote the boundaries: $\Gamma_\downarrow = \{z = 0\}$ is the lower boundary to which the cilia are fixed. $\Gamma_\uparrow = \{z = L_z\}$ is the upper boundary that corresponds to the top of the mucus layer. The fluid domain divides into two areas: the PCL, occupied by a fluid of viscosity μ_1, is the subdomain $\{z < H\}$; the mucus, occupied by a fluid of viscosity $\mu_2 > \mu_1$ is the subdomain $\{z > H\}$. In this context, we define

$$\mu(z) = \begin{cases} \mu_1 & \text{if } z < H, \\ \mu_2 & \text{if } z > H. \end{cases}$$

The interface between the PCL and the mucus is located at $\Gamma_* = \{z = H\}$. We consider a list of thin structures (i,j), where $i \in [\![1, n_x]\!]$ and $j \in [\![1, n_y]\!]$, immersed in Ω and fixed to the bottom of the domain $\Gamma_\downarrow$. We denote by $s \mapsto \boldsymbol{\xi}^{(ij)}(s,t)$ the parametrization of their motion at time t. Note that in the context of a viscous flow governed by Stokes equations, the system is instantaneous and time only plays the role of a parameter (therefore it will be regularly omitted when no ambiguity emerges from the equations). The resulting mathematical problem consists in finding a velocity field $\mathbf{x} \mapsto \mathbf{u}(\mathbf{x})$, a pressure field $\mathbf{x} \mapsto p(\mathbf{x})$, and a surface tension $(x,y) \mapsto \gamma(x,y)$ such that $(\mathbf{u}, p, \gamma)$ are periodic in x and

y and

$$\left\{\begin{array}{rcll} -\mathrm{div}(\mu\nabla\mathbf{u}) + \nabla p + \gamma\mathbf{e}_z\delta_{\Gamma_*} &=& \displaystyle\sum_{i,j}\mathbf{f}_{ij}[\mathbf{u}]\,\delta_{\Gamma_{ij}} & \text{in } \Omega,\\ \mathrm{div}(\mathbf{u}) &=& 0 & \text{in } \Omega,\\ [(\mu\nabla\mathbf{u} - p\mathbb{I})\cdot\mathbf{n}]\cdot\mathbf{t} &=& 0 & \text{on } \Gamma_\uparrow,\\ \mathbf{u}\cdot\mathbf{n} &=& 0 & \text{on } \Gamma_\uparrow\cup\Gamma_*,\\ \mathbf{u} &=& 0 & \text{on } \Gamma_\downarrow. \end{array}\right. \tag{1.2}$$

Here Γ_{ij} denotes the 1D curve describing the centerline of the (i,j)-th structure, and $\mathbf{f}_{ij}[\mathbf{u}](\cdot,t)$ is the force distribution it exerts by the structure at time t on the fluid (it has been partially described previously, through the slender body theory and we recall that it may depend on the solution $\mathbf{u}$ because of the influence of the background flow - as this will be detailed further). Let us argue on the condition $u_z = 0$ on the PCL-mucus interface Γ_*: it is noticed in experiments that the interface does not evolve in time, presumably due to surface tension. From the mathematical point of view, this constraint is imposed by duality: for that purpose we introduce the surface tension γ (to be determined) located at the interface, which serves as a Lagrange multiplier for the constraint $u_z = 0$ on Γ_*.

At the bottom we impose a no-slip boundary condition ($\mathbf{u} = 0$) on $\Gamma_\downarrow$, while at the top of the box we prescribe so-called free-slip conditions on $\Gamma_\uparrow$: $\mathbf{u}\cdot\mathbf{n} = 0$ is the kinematic condition, whereas $[(\mu\nabla\mathbf{u} - p\mathbb{I})\cdot\mathbf{n}]\cdot\mathbf{t} = 0$ is the dynamic condition. Here $\mathbf{n}$ is the normal outward unit vector, $\mathbf{t}$ the tangential unit vector associated to the interface. Prescribing this kinematic condition means that we assume that the particles of fluid do not cross the mucus/air interface, so that this interface remains flat and constant during the whole simulation, which is a reasonable assumption with regard to the experimental results available. The dynamic condition implies that we neglect friction of the air layer. More complex boundary conditions could be considered in order to take into account the effect of the airflow on the mucus layer, as for instance a prescribed shear stress (see for instance [48] and [54]). Finally, the box we consider is seen as a window focused on a part of a bronchus, and mucociliary transport goes on outside this box. Therefore it is natural to impose biperiodic boundary conditions in both directions (this requires that the computation domain extends so that a full metachronal wavelength is taken into account).

Source terms

Let us come back to the term $\mathbf{f}_{ij}[\mathbf{u}]$ that describes the force distribution the cilium exerts on the fluid. As previously mentioned, the definition relies on Eq. (1.1) but the background flow velocity needs to be specified. Because of the configuration of the cilia forest, we assume the following:

Assumption 1. *We denote the fluid flow by $\mathbf{u} = (u_x, u_y, u_z)$ and we approximate the background flow velocity defined over Ω by*

$$\mathbf{u}_{\mathrm{bg}}(x,y,z) = \begin{pmatrix} \overline{u_x}^{x,y}(z) \\ 0 \\ 0 \end{pmatrix},$$

where $\overline{\cdot}^{x,y}$ denotes the classical averaging process with respect to to x and y. As a consequence the background flow in the slender body theory follows:

$$\hat{\mathbf{u}}_{\mathrm{bg}}(s,t) = \mathbf{u}_{\mathrm{bg}}(\boldsymbol{\xi}(s,t)) = \begin{pmatrix} \overline{u_x}^{x,y}(\xi_z(s,t)) \\ 0 \\ 0 \end{pmatrix}.$$

Remark 4. *From Assumption 1, denoting*

$$\hat{\mathbb{M}}^{(ij)} = \begin{pmatrix} \hat{m}_{xx}^{(ij)} & \hat{m}_{xy}^{(ij)} & \hat{m}_{xz}^{(ij)} \\ \hat{m}_{yx}^{(ij)} & \hat{m}_{yy}^{(ij)} & \hat{m}_{yz}^{(ij)} \\ \hat{m}_{zx}^{(ij)} & \hat{m}_{zy}^{(ij)} & \hat{m}_{zz}^{(ij)} \end{pmatrix}, \quad \hat{\mathbf{u}}_{\mathit{cil.}}^{(ij)} = (\hat{u}_{\mathit{cil.},x}^{(ij)}, \hat{u}_{\mathit{cil.},y}^{(ij)}, \hat{u}_{\mathit{cil.},z}^{(ij)}), \quad \hat{\mathbf{u}}_{\mathit{bg}}^{(ij)} = (\hat{u}_{\mathrm{bg.},x}^{(ij)}, 0, 0),$$

and recalling that $\hat{u}_{\mathit{cil.},y}^{(ij)} = 0$ *and* $\hat{m}_{xy}^{(ij)} = \hat{m}_{yx}^{(ij)} = \hat{m}_{yz}^{(ij)} = \hat{m}_{zy}^{(ij)} = 0$ *(see Remark 3), we can write:*

$$\hat{\mathbf{f}}_{ij}[\mathbf{u}] = \underbrace{\begin{pmatrix} \hat{m}_{xx}^{(ij)} \hat{u}_{\mathit{cil.},x}^{(ij)} + \hat{m}_{xz}^{(ij)} \hat{u}_{\mathit{cil.},z}^{(ij)} \\ 0 \\ \hat{m}_{zx}^{(ij)} \hat{u}_{\mathit{cil.},x}^{(ij)} + \hat{m}_{zz}^{(ij)} \hat{u}_{\mathit{cil.},z}^{(ij)} \end{pmatrix}}_{\hat{\mathbf{f}}_{ij}^0} - \underbrace{\begin{pmatrix} \hat{m}_{xx}^{(ij)} \\ 0 \\ \hat{m}_{zx}^{(ij)} \end{pmatrix}}_{\hat{\mathbf{m}}^{(ij)}} \hat{u}_{\mathit{bg},x}^{(ij)}.$$

This allows us to consider the force as the summation of the contribution due to isolated cilia and a contribution due to the background flow, namely,

$$\hat{\mathbf{f}}_{ij}[\mathbf{u}](s,t) = \hat{\mathbf{f}}_{ij}^0(s,t) - \overline{u_x}^{x,y}(\xi_z^{(ij)}(s,t))\, \hat{\mathbf{m}}^{(ij)}(s,t).$$

As a straightforward consequence, the momentum equation in System (1.2) *writes:*

$$-\mathrm{div}(\mu \nabla \mathbf{u}) + \sum_{i,j} \overline{u}_x^{x,y} \mathbf{m}^{(ij)} \delta_{\Gamma_{ij}} + \nabla p + \gamma \mathbf{e}_z \delta_{\Gamma_*} = \sum_{i,j} \mathbf{f}_{ij}^0 \delta_{\Gamma_{ij}}.$$

It is worthwhile noticing that, due to the background flow:

- *the system is linear but...*
- *the system is* nonlocal*.*

Remark 5. *Note that in the 3D model the punctual value of* u_x *is not defined on* Γ_{ij} *because of the loss of regularity induced by the lineic Dirac mass. However the averaging process over the velocity field does not suffer the same drawback:* $\overline{u_x}^{x,y}$ *is well defined on* $(0, L_z)$ *and, by extension, on* Γ_{ij}*.*

Variational formulation

Because of the singularity induced by the lineic Dirac source term, the functional framework requires some adaptation with respect to the classical one. Let us temporarily omit time t (which plays the role of a parameter) for the sake of simplicity, we aim at writing the variational formulation of the 3D problem (restoring time t in the notations does not raise any difficulty). The source term $\delta_{\Gamma_{ij}}$ satisfies $\delta_{\Gamma_{ij}} \in (W^{1,r^*}(\Omega))'$ with $r^* > 2$. Let

$$\mathcal{V}_{r^*} := \{\mathbf{v} = (v_x, v_y, v_z) \in (W^{1,r^*}(\Omega))^3,\ \mathbf{v}_{|\Gamma_\downarrow} = 0 \text{ in } (L^{r^*}(\Gamma_\downarrow))^3,\ v_{z|\Gamma_\uparrow} = 0 \text{ in } L^{r^*}(\Gamma_\uparrow),\ v_{z|\Gamma_*} = 0 \text{ in } L^{r^*}(\Gamma_*)\}$$

and $(\mathcal{V}_{r^*})'$ its dual space. The variational formulation requires some precision on the source term. Let $\mathbf{v} \in \mathcal{V}_{r^*}$. We have

$$\begin{aligned} \left\langle \mathbf{f}_{ij}[\mathbf{u}]\delta_{\Gamma_{ij}}, \mathbf{v} \right\rangle_{(\mathcal{V}_{r^*})',\mathcal{V}_{r^*}} &= \int_{\Gamma^{(ij)}(t)} \mathbf{f}_{ij}[\mathbf{u}](x,y,z) \cdot \mathbf{v}(x,y,z)\, \mathrm{d}x\, \mathrm{d}y\, \mathrm{d}z \\ &= \int_0^L \mathbf{f}_{ij}[\mathbf{u}](\boldsymbol{\xi}^{(ij)}(s)) \cdot \mathbf{v}(\boldsymbol{\xi}^{(ij)}(s))\, |\nabla \boldsymbol{\xi}^{(ij)}(s)|\, \mathrm{d}s \\ &= \int_0^L \left[\hat{\mathbf{f}}_{ij}^0(s) - \overline{u_x}^{x,y}(\xi_z^{(ij)}(s))\, \hat{\mathbf{m}}^{(ij)}(s)\right] \cdot \mathbf{v}(\boldsymbol{\xi}^{(ij)}(s))\, |\nabla \boldsymbol{\xi}^{(ij)}(s)|\, \mathrm{d}s. \end{aligned}$$

The source term thus contains two contributions:

- a classical contribution due to the action of each isolated cilium :

$$\int_0^L \hat{\mathbf{f}}_{ij}^0(s) \cdot \mathbf{v}(\boldsymbol{\xi}^{(ij)}(s)) \, |\nabla \boldsymbol{\xi}^{(ij)}(s)| \, \mathrm{d}s$$

- a nonlocal contribution due to the background flow :

$$\int_0^L \left[\overline{u_x}^{x,y}(\xi_z^{(ij)}(s)) \, \hat{\mathbf{m}}^{(ij)}(s) \right] \cdot \mathbf{v}(\boldsymbol{\xi}^{(ij)}(s)) \, |\nabla \boldsymbol{\xi}^{(ij)}(s)| \, \mathrm{d}s.$$

Let $r = \frac{r^*}{r^*-1}$, so that $1 \leq r < 2$. The variational formulation writes:

$$\left\{ \begin{array}{l} \text{find } \mathbf{u} \in \mathcal{V}_r, p \in L_0^r(\Omega) \text{ such that} \\ \quad a(\mathbf{u},\mathbf{v}) + nl(\mathbf{u},\mathbf{v}) - b(p,\mathbf{v}) = \ell(\mathbf{v}), \quad \forall \mathbf{v} \in \mathcal{V}_{r^*}, \\ \qquad\qquad\qquad\qquad b(q,\mathbf{u}) = 0, \qquad \forall q \in L_0^{r^*}(\Omega), \end{array} \right. \tag{1.3}$$

with the following bilinear forms

$$\begin{array}{rcl} a(\mathbf{u},\mathbf{v}) & := & \displaystyle\int_\Omega \mu \nabla \mathbf{u} \cdot \nabla \mathbf{v}, \\ nl(\mathbf{u},\mathbf{v}) & := & \displaystyle\sum_{i,j} \int_0^L \overline{u_x}^{x,y}(\xi_z^{(ij)}(s)) \, \hat{\mathbf{m}}^{(ij)}(s) \cdot \mathbf{v}(\boldsymbol{\xi}^{(ij)}(s)) \, |\nabla \boldsymbol{\xi}^{(ij)}(s)| \, \mathrm{d}s, \\ b(p,\mathbf{v}) & := & \displaystyle\int_\Omega p \, \mathrm{div}(\mathbf{v}), \end{array}$$

and the following linear form

$$\ell(\mathbf{v}) := \sum_{i,j} \int_0^L \hat{\mathbf{f}}_{ij}^0(s) \cdot \mathbf{v}(\boldsymbol{\xi}^{(ij)}(s)) \, |\nabla \boldsymbol{\xi}^{(ij)}(s)| \, \mathrm{d}s.$$

The well-posedness of this problem will be proved in the next section.

1.2 Derivation of a one-dimensional average model

We propose a way to deal with the averaged velocity term in the 3D model (1.3) and avoid the difficult numerical treatment of the non-local term. It consists in averaging the 3D equations in the x and y directions, taking advantage of the periodic conditions, in order to obtain a 1D equation on $\overline{u_x}^{x,y}$. The numerical solution of this equation can then be injected into the 3D problem. Besides, the existence and uniqueness of the solution to this 1D equation allows to prove the well-posedness of the 3D problem (1.3).

Averaged equations

The averaging process is detailed in Appendix and leads to the following reduced model:

$$\left\{ \begin{array}{rcl} -\partial_z(\mu \partial_z \overline{u_x}^{x,y}) & = & \displaystyle\sum_{i,j} \overline{f_{ij,x}[\overline{u_x}^{x,y}]\delta_\Gamma}^{x,y} \quad \text{in } \mathcal{D}'(0,L_z), \\ \overline{u_x}^{x,y}(0) & = & 0, \\ \partial_z \overline{u_x}^{x,y}(L_z) & = & 0. \end{array} \right. \tag{1.4}$$

Each source term in the sum over i and j is a distribution in $\mathcal{D}'(0,L_z)$ that needs to be defined properly, since its derivation follows from the averaging process with respect to x and y of the 3D singular source terms, which is not straightforward. Choosing $v := v(z)$, we define

$$\left\langle \overline{f_x\delta}^{x,y}, v \right\rangle_{\mathcal{D}'(0,L_z),\mathcal{D}(0,L_z)} = \frac{1}{L_xL_y}\left\langle f_x\delta, \tilde{v}\right\rangle_{\mathcal{D}'(\Omega),\mathcal{D}(\Omega)}$$

by considering the natural extension from $(0,L_z)$ to Ω (we recall that Ω is periodic in x and y):

$$\begin{array}{rccc} \tilde{\cdot} \ : & \mathcal{D}(0,L_z) & \mapsto & \mathcal{D}(\Omega) \\ & [z\mapsto v(z)] & \to & [(x,y,z)\mapsto \tilde{v}(x,y,z)=v(z)]. \end{array}$$

As a consequence, using the parametrization $s\mapsto \boldsymbol{\xi}(s,t)$ of the cilium, each source term reads :

$$\begin{aligned} \left\langle \overline{f_{ij,x}(\cdot,t)\delta_{\Gamma(t)}}^{x,y}, v \right\rangle_{\mathcal{D}'(0,L_z),\mathcal{D}(0,L_z)} &= \frac{1}{L_xL_y}\int_{\Gamma(t)} f_{ij,x}((x,y,z);t)\, v(z)\,\mathrm{d}x\,\mathrm{d}y\,\mathrm{d}z \\ &= \frac{1}{L_xL_y}\int_0^L f_{ij,x}(\boldsymbol{\xi}^{(ij)}(s,t);t)\, v(\xi_z^{(ij)}(s,t))\,|\nabla\boldsymbol{\xi}^{(ij)}(s,t)|\,\mathrm{d}s. \end{aligned}$$

In the context of mucociliary transport,

$$\hat{\mathbf{f}}_{(ij)}[\mathbf{u}](s,t) = \hat{\mathbb{M}}^{(ij)}(s,t)\cdot\left(\hat{\mathbf{u}}_{\text{cil.}}^{(ij)}(s,t) - \begin{pmatrix} \overline{u_x}^{x,y}(\xi_z^{(ij)}(s,t)) \\ 0 \\ 0 \end{pmatrix}\right).$$

Thus

$$\begin{aligned} \left\langle \overline{f_{ij,x}[\overline{u_x}^{x,y}](\cdot,t)\delta_{\Gamma(t)}}^{x,y}, v \right\rangle_{\mathcal{D}'(0,L_z),\mathcal{D}(0,L_z)} &= \frac{1}{L_xL_y}\int_0^L [\hat{m}_{xx}^{(ij)}\hat{u}_{\text{cil.},x}^{(ij)} + \hat{m}_{xz}^{(ij)}\hat{u}_{\text{cil.},z}^{(ij)}](s,t)\, v(\xi_z^{(ij)}(s,t))\,|\nabla\boldsymbol{\xi}^{(ij)}(s,t)|\,\mathrm{d}s \\ &\quad -\frac{1}{L_xL_y}\int_0^L \hat{m}_{xx}^{(ij)}(s,t)\overline{u_x}^{x,y}(\xi_z^{(ij)}(s,t))\, v(\xi_z^{(ij)}(s,t))\,|\nabla\boldsymbol{\xi}^{(ij)}(s,t)|\,\mathrm{d}s. \end{aligned}$$

Let us now introduce the variational formulation associated to the 1D problem. Defining $V=\{v\in H^1(0,L_z),\ v(0)=0\}$, the variational formulation of the reduced problem (including the summation over all the cilia) reads:

$$\left\{\begin{array}{l} \text{find } \overline{u_x}^{x,y}(\cdot,t)\in V \text{ such that, for all } v\in V, \\ \displaystyle\int_0^{L_z}\mu(z)\,\partial_z\overline{u_x}^{x,y}(z,t)\cdot\partial_z v(z)\,\mathrm{d}z \\ \qquad + \ \displaystyle\frac{1}{L_xL_y}\sum_{i,j}\int_0^L \hat{m}_{xx}^{(ij)}(s,t)\,\overline{u_x}^{x,y}(\xi_z^{(ij)}(s,t);t)\, v(\xi_z^{(ij)}(s,t))\,|\nabla\boldsymbol{\xi}^{(ij)}(s,t)|\,\mathrm{d}s \\ \qquad = \ \displaystyle\frac{1}{L_xL_y}\sum_{i,j}\int_0^L \left(\hat{m}_{xx}^{(ij)}\hat{u}_{\text{cil.},x}^{(ij)} + \hat{m}_{xz}^{(ij)}\hat{u}_{\text{cil.},z}^{(ij)}\right)(s,t)\, v(\xi_z^{(ij)}(s,t))\,|\nabla\boldsymbol{\xi}^{(ij)}(s,t)|\,\mathrm{d}s. \end{array}\right. \tag{1.5}$$

It is worthwhile noticing that the variational formulation of the 1D reduced problem can be derived from the variational formulation of the 3D problem: up to a constant related to the averaging process, it is then sufficient to use a test function $v\in\mathcal{D}(\Omega)$ which does not depend on x and y, then use the periodicity arguments.

We emphasize that the model is rich and simple: the unknown of the reduced model is $z\mapsto \overline{u_x}^{x,y}(z,t)$ i. e. the first component of the mean velocity. This is exactly the observable quantity which allows for the quantification of the mucociliary efficiency. Then the 1D problem divides into three contributions:

- a classical second-order 1D operator, modelling a bifluid description of the medium:

$$\int_0^{L_z} \mu(z)\, \partial_z \overline{u_x}^{x,y}(z,t) \cdot \partial_z v(z)\, \mathrm{d}z$$

- a source term modelling the action of each cilium over the fluid

$$\frac{1}{L_x L_y} \sum_{ij} \int_0^L \left(\hat{m}_{xx}^{(ij)} \hat{u}_{\text{cil.},x}^{(ij)} + \hat{m}_{xz}^{(ij)} \hat{u}_{\text{cil.},z}^{(ij)} \right) (s,t)\, v(\xi_z^{(ij)}(s,t)) \, |\nabla \boldsymbol{\xi}^{(ij)}(s)| \, \mathrm{d}s.$$

- a counter-part contribution due to the collective transport:

$$\frac{1}{L_x L_y} \sum_{i,j} \int_0^L \hat{m}_{xx}^{(ij)}(s,t)\, \overline{u_x}^{x,y}(\xi_z^{(ij)}(s,t))\, v(\xi_z^{(ij)}(s)) \, |\nabla \boldsymbol{\xi}^{(ij)}(s,t)| \, \mathrm{d}s.$$

Remark 6. *We point out the fact that if the averaging process is performed over a domain that fits the metachronal wave in the $x-$direction (recall that cilia only evolve in the $x-z$ plane) then the solution of the reduced problem does not depend on time anymore (by invariance of the setting with respect to time), highlighting the notion of* mucociliary elevator*.*

Let us conclude this section with the mathematical properties of the 1D problem:

Theorem 1. *The 1D problem* (1.5) *admits a unique solution.*

Proof. Well-posedness of the 1D problem is a consequence of Lax-Milgram theorem, noticing (as in the proof of Theorem 2) that

$$\hat{m}_{xx}^{(ij)} = \frac{2\pi\mu}{\ln(L/r)} \left(2 - \frac{|\partial_s \xi_x|^2}{\|\partial_s \boldsymbol{\xi}(s,t)\|^2} \right) \geq \frac{2\pi\mu}{\ln(L/r)} > 0.$$

Thus the bilinear form

$$a_{1\mathrm{D}} : (u,v) \mapsto \int_0^{L_z} \mu(z)\, \partial_z u(z) \cdot \partial_z v(z)\, \mathrm{d}z + \frac{1}{L_x L_y} \sum_{i,j} \int_0^L \hat{m}_{xx}^{(ij)}(s,t)\, u(\xi_z^{(ij)}(s,t))\, v(\xi_z^{(ij)}(s)) \, |\nabla \boldsymbol{\xi}^{(ij)}(s,t)| \, \mathrm{d}s$$

satisfies

$$a_{1\mathrm{D}}(u,u) \geq \min(\mu_1, \mu_2) \|u\|_V^2$$

as V may be equipped with the norm $v \mapsto \|v\|_V := \|\partial_z v\|_{L^2(0,L_z)}$. □

Strong formulation

The easiest way to implement the reduced 1D model relies on the above variational formulation. However it is possible to rewrite the reduced problem in a strong formulation: this requires to interpret the source term. Let us recall that the description of a cilium $\Gamma(t)$ is performed with a parametrization of the form (subscripts (i,j) have been skipped):

$$s \mapsto \boldsymbol{\xi}(s,t) = (\xi_x(s,t), \xi_y(s,t), \xi_z(s,t)).$$

For a function $f(\cdot,t)$, we have used the identity

$$\int_{\Gamma(t)} f((x,y,z);t)\, v(z)\, \mathrm{d}x\, \mathrm{d}y\, \mathrm{d}z = \int_0^L f(\boldsymbol{\xi}(s,t);t) v(\xi_z(s,t))(z) \, |\nabla \boldsymbol{\xi}(s,t)| \, \mathrm{d}s.$$

Now we propose a parametrization that allow us to recover a classical formulation. Instead of using the "natural" parametrization of the cilium, we may use the third component as the leading parameter and describe $\Gamma(t)$ by

$$z \mapsto \mathbf{\Phi}(z,t) = (X(z,t), Y(z,t), z).$$

Now defining $h(t) := \max_s(\xi_z(s,t))$ we have

$$\begin{aligned}\int_{\Gamma(t)} f((x,y,z);t)\, v(z)\,\mathrm{d}x\,\mathrm{d}y\,\mathrm{d}z &= \int_0^{h(t)} f(\mathbf{\Phi}(z,t);t)\, v(z)\,|\nabla\mathbf{\Phi}(z,t)|\,\mathrm{d}z \\ &= \int_0^{L_z} f(\mathbf{\Phi}(z,t);t)\,|\nabla\mathbf{\Phi}(z,t)|\,\mathbb{1}_{(0,h(t))}(z)\, v(z)\,\mathrm{d}z\end{aligned}$$

which allows us to rewrite the 1D variational formulation (1.5):

$$\left\{\begin{array}{l} \text{find } \overline{u_x}^{x,y}(\cdot,t) \in V \text{ such that, for all } v \in V, \\ \displaystyle\int_0^{L_z} \mu(z)\,\partial_z\overline{u_x}^{x,y}(z,t)\cdot\partial_z v(z)\,\mathrm{d}z \\ \qquad \displaystyle+\frac{1}{L_xL_y}\int_0^{L_z}\left(\sum_{i,j} m_{xx}^{(ij)}(\mathbf{\Phi}^{(ij)}(z,t);t)\cdot|\nabla\mathbf{\Phi}^{(ij)}(z,t)|\cdot\mathbb{1}_{(0,h^{(ij)}(t))}(z)\right)\cdot\overline{u_x}^{x,y}(z,t)\cdot v(z)\,\mathrm{d}z \\ \qquad \displaystyle=\frac{1}{L_xL_y}\int_0^{L_z}\left(\sum_{i,j}\left[\hat{m}_{xx}^{(ij)}\hat{u}_{\text{cil.},x}^{(ij)}+\hat{m}_{xz}^{(ij)}\hat{u}_{\text{cil.},z}^{(ij)}\right](\mathbf{\Phi}^{(ij)}(z,t);t)\cdot|\nabla\mathbf{\Phi}^{(ij)}(z,t)|\cdot\mathbb{1}_{(0,h^{(ij)}(t))}(z)\right)\cdot v(z)\,\mathrm{d}z \end{array}\right.$$

with subsequent notations adapted to each cilium, in particular $h^{(i,j)}(t) = \max_s(\xi_z^{(i,j)}(s,t))$. Thus the strong formulation of this problem reads:

$$\left\{\begin{array}{rcl} -\partial_z(\mu(z)\partial_z\overline{u_x}^{x,y}(z,\cdot)) + c_1(z,\cdot)\cdot\overline{u_x}^{x,y}(z,\cdot) &=& c_2(z,\cdot), \quad \forall z\in(0,L_z), \\ \overline{u_x}^{x,y}(0,\cdot) &=& 0, \\ \partial_z\overline{u_x}^{x,y}(L_z,\cdot) &=& 0. \end{array}\right. \tag{1.6}$$

with

$$\begin{aligned} c_1(z,t) &= \frac{1}{L_xL_y}\sum_{i,j} m_{xx}^{(ij)}(\mathbf{\Phi}^{(ij)}(z,t);t)\cdot|\nabla\mathbf{\Phi}^{(ij)}(z,t)|\cdot\mathbb{1}_{(0,h^{(ij)}(t))}(z), \\ c_2(z,t) &= \frac{1}{L_xL_y}\sum_{i,j}\left[\hat{m}_{xx}^{(ij)}\hat{u}_{\text{cil.},x}^{(ij)}+\hat{m}_{xz}^{(ij)}\hat{u}_{\text{cil.},z}^{(ij)}\right](\mathbf{\Phi}^{(ij)}(z,t);t)\cdot|\nabla\mathbf{\Phi}^{(ij)}(z,t)|\cdot\mathbb{1}_{(0,h^{(ij)}(t))}(z). \end{aligned}$$

The use of the strong formulation (1.6) is quite limited in terms of numerical computations as the evaluation of c_1 and c_2 may be intricate. However numerical computations may be easily led with the variational formulation (1.5) whereas the strong formulation (1.6) is helpful for understanding the mathematical structure of the reduced problem. In particular:

- coefficients c_1 and c_2 concentrate all the effects of the active cilia, by a summation process;
- the average velocity $\overline{u_x}^{x,y}$ is continuous with respect to z;
- it is worthwhile noticing that

  $$c_1(z,\cdot) = c_2(z,\cdot) = 0 \quad \text{if } z > h := \max_{i,j} h^{(ij)}.$$

  Here h denotes the altitude above which no cilium emerges: in this *passive* area, the average velocity $\overline{u_x}^{x,y}$ is constant (because of the homogeneous Neumann boundary condition).

Well-posedness of the 3D problem

We can now prove the well-posedness of the 3D problem (1.3).

Theorem 2. *The 3D problem* (1.3) *admits a unique solution.*

Proof. Let $\overline{u_x}^{x,y}$ be the unique solution of the 1D problem, and define $\mathcal{W}_{r^*} := \{\mathbf{v} = (v_x, v_y, v_z) \in \mathcal{V}_{r^*},\ \mathrm{div}(\mathbf{v}) = 0\}$. It is straightforward that problem (1.3) is equivalent to

$$\begin{cases} \text{find } \mathbf{u} \in \mathcal{W}_r \text{ such that} \\ a(\mathbf{u}, \mathbf{v}) \quad = \quad \tilde{\ell}[\overline{u_x}^{x,y}](\mathbf{v}), \quad \forall \mathbf{v} \in \mathcal{W}_{r^*}, \end{cases} \tag{1.7}$$

where

$$\tilde{\ell}[\overline{u_x}^{x,y}](\mathbf{v}) \quad := \qquad \ell(\mathbf{v}) - \sum_{i,j} \int_0^L \overline{u_x}^{x,y}(\xi_z^{(ij)}(s))\, \hat{\mathbf{m}}^{(ij)}(s) \cdot \mathbf{v}(\boldsymbol{\xi}^{(ij)}(s))\, |\nabla \boldsymbol{\xi}^{(ij)}(s)|\, \mathrm{d}s,$$

Well-posedness of (1.7) follows from a representation theorem in reflexive Banach spaces (see Theorem 1 in [33]), which we apply to the Sobolev spaces $\mathcal{W}_r$ and $\mathcal{W}_{r^*}$. The bilinear form $a(,.)$ is continuous on $\mathcal{W}_r \times \mathcal{W}_{r^*}$, and non-degenerate with respect to the second variable (this follows from the coercivity of $a(\cdot,\cdot)$ on $H_0^1 \times H_0^1$). Then, a necessary and sufficient condition for (1.7) to admit a unique solution is that there exists a positive number $\alpha > 0$ such that for each $\mathbf{u} \in \mathcal{W}_r$:

$$\sup_{\|\mathbf{v}\|_{\mathcal{W}_{r^*}}=1} a(\mathbf{u}, \mathbf{v}) \geq \alpha \|\mathbf{u}\|_{\mathcal{W}_r}.$$

This property is proven in [68] for a general class of elliptic bilinear operators which are strongly uniformly elliptic and include the case of the bilinear form $a(\cdot,\cdot)$. □

1.3 Application to mucociliary transport in the lung

The 3D and 1D models presented in the previous sections to simulate many thin structures in a viscous fluid may be investigated through the simulation of mucociliary transport.

1.3.1 Numerical methods

Unless otherwise stated, the parameters are the ones used in all the simulations. Data related to the fluid domain $\Omega = (0, L_x) \times (0, L_y) \times (0, L_z)$ are the following ones:

$$L_x = 30\,\mu\mathrm{m}, \quad L_y = 4.8\,\mu\mathrm{m}, \quad L_z = 10\,\mu\mathrm{m}.$$

The airway surface liquid is composed of two overlayed layers: the periciliary layer (located in the region $\{(x,y,z) \in \Omega,\ 0 < z < H\}$) and the mucus (located in the region $\{(x,y,z) \in \Omega,\ H < z < L_z\}$). Viscosity of the periciliary layer is $\mu_1 = 1 \cdot 10^{+0}\,\mathrm{mPa{\cdot}s}$ and viscosity of the mucus is $\mu_2 = 1 \cdot 10^{+4}\,\mathrm{mPa{\cdot}s}$. Moreover the interface between the two layers is defined as $\{(x,y,z) \in \Omega,\ z = H\}$ with $H = 4.8\,\mu\mathrm{m}$.

Table 2.2 summarizes the data related to the cilia, as given in [26]. Those default parameter values lead us to consider a forest of 100×16 cilia in the computational domain Ω. The simulations should present the time evolution of the flow field. In our model the movement of the cilia is prescribed, and it is periodic (the period T is $1/f$). We recall that we need to retrieve the distribution of forces exerted by the cilia on the fluid from their prescribed movement, and for that purpose we use relation

Fluid			
Domain dimensions:			
– in axial direction	L_x	30.0	μm
– in azimuthal direction	L_y	4.8	μm
– in radial direction	L_z	10.0	μm
Fluid viscosity in PCL	μ_1	$1 \cdot 10^{+0}$	mPa $\cdot$ s
Fluid viscosity in mucus	μ_2	$1 \cdot 10^{+4}$	mPa $\cdot$ s
Airway surface liquid (ASL)	H	4.8	μm
Cilia			
Length of a cilium	L	6.0	μm
Cross-sectional radius of a cilium	a	0.1	μm
Beat frequency of a cilium	f	15.0	Hz
In axial direction:			
– Number of cilia in the computational domain	n_x	100	
– Cilia spacing	ℓ_x^0	0.3	μm
– Number of cilia per unit length	d_x	3.33	μm^{-1}
In azimuthal direction:			
– Number of cilia in the computational domain	n_y	16	
– Cilia spacing	ℓ_y^0	0.3	μm
– Number of cilia per unit length	d_y	3.33	μm^{-1}
Density of cilia	$D_{\text{cil.}}$	11.11	μm^{-2}
Metachronal wavelength	λ	30.0	μm

Table 1.2 – Summary of data for fluid cilia in the lung, from [26].

(1.1). Now in the case of a two-viscosity fluid this relation, based on the slender-body theory described by Cox [20], is no longer valid. However Fulford and Blake [25] established the expression of the distribution of forces along a slender body which straddles an interface. At the first order (in the regime $\ln(L/r)^{-1}$ tends to zero) and far from the interface, the expression of the force is the same as for constant viscosity. Close to the interface, more precisely at a distance smaller than the radius a of the body, relation (1.1) is no more valid and should be corrected. In our case, we neglect this correction and we consider expression (1.1) for the forces along the whole cilium with a variable viscosity.

Solving the 1D reduced model

The 1D reduced model is solved using the variational formulation (1.5). More precisely we solve a finite-element approximation of (1.5). Define a regular triangulation of $[0, L_z]$, denoted $\mathcal{T}_{h_z}$, that involves N_z nodes (set $h_z = \frac{L_z}{N_z}$) and

$$V_{h_z} := \{v \in \mathcal{C}^0([0, L_z]), v_{|T} \in P_1[T], \forall T \in \mathcal{T}_{h_z} \text{ and } v(0) = 0\}.$$

In the numerical approximation of problem (1.5), we substitute functional space V by the subspace V_{h_z}.

Solving the 3D model

The 3D model is solved using the variational formulation (1.7) once the averaged solution $(\overline{u_x}^{x,y})_h$ has been determined and the resolution is based on a finite-element approximation of the problem.

Define a regular triangulation of Ω, denoted $\mathcal{T}_h$, that involves $N_x \times N_y \times N_z$ nodes and the following approximation spaces:

- for the velocity field:

$$\mathcal{V}_h \;:=\; \{\mathbf{v} \in (\mathcal{C}^0(\overline{\Omega}))^3,\ \mathbf{v}_{|T} \in (P_1[T] \oplus \text{span}(b_T))^3,\ \forall T \in \mathcal{T}_h \text{ and } \mathbf{v}_{|\Gamma_\downarrow} = 0,\ v_{z|\Gamma_\uparrow} = 0 \text{ and } v_{z|\Gamma_*} = 0\},$$

  where the so-called bubble-function b_T is defined by

$$b_T(\mathbf{x}) = \begin{cases} \lambda_1^T(\mathbf{x}) \cdot \lambda_2^T(\mathbf{x}) \cdot \lambda_3^T(\mathbf{x}), & \text{if } \mathbf{x} \in T, \\ 0, & \text{otherwise,} \end{cases}$$

  and λ_1^T, λ_2^T, λ_3^T are the barycentric coordinates of $\mathbf{x}$ in relation to the mesh element T.

- for the pressure field:

$$\mathcal{W}_h \;:=\; \{q \in \mathcal{C}^0(\overline{\Omega}),\ q_{|T} \in P_1[T],\ \forall T \in \mathcal{T}_h\}.$$

In the discrete setting, we now consider the variational problem:

$$\begin{cases} \text{find } \mathbf{u}_h \in \mathcal{V}_h,\ p_h \in \mathcal{W}_h \text{ such that} \\ \quad a(\mathbf{u}_h, \mathbf{v}_h) - b(p_h, \mathbf{v}_h) + \varepsilon d(p_h, q_h) &=& \tilde{\ell}[(\overline{u_x}^{x,y})_h](\mathbf{v}_h), & \forall \mathbf{v}_h \in \mathcal{V}_h, \\ \quad b(q_h, \mathbf{u}_h) &=& 0, & \forall q_h \in \mathcal{W}_h. \end{cases} \tag{1.8}$$

Notice that a small perturbative term $d(p_h, q_h) := \int_\Omega p_h q_h$ with factor $\varepsilon \ll 1$ has been introduced in order to fix the constant associated to the pressure field which is determined up to a constant in the initial problem.

Remark 7. *The main difficulty of the 3D problem relies on its nonlocal property, due to the background flow. It means that the direct resolution of the problem is associated to a linear system involving matrix which is not sparse. In our case, we took advantage of the 1D reduced model to overcome this difficulty, reducing the complexity to the one of a classical Stokes problem (up to the resolution of a 1D problem that provides the mean velocity that is used as a source term in the subsequent 3D problem). An alternative way to solve the 3D problem consists in using the linearity of the problem to avoid the resolution of the linear system with a full matrix: for this, let us recall that the finite element approximation of the background flow velocity $\overline{u_x}^{x,y}$ is decomposed on a P_1 finite element basis $\{\phi_k\}_{k=1,\dots,N_z}$ with $\phi_k(z_i) = \delta_{ik}$, $\{z_k\}_{k=1,\dots,N_z}$ being the nodes of the 1D mesh. Then define the following problem*

$$\begin{cases} \textit{find } \mathbf{u}_h^{[0]} \in \mathcal{V}_h,\ p_h^{[0]} \in \mathcal{W}_h,\ \gamma_h^{[0]} \in \mathcal{M}_h \textit{ such that} \\ \quad a\left(\mathbf{u}_h^{[0]}, \mathbf{v}_h\right) - b\left(p_h^{[0]}, \mathbf{v}_h\right) + c\left(\gamma_h^{[0]}, \mathbf{v}_h\right) + \varepsilon d\left(p_h^{[0]}, q_h\right) &=& \ell\left(\mathbf{v}_h\right), & \forall \mathbf{v}_h \in \mathcal{V}_h, \\ \quad b\left(q_h, \mathbf{u}_h^{[0]}\right) &=& 0, & \forall q_h \in \mathcal{W}_h, \\ \quad c\left(\beta_h, \mathbf{u}_h^{[0]}\right) &=& 0, & \forall \beta_h \in \mathcal{M}_h, \end{cases} \tag{1.9}$$

and also the following N_z auxiliary problems:

$$\begin{cases} \textit{find } \mathbf{u}_h^{[k]} \in \mathcal{V}_h,\ p_h^{[k]} \in \mathcal{W}_h,\ \gamma_h^{[k]} \in \mathcal{M}_h \textit{ such that} \\ \quad a\left(\mathbf{u}_h^{[k]}, \mathbf{v}_h\right) - b\left(p_h^{[k]}, \mathbf{v}_h\right) + c\left(\gamma_h^{[k]}, \mathbf{v}_h\right) + \varepsilon d\left(p_h^{[k]}, q_h\right) &=& \ell^{[k]}\left(\mathbf{v}_h\right), & \forall \mathbf{v}_h \in \mathcal{V}_h, \\ \quad b\left(q_h, \mathbf{u}_h^{[k]}\right) &=& 0, & \forall q_h \in \mathcal{W}_h, \\ \quad c\left(\beta_h, \mathbf{u}_h^{[k]}\right) &=& 0, & \forall \beta_h \in \mathcal{M}_h, \end{cases} \tag{1.10}$$

with

$$\ell^{[k]}(\mathbf{v}_h) = -\sum_{i,j} \int_0^L \phi_k(\xi_z^{(ij)}(s))\, \hat{\mathbf{m}}^{(ij)}(s) \cdot \mathbf{v}(\boldsymbol{\xi}^{(ij)}(s))\, |\nabla \boldsymbol{\xi}^{(ij)}(s)|\, \mathrm{d}s.$$

By linearity, the solution $(\mathbf{u}_h, p_h, \gamma_h)$ *is a linear combination of the auxiliary solutions* $\{(\mathbf{u}_h^{[k]}, p_h^{[k]}, \gamma_h^{[k]})\}_{k=0,\dots,N_z}$*, namely*

$$\begin{aligned} \mathbf{u}_h &= \mathbf{u}_h^{[0]} + \sum_{k=1}^{N_z} \lambda_k \mathbf{u}_h^{[k]}, \\ p_h &= p_h^{[0]} + \sum_{k=1}^{N_z} \lambda_k p_h^{[k]}, \\ \gamma_h &= \gamma_h^{[0]} + \sum_{k=1}^{N_z} \lambda_k \gamma_h^{[k]}. \end{aligned} \tag{1.11}$$

It remains to determine $\{\lambda_k\}_k$*. Using Eq.* (1.11) *in problem* (1.8) *shows that the linear combination solves the initial problem if*

$$\ell + \sum_{k=1}^{N_z} \lambda_k \ell^{[k]} = \widetilde{\ell[\overline{(\mathbf{u}_h)_x}^{x,y}]}$$

that is to say

$$\begin{aligned} \sum_{k=1}^{N_z} \lambda_k \phi_k &= \overline{(\mathbf{u}_h)_x}^{x,y} \\ &= \overline{(\mathbf{u}_h^{[0]})_x}^{x,y} + \sum_{k=1}^{N_z} \lambda_k \overline{(\mathbf{u}_h^{[k]})_x}^{x,y}. \end{aligned}$$

In order to determine $\{\lambda_k\}_k$*, we proceed to the evaluation of the above expression in each 1D node* z_i*. Denoting* $U_i^{[0]} := \overline{(\mathbf{u}_h^{[0]})_x}^{x,y}(z_i)$ *and* $U_i^{[k]} := \overline{(\mathbf{u}_h^{[k]})_x}^{x,y}(z_i)$ *we get*

$$\lambda_i = U_i^{[0]} + \sum_{k=1}^{N_z} \lambda_k U_i^{[k]}, \qquad i = 1, \dots, N_z.$$

The resolution of the linear system

$$\left[\mathrm{I}_{N_z \times N_z} - \begin{pmatrix} U_1^{[1]} & U_1^{[2]} & \cdots & U_1^{[N_z]} \\ U_2^{[1]} & U_2^{[2]} & \cdots & U_2^{[N_z]} \\ \vdots & \vdots & \ddots & \vdots \\ U_{N_z}^{[1]} & U_{N_z}^{[2]} & \cdots & U_{N_z}^{[N_z]} \end{pmatrix} \right] \cdot \begin{pmatrix} \lambda_1 \\ \lambda_2 \\ \vdots \\ \lambda_{N_z} \end{pmatrix} = \begin{pmatrix} U_1^{[0]} \\ U_2^{[0]} \\ \vdots \\ U_{N_z}^{[0]} \end{pmatrix}$$

determines the solution of the 3D nonlocal problem. However one should notice that this requires, at a preliminary step, the resolution of $N_z + 1$ *Stokes problems in 3D, which is much more costly than the approach based upon the resolution of the 1D reduced problem attached to the 3D problem.*

1.3.2 Numerical results

3D velocity distribution in the reference situation

We have computed the flow produced by a whole forest of cilia, with data given by Table 2.2: we consider a three dimensional box, with an axial length equivalent to the length of one metachronal

wave, $L_x = 30\,\mu\mathrm{m}$, a radial depth of $L_z = 10\,\mu\mathrm{m}$ (which is the average depth of the mucus layer in the human trachea), and an azimuthal width of $L_y = 4.8\,\mu\mathrm{m}$. A 100×16 array of cilia is attached to the bottom of this box and biperiodic boundary conditions on the solution of the Stokes equations are imposed in the axial and azimuthal directions, in order to represent the configuration of an "infinite" array of cilia. The box is filled with a Newtonian fluid with piecewise constant viscosity μ: $\mu = \mu_1$ in the PCL layer and $\mu = \mu_2$ in the mucus layer. The interface between the two layers is located at $z = H$ which is set to $4.8\,\mu\mathrm{m}$, so that cilia penetrate the mucus layer during the effective stroke, but not during the recovery stroke.

Computations have been performed with `FreeFem++`, see [**?**]: 3D Stokes problems are solved using P_1b-P_1 finite elements, in order to satisfy a uniform inf-sup condition at the discrete level. Note that in this context the rigorous error analysis has been led in [7]: the method is proven to be convergent with optimal rates when "far from singularities": thus, in our case, error converges to 0 with order 1 in H^1-norm in the mucus region. Note also that the nonlocal term is treated by computing the solution of the average 1D problem: for this, `FreeFem++` is used as well and the resulting 1D solution serves as a contributing source term for the 3D Stokes problem. The 3D problems have been solved with a mesh size

$$N_x \times N_y \times N_z = 100 \times 10 \times 100.$$

In particular we choose to limit the number of degrees of freedom in the azimuthal (y) direction as little variation of the velocity field is expected, due to the geometrical configuration; this allows us to use fine mesh in axial (x) and radial (z) directions. Note also that the chosen mesh is conformal with the PCL-mucus interface. The mesh is sufficiently fine to capture the dynamics of the collective ciliary beating with good precision.

Figure 1.4 illustrates the results obtained in the reference configuration. The density of cilia is high enough for the flow to be independent on time, up to a translation at the velocity of the metachronal wave. As a consequence, drawing one time step only is sufficient. We observe important recirculations in the PCL, with high magnitude variations, while in the mucus layer the flow is rather homogeneous. Actually, mucus is transported at an almost constant velocity, like a block "sliding" over the PCL. To the best of our knowledge, only mucus velocity can be experimentally measured and our numerical results fit the magnitudes of the mucus velocity in experimental measurements: for instance, tracheal mucus velocity is found to be about $100\,\mu\mathrm{m} \cdot \mathrm{s}^{-1}$ in [**?**, **?**], $60\,\mu\mathrm{m} \cdot \mathrm{s}^{-1}$, between 80 and $150\,\mu\mathrm{m} \cdot \mathrm{s}^{-1}$ in [**?**], $150\,\mu\mathrm{m} \cdot \mathrm{s}^{-1}$ in [**?**] and it ranges from 160 (young adults) to $110\,\mu\mathrm{m} \cdot \mathrm{s}^{-1}$ (older adults) in [**?**]. But, as a matter of fact, no experiment gives access to the 3D or axial velocity profile. In a more general way data related to the mucociliary transport are very sparse, often related to morphometric data in small animals (beating frequency, ciliary density...) and the measurement of the mucociliary transport mainly relies on scalar quantities (e.g. mean velocity) and not on distributional quantities (such as velocity profiles).

Figures 1.5 and 1.6 present the velocity profile for the very same situation as in Figure 1.4 except that the forest is sparse (50×8 and 25×4 cilia respectively instead of 100×16). We still observe the "block property" of the mucus: this is due to the high viscosity of the mucus, the surface tension at the interface with PCL and the fact that cilia hardly penetrate the mucus. We also observe that in the PCL recirculations are limited when sparsity is enough.

Figure 1.7 presents the velocity profile for the very same situation as in Figure 1.4 up to two (major) differences: on the one hand, the viscosity ratio is $\mu_2/\mu_1 = 10^{+0}$ (instead of 10^{+4}) as μ_2 has been set to $\mu_2 = 10^{+0}\,\mathrm{mPa} \cdot \mathrm{s}$; on the other hand, the surface tension constraint has been relaxed (so that the normal velocity at the PCL-mucus interface is not 0). Therefore the situation corresponds to an isoviscous fluid moved by a dense forest of cilia. It can be observed that the "block property" of the

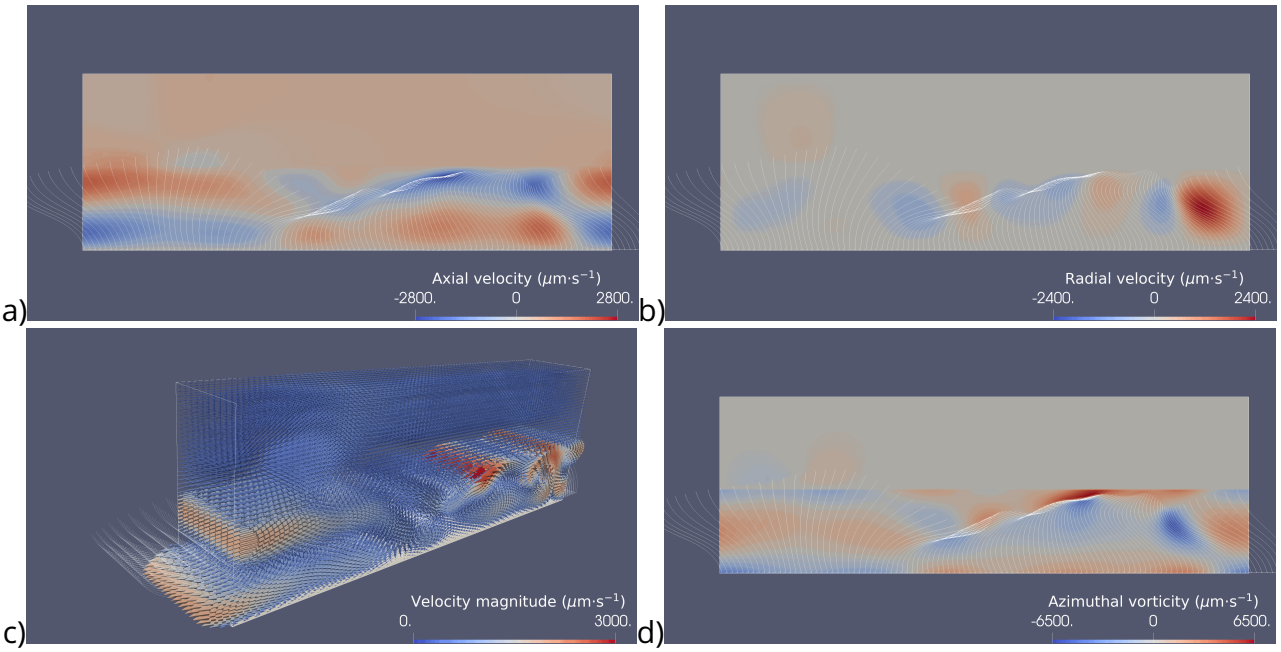

Figure 1.4 – Velocity distribution associated to a dense forest of cilia. All data from Table 2.2.

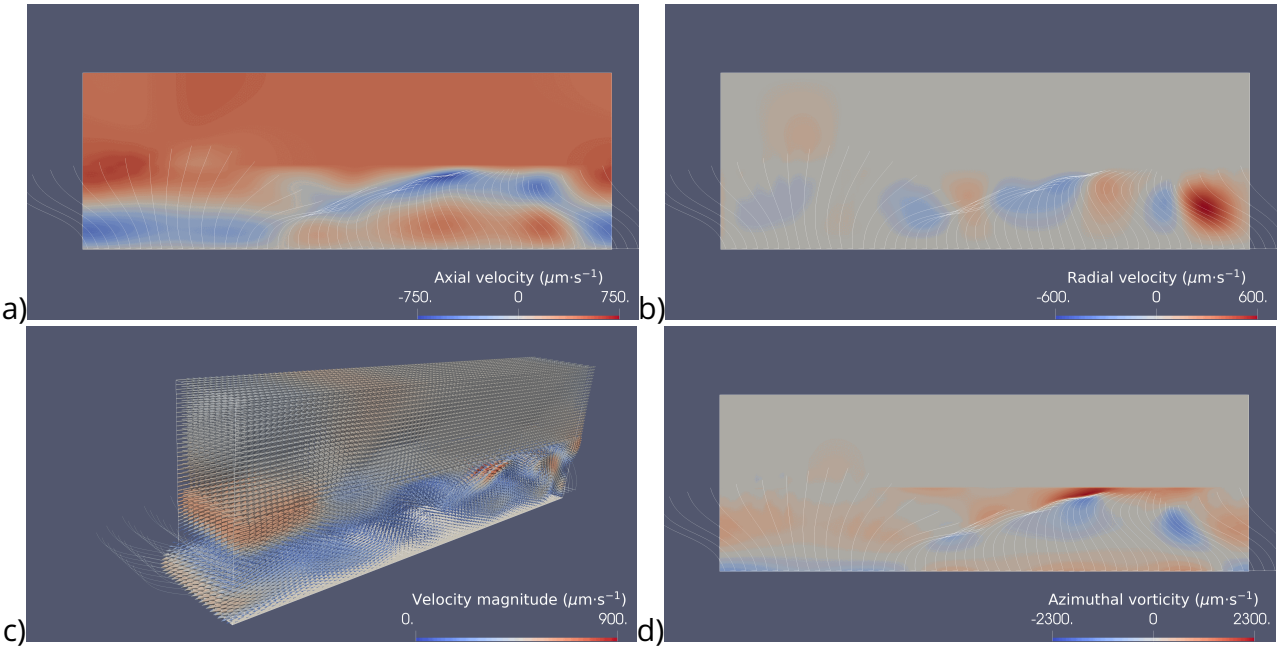

Figure 1.5 – Velocity distribution associated to a sparse forest of cilia. Data from Table 2.2 except for the cilia spacing: $\ell_x^0 = \ell_y^0 = 0.6\,\mu\mathrm{m}$ (instead of $0.3\,\mu\mathrm{m}$) and, as a consequence, the number of cilia has become $n_x = 50$ (instead of 100) and $n_y = 8$ (instead of 16).

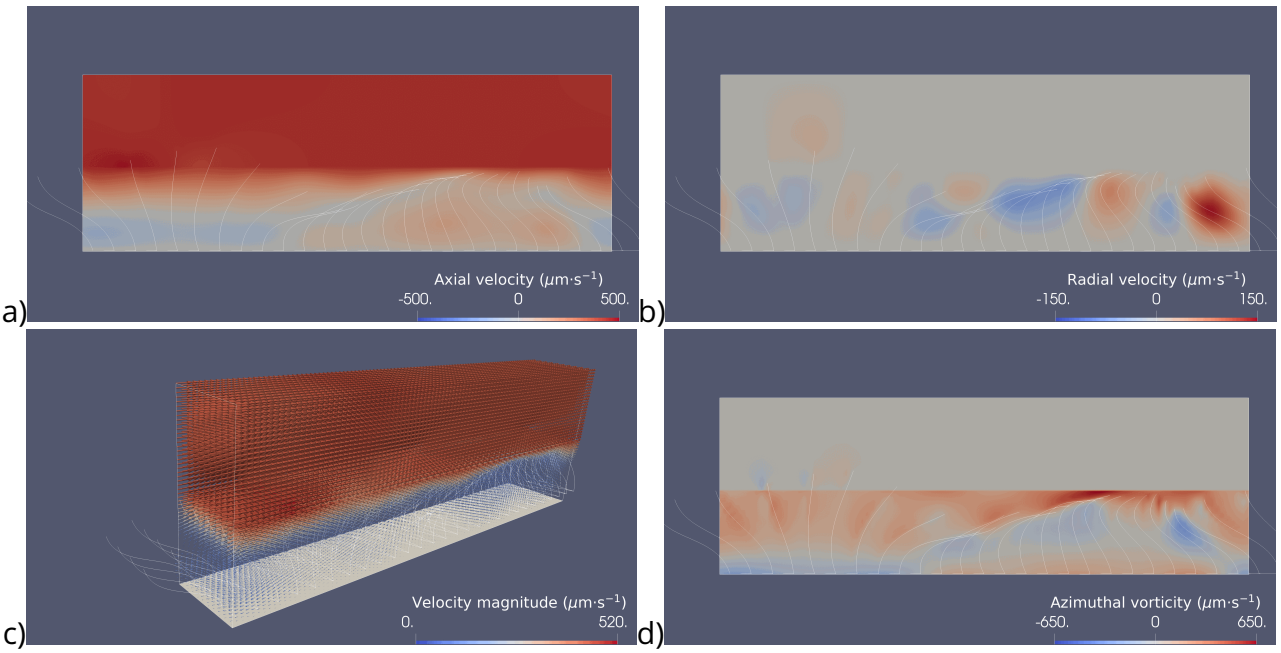

Figure 1.6 – Velocity distribution associated to a sparse forest of cilia. Data from Table 2.2 except for the cilia spacing: $\ell_x^0 = \ell_y^0 = 0.6\,\mu\mathrm{m}$ (instead of $0.3\,\mu\mathrm{m}$) and, as a consequence, the number of cilia has become $n_x = 25$ (instead of 100) and $n_y = 4$ (instead of 16).

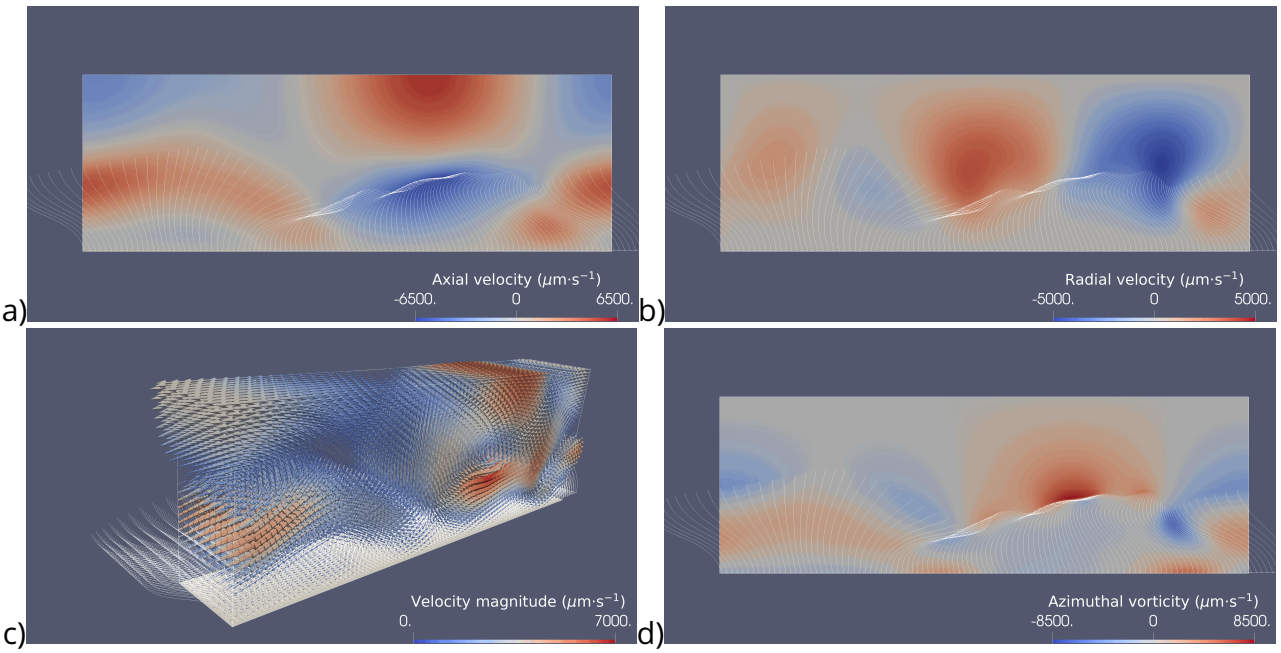

Figure 1.7 – Velocity distribution associated to a dense forest of cilia *in the monofluid case* and *relaxing the surface tension constraint*. Data from Table 2.2 except for the viscosity ratio: $\mu_2 = 1 \cdot 10^{+0}\,\mathrm{mPa \cdot s}$

mucus is not preserved, as velocity variations are significant in the mucus because of the standard viscosity in the whole domain (not only in the PCL) and recirculations are not limited by the surface tension at the interface.

The conclusion is that both high viscosity in the mucus and surface tension allow for a homogeneous flow in the mucus, whereas ciliary density allows for a more efficient mucociliary transport. The impact of these parameters will be investigated in the following subsections.

Influence of the viscosity ratio

Figure 1.8 presents the influence of the viscosity ratio over the mean axial velocity $z \mapsto u(z) := \overline{u_x}^{x,y}(z)$, resulting from the averaged model (which is also identified as the background flow). This profile is important as it allows for the quantification of the mucociliary efficiency. Data are taken from Table 2.2, except for the viscosity of the fluid: μ_1 is set to $1 \cdot 10^{+0}\,\mathrm{mPa \cdot s}$, whereas μ_2 may vary from $1 \cdot 10^{+0}$ to $1 \cdot 10^{+4}\,\mathrm{mPa \cdot s}$. We observe that the *high viscosity ratio* regime is already nearly achieved for $\mu_2/\mu_1 = 50$, showing some robustness of the mucus transport with respect to μ_2, when sufficiently high.

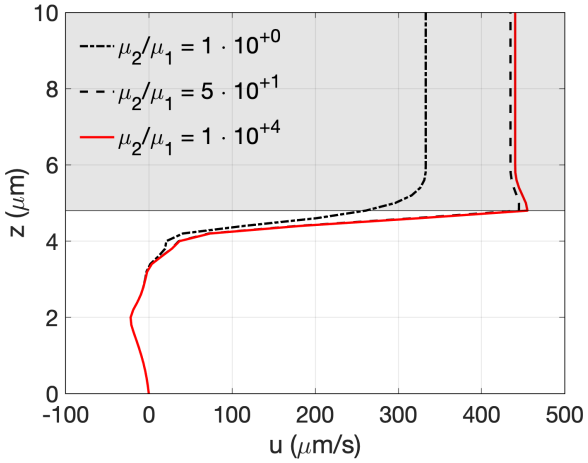

Figure 1.8 – Mean axial velocity $z \mapsto u(z) := \overline{u_x}^{x,y}(z)$ in the radial direction, for different viscosity ratios. Data from Table 2.2, except for mucus viscosity μ_2 (that takes the following values: $1 \cdot 10^{+0}$, $5 \cdot 10^{+1}$ and $1 \cdot 10^{+4}$).

Influence of the surface tension

Figures 1.9 and 1.10 present the numerical results obtained with/without surface tension (all data are taken from Table 2.2). Let us recall that, in Eq. (1.2), the surface tension γ is the Lagrange multiplier associated to the constraint $\mathbf{u} \cdot \mathbf{n} = 0$ on Γ_* and it ensures the stability of the interface between the PCL and the mucus. The influence of the surface tension is investigated in terms of velocity distribution. As already outlined, it has no influence on the averaged 1D model: the mean axial velocity does not depend on the surface tension. However surface tension has great influence on the 3D velocity distribution, especially when the viscosity ratio is around 1 (monofluid case); the influence of the surface tension tends to be damped for both axial and radial velocities when the viscosity ratio increases.

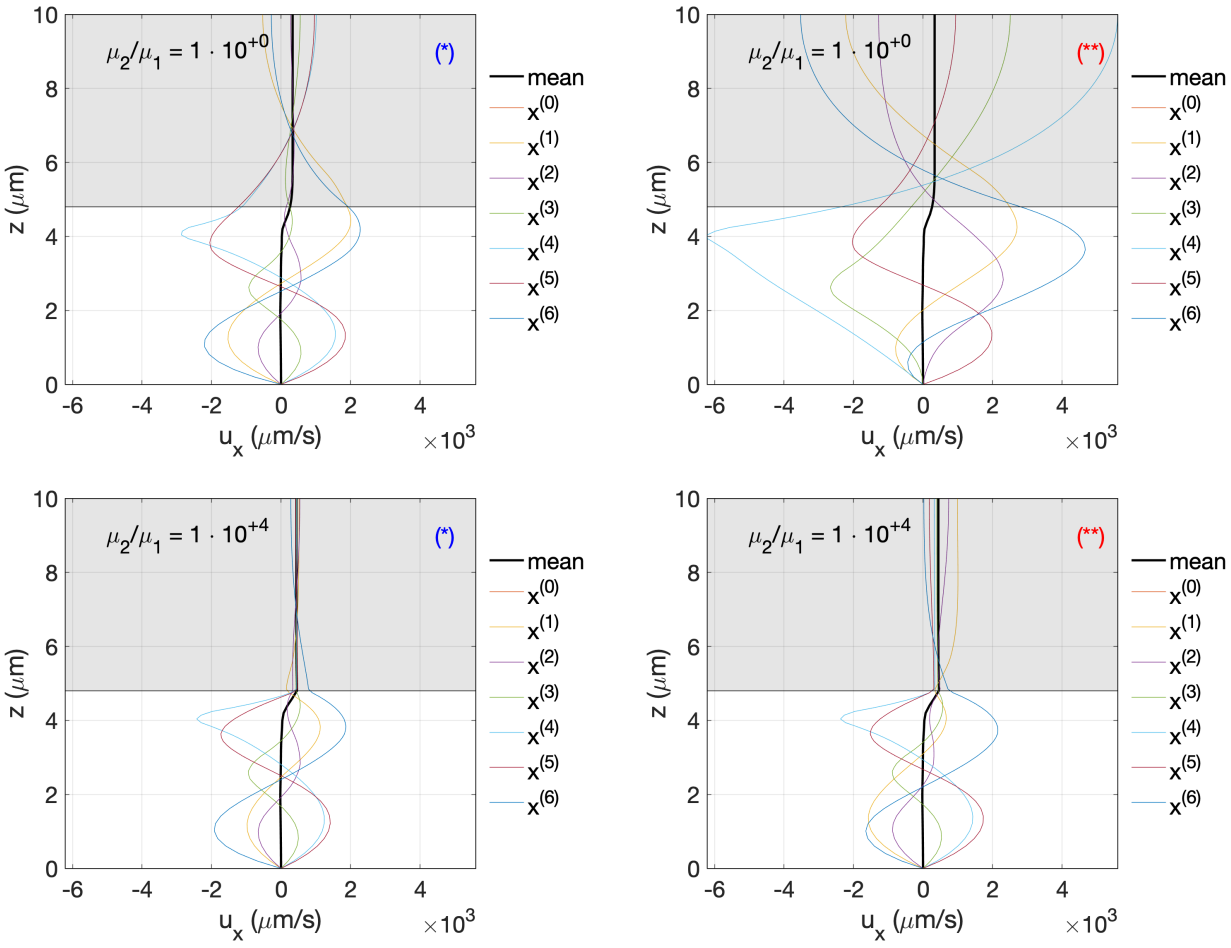

Figure 1.9 – Axial velocity profiles in the radial direction, for different axial positions $x = x^{(j)} = j\Delta$ (with $\Delta = 5\,\mu\mathrm{m}$). The velocity is averaged in the azimuthal direction y (note that the velocity little varies in this direction) so that we show the following profiles: $z \mapsto \overline{u_x}^y(x^{(j)}, z)$ $(*)$ refers to the standard model with surface tension (hence $u_z = 0$ is imposed at the PCL-mucus interface) whereas $(**)$ refers to the model in which no surface tension is taken into account (hence u_z is not constrained at the PCL-mucus interface).

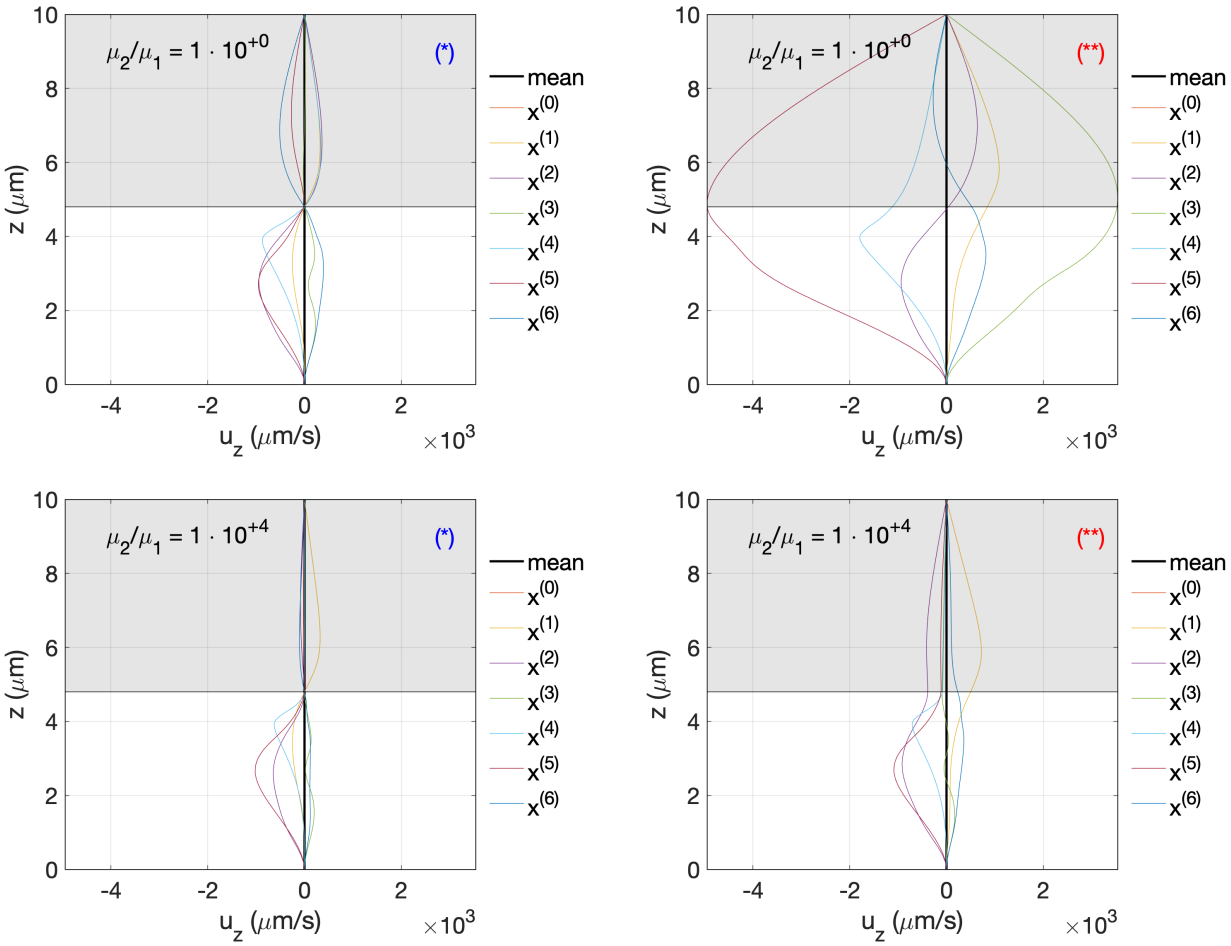

Figure 1.10 – Radial velocity profiles in the radial direction, for different axial positions $x = x^{(j)} = j\Delta$ (with $\Delta = 5\,\mu\mathrm{m}$). The velocity is averaged in the azimuthal direction y so that we show the following profiles: $z \mapsto \overline{u_z}^y(x^{(j)}, z)(*)$ refers to the standard model with surface tension (hence $u_z = 0$ is imposed at the PCL-mucus interface) whereas $(**)$ refers to the model in which no surface tension is taken into account (hence u_z is not constrained at the PCL-mucus interface).

Influence of the position of the ASL

Figure 1.11 investigates the influence of the position of the PCL-mucus interface on the mucociliary transport, for different viscosity ratios. Actually $H = 4.8\,\mu\mathrm{m}$ is a near-maximizer of the mean mucus velocity. Note that for $H > 6\,\mu\mathrm{m}$, the cilia are completely immersed in the PCL only and do not reach the mucus: as a consequence, the mean axial velocity does not depend on the position of the interface in this regime. But for $H < 6\,\mu\mathrm{m}$, cilia are partially immersed in the mucus, providing energy to the highly viscous fluid in a more direct way. Note that this behaviour quantitatively depends on the viscosity contrast.

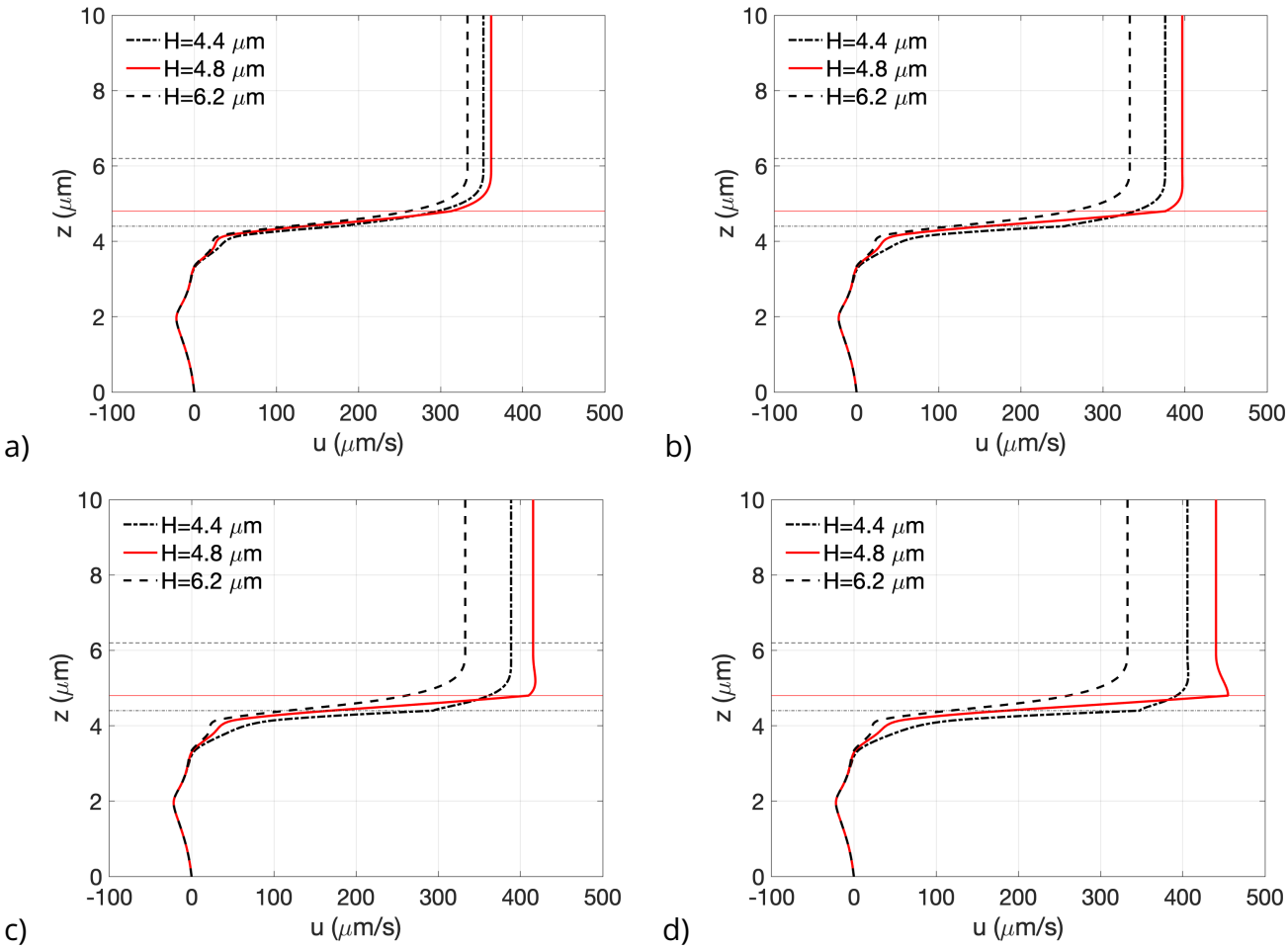

Figure 1.11 – Influence of the position of the ASL (H) on the mean axial velocity $z \mapsto \overline{u_x}^{x,y}(z)$ in the radial direction (through PCL and mucus). a) $\mu_2 = 2{\cdot}10^{+0}\,\mathrm{mPa{\cdot}s}$, b) $\mu_2 = 5{\cdot}10^{+0}\,\mathrm{mPa{\cdot}s}$, c) $\mu_2 = 1{\cdot}10^{+1}\,\mathrm{mPa{\cdot}s}$, d) $\mu_2 = 1 \cdot 10^{+4}\,\mathrm{mPa \cdot s}$.

Figure 1.12 investigates the influence of the position of the PCL-mucus interface on the mucociliary transport. Figure 1.12 a) only depends on the parametrization of the cilia movement (see Table 1.1). The mucus velocity profile exhibits three zones. Range (III) corresponds to $H > 5.9038\,\mu\mathrm{m}$ for which the cilia are completely immersed in the PCL in both effective and recovery strokes: the velocity is constant with respect to H. Range (III) is characterized by the fact that the cilia partially penetrate the mucus in the effective stroke but do not in the recovery stroke: this corresponds to some optimal situation in terms of mucociliary efficiency. In Section (I), cilia penetrate the mucus in the effective stroke but

also in the recovery stroke, which explains the decrease of the mucus velocity when compared to the one obtained in Range (II). Note that the mean velocity profile exhibits some discontinuity at the transition between (II) and (III), for high viscosity ratios (actually this trend emerges when the viscosity ratio increases (between 10 and 100) and is stabilized for high viscosity ratios). This is due to some model artefact: in Range (III) the cilia are all immersed in the PCL only; but when we get into Range (II), the head of some cilia penetrate the highly viscous mucus: this leads to local forces that become extremely high (recall that in the slender body theory the force is proportional to the viscosity) with no transition. Thus in this model governed by the slender body theory the energy transferred to the fluid by the cilia is not continuous with respect to H, even if the background flow term stabilizes the solution profiles with respect to high viscosity ratios.

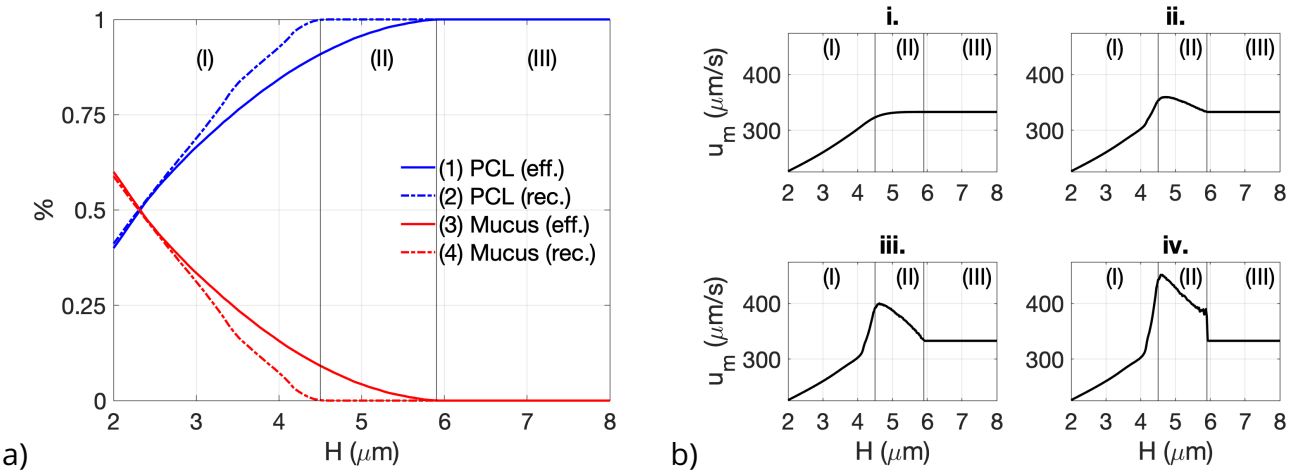

Figure 1.12 – Influence of the position of the ASL (H). a) The percentage (%) of time spent by cilia in the mucus and PCL is shown for both phases: effective stroke (eff.) and recovery stroke (rec.). b) Influence of the position of the ASL on mucus velocity $u_m = (L_z - H)^{-1} \int_H^{L_z} \overline{u_x}^{x,y}(z)\,\mathrm{d}z$ for different viscosity ratios (data from Table 2.2, except for the position of the PCL-mucus interface which varies from 2 to $8\,\mu\mathrm{m}$ and the viscosity μ_2 that takes the following values: **i.** $\mu_2 = 1\cdot 10^{+0}\,\mathrm{mPa\cdot s}$, **ii.** $\mu_2 = 2\cdot 10^{+0}\,\mathrm{mPa\cdot s}$, **iii.** $\mu_2 = 5\cdot 10^{+0}\,\mathrm{mPa\cdot s}$, **iv.** $\mu_2 = 1\cdot 10^{+4}\,\mathrm{mPa\cdot s}$).

Influence of the ciliary density

Figures 1.13 and 1.14 investigate the influence of the ciliary density over the mucociliary transport for $H = 4.8\,\mu\mathrm{m}$ and $H = 6.2\,\mu\mathrm{m}$. Note that

- For $H < 6\,\mu\mathrm{m}$, the cilia penetrate the mucus during the effective stroke;
- For $H > 6\,\mu\mathrm{m}$, the cilia are completely immersed in the PCL only and do not penetrate the mucus.

Other data are taken from Table 2.2, except for the cilia densities ℓ_x^0 and ℓ_y^0 (or the number of cilia in each direction, n_x and n_y, as $n_x\ell_x^0 = L_x$ and $n_y\ell_y^0 = L_y$). The reference density of cilia is $11.11\ \mu\mathrm{m}^{-2}$, which corresponds to a forest of $n_x \times n_y$ cilia with $n_x = 100$ and $n_y = 16$, placed on surface whose area is $L_x \times L_y$ with $L_x = 30.0\,\mu\mathrm{m}$ and $L_y = 4.8\,\mu\mathrm{m}$.

Figure 1.13 investigates the influence of the ciliary density over the mucociliary transport with $H = 4.8\,\mu\mathrm{m}$. In Figure 1.13 a), we let d_x vary (whereas the density of cilia in the azimuthal direction is fixed to its reference value). In Figure 1.13 b), we let d_y vary (whereas the density of cilia in the

axial direction is fixed to its reference value). In Figure 1.13 c), we investigate the crossed influence of the axial/azimuthal densities. We observe that the mucus velocity becomes stable when n_x or n_y increase: these results are due to the background flow term in the 3D model or, equivalently, the counter-part contribution due to the collective transport in the 1D model. Indeed the source term (without background flow) is proportional to n_x and n_y but so does the damping term coefficient due to the background flow. The latter argument prevents the model from being linear with respect to n_x and n_y and it provides some remarkable robustness of the mucus transport with respect to the cilia density, when reaching a sufficiently high value.

Figure 1.14 investigates the influence of the ciliary density over the mucociliary transport with $H = 6.2\,\mu\mathrm{m}$ (instead of $H = 4.8\,\mu\mathrm{m}$). In this case, the cilia do not penetrate the mucus. The mean axial velocity profile does not depend on the position of the interface: this results from the fact that, as long as the cilia do not penetrate the mucus, the mucus area is passive (i.e. source term is null) which, combined with homogeneous Neumann condition, leads to a constant velocity profile in the mucus. Noteworthily the robustness of the ciliary transport with respect to the cilia density is achieved when it reaches a sufficiently high value.

Figures 1.15 and 1.16 exhibit the axial velocity profiles with low density for $H = 4.8\,\mu\mathrm{m}$ and $H = 6.2\,\mu\mathrm{m}$ respectively. When the cilia penetrate the mucus during the effective stroke (see Figure 1.15, corresponding to $H = 4.8\,\mu\mathrm{m}$), we notice that *low* ciliary density does not modify the magnitude of the mean axial velocity, but it damps the dispersion of velocity profiles around the mean profile: the loss of activity makes the velocity distribution more homogeneous, in particular in the PCL. When the cilia do not penetrate the mucus (see Figure 1.16, corresponding to $H = 6.2\,\mu\mathrm{m}$), not only dispersion of velocity profiles around the mean profile tends to be damped, but also the magnitude of the mean velocity decreases.

1.4 Conclusion

In this article we modelled the mucociliary transport through a 3D model connecting all the main features of the process: 1) (dense) forests of cilia immersed in a fluid, with an individual description of the cilia; 2) the fluid is a two-layer fluid (PCL+mucus with a sharp viscosity ratio) separated by an interface which is made stable due to surface tension. The main limitation lies in the fact that the ciliary movement is prescribed and the forces exerted by the cilia on the fluid are evaluated using an approximated formula provided by the slender body theory. Beyond these limitations, the model is based upon fundamental equations of dynamics and results in a nonlocal Stokes system with singular source terms; from the mathematical point of view, the model is well-posed (in suitable functional spaces) and, from the numerical point of view, the computation of the 3D velocity profiles is performed using numerical methods characterized by rigorous error analysis (even in the singular case). Numerical results allow us to describe the 3D velocity distribution in a non-pathological situation and to highlight, by comparison, the influence of critical parameters (beating frequency of the cilia, mucus viscosity, surface tension, ciliary density in the forest, position of the PCL/mucus interface etc.) on the velocity distribution and, finally, on the efficiency of the mucociliary transport. Note that several extensions can be made:

- *Influence of the airflow on the mucociliary efficiency*. In a bronchus, the bronchial wall is lined with a bifluid made of two layers (the PCL and mucus) and the center of the bronchus is filled with air. Thus mucus has an interface not only with PCL (at $\{z = H\}$) but also with air (at $\{z = L_z\}$). In this article, the influence of air has been neglected (hence we impose a free-slip boundary

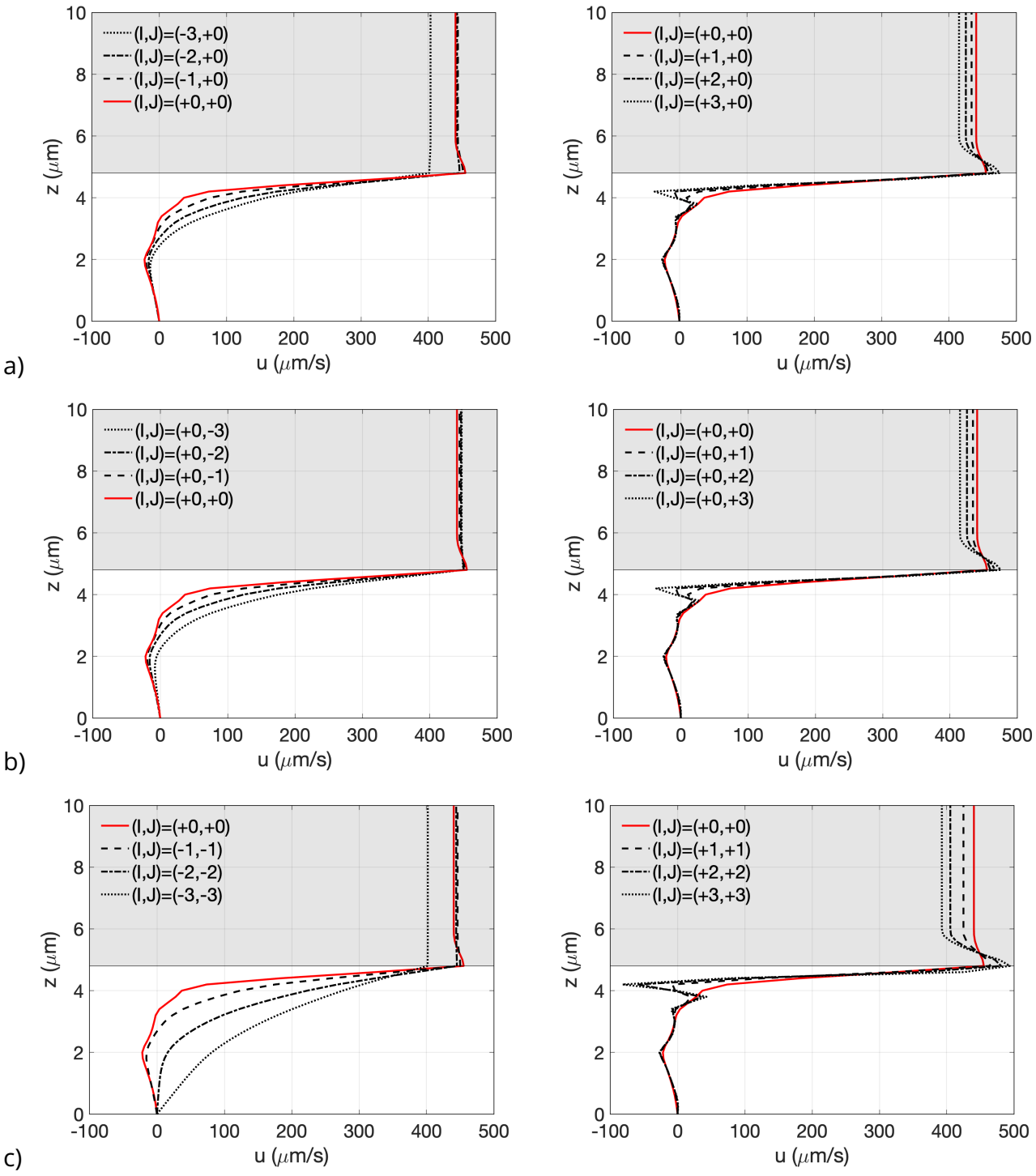

Figure 1.13 – Influence of the density of cilia on the mean axial velocity $z \mapsto u(z) := \overline{u_x}^{x,y}(z)$, for $H = 4.8\,\mu\mathrm{m}$. All data from Table 2.2 except for the density of cilia. Index (I, J) relates to the following density: $d_x = 2^I d_x^0$ (axial direction), $d_y = 2^J d_y^0$ (azimuthal direction), with reference values: $d_x^0 = d_y^0 := 3.33\,\mu\mathrm{m}^{-1}$.

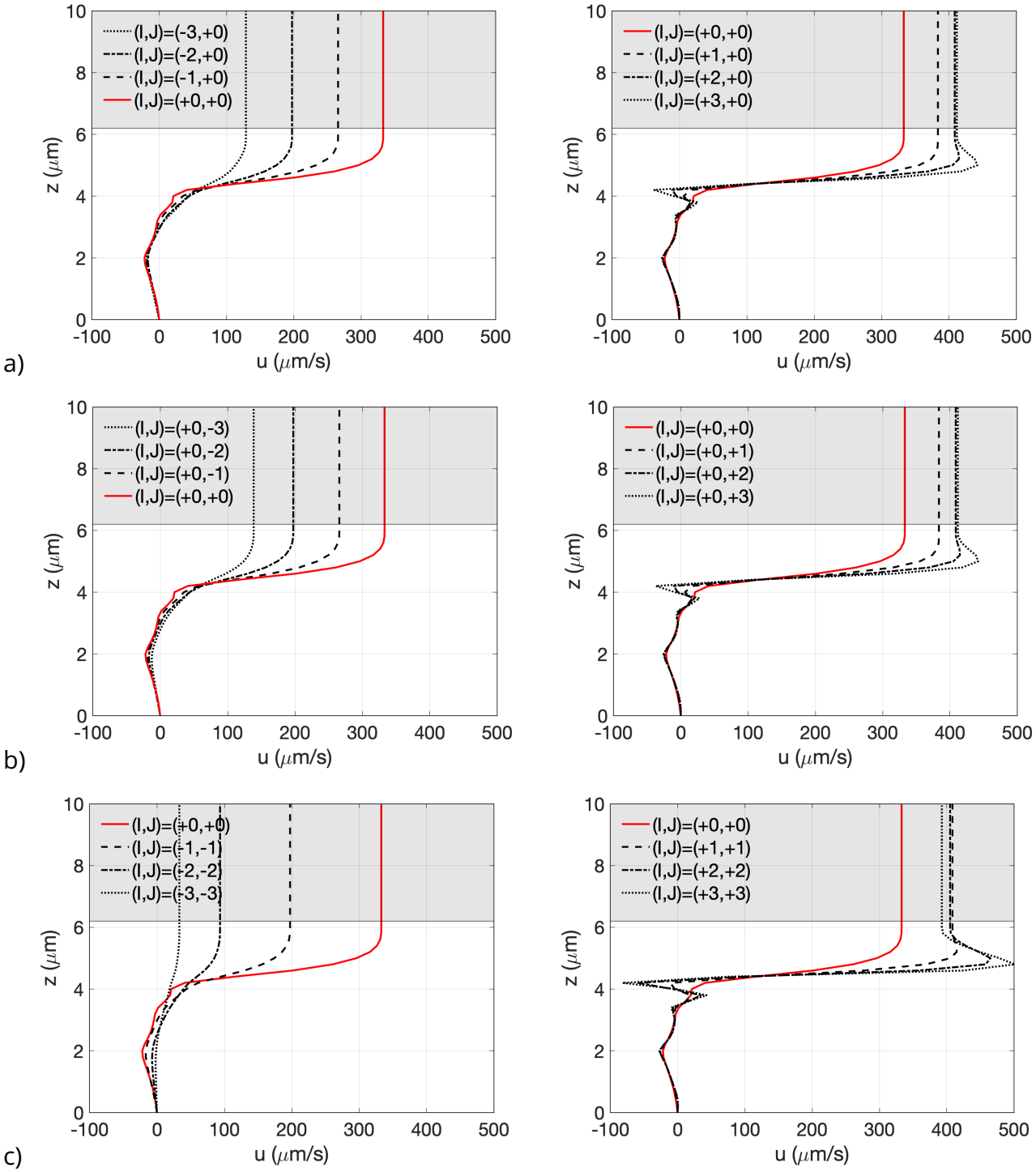

Figure 1.14 – Influence of the density of cilia on the mean axial velocity $z \mapsto u(z) := \overline{u_x}^{x,y}(z)$, for $H = 6.2\,\mu\mathrm{m}$. All data from Table 2.2 except for the density of cilia and the position of the interface. Index (I, J) relates to the following density: $d_x = 2^I d_x^0$ (axial direction), $d_y = 2^J d_y^0$ (azimuthal direction), with reference values: $d_x^0 = d_y^0 := 3.33\,\mu\mathrm{m}^{-1}$.

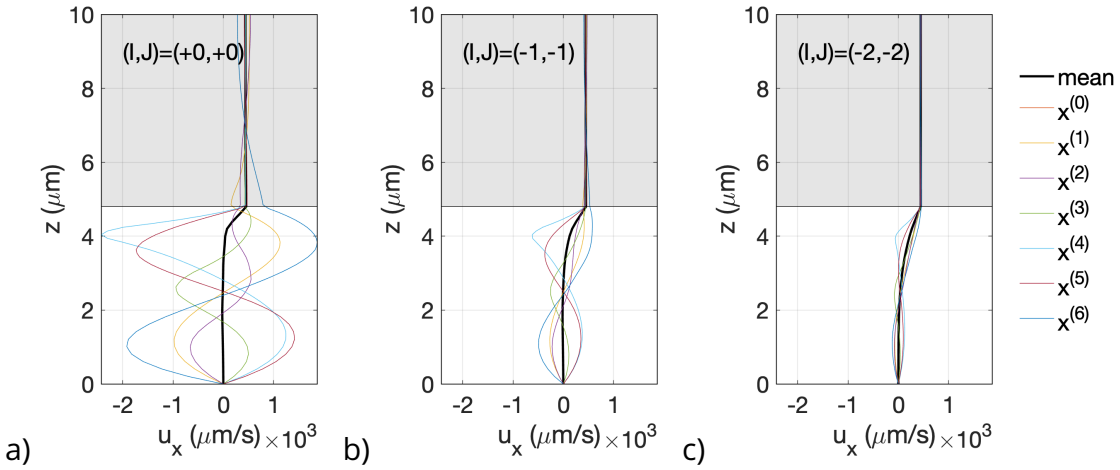

Figure 1.15 – Influence of the density of cilia on the axial velocity, for $H = 4.8\,\mu\mathrm{m}$. All data from Table 2.2 except for the density of cilia. The axial velocity is averaged in the azimuthal direction y (note that the velocity little varies in this direction) so that we show the following profiles: $z \mapsto \overline{u_x}^y(x^{(j)}, z)$ for different axial positions $x = x^{(j)} = j\Delta$ (with $\Delta = 5\,\mu\mathrm{m}$). Index (I, J) relates to the following density: $d_x = 2^I d_x^0$ (axial direction), $d_y = 2^J d_y^0$ (azimuthal direction), with reference values: $d_x^0 = d_y^0 := 3.33\,\mu\mathrm{m}^{-1}$.

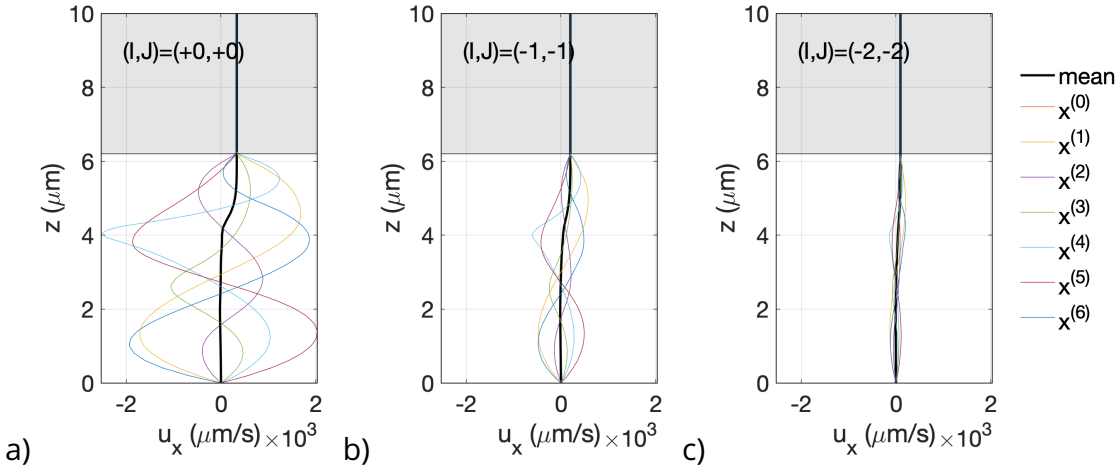

Figure 1.16 – Influence of the density of cilia on the axial velocity, for $H = 6.2\,\mu\mathrm{m}$. All data from Table 2.2 except for the density of cilia. The axial velocity is averaged in the azimuthal direction y (note that the velocity little varies in this direction) so that we show the following profiles: $z \mapsto \overline{u_x}^y(x^{(j)}, z)$ for different axial positions $x = x^{(j)} = j\Delta$ (with $\Delta = 5\,\mu\mathrm{m}$). Index (I, J) relates to the following density: $d_x = 2^I d_x^0$ (axial direction), $d_y = 2^J d_y^0$ (azimuthal direction), with reference values: $d_x^0 = d_y^0 := 3.33\,\mu\mathrm{m}^{-1}$.

condition at $\{z = L_z\}$) but the influence of air cycles combined with the ciliary activity can be done as follows: because the airflow goes through the bronchus, the shear effect at the air-mucus interface imposed by the respiratory cycle can alternatively increase (at expiration) or decrease (at expiration) the mucus velocity; this phenomenon can be taken into account by introducing a pressure drop in the fluid flow and replacing the free-slip boundary conditions at $\{z = L_z\}$ by boundary conditions that model the shear effect of the air flow in the bronchus, which can be represented by a Poiseuille flow.

- *Viscoelasticity of the mucus*. Viscoelastic properties of the mucus may have an impact on the mucociliary transport, in particular in pathological situations [19, 66]. We could extend our 3D model to take into account viscoelasticity: for instance, using an Oldroyd-type model, under the assumption that cilia do not penetrate the mucus, the constitutive equations relating the elastic tensor to the velocity field can be computed using a splitting scheme combined with a characteristics method as in [21]. If cilia penetrate the mucus, the lack of regularity of the velocity field, due to the singular source term in the active part of the mucus, would certainly lead to mathematical and numerical difficulties: indeed, to the best of our knowledge, the regularity of the solution for the Stokes-Oldroyd problem with singular source term is an open question and, thus, it requires a suitable functional framework in order to derive a rigorous mathematical formulation and error analysis for the finite element method in this case.

1.5 Appendix

Let us describe the derivation of the reduced model.

Averaging process

We denote by $\overline{\cdot}^x$ (resp. $\overline{\cdot}^y$; $\overline{\cdot}^{x,y}$) the (classical) averaging process with respect to x (resp. y ; x and y). For instance, for a regular function $(x, y, z) \mapsto f(x, y, z)$ we denote $\overline{f}^{x,y} : (0, L_z) \mapsto \mathbb{R}$ the function defined by

$$\overline{f}^{x,y}(z) = \frac{1}{L_x L_y} \int_0^{L_x} \int_0^{L_y} f(x, y, z) \, \mathrm{d}x \, \mathrm{d}y.$$

Averaging the continuity equation $\partial_x u_x + \partial_y u_y + \partial_z u_z = 0$ combined with the periodicity of the velocity field $\mathbf{u}$ yields

$$\partial_z \overline{u_z}^{x,y} = 0$$

which, combined with the homogeneous Dirichlet condition at $\Gamma_\downarrow$, gives:

$$\overline{u_z}^{x,y} = 0.$$

Let us average the momentum equation. Note that the source terms involved by the ciliary beat are not regular but we first derive the average model by skipping this difficulty which will be treated thereafter. Therefore assume that F_x, F_y and F_z are regular source terms (e.g. in $L^2(\Omega)$), we have

$$\begin{cases} -\partial_x(\mu\partial_x u_x) - \partial_y(\mu\partial_y u_x) - \partial_z(\mu\partial_z u_x) + \partial_x p & = F_x \quad \text{on } \Omega, \\ -\partial_x(\mu\partial_x u_y) - \partial_y(\mu\partial_y u_y) - \partial_z(\mu\partial_z u_y) + \partial_y p & = F_y \quad \text{on } \Omega, \\ -\partial_x(\mu\partial_x u_z) - \partial_y(\mu\partial_y u_z) - \partial_z(\mu\partial_z u_z) + \partial_z p + \gamma\delta_{\Gamma_*} & = F_z \quad \text{on } \Omega. \end{cases}$$

Averaging in x and y, using the fact that μ only depends on z and using the periodicity of $\mathbf{u}$ and p we obtain

$$\begin{cases} -\partial_z(\mu\partial_z\overline{u_x}^{x,y}) & = & \overline{F_x}^{x,y} & \text{on } (0,L_z), \\ -\partial_z(\mu\partial_z\overline{u_y}^{x,y}) & = & \overline{F_y}^{x,y} & \text{on } (0,L_z), \\ -\partial_z(\mu\partial_z\overline{u_z}^{x,y}) + \partial_z\overline{p}^{x,y} & + & \overline{\gamma}^{x,y}\delta_{z=H} = \overline{F_z}^{x,y} & \text{on } (0,L_z). \end{cases}$$

Next as the cilia movement only occurs in the $(x-z)$ plane (see the parametrization of the ciliary beat patterns), then $F_y = 0$ and the second equation of the system writes:

$$-\partial_z(\mu\partial_z\overline{u_y}^{x,y}) = 0 \quad \text{on } (0,L_z),$$

which, by the homogeneous boundary condition on $\Gamma_\downarrow$, gives:

$$\overline{u_y}^{x,y} = 0.$$

Besides, as previously shown, $\overline{u_z}^{x,y} = 0$ so that the third equation of the system writes

$$\partial_z\overline{p}^{x,y} + \overline{\gamma}^{x,y}\delta_{\Gamma_*} = \overline{F_z}^{x,y} \quad \text{on } (0,L_z).$$

The reduced system (with regular source term) writes

$$\begin{cases} -\partial_z(\mu\partial_z\overline{u_x}^{x,y}) = \overline{F_x}^{x,y} & \text{on } (0,L_z), \\ \overline{u_y}^{x,y} = 0 & \text{on } (0,L_z), \\ \overline{u_z}^{x,y} = 0 & \text{on } (0,L_z), \\ \partial_z\overline{p}^{x,y} + \overline{\gamma}^{x,y}\delta_{z=H} = \overline{F_z}^{x,y} & \text{on } (0,L_z). \end{cases} \tag{1.12}$$

Notice that the last equation relates the average pressure $\overline{p}^{x,y}$ and the surface tension $\overline{\gamma}^{x,y}$ to the force exerted by the cilia onto the fluid. Hower this equation is not required when one aims at determining the average velocity field, in particular $z \mapsto \overline{u_x}^{x,y}(z)$ which describes the average velocity profile of the PCL+mucus system. Additionally let us deal with the boundary conditions. In a straightforward way, the Dirichlet condition readily adapts into:

$$\overline{u_x}^{x,y}(0) = \overline{u_y}^{x,y}(0) = \overline{u_z}^{x,y}(0) = 0.$$

The kinematic and dynamic conditions on $\Gamma_\uparrow$ read $u_z = 0$ and $\partial_z u_x = 0$ on $\Gamma_\uparrow$ which, after averaging in x and y, yields:

$$\begin{cases} \overline{u_z}^{x,y}(L_z) = 0, \\ \partial_z\overline{u_x}^{x,y}(L_z) = 0. \end{cases}$$

As a consequence, the reduced model (with regular source term) reads:

- First component of the velocity:

$$\begin{cases} -\partial_z(\mu(z)\partial_z\overline{u_x}^{x,y}(z)) = \overline{F_x}^{x,y}(z), \quad \forall z \in (0,L_z), \\ \overline{u_x}^{x,y}(0) = 0, \\ \partial_z\overline{u_x}^{x,y}(L_z) = 0. \end{cases} \tag{1.13}$$

- Second component of the velocity:

$$\overline{u_y}^{x,y}(z) = 0, \quad \forall z \in (0, L_z).$$

- Third component of the velocity:

$$\overline{u_z}^{x,y}(z) = 0, \quad \forall z \in (0, L_z).$$

- Pressure field:

$$\partial_z \overline{p}^{x,y}(z) + \overline{\gamma}^{x,y}(z)\delta_{z=H} = \overline{F_z}^{x,y}(z) \quad \forall z \in (0, L_z).$$

Remark 8. *Partial derivatives with respect to z have been maintained because the functions may depend on time, even if it plays the role of a parameter. In particular, if the source terms F_x, F_y and F_z do depend on time, so do the solution $\mathbf{u}$ and its subsequent average first component $\overline{u_x}^{x,y}$.*

Reduction of the source term

Let us now provide some details about the derivation of the source terms $\overline{F_x}^{x,y}$ and $\overline{F_z}^{x,y}$ in the context of the ciliary study. More precisely we need to define in a rigorous way the averaging process of the source term defined in Problem (1.2), namely:

$$\mathbf{F} := \begin{pmatrix} F_x \\ F_y \\ F_z \end{pmatrix} = \sum_{i,j} \mathbf{f}_{ij}(\cdot, t)\delta_{\Gamma_{ij}(t)}.$$

In order to define the averaging process for the singular source term, let us deal with one single Dirac term (the extension to an arbitrary number of singular source terms follows from linearity).

For any (i, j), $i \in [\![1, n_x]\!]$ and $j \in [\![1, n_y]\!]$, consider the $(i, j)-$th cilium associated with the source term $\mathbf{f}_{ij}\delta_{\Gamma_{ij}}$ (we omit in this subsection the subscript (i, j), for the sake of simplicity). In the variational formulation of the source term, using a test function $\mathbf{v} \in (\mathcal{D}(\Omega))^3$, the source term would be

$$\left\langle \mathbf{f}(\cdot, t)\delta_{\Gamma(t)}, \mathbf{v} \right\rangle_{(\mathcal{D}'(\Omega))^3,(\mathcal{D}(\Omega))^3} = \int_{\Gamma(t)} \mathbf{f}(\cdot, t) \cdot \mathbf{v} \, \mathrm{d}x \, \mathrm{d}y \, \mathrm{d}z.$$

Aiming at studying the first component of the system, namely choosing $\mathbf{v} = (v, 0, 0)$, we focus on

$$\left\langle f_x(\cdot, t)\delta_{\Gamma(t)}, v \right\rangle_{\mathcal{D}'(\Omega),\mathcal{D}(\Omega)} = \int_{\Gamma(t)} f_x(\cdot, t)\, v \, \mathrm{d}x \, \mathrm{d}y \, \mathrm{d}z.$$

Next choosing $v := v(z)$, we define

$$\left\langle \overline{f_x(\cdot, t)\delta_{\Gamma(t)}}^{x,y}, v \right\rangle_{\mathcal{D}'(0,L_z),\mathcal{D}(0,L_z)} = \frac{1}{L_x L_y} \left\langle f_x(\cdot, t)\delta_{\Gamma(t)}, \tilde{v} \right\rangle_{\mathcal{D}'(\Omega),\mathcal{D}(\Omega)}$$

by considering the natural extension from $(0, L_z)$ to Ω (we recall that Ω is periodic in x and y):

$$\begin{array}{rccc} \tilde{\cdot} & : & \mathcal{D}(0, L_z) & \mapsto & \mathcal{D}(\Omega) \\ & & [z \mapsto v(z)] & \to & [z \mapsto \tilde{v}(x, y, z) = v(z)]. \end{array}$$

This process actually defines the averaging process with respect to x and y in the treatment of the source term. As a consequence, using the parametrization $s \mapsto \boldsymbol{\xi}(s, t)$ of the cilium

$$\begin{aligned} \left\langle \overline{f_x(\cdot, t)\delta_{\Gamma(t)}}^{x,y}, v \right\rangle_{\mathcal{D}'(0,L_z),\mathcal{D}(0,L_z)} &= \frac{1}{L_x L_y} \int_{\Gamma(t)} f_x((x, y, z); t)\, v(z) \, \mathrm{d}x \, \mathrm{d}y \, \mathrm{d}z \\ &= \frac{1}{L_x L_y} \int_0^L f_x(\boldsymbol{\xi}(s, t); t)\, v(\xi_z(s, t)) \, |\nabla \boldsymbol{\xi}(s, t)| \, \mathrm{d}s \\ &= \frac{1}{L_x L_y} \int_0^L \hat{f}_x(s, t)\, v(\xi_z(s, t)) \, |\nabla \boldsymbol{\xi}(s, t)| \, \mathrm{d}s. \end{aligned}$$

Chapter 2

Estimation of the mucus secretion rate in the bronchial tree

2.1 Introduction

In Chapter 1, we studied a 3D model of mucociliary transport in a sample of pulmonary bronchus. Now we would like to extend this work over an entire bronchial tree but with a 1D reduced model. Through this work, we will estimate mucus thickness in each generation of bronchus. As a reminder, mucus is a fluid naturally secreted by the epithelium, more precisely at the level of the submucosal glands and goblet cells. The cells secreting mucus become less and less numerous as we move towards the peripheral respiratory tract [51]. Likewise, the ciliary density is less and less important as one advances towards the peripheral respiratory airways [51]. Moreover, there is no secretion of mucus at the level of the alveoli. In our model, we will simplify by taking a constant ciliary and cell secretion density in each bronchus.

One of the great difficulties in the study of mucociliary clearance is the lack of experimental data. The complex structure of the bronchial tree makes in vivo measurements impossible from the sixth generation. Furthermore, very little data has been provided on the rate of mucus production as well as on the thickness of the mucus layer in each generation of bronchus. This is why it would be interesting to develop a mathematical model providing access to estimates of the rate of mucus secretion, which is difficult to obtain through experiments.

Mathematical modeling of mucociliary clearance has been the center of attention since the late 1960s. A recent work have been devoloped by Kurbatova et al [37]. Based on a model of Smith et al [71], Kurbatova et al [37] studied the evolution of the quantity of mucus secreted by the submucosal glands, in a bronchial tree model. In cystic fibrosis lungs, the authors studied the influence of the aerosolized and inhaled drug dornase alfa on mucus viscosity, and therefore the effectiveness of mucociliary clearance. Another recent work on modeling of mucociliary clearance that we can cite is that of Volpert et al [8]. The authors studied mucociliary clearance in a case of viral infection in the lungs. Based on a model developed by [37] that studies mucus velocity due to cilia beating, coupled with a model describing the spreading of the viral infection through generations of the bronchial tree. The authors studied mucus accumulation and stagnation both because of its production, but also because of an impairment of cilia beating velocity due to an increase of mucus viscosity resulting from the infection.

In our model, we aim to obtain a realistic representation of mucociliary clearance. Also, through our work, we would like to estimate the rate of mucus production by the submucosal glands. To make

the model feasible, the study of the thicknesses of the mucus layer will be done only as a function of generation. We will then associate to each generation a constant thickness of the mucus layer and an average speed of mucus flow obtained thanks to a 1d reduced model for ciliary activity. We will only consider the first 17 generations of bronchi of a symmetrical tree while taking into account the sizes of each bronchus of a certain generation. Also, cilia are supposed to have the same length and thickness. The frequency of beating of the cilia is assumed to be equal to 22Hz at the level of the trachea and it decreases as we advance through the generations until 7Hz at the level of the last generation.

Also, mucus is a non-Newtonian viscoelastic fluid [39], it therefore has elastic properties. Filloche et al [19] studied a model of mucociliary transport where mucus is considered viscoelastic. It comes to a consequence that for a healthy mucus, and a frequency of cilia beating from 5 to 20 Hz, the viscoelastic effects of the mucus can be neglected. In our model, the mucus will thus be considered as a Newtonian fluid, the same as for the PCL.

2.2 Model, notations and assumptions

2.2.1 Model of mucus flow in the bronchial tree

We consider a bronchial tree of N generations, numbered from 0 to $N-1$. Each generation i is characterized by a typical bronchus of (fixed) length ℓ_i^b, (fixed) radius r_i^b. But the bronchus wall is covered with a bifluid composed of PCL+mucus: the low viscous PCL adheres to the bronchial walls and the radial position of the (fixed) PCL/mucus interface is located at $r_i^m := r_i^b - h$ (which means that the PCL thickness is h, which is assumed to be fixed). Then the mucus may be observed within the radial range (r_i^a, r_i^m), where r_i^a denotes the (variable) radial position of the mucus/air interface, as air is driven in the center of the bronchus, namely in the radial range $(0, r_i^a)$. Therefore we have

$$0 < r_i^a < r_i^m < r_i^b.$$

The mean axial velocity of mucus in each generation is governed by the 1D model referred to the (M+A) problem, which is derived in section 2.2.2 by averaging with respect to z and θ the Stokes equations expressed in cylindrical coordinates. The dynamic of the mucus arises from the *motility* of cilia (modeled by c_1 and c_2) and by the *airflow* induced by a breathing scenario.

- (M+A) problem:

$$\left\{\begin{array}{rcl} -\frac{1}{r}\frac{\mathrm{d}}{\mathrm{d}r}\left(r\mu(r)\frac{\mathrm{d}U_i}{\mathrm{d}r}(r)\right) + c_1(r)U_i(r) &=& c_2(r)+f_1, \quad r \in (r_i^a, r_i^b), \\ U_i(r_i^b) &=& 0, \\ -\left[\mu\frac{\mathrm{d}U_i}{\mathrm{d}r}\right](r_i^a) &=& f_2, \end{array}\right.$$

  where c_1, c_2, f_1, f_2 are described in the forthcoming subsections, and the viscosity is defined as

$$\mu(r) = \left\{\begin{array}{ll} \mu_{\mathrm{m}}, & r \in (r_i^a, r_i^m) \quad \text{i.e. in the mucus,} \\ \mu_{\mathrm{w}}, & r \in (r_i^m, r_i^b) \quad \text{i.e. in the PCL.} \end{array}\right.$$

As a matter of fact, the (M+A) problem can be divided into two contributions:

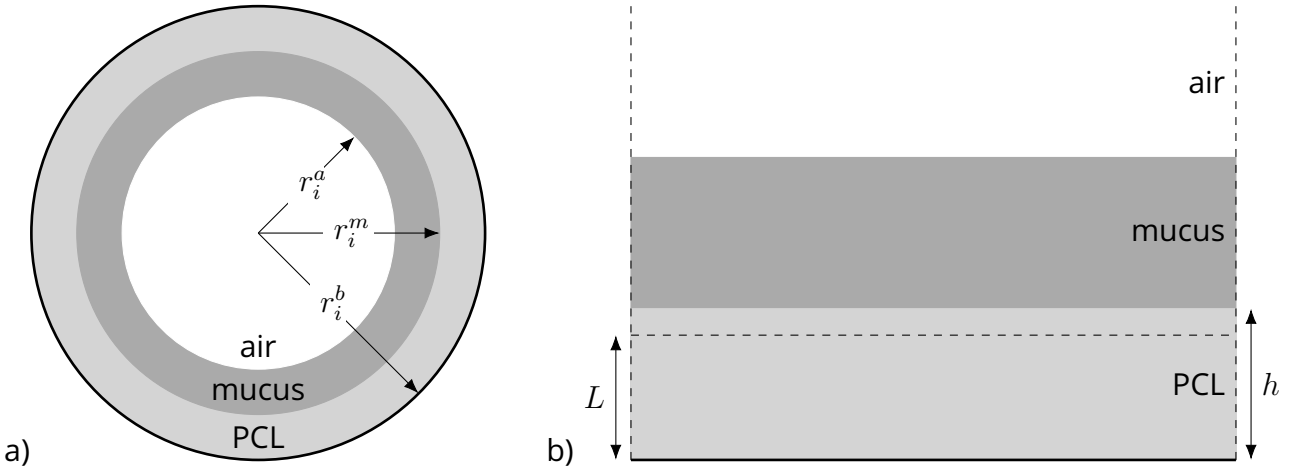

Figure 2.1 – Schematic view of a bronchus at generation i. a) : Radial section. The rigid wall is located at $\{r = r_i^b\}$. The bronchial wall is lined with a bifluid made of two layers: the PCL and mucus (the PCL-mucus interface is located at $\{r = r_i^m\}$). The center of the bronchus is filled with air (the air-mucus interface is located at $\{r = r_i^a\}$. b) Axial section, near the bronchus wall. Active cilia (length L) are attached to the wall and completely immersed in the PCL (i.e. $L < h = r_i^b - r_i^m$); the collective beating of the cilia leads to a motion of the PCL+mucus fluid.

- (M) problem:

$$\begin{cases} -\frac{1}{r}\frac{\mathrm{d}}{\mathrm{d}r}\left(r\mu(r)\frac{\mathrm{d}u_i}{\mathrm{d}r}(r)\right) + c_1(r)u_i(r) &= c_2(r), \quad r \in (r_i^a, r_i^b), \\ u_i(r_i^b) &= 0, \\ -\left[\mu\frac{\mathrm{d}u_i}{\mathrm{d}r}\right](r_i^a) &= 0. \end{cases}$$

- (A) problem:

$$\begin{cases} -\frac{1}{r}\frac{\mathrm{d}}{\mathrm{d}r}\left(r\mu(r)\frac{\mathrm{d}v_i}{\mathrm{d}r}(r)\right) + c_1(r)v_i(r) &= f_1, \quad r \in (r_i^a, r_i^b), \\ v_i(r_i^b) &= 0, \\ -\left[\mu\frac{\mathrm{d}v_i}{\mathrm{d}r}\right](r_i^a) &= f_2. \end{cases}$$

Remark 9. *The velocities $r \mapsto U_i(r)$, $r \mapsto u_i(r)$, $r \mapsto v_i(r)$ are defined on (r_i^a, r_i^b) where r_i^a denotes the (variable) radial position of the mucus/air interface and r_i^b is the (fixed) radial position of the bronchus wall.*

Definition 1. *We denote, without possible ambiguity, the mucus flows at generation i*

$$Q_i(U_i; r_i^a) = 2\pi \int_{r_i^a}^{r_i^m} r\, U_i(r)\, \mathrm{d}r, \quad Q_i(u_i; r_i^a) = 2\pi \int_{r_i^a}^{r_i^m} r\, u_i(r)\, \mathrm{d}r, \quad Q_i(v_i; r_i^a) = 2\pi \int_{r_i^a}^{r_i^m} r\, v_i(r)\, \mathrm{d}r$$

where U_i, u_i, v_i are the solutions of the (M+A), (M), (A) problems respectively.

Remark 10. *By linearity, the solution U_i of the (M+A) problem is the sum of the solution of (M) problem and of the (A) problem:*

$$U_i = u_i + v_i.$$

Note that

- *u_i corresponds to the solution for which airflow is neglected ($f_1 = f_2 = 0$);*
- *v_i corresponds to the solution taking into account the effects induced by the airflow in the center of the bronchus; in this problem, the ciliary activity is neglected, even if the backflow term (modeled by $c_1(r)v_i(r)$) is still taken into account as a resistive force due to the presence of the (passive) cilia.*

After describing the mucus dynamics within each generation, let us describe the evolution of the mucus distribution all along the bronchial tree. Based upon mass flow conservation, the model is governed by the set of equations:

$$\frac{\mathrm{d}r_i^a}{\mathrm{d}t}(t) = \frac{Q_i(U_i; r_i^a(t)) - 2Q_{i+1}(U_{i+1}; r_{i+1}^a(t)) - \phi_i}{2\pi \ell_i^b r_i^a(t)}, \qquad i \in \{0, ..., N-1\}, \tag{2.1}$$

where $t \mapsto r_i^a(t)$ is the (variable) radial position of the air/mucus interface within generation at generation i, Q_i is the flow of mucus at generation i (the flow depends on the radial position r_i^a of the air/mucus interface and also on the mean axial velocity of the fluid U within the mucus, to be described later), ϕ_i is the flux of mucus secreted at generation i. Note that mucus production occurs from generations 0 to $N = 16$, so that we artificially define $Q_N \equiv 0$.

Assumption 1. *Cilia do not penetrate the mucus: $L < h$. In particular it implies that u_i is constant in the mucus in each generation i.*

Assumption 2. *The secretion term is proportional to the bronchial surface:*

$$\phi_i = 2\pi\, r_i^b\, \ell_i^b\, \tilde{\phi}.$$

Assumption 3. *The bronchus length $\ell_i^b \gg \lambda$ in every generation, where λ is the length of the metachronal wave.*

We assume that Assumptions 1 and 2 and 3 hold from now on.

Remark 11. *The normalization process of the secretion term induces that $\tilde{\phi}$ is homogeneous to $\mu m \cdot s^{-1}$. It means that an epithelial cell of surface h^2 (in μm^2) produces a flux of mucus corresponding to $\tilde{\phi}h^2$ expressed in $\mu m^3 \cdot s^{-1}$.*

Remark 12. *In the forthcoming section, the velocity distribution $\mathbf{u}$ is periodic in z with a period of λ, so for $n \in \mathbb{N}$ the periodicity of $\mathbf{u}$ holds in a bronchus with $\ell_i^b = n\lambda$ in every generation, which is not the case but can be neglected using the assumption 3.*

2.2.2 Derivation of the model of mucus flow in the bronchial tree

Let us describe how (M+A) problem has been derived. For that purpose we deal with a generic bronchial generation. Let

$$\Omega_i = \{(r, \theta, z),\ 0 \le \theta \le 2\pi,\ 0 \le z \le \ell_i^b,\ r_i^a \le r \le r_i^b\},$$

denote the space occupied by the liquid within the bronchus. The fluid domain divides into two areas: the PCL, occupied by a fluid of viscosity μ_1, is the subdomain $\Omega_i^{\mathrm{m}} := \{(r, \theta, z),\ r_i^m \le r \le r_i^b\}$; the mucus, occupied by a fluid of viscosity $\mu_2 > \mu_1$ is the subdomain $\Omega_i^{\mathrm{PCL}} := \{(r, \theta, z),\ r_i^a \le r \le r_i^m\}$. In this context, we define

$$\mu(r) = \begin{cases} \mu_{\mathrm{m}} & \text{if } (r, \theta, z) \in \Omega_i^{\mathrm{m}}, \\ \mu_{\mathrm{PCL}} & \text{if } (r, \theta, z) \in \Omega_i^{\mathrm{PCL}}. \end{cases}$$

The interface between the PCL and the mucus is located at $\Gamma_i^{\mathrm{m}} = \{r = r_i^m\}$. The interface between the mucus and air that flows in the bronchial lumen is located at $\Gamma_i^{\mathrm{a}} = \{r = r_i^a\}$. We consider a list of N thin structures immersed in Ω_i and fixed to the bronchial wall $\Gamma_i^{\mathrm{b}} := \{r = r_i^b\}$. We denote by $\{s \mapsto \boldsymbol{\xi}^{(j)}(s,t)\}_{j=0,\cdots,N-1}$ the parametrization of their motion at time t. Note that in the context of a viscous flow governed by Stokes equations, the system is instantaneous and time only plays the role of a parameter (therefore it will be regularly omitted when no ambiguity emerges from the equations). The resulting mathematical problem consists in finding a velocity field $(r,\theta,z) \mapsto \mathbf{u}(r,\theta,z)$ and a pressure field $(r,\theta,z) \mapsto p(r,\theta,z)$ such that $(\mathbf{u}, p)$ are periodic in z and θ and

$$\left\{\begin{array}{rcll} -\mathrm{div}(\mu\nabla\mathbf{u}) + \nabla p &=& \displaystyle\sum_j \mathbf{f}_j[\mathbf{u}]\,\delta_{\Gamma_j} & \text{in } \Omega_i, \\ \mathrm{div}(\mathbf{u}) &=& 0 & \text{in } \Omega_i, \\ \mathbf{u}\cdot\mathbf{n} &=& 0 & \text{on } \Gamma_i^{\mathrm{a}}, \\ [(\mu\nabla\mathbf{u} - p\mathbb{I})\cdot\mathbf{n}]\cdot\mathbf{t} &=& [\sigma_{\mathrm{air}}\cdot\mathbf{n}]\cdot\mathbf{t} & \text{on } \Gamma_i^{\mathrm{a}}, \\ \mathbf{u} &=& 0 & \text{on } \Gamma_i^{\mathrm{b}}. \end{array}\right. \tag{2.2}$$

Note that boundary conditions express the following properties: at the bronchial wall, the viscous fluid adheres to the wall; at the mucus-air interface, free slip boundary conditions (or no-penetration boundary conditions) are considered, involving the shear stress σ_{air} of air flowing within the lumen.

About the terms related to the action of air over the fluid

Air flows through the bronchus in the lumen which corresponds to the domain

$$\Omega_i^{\mathrm{air}} = \{(r,\theta,z),\ 0 \le \theta \le 2\pi,\ 0 \le z \le \ell_i^b,\ 0 \le r \le r_i^a\},$$

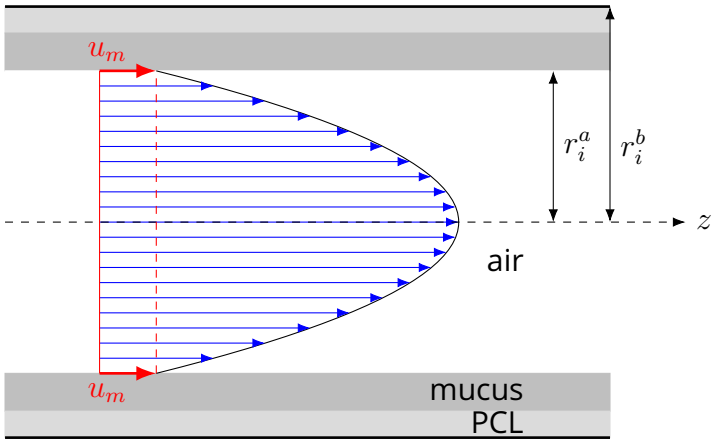

Figure 2.2 – Idealized air flow in a bronchus, whose lumen is reduced by the mucus at the bronchial walls.

We assume that air is an incompressible fluid with viscosity μ_{air} and it is driven by a Poiseuille flow in Ω_i^{air}. Let us first describe the flow profile:

- the air pressure field varies linearly in z:

$$p_{|\text{air}}(r,\theta,z) = P_{\text{in},i} + \frac{z}{\ell_i^b}\left(P_{\text{out},i} - P_{\text{in},i}\right).$$

  Here $P_{\text{in},i}$ (resp. $P_{\text{out},i}$) represents the pressure field at the entrance (resp. exit) of the bronchus. The airflow is precisely driven by the pressure drop.

- the air velocity profile is defined as $\mathbf{u}_{|\text{air}}(r,\theta,z) = (0,0,u_{z|\text{air}}(r))$ with

$$u_{z|\text{air}}(r) = \frac{r_{a,i}^2}{4\mu_{air}}\frac{P_{\text{in},i} - P_{\text{out},i}}{\ell_i^b}\left(1 - \frac{r^2}{r_{a,i}^2}\right) + u_m, \qquad r \in (0, r_i^a).$$

  where u_m is the air velocity at the mucus/air interface corresponding, by continuity, to the mucus velocity.

Let us now compute the shear rate at the mucus/air interface:

$$\partial_r u_{z|\text{air}}(r_i^a) = -\frac{a}{2\mu_{air}\ell_i^b}(P_{\text{in},i} - P_{\text{out},i}).$$

Let us now relate the airflow to the pressure drop:

$$\Phi_i^{\text{air}} := 2\pi\int_0^{r_i^a} r\, u_{z|\text{air}}(r)\,\mathrm{d}r = \underbrace{\frac{\pi(r_i^a)^4}{8\mu_{\text{air}}\ell_i^b}(P_{\text{in},i} - P_{\text{out},i})}_{(*)} + \underbrace{\pi(r_i^a)^2 u_m}_{(**)}.$$

We may notice that the relationship has a classical contribution $(*)$ that expresses the Poiseuille law and an extra term $(**)$ due to the mucus velocity.

As a concluding remark, we may express the shear rate at the mucus/air interface and the mean pressure drop as a function of the air flux that flows through the bronchus:

$$\begin{aligned}
\frac{P_{\text{in},i} - P_{\text{out},i}}{\ell_i^b} &= \frac{8\mu_{\text{air}}\Phi_i^{\text{air}}}{\pi(r_i^a)^4} - \frac{8\mu_{\text{air}}}{(r_i^a)^2}u_m,\\
\partial_r u_{z|\text{air}}(r_i^a) &= -\frac{4\Phi_i^{\text{air}}}{\pi(r_i^a)^3} + \frac{4}{r_i^a}u_m.
\end{aligned}$$

Notice that the mucus velocity u_m provides an extra term in the computation of the pressure drop and shear rate. However these extra terms will be neglected due to the smallness of the mucus velocity, see the following Remark, and we get:

$$\frac{P_{\text{in},i} - P_{\text{out},i}}{\ell_i^b} = \frac{8\mu_{\text{air}}\Phi_i^{\text{air}}}{\pi(r_i^a)^4}, \tag{2.3}$$

$$\partial_r u_{z|\text{air}}(r_i^a) = -\frac{4\Phi_i^{\text{air}}}{\pi(r_i^a)^3}. \tag{2.4}$$

Remark 13. *The above assumption relies on the following properties*

$$\frac{8\mu_{\text{air}}}{(r_i^a)^2}u_m \ll \frac{8\mu_{\text{air}}\Phi_i^{\text{air}}}{\pi(r_i^a)^4}, \qquad \frac{4}{r_i^a}u_m \ll \frac{4\Phi_i^{\text{air}}}{\pi(r_i^a)^3},$$

which are both equivalent to

$$\frac{\pi u_m (r_i^a)^2}{\Phi_i^{\text{air}}} \ll 1.$$

This holds true at any generation:

- *in the most proximal generation (the trachea, corresponding to $i = 0$), the mucus velocity u_m is about $100\,\mu m \cdot s^{-1}$; the bronchial radius is about $r_0^a \sim 1 \cdot 10^{+4}\,\mu m$ (see Table 2.1) and air flow $\Phi_0^{\rm air} = \Phi_0^{\rm air}$, where $\Phi_0^{\rm air} \sim 1\,l \cdot s^{-1} = 10^{+15}\,\mu m^3 \cdot s^{-1}$ is the air flow at mouth. Thus we get:*

$$\frac{\pi u_m (r_0^a)^2}{\Phi_0^{\rm air}} \sim 10^{-5}.$$

- *in the most distal generation ($i = 16$), the mucus velocity u_m is about $100\,\mu m \cdot s^{-1}$; the bronchial radius is about $r_{16}^a \sim 250\,\mu m$ (see Table 2.1) and air flow $\Phi_{16}^{\rm air} = \Phi_0^{\rm air}/2^{16}$. Thus we get:*

$$\frac{\pi u_m (r_{16}^a)^2}{\Phi_{16}^{\rm air}} \sim 10^{-3}.$$

Derivation of a reduced model in cylindrical coordinates

Using cylindrical coordinates, we write the velocity field as $\mathbf{u}(r,\theta,z,t) = u_r(r,\theta,z,t)\mathbf{e}_r + u_\theta(r,\theta,z,t)\mathbf{e}_\theta + u_z(r,\theta,z,t)\mathbf{e}_z$. In the same way, the parametrized description of the cilia reads: for all $s \in [0,L]$, $t > 0$,

$$\begin{aligned} \boldsymbol{\xi}(s,t) &= \xi_r(s,t)\mathbf{e}_r + \xi_z(s,t)\mathbf{e}_z \\ \mathbf{f}(s,t) &= f_r(s,t)\mathbf{e}_r + f_z(s,t)\mathbf{e}_z \end{aligned} \tag{2.5}$$

Using cylindrical coordinates, Eq. (2.2)$_{(1,2)}$ become

$$\left\{ \begin{array}{rcll} -\frac{1}{r}\frac{\partial}{\partial r}(r\mu\frac{\partial u_r}{\partial r}) - \mu(\frac{1}{r^2}\frac{\partial^2 u_r}{\partial \theta^2} + \frac{\partial^2 u_r}{\partial z^2} - \frac{u_r}{r^2} + \frac{2}{r^2}\frac{\partial u_\theta}{\partial \theta}) + \frac{\partial p}{\partial r} &=& \sum_{j=1}^M f_r^j \delta_{\Gamma_i(t)} & \text{in } \Omega_i, \\ -\frac{1}{r}\frac{\partial}{\partial r}(r\mu\frac{\partial u_\theta}{\partial r}) - \mu(\frac{1}{r^2}\frac{\partial^2 u_\theta}{\partial \theta^2} + \frac{\partial^2 u_\theta}{\partial z^2} - \frac{u_\theta}{r^2} + \frac{2}{r^2}\frac{\partial u_r}{\partial \theta}) + \frac{\partial p}{\partial \theta} &=& 0 & \text{in } \Omega_i, \\ -\frac{1}{r}\frac{\partial}{\partial r}(r\mu\frac{\partial u_z}{\partial r}) - \mu(\frac{1}{r^2}\frac{\partial^2 u_z}{\partial \theta^2} + \frac{\partial^2 u_z}{\partial z^2}) + \frac{\partial p}{\partial z} &=& \sum_{j=1}^M f_z^j \delta_{\Gamma_j(t)} & \text{in } \Omega_i, \\ \frac{1}{r}\frac{\partial (r u_r)}{\partial r} + \frac{1}{r}\frac{\partial u_\theta}{\partial \theta} + \frac{\partial u_z}{\partial z} &=& 0 & \text{in } \Omega_i. \end{array} \right. \tag{2.6}$$

whereas Eq. (2.2)$_{(3,4,5)}$, that describe boundary conditions at the mucus-air interface $\{r = r_i^a\}$ and on the bronchial wall $\{r = r_i^b\}$ read (note that $\mathbf{n} = \mathbf{e}_r$ and $\boldsymbol{\tau} = \mathbf{e}_z$ or $\mathbf{e}_\theta$):

$$\left\{ \begin{array}{rcll} \sigma_{r\theta} = \mu(\frac{1}{r}\frac{\partial u_r}{\partial \theta} + \frac{\partial u_\theta}{\partial r} - \frac{u_\theta}{r}) &=& \sigma_{r\theta|\rm air} & \text{on } \Gamma_i^{\rm a}, \\ \sigma_{rz} = \mu(\frac{1}{r}\frac{\partial u_r}{\partial z} + \frac{\partial u_z}{\partial r}) &=& \sigma_{rz|\rm air} & \text{on } \Gamma_i^{\rm a}, \\ u_r &=& 0 & \text{on } \Gamma_i^{\rm a}, \\ u_r = u_\theta = u_z &=& 0 & \text{on } \Gamma_i^{\rm b}. \end{array} \right. \tag{2.7}$$

Now let us describe how to derive an averaged 1D model. We first use the periodicity structure of the problem:

- The velocity and pressure fields are $\theta-$periodic and thus

$$\int_0^{2\pi} \partial_\theta^n u_r \,\mathrm{d}\theta = 0, \quad \int_0^{2\pi} \partial_\theta^n u_z \,\mathrm{d}\theta = 0, \quad \int_0^{2\pi} \partial_\theta^n u_\theta \,\mathrm{d}\theta = 0, \quad \int_0^{2\pi} \partial_\theta p \,\mathrm{d}\theta = 0, \qquad n = 1, 2.$$

- The velocity field is $z-$periodic, with period λ (the length of the metachronal wave), so that considering bronchi with length $\ell_i^b = k_i\lambda$ ($k_i \in \mathbb{N}$), we have

$$\int_0^{\ell_i^b} \partial_z^n u_r \,\mathrm{d}z = 0, \quad \int_0^{\ell_i^b} \partial_z^n u_z \,\mathrm{d}z = 0, \quad \int_0^{\ell_i^b} \partial_z^n u_\theta \,\mathrm{d}z = 0, \qquad n = 1, 2.$$

We now define the averaging process as

$$\overline{\mathcal{F}}^{\theta,z}(r) = \frac{1}{2\pi\ell_i^b}\int_0^{\ell_i^b}\int_0^{2\pi}\mathcal{F}(r,\theta,z)\,\mathrm{d}z\,\mathrm{d}\theta.$$

Next averaging Eq. (2.6) with respect to z et θ, we get

$$\left\{\begin{array}{rcll} \frac{\mathrm{d}\overline{p}^{\theta,z}}{\mathrm{d}r} & = & \sum_{j=1}^M \overline{f_r^j\delta_{\Gamma_i(t)}}^{\theta,z} & \text{in } (r_i^a, r_i^b), \\ -\frac{1}{r}\frac{\mathrm{d}}{\mathrm{d}r}(r\mu\frac{\mathrm{d}\overline{u}_\theta^{\theta,z}}{\mathrm{d}r}) + \frac{\mu}{r^2}\overline{u}_\theta^{\theta,z} & = & 0 & \text{in } (r_i^a, r_i^b), \\ -\frac{1}{r}\frac{\mathrm{d}}{\mathrm{d}r}(r\mu\frac{\mathrm{d}\overline{u_z}^{\theta,z}}{\mathrm{d}r}) + \frac{1}{\ell_i^b}(\overline{p}_{\mathrm{out}}^\theta - \overline{p}_{\mathrm{in}}^\theta) & = & \sum_{j=1}^M \overline{f_z^j\delta_{\Gamma_j(t)}}^{\theta,z} & \text{in } (r_i^a, r_i^b), \\ \frac{1}{r}\frac{\mathrm{d}}{\mathrm{d}r}(r\overline{u_r}^{\theta,z}) & = & 0 & \text{in } (r_i^a, r_i^b), \end{array}\right. \tag{2.8}$$

where $p_{\mathrm{in}} =: p(\cdot,\cdot,0)$ (resp. $p_{\mathrm{out}} =: p(\cdot,\cdot,\ell_i^b)$) stands for the pressure at the entrance (resp. exit) of the bronchus.

Remark 14. *We may notice that the average system introduces the $\theta-$average pressure drop within the bronchus $r \mapsto \overline{p}_{\mathrm{out}}^\theta(r) - \overline{p}_{\mathrm{in}}^\theta(r)$.*

Actually integrating Eq. (2.6)$_{(1)}$ *with respect to θ only gives*

$$-\frac{1}{r}\frac{\partial}{\partial r}(r\mu\frac{\partial\overline{u_r}^\theta}{\partial r}) - \mu(\frac{\partial^2\overline{u_r}^\theta}{\partial z^2} - \frac{\overline{u_r}^\theta}{r^2}) + \frac{\partial\overline{p}^\theta}{\partial r} = \sum_{j=1}^M \overline{f_r^j\delta_{\Gamma_i(t)}}^\theta$$

and evaluation of this equation at $z=0$ and $z=\ell_i^b$ gives, by subtraction and periodicity of the involved quantities (including the source term) :

$$\frac{\partial\overline{p}^\theta}{\partial r}(r, z=\ell_i^b) - \frac{\partial\overline{p}^\theta}{\partial r}(r, z=0) = 0$$

that is

$$\frac{\mathrm{d}}{\mathrm{d}r}(\overline{p}_{\mathrm{out}}^\theta - \overline{p}_{\mathrm{in}}^\theta) = 0.$$

In other words, the pressure drop $\overline{p}_{\mathrm{out}}^\theta - \overline{p}_{\mathrm{in}}^\theta$ does not depend on the radial variable and we will use this quantity as a constant denoted $P_{\mathrm{in},i} - P_{\mathrm{out},i}$.

Terms involved in the boundary conditions (2.7) may be also averaged with respect to z and θ. This gives:

$$\left\{\begin{array}{rcll} \mu(\partial_r\overline{u}_\theta^{\theta,z} - \frac{\overline{u}_\theta^{\theta,z}}{r}) & = & \overline{\sigma}_{r\theta|\mathrm{air}}^{\theta,z} & \text{on } \{r=r_i^a\}, \\ \mu\partial_r\overline{u}_z^{\theta,z} & = & \overline{\sigma}_{rz|\mathrm{air}}^{\theta,z} & \text{on } \{r=r_i^a\}, \\ u_r & = & 0 & \text{on } \{r=r_i^a\}, \\ \overline{u}_r^{\theta,z} = \overline{u}_\theta^{\theta,z} = \overline{u}_z^{\theta,z} & = & 0 & \text{on } \{r=r_i^b\}. \end{array}\right. \tag{2.9}$$

We may notice that some precise meaning has to be given for the average source terms $\overline{f_r^j\delta_{\Gamma_i(t)}}^{\theta,z}$ and $\overline{f_z^j\delta_{\Gamma_j(t)}}^{\theta,z}$. Beyond this precise definition, let us briefly comment each equation of Eq. (2.8):

- Eq. (2.8)$_{(1)}$ relates the radial variation of the pressure along the bronchus with respect to the ciliary activity: a simple integration provides the pressure distribution.

- Eq. (2.8)$_{(2)}$ combined with Eq. (2.9)$_{(4)}$ (in particular $\overline{u}_\theta^{\theta,z}(r_i^a) = 0$, at the bronchial wall) implies

$$\overline{u}_\theta^{\theta,z} \equiv 0.$$

  This is compatible with a suitable choice for $\overline{\sigma}_{r\theta|\text{air}}^{\theta,z}$ that has to be 0 (so that Eq. (2.9)$_{(1)}$ is satisfied): for instance, this property holds if the airflow is axisymmetric in the lumen of the bronchus.

- Eq. (2.8)$_{(3)}$ relates the mean axial velocity of the mucus to the ciliary activity and airflow; note that airflow has a twofold influence on the mucus dynamics: first through the pressure drop $\frac{1}{\ell_i^b}(\overline{p}_{\text{out}}^\theta - \overline{p}_{\text{in}}^\theta)$, second through the shear stress imposed on the mucus at the mucus-air interface (see Eq. (2.9)$_{(2)}$).

- Eq. (2.8)$_{(4)}$ combined with Eq. (2.9)$_{(4)}$ (in particular $\overline{u}_r^{\theta,z}(r_i^a) = 0$, at the bronchial wall) implies

$$\overline{u}_r^{\theta,z} \equiv 0.$$

The average 1D model that governs the behaviour of the mean axial velocity $\overline{u_z}^{\theta,z}$ finally writes:

$$\begin{cases} -\frac{1}{r}\frac{\mathrm{d}}{\mathrm{d}r}(r\mu\frac{\mathrm{d}\overline{u_z}^{\theta,z}}{\mathrm{d}r}) + \frac{P_{\text{out},i}-P_{\text{in},i}}{\ell_i^b} &=& \sum_{j=1}^M \overline{f_z^j}^{\theta,z}\delta_{\Gamma_j(t)} & \text{in } (r_i^a, r_i^b), \\ \mu\frac{\mathrm{d}}{\mathrm{d}r}\overline{u}_z^{\theta,z} &=& \overline{\sigma}_{rz|\text{air}}^{\theta,z} & \text{on } \{r = r_i^a\}, \\ \overline{u}_z^{\theta,z} &=& 0 & \text{on } \{r = r_i^b\}. \end{cases} \tag{2.10}$$

Still postponing the averaging process of the source term, let us highlight the influence of air on the whole process, i.e. let us describe f_1 and f_2:

- **Source term f_1.** The pressure drop is associated to the airflow in generation i. Poiseuille law in a bronchus of generation i relates the pressure drop ($p_{\text{in},i} - p_{\text{out},i}$) to the fluid flow ($\phi_i^{\text{air}}$) through the dimensions of the bronchus (length ℓ_i^b, radius r_i^a) and the properties of the fluid (viscosity μ_{air}):

$$\frac{P_{\text{in},i} - P_{\text{out},i}}{\ell_i^b} = \frac{8\mu_{\text{air}}}{\pi(r_i^a)^4}\phi_i^{\text{air}}.$$

  The flux of air at generation i, denoted ϕ_i^{air}, divides in two at the next generation: therefore $\phi_i^{\text{air}} = 2\phi_{i+1}^{\text{air}}$. Furthermore we denote by $\Phi_{\text{mouth}}^{\text{air}}$ the flux of air at the trachea (generation 0), so that $\phi_i^{\text{air}} = \Phi_{\text{mouth}}^{\text{air}}/2^i$. Thus, in the definition of the (M+A) problem, we get

$$f_1 = \frac{8\mu_{\text{air}}\Phi_{\text{mouth}}^{\text{air}}}{2^i\pi(r_i^a)^4}. \tag{2.11}$$

- **Boundary source term f_2.** It comes from boundary condition that holds at the mucus-air interface: in the air, we have $\sigma_{rz|\text{air}} = \mu_{\text{air}}(\frac{1}{r}\partial_z u_{r|\text{air}} + \partial_r u_{z|\text{air}})$, hence $\overline{\sigma}_{rz|\text{air}}^{\theta,z} = \mu_{\text{air}}\partial_r\overline{u}_{z|\text{air}}^{\theta,z}$. Thus the boundary condition reads $\mu_{\text{m}}\partial_r\overline{u}_z^{\theta,z} = \mu_{\text{air}}\partial_r\overline{u}_{z|\text{air}}^{\theta,z}$, on $\{r = r_i^a\}$ or

$$-\mu_{\text{m}}\partial_r\overline{u}_z^{\theta,z} = -\mu_{\text{air}}\partial_r\overline{u}_{z|\text{air}}^{\theta,z}, \quad \text{on } \{r = r_i^a\}$$

Let us recall that, by Eq. (2.4), we have $\partial_r u_{z|\mathrm{air}}(r_i^a) = -\dfrac{4\Phi_i^{\mathrm{air}}}{\pi(r_i^a)^3}$. Thus we get

$$-\mu_{\mathrm{m}}\partial_r \overline{u}_z^{\theta,z} = \mu_{\mathrm{air}}\frac{4\Phi_{\mathrm{mouth}}^{\mathrm{air}}}{2^i\pi(r_i^a)^3}, \quad \text{on } \{r = r_i^a\}$$

hence

$$f_2 = \frac{4\mu_{\mathrm{air}}\Phi_{\mathrm{mouth}}^{\mathrm{air}}}{2^i\pi(r_i^a)^3}. \tag{2.12}$$

Now let us describe the averaging process of the singular source term, namely $\sum_{j=1}^{M} \overline{f_z^j \delta_{\Gamma_j(t)}}^{\theta,z}$. All the previous terms can be obtained through the variational formulation of the 3d problem: using a test function $\phi \in \mathcal{V} := \{\phi \in \mathcal{D}([r_i^a, r_i^b) \times (2\pi\mathbb{T}) \times (\ell_i^b\mathbb{T}))^3$, such that ϕ is periodic in θ and $z\}$ (here $\mathbb{T}$ denotes the 1-periodic torus) and integrating over the whole domain, we build the variational formulation of the 3d problem. Then taking test functions that do not depend on θ and z (this is possible because of the periodicity with respect to θ and z, which is included in the functional space), and considering the functional space (obtained by a simple density argument)

$$V = \{v \in H^1(r_i^a, r_i^b),\ v(r_i^b) = 0\},$$

the variational formulation of the (A+M) problem (including the summation over all the cilia) reads:

$$\left\{\begin{array}{l} \text{find } u \in V \text{ such that, for all } v \in V, \\ \displaystyle\int_{r_i^a}^{r_i^b} r\mu(r)\,\frac{\mathrm{d}u}{\mathrm{d}r}(r)\,\frac{\mathrm{d}v}{\mathrm{d}r}(r)\,\mathrm{d}r \\ \qquad + \ \dfrac{1}{2\pi L_z}\displaystyle\sum_j \int_0^L \xi_r^{(j)}(s,t))\,\hat{m}_{zz}^{(j)}(s,t)\,u(\xi_r^{(j)}(s,t))\,v(\xi_r^{(j)}(s,t))\,|\partial_r \boldsymbol{\xi}^{(j)}(s,t)|\,\mathrm{d}s \\ \qquad = \ \dfrac{1}{2\pi L_z}\displaystyle\sum_j \int_0^L \xi_r^{(j)}(s,t))\left(\hat{m}_{zz}^{(j)}\hat{u}_{\mathsf{cil.},z}^{(j)} + \hat{m}_{zr}^{(j)}\hat{u}_{\mathsf{cil.},r}^{(j)}\right)(s,t)\,v(\xi_r^{(j)}(s,t))\,|\partial_r \boldsymbol{\xi}^{(j)}(s,t)|\,\mathrm{d}s \\ \qquad + \ \displaystyle\int_{r_i^a}^{r_i^b} r\,f_1\,v(r)\,\mathrm{d}r + r_i^a\,f_2\,v(r_i^a). \end{array}\right. \tag{2.13}$$

where $s \mapsto \boldsymbol{\xi}^{(j)}(s,t)$ denotes the parametrization of cilium (i,j), L_z is the length of the metachronal wave, index i relates to the number of cilia in the axial direction (z) over the length of a metachronal wave, index j relates to the number of cilia in the azimuthal direction (θ) over the complete annulus. Thus, the above variational formulation allows us to formally describe $c_1 \in V'$ and $c_2 \in V'$ as:

$$\begin{aligned} <c_1, v>_{V',V} \ &:= \ \frac{1}{2\pi L_z}\sum_j \int_0^L \xi_r^{(j)}(s,t))\,\hat{m}_{zz}^{(j)}(s,t)\,u(\xi_r^{(j)}(s,t))\,v(\xi_r^{(j)}(s,t))\,|\partial_r \boldsymbol{\xi}^{(j)}(s,t)|\,\mathrm{d}s, \\ <c_2, v>_{V',V} \ &:= \ \frac{1}{2\pi L_z}\sum_j \int_0^L \xi_r^{(j)}(s,t))\left(\hat{m}_{zz}^{(j)}\hat{u}_{\mathsf{cil.},z}^{(j)} + \hat{m}_{zr}^{(j)}\hat{u}_{\mathsf{cil.},r}^{(j)}\right)(s,t)\,v(\xi_r^{(j)}(s,t))\,|\partial_r \boldsymbol{\xi}^{(j)}(s,t)|\,\mathrm{d}s. \end{aligned}$$

Noteworthily it may be possible to give a strong interpretation of c_1 and c_2 under some (possibly unrealistic) assumptions on the cilia movement. But the formulation of the (M+A) problem should always be interpreted in the sense of its weak formulation.

2.3 Stability of the mucus distribution

In this section, we determine the stationary states r_i^a associated to permanent airflow situations. This has the advantage of giving us a hint on the estimate of the secretion term $\tilde{\phi}$, which is not easily observable. Indeed, let us discuss some fictional scenarios:

- Assume that $\tilde{\phi} = 0$. If there is no secretion term, the mucus of the last generation ($N = 17$) will tend to vanish, as the ciliary activity of generation N tends to push mucus into generation $N-1$, but nothing comes from generation $N+1$ (whose mucus flow is artificially set to 0). In the same way, the mucus of generation $N-1$ will tend to vanish too as the "well" of generation N has gone "dry", although the mucociliary activity of generation $N-1$ tends to push mucus into generation $N-2$. And so on... In the end, the stationary states are $r_i^a = r_i^m$, i.e. the mucus has been completely excreted in every generation. As a consequence, secretion is necessary to counterbalance the mucus loss at the mouth, to guarantee the functional role of mucociliary transport.

- Now assume that a high value for $\tilde{\phi}$ is considered. Then the bronchi will tend to be filled with mucus if the mucus flow balance dynamics is not strong enough to counterbalance the secretion term. In the end, no air can flow through the bronchial tree.

As a consequence, the evaluation of the secretion term is a critical aspect of the modeling. Stability of the mucus distribution is useful to estimate a suitable value, based upon a simple observable quantity (the mucus quantity in the trachea in a healthy situation).

2.3.1 Stationary states of mucus distribution when neglecting the airflow ($f_1 = f_2 = 0$)

The dynamics of the mucus distribution is governed by Eq. (2.1). Combined with Assumption 1 and neglecting the airflow (i.e. $f_1 = f_2 = 0$, which implies that $U_i = u_i$), stationary states $\{r_i^{a\star}\}_{i=0,\cdots,N-1}$ are defined by

$$Q_i(u_i; r_i^{a\star}) - 2Q_{i+1}(u_{i+1}; r_{i+1}^{a\star}) - \phi_i = 0. \tag{2.14}$$

Because Eq. (2.14$_{[N-1]}$) formally writes $Q_{N-1}(u_{N-1}; r_{N-1}^{a\star}) - \phi_{N-1} = 0$ (recall that $Q_N \equiv 0$), we have:

$$Q_{N-1}(u_{N-1}; r_{N-1}^{a\star}) = \phi_{N-1}.$$

Then Eq. (2.14$_{[N-2]}$) formally writes $Q_{N-2}(u_{N-2}; r_{N-2}^{a\star}) - 2Q_{N-1}(u_{N-1}; r_{N-1}^{a\star}) - \phi_{N-2} = 0$, so that

$$Q_{N-2}(u_{N-2}; r_{N-2}^{a\star}) = \phi_{N-2} + 2\phi_{N-1}.$$

Proceeding iteratively, in the general case,

$$Q_i(u_i; r_i^{a\star}) = \sum_{J=i}^{N-1} 2^{J-i}\phi_J, \qquad i \in \{0, \cdots, N-1\}. \tag{2.15}$$

Remark 15. *To fix ideas, motility parameters are chosen to get $u_i > 0$ in the mucus. Thus $\overline{u_i} > 0$ and $Q_i(u_i; r_i^{a\star}) > 0$.*

Proposition 2.3.1 (Stationary states with $f_1 = f_2 = 0$)**.** *Under Assumptions 1 and 2, stationary states are defined by:*

$$r_i^{a\star} = \sqrt{(r_i^m)^2 - \tilde{\phi}\left(\frac{2}{\overline{u_i}}\sum_{J=i}^{N-1} 2^{J-i} r_J^b\, \ell_J^b\right)}, \qquad i \in \{0, ..., N-1\}, \tag{2.16}$$

where $\overline{u_i}$ denotes the velocity fluid of the mucus at each generation. Stationary states are asymptotically stable.

Proof. Under Assumption 1, we have $u_i(r) \equiv \overline{u_i}$, for $r \in (r_i^a, r_i^m)$, as the fluid velocity is constant in the mucus. Moreover

$$Q_i(u_i; r_i^{a\star}) = 2\pi \int_{r_i^{a\star}}^{r_i^m} r u_i(r)\, \mathrm{d}r = 2\pi\overline{u_i} \int_{r_i^{a\star}}^{r_i^m} r\, \mathrm{d}r = 2\pi\overline{u_i}\left[\frac{(r_i^m)^2}{2} - \frac{(r_i^{a\star})^2}{2}\right].$$

Assumption 2 combined with Eq. (2.15) gives:

$$2\pi\overline{u_i}\left[\frac{(r_i^m)^2}{2} - \frac{(r_i^{a\star})^2}{2}\right] = 2\pi\,\tilde{\phi}\sum_{J=i}^{N} 2^{J-i} r_J^b\, \ell_J^b,$$

which defines the stationary states. Note that, as $\overline{u_i} > 0$ and $\tilde{\phi} > 0$, stationary states satisfy

$$0 < r_i^{a\star} < r_i^m,$$

i.e. mucus does not vanish. We have also

$$\frac{\mathrm{d}Q_i(u_i; r_i^a)}{\mathrm{d}r} = -2\pi\,\overline{u_i}\, r_i^a < 0$$

which provides the asymptotic stability of the stationary states. □

Remark 16. *For practical computations:*

- *if the secretion term $\tilde{\phi}$ is unknown, it can be estimated as follows: assume that $r_0^m - r_0^{a\star} := 10\,\mu\mathrm{m}$ (the level of mucus is observed in the trachea), then $\tilde{\phi}$ is deduced from Eq. (2.16$_{[0]}$) and $r_1^{a\star}$, $r_2^{a\star}$,... $r_{N-1}^{a\star}$ can be computed as well.*
- *if the secretion term $\tilde{\phi}$ is known, then $r_0^{a\star}$, $r_1^{a\star}$,... $r_{N-1}^{a\star}$ can be computed with Eq.* (2.16)*.*

2.3.2 Stationary states of mucus distribution in the general case

Assumptions 1 and 2 still hold. The velocity field $r \mapsto U_i(r)$ in generation i is governed by the (M+A) problem. Recall that f_1 and f_2 *linearly* depend on the airflow in the trachea, denoted $\Phi_{\mathrm{mouth}}^{\mathrm{air}}$.

Remark 17. *We may consider the following situations:*

- $\Phi_{\mathrm{mouth}}^{\mathrm{air}} = 0$*: neutral case ($f_1 = f_2 = 0$), in which no airflow is considered: $U_i = u_i$.*
- $\Phi_{\mathrm{mouth}}^{\mathrm{air}} > 0$*: expiration case, that contributes to some increase of the velocity in the mucus, w.r.t. the neutral case $f_1 = f_2 = 0$: $U_i > u_i$ in the mucus.*
- $\Phi_{\mathrm{mouth}}^{\mathrm{air}} < 0$*: inspiration case, that contributes to some decrease of the velocity in the mucus, w.r.t. the neutral case $f_1 = f_2 = 0$: $U_i < u_i$ in the mucus.*

However in standard regimes, we expect airflow to have little influence on the velocity magnitude, i.e. $U_i = u_i + v_i$ *is mainly driven by* u_i *(whereas* v_i *is a perturbation of* u_i*).*

As for the derivation of Eq. (2.16), we have:

Proposition 2.3.2. *Under Assumptions 1 and 2, stationary states of mucus* $\{r_i^{a\star}\}_{i=0,\dots,N-1}$ *are defined by:*

$$f(r_i^{a\star}) := Q_i(U_i, r_i^{a\star}) - 2\pi\,\tilde{\phi}\sum_{J=i}^{N-1} 2^{J-i} r_J^b \ell_J^b = 0, \qquad i \in \{0, \dots, N-1\}. \tag{2.17}$$

Remark 18. *Let us recall that, as* $U_i = u_i + v_i$*, the mucus flow divides into two corresponding contributions:*

$$\begin{array}{rcccl} Q_i(U_i, r_i^a) & = & Q_i(u_i, r_i^a) & + & Q_i(v_i, r_i^a) \\ & = & 2\pi\overline{u_i}\left[\frac{(r_i^m)^2}{2} \frac{-(r_i^a)^2}{2}\right] & + & 2\pi\int_{r_i^a}^{r_i^m} r v_i(r)\,\mathrm{d}r. \end{array}$$

Under Assumption 2, the problem consists in finding r_i^a, $i \in \{0, \dots, N-1\}$, such that Eq. (2.17) holds. Furthermore, solving Eq. (2.17)$_{[i]}$ can be done using a Newton iterative process:

Algorithm 1 (Solving Eq. (2.17) with a Newton procedure)**.**

- Initialization. *Define* $[r_i^a]^{(0)}$ *(for instance Eq. (2.16) may provide the initial guess).*
- Iterations. *For* $k \geq 0$, $[r_i^a]^{(k+1)} := [r_i^a]^{(k)} - \dfrac{f([r_i^a]^{(k)})}{f'([r_i^a]^{(k)})}$.
- Conclusion. $r_i^{a\star} := [r_i^a]^{(\infty)}$.

Remark 19. *Note that each Newton iteration requires to solve a 1D problem:*

- *Either compute* U_i *the solution of* $(\mathrm{M}+\mathrm{A})$ *defined on* $([r_i^a]^{(k)}, r_i^b)$*. Then the Newton update can be written as:*

$$[r_i^a]^{(k+1)} = [r_i^a]^{(k)} + \frac{\displaystyle\int_{[r_i^a]^{(k)}}^{r_i^m} r U_i(r)\,\mathrm{d}r - \tilde{\phi}\sum_{J=i}^{N-1} 2^{J-i} r_J^b \ell_J^b}{[r_i^a]^{(k)}\, U_i([r_i^a]^{(k)})}.$$

- *Or compute* v_i *the solution of problem* (A) *defined on* $([r_i^a]^{(k)}, r_i^b)$ *(and also* u_i *the solution of problem* (M) *but this can to done offline and only once). Then the Newton update can be written as:*

$$[r_i^a]^{(k+1)} = [r_i^a]^{(k)} + \frac{\overline{u_i}\left[\frac{(r_i^m)^2}{2} - \frac{([r_i^a]^{(k)})^2}{2}\right] + \displaystyle\int_{[r_i^a]^{(k)}}^{r_i^m} r v_i(r)\,\mathrm{d}r - \tilde{\phi}\sum_{J=i}^{N-1} 2^{J-i} r_J^b \ell_J^b}{[r_i^a]^{(k)}(\overline{u_i} + v_i([r_i^a]^{(k)})}.$$

Remark 20. *For practical computations:*

- $r \mapsto v_i(r)$ *linearly depends on* $\Phi^{\mathrm{air}}_{\mathrm{mouth}}$*, so that* v_i *contributes as a perturbative velocity field (due to airflow) in the velocity field* u_i*. Numerical simulations show the fact that* $v_i \ll u_i$ *in the normal regimes (inspiration or expiration). It may play a significant role in severe regimes (forced breathing).*
- *if the secretion term* $\tilde{\phi}$ *is unknown, it can be estimated as follows: assume that* $r_0^m - r_0^{a\star} := 10\,\mu\mathrm{m}$ *(the level of mucus is observed in the trachea), then* $\tilde{\phi}$ *is deduced from Eq. (2.17*$_{[0]}$*) and* $r_1^{a\star}$*,* $r_2^{a\star}$*,...* $r_{N-1}^{a\star}$ *can be computed as well. However, it means that each airflow* $\Phi^{\mathrm{air}}_{\mathrm{mouth}}$ *(*> 0 *or* < 0*) is associated to a corresponding secretion source term* $\tilde{\phi}$*... However in the prospect of a breathing scenario that consists in a sequence of inspiration/expiration patterns,* $\tilde{\phi}$ *should be fixed once for all (instead of being modified for each sub-case): therefore we suggest to fix the value of* $\tilde{\phi}$ *using* $\Phi^{\mathrm{air}}_{\mathrm{mouth}} = 0$*.*
- *if the secretion term* $\tilde{\phi}$ *is known, then* $r_0^{a\star}$*,* $r_1^{a\star}$*,...* $r_{N-1}^{a\star}$ *can be computed with Eq. (2.17).*

2.3.3 Numerical results

Data related to the geometry of the bronchial tree

The human tree is a 23 generations dichotomic tree but mucus is present in generations 0 to 16 only (then generations 17 to 22 are part of the acini, i.e. they are alveolated). Two geometrical models are considered:

- the so-called Weibel model, which is an idealized version of the data. In this case, the tree geometry is assumed to obey a scaling law, which is a typical assumption for lung modeling [49]. At each bifurcation, the radius and length of its daughter branches are reduced by a constant homothetic ratio $h = 2^{-\frac{1}{3}} \simeq 0.79$. Such a tree is known to be a good first approximation model for the lungs [49, 78, 50, 75]. Thus we define

$$r_i^b = r_0^b \cdot 2^{-\frac{i}{3}}, \qquad \ell_i^b = \ell_0^b \cdot 2^{-\frac{i}{3}},$$

  with $r_0^b = 5.0 \cdot 10^{+3}\,\mu$m (diameter of the trachea: 1 cm) and $\ell_0^b = 3.0 \cdot 10^{+4}\,\mu$m (length of the trachea: 30 cm).

- the so-called morphometric model, which is based upon experimental data [73, 74], see Table 2.1.

generation	length in μm	radius in μm
0	$9.400 \times 10^{+4}$	$9.000 \times 10^{+3}$
1	4.050	6.100
2	1.080	4.150
3	0.918	2.800
4	0.780	2.250
5	0.660	1.750
6	0.560	1.400
7	0.480	1.150
8	0.410	0.930
9	0.350	0.770
10	0.290	0.650
11	0.250	0.545
12	0.210	0.475
13	0.180	0.410
14	0.150	0.370
15	0.140	0.250
16	0.133	0.245

Table 2.1 – Morphometry of the conductive airways [73].

Data related to the ciliary activity

Table 2.2 summarizes the data related to the cilia, as given in [26]. Those default parameter values lead us to consider a forest of 100×16 cilia in the 3d computational domain Ω, leading to the computation of the 1D data $r \mapsto c_1(r)$ and $r \mapsto c_2(r)$.

Fluid			
Domain dimensions:			
– in axial direction	L_x	30.0	μm
– in azimuthal direction	L_y	4.8	μm
– in radial direction	L_z	10.0	μm
Fluid viscosity in PCL	μ_{w}	$1 \cdot 10^{+0}$	$\mathrm{mPa} \cdot \mathrm{s}$
Fluid viscosity in mucus	μ_{m}	$1 \cdot 10^{+4}$	$\mathrm{mPa} \cdot \mathrm{s}$
Airway surface liquid (ASL)	h	6	μm
Cilia			
Length of a cilium	L	6.0	μm
Cross-sectional radius of a cilium	a	0.1	μm
Beat frequency of a cilium (mean value)	f	15	Hz
Beat frequency of a cilium (range)	f	$7 - 22$	Hz
In axial direction:			
– Number of cilia in the computational domain	n_x	100	
– Cilia spacing	ℓ_x^0	0.3	μm
– Number of cilia per unit length	d_x	3.33	$\mu\mathrm{m}^{-1}$
In azimuthal direction:			
– Number of cilia in the computational domain	n_y	16	
– Cilia spacing	ℓ_y^0	0.3	μm
– Number of cilia per unit length	d_y	3.33	$\mu\mathrm{m}^{-1}$
Density of cilia	$D_{\text{cil.}}$	11.11	$\mu\mathrm{m}^{-2}$
Metachronal wavelength	λ	30.0	μm

Table 2.2 – Summary of data for fluid cilia in the lung, from [26].

Results I: Weibel model and morphometric model

Estimation of the secretion term is obtained by neglecting the airflow (i.e. $\Phi^{\text{air}}_{\text{mouth}} = 0$): assume that $r_1^m - r_1^{a\star} := 10\,\mu$m (the level of mucus is observed in the trachea), then $\tilde{\phi}$ is deduced from Eq. (2.16$_{[1]}$). We obtain:

$$\tilde{\phi} = \begin{cases} 5.779 \cdot 10^{-4} & \mu\mathrm{m} \cdot \mathrm{s}^{-1} \quad \text{for the Weibel model,} \\ 4.772 \cdot 10^{-4} & \mu\mathrm{m} \cdot \mathrm{s}^{-1} \quad \text{for the morphometric model.} \end{cases}$$

We thus obtain a value which slightly depends on the geometrical model but the order of magnitude remains the same. Then equilibrium states are numerically computed for various airflows (air viscosity is set to $1.9 \cdot 10^{-2}\ \mathrm{mPa} \cdot \mathrm{s}$).

- Fig. 2.3 (Weibel model) and Fig. 2.4 (morphometric model) present the bronchial distribution of the mucus thickness $\delta_i := r_i^m - r_i^{a\star}$ at equilibrium for various airflows; in a similar way, we present the bronchial distribution of the mucus filling rates $\tau_{\text{mucus},i}$ at equilibrium for various airflows:

$$\tau_{\text{mucus},i} = \frac{r_i^m - r_i^{a\star}}{r_i^m}.$$

  corresponding to the ratio between the space occupied by mucus ($r_i^m - r_i^{a\star}$) and the maximal available space (r_i^m). Several comments can be made:

  - In the literature, mucus layer thickness is 10-30 μm in the trachea [34, 72, 40, 51, 62] and 2-5 μm in distal generations [34, 51, 79]. Numerical results evidence differences in the

distribution shapes according to the geometrical model. However in both cases, in the reference case (no airflow), the mucus thickness is set to $10\ \mu$m at the trachea whereas, in the 17th generation, it is very small (the model fails at getting a value around $2\ \mu$m). This suggests that the assumption of a **homogeneous secretion rate** and the assumption of a **uniform beat frequency of the cilia** (here fixed to 15 Hz in all the generations) should be relaxed if we aim at obtaining reference values of the mucus thickness in the distal regions.

- Airflows in normal regimes have little influence on the equilibrium mucus thickness, thus showing that the main process leading to mucus excretion is due to ciliary beating. The process can be significantly increased during forced expiration associated with high airflow magnitude.

- Fig. 2.5 (Weibel model) and Fig. 2.6 (morphometric model) present the bronchial distribution of the mucus velocity $\overline{u}_i$ at equilibrium for various airflows. We may observe that airflows in normal regimes have little influence on the mucus velocity, whereas airflows with high magnitude can significantly increase (resp. decrease) the mucus velocity during forced expiration (resp. forced inspiration).

- Fig. 2.7 (Weibel model) and Fig. 2.8 (morphometric model) present the velocity distribution in the PCL+mucus at equilibrium for various airflows at the 9th generation (i.e. $i = 8$), in the transition between the proximal and distal bronchi. As in the previous cases, airflows associated to normal regimes do not modify the magnitude of the velocity profile, whereas airflows associated to extreme maneuvers lead to a significant change of the velocity profile. Note however that the geometry may have an impact on this observation, as the morphometric model (when compared to the Weibel model) tends to damp the influence of the airflow over the velocity distribution.

Results II: Spatial heterogeneity of the ciliary beat frequency

Previous numerical results are obtained with constant ciliary beat frequency ($f = 15$ Hz) all along the bronchial tree. However the ciliary beat frequency varies from approximately $f = f_{\text{dist.}} := 7$ Hz in the distal airways to about $f = f_{\text{prox.}} := 22$ Hz in the trachea [69]. Variations may also be defined within the range 13-25 Hz, see [65]. Therefore we introduce two different scenarios:

1. the *constant frequency scenario:*

$$f := f(i) = \frac{f_{\text{prox.}} + f_{\text{dist.}}}{2}, \qquad i \in \{0, \cdots, 16\},$$

2. the *linear frequency scenario:*

$$f := f(i) = f_{\text{prox.}} + \frac{i}{16}(f_{\text{dist.}} - f_{\text{prox.}}), \qquad i \in \{0, \cdots, 16\},$$

where i denotes the number of the considered generation ($i = 0$ for the trachea, $i = 16$ for the deepest distal generation located before the entrance of the acinus).

Fig. 2.9 highlights the following facts: for each scenario, if we impose the mucus thickness in the trachea $\delta_0 := r_0^m - r_0^{a\star}$ to be $10\ \mu$m, then there is no significant difference in the distribution of mucus

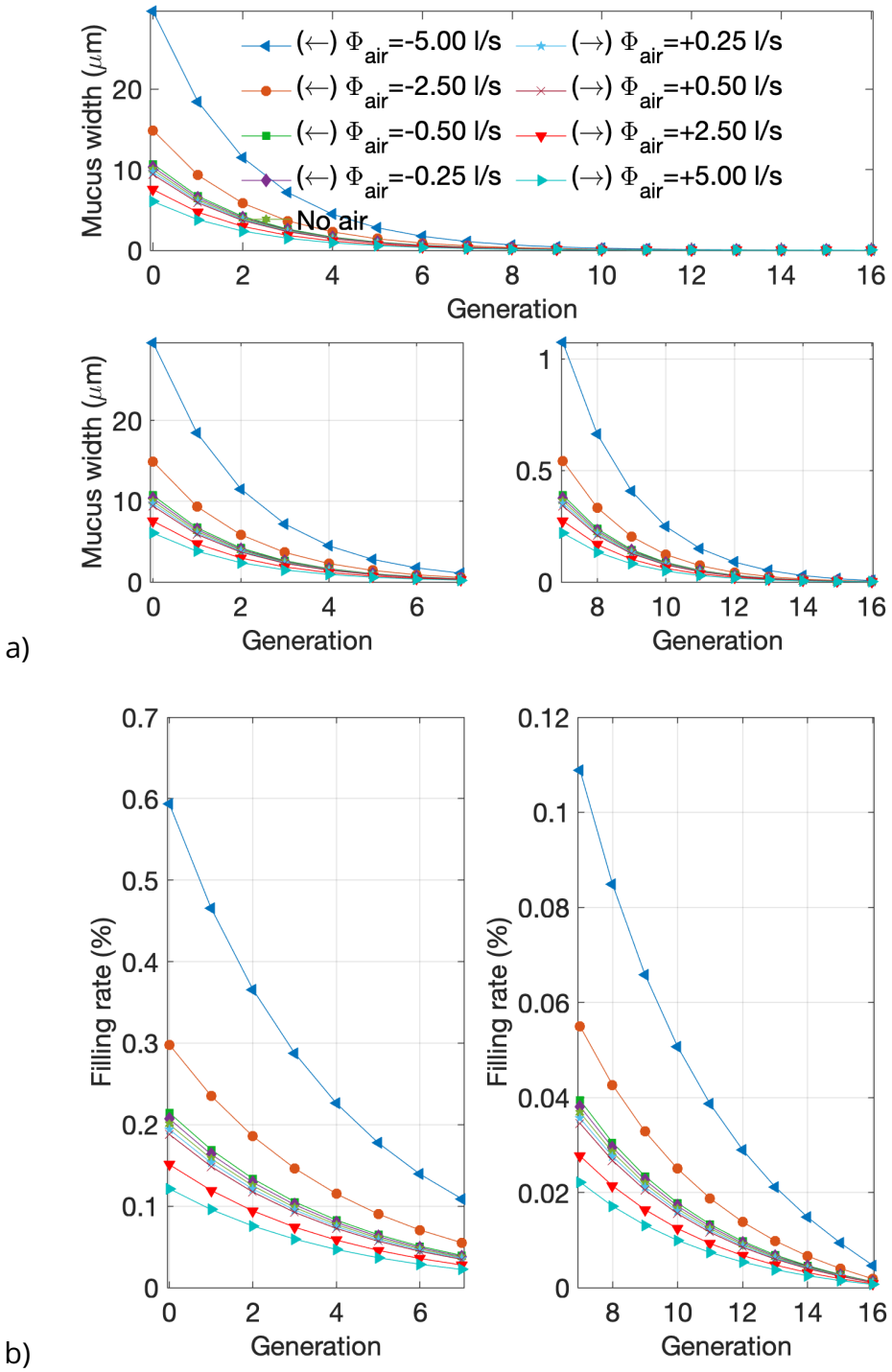

Figure 2.3 – **Weibel model.** a) Bronchial distribution of the mucus thickness $\delta_i := r_i^m - r_i^{a\star}$ at equilibrium for various airflows (← stands for inspiration, → stands for expiration). b) Bronchial distribution of the mucus filling rates at equilibrium for various airflows.

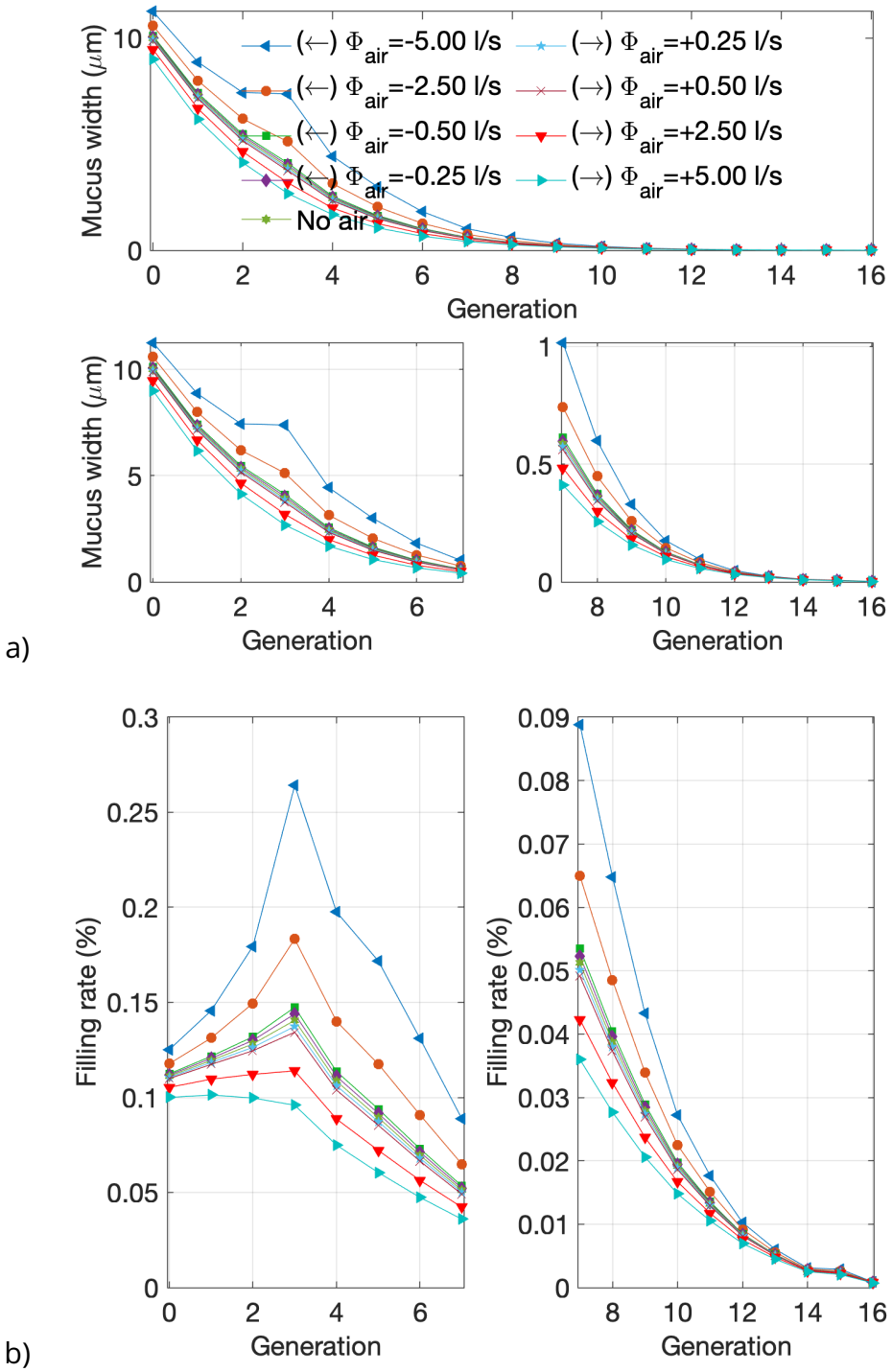

Figure 2.4 – **Morphometric model.** a) Bronchial distribution of the mucus thickness $\delta_i := r_i^m - r_i^{a\star}$ at equilibrium for various airflows (← stands for inspiration, → stands for expiration). b) Bronchial distribution of the mucus filling rates $\tau_{\text{mucus},i}$ at equilibrium for various airflows.

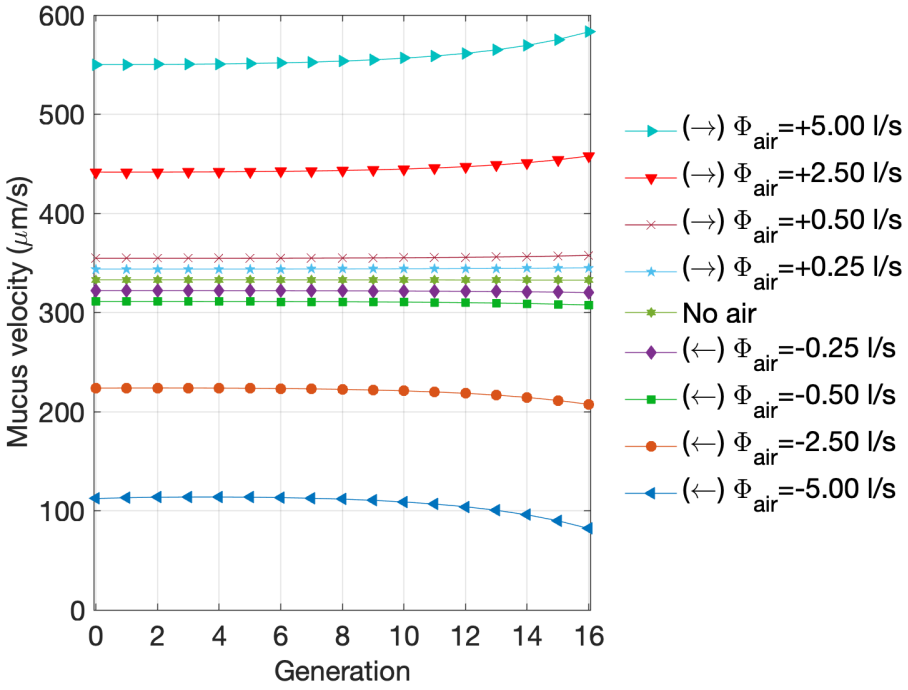

Figure 2.5 – **Weibel model.** Bronchial distribution of the mucus velocity $\overline{u}_i$ at equilibrium for various airflows ($\leftarrow$ stands for inspiration, $\rightarrow$ stands for expiration).

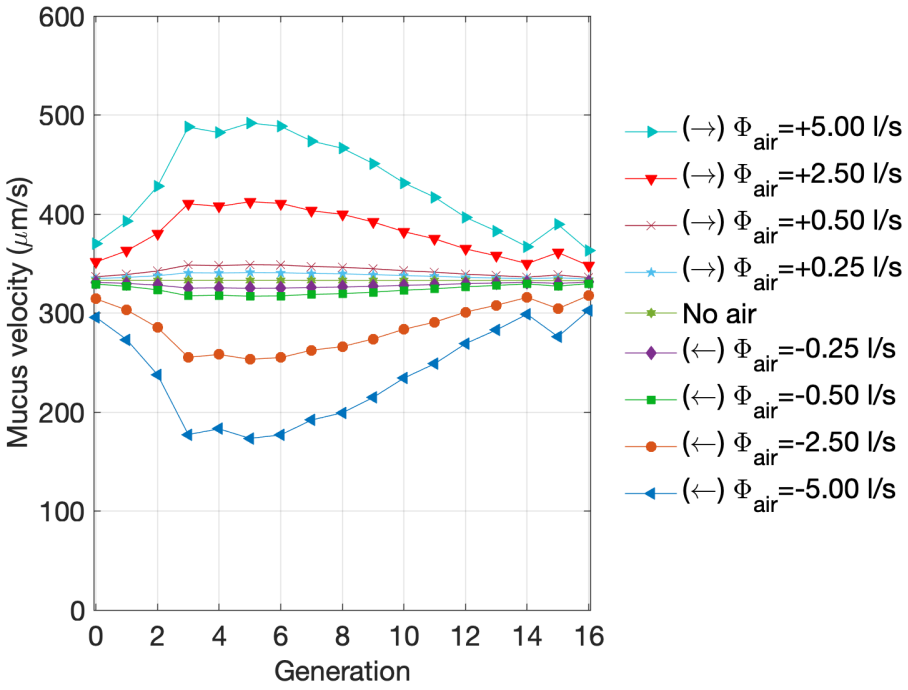

Figure 2.6 – **Morphometric model.** Bronchial distribution of the mucus velocity $\overline{u}_i$ at equilibrium for various airflows ($\leftarrow$ stands for inspiration, $\rightarrow$ stands for expiration).

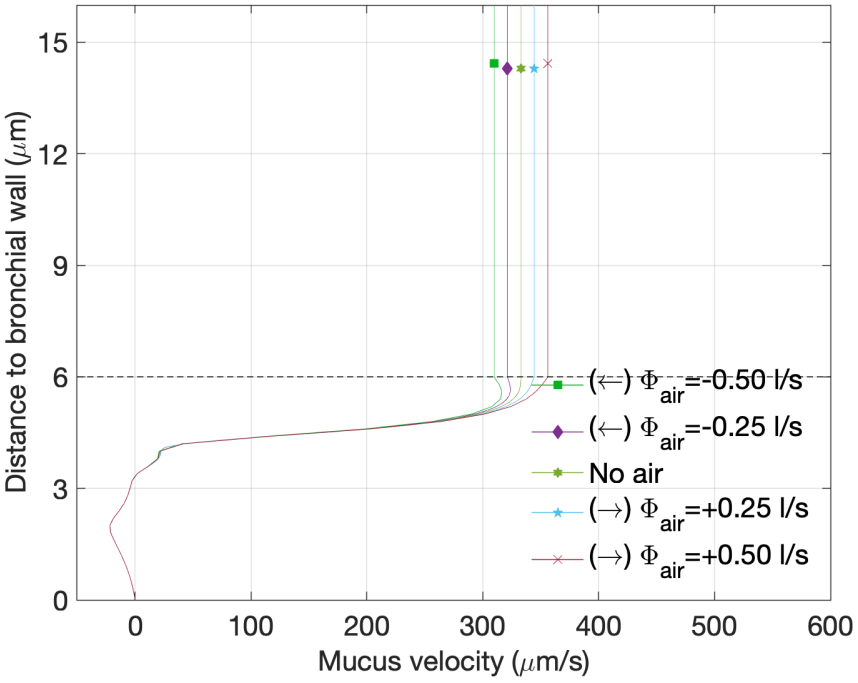

a)

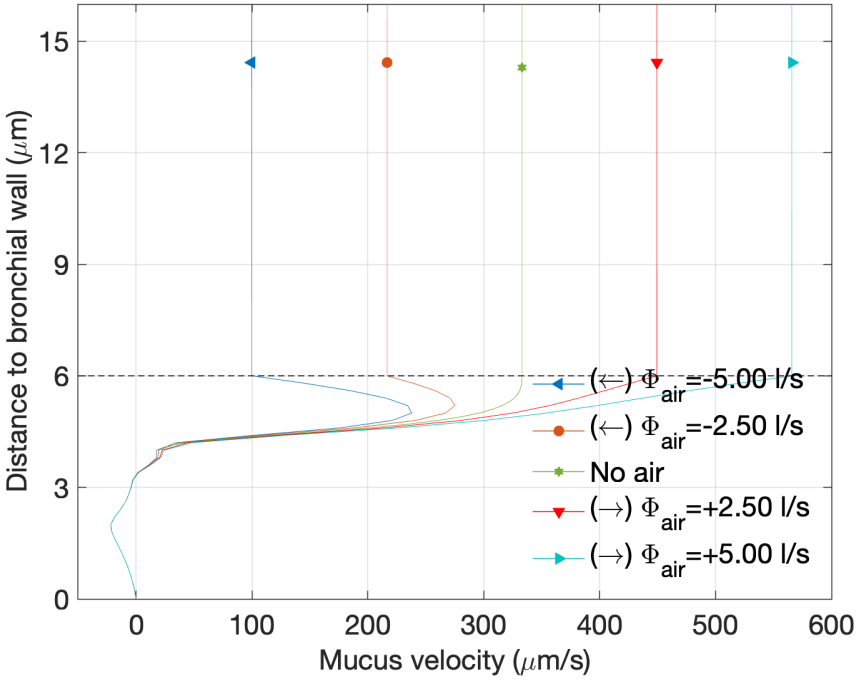

b)

Figure 2.7 – **Weibel model.** Velocity distribution in the PCL+mucus at equilibrium for various airflows (← stands for inspiration, → stands for expiration) at generation 8 (i.e. in the transition of the proximal/distal bronchi). a) for normal breathing to exercice b) for extreme airflows (e.g. during forced maneuvers involved in spirometry).

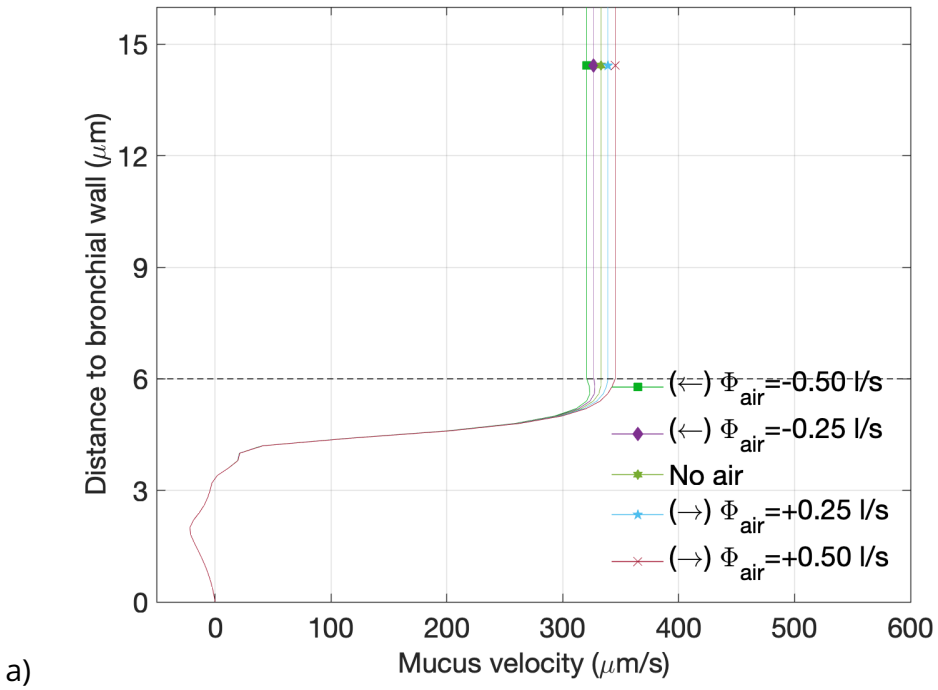

a)

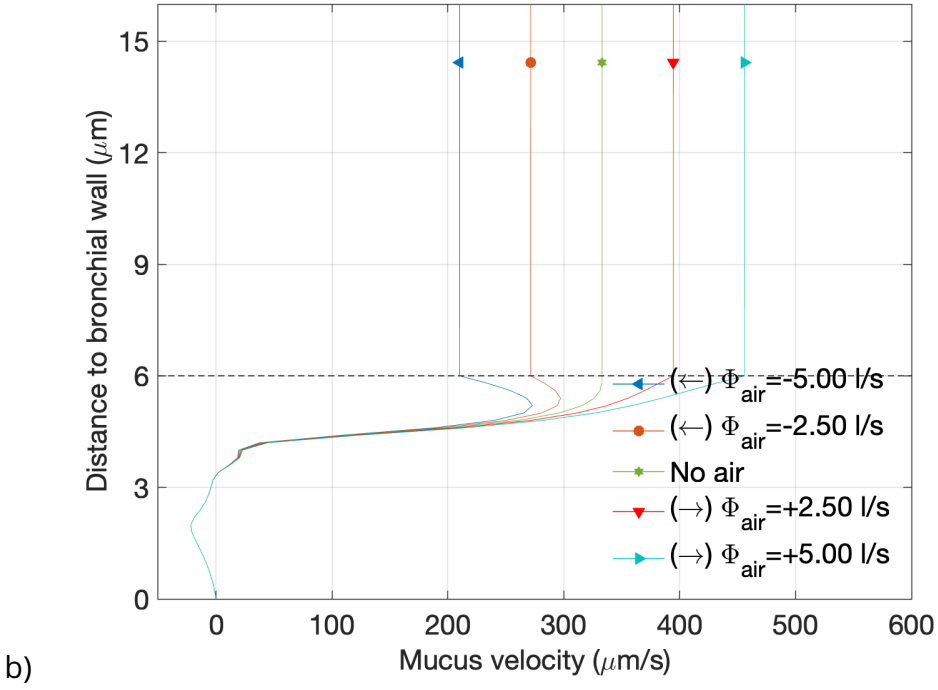

b)

Figure 2.8 – **Morphometric model.** Velocity distribution in the PCL+mucus at equilibrium for various airflows (← stands for inspiration, → stands for expiration) at generation 8 (i.e. in the transition of the proximal/distal bronchi). a) for normal breathing to exercice b) for extreme airflows (e.g. during forced maneuvers involved in spirometry).

thickness between the linear frequency scenario (from 22 Hz to 7 Hz) and the constant one (15 Hz in every generation). Note however that the value of $\tilde{\phi}$ depends on the chosen scenario: more precisely the mucus thickness distribution profiles are similar but the linear scenario requires a *stronger* secretion rate ($6.999 \cdot 10^{-4}\,\mu\mathrm{m} \cdot \mathrm{s}^{-1}$) than the constant scenario ($4.772 \cdot 10^{-4}\,\mu\mathrm{m} \cdot \mathrm{s}^{-1}$). If we now use the same value of the secretion rate (e.g. $4.772 \cdot 10^{-4}\,\mu\mathrm{m} \cdot \mathrm{s}^{-1}$) in the two scenarios, then the mucus thickness is the same in the terminal generation but we may observe that the mucus thickness at the trachea for the linear frequency scenario is divided by 3 approximatively, when compared to the value of the constant frequency scenario. The numerical results suggest that the constant frequency scenario, based upon the mean value of the ciliary beat frequency, overestimates the mucus thickness distribution. Equivalently it underestimates the ability of the bronchial tree to evacuate mucus. *In all the forthcoming simulations, the ciliary beat frequency is chosen as the linear profile varying from 22 (at gen. 0) to 7 Hz (at gen. 16).*

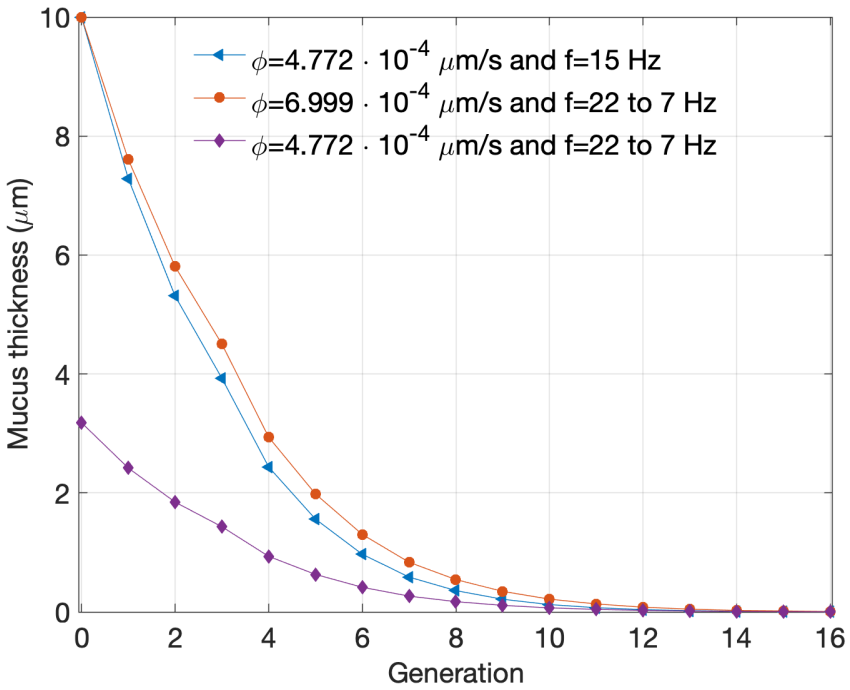

Figure 2.9 – Influence of the ciliary beat frequency distribution on the mucus thickness: Bronchial distribution of the mucus thickness $\delta_i := r_i^m - r_i^{a\star}$ at equilibrium. All data provided in Table 2.2 except for the ciliary beat frequency and the secretion rate.

2.4 Discussion on the mucus secretion rate

2.4.1 Constant mucus secretion rate

Let us discuss the value of the secretion rate, based upon Assumption 2. It is clear that each chosen value of the secretion rate $\tilde{\phi}$ corresponds to a distribution of the mucus thickness and, incidentally, to the mucus thickness in the trachea $\delta_0 := r_0^m - r_0^{a\star}$ and the mucus thickness in the deepest generation $\delta_{16} := r_{16}^m - r_{16}^{a\star}$. The choice for the secretion rate $\tilde{\phi}$ is thus strongly related to informations about mucus thickness that are available in the literature. Data, such as mucus thickness in the trachea and

in the distal generation, that are available in the literature should guide us for the identification of the secretion rate that is compatible with the data.

Table 2.3 provides a selection of values for the secretion rate along with the associated mucus thickness δ_0 (trachea) and δ_{16} (deepest generation). These values have to be confronted to the ones that are available in the literature:

- According to [34], mucus layer thickness is about $10 - 20\,\mu\mathrm{m}$ in the trachea (cited references are [72, 40, 51, 62]) and $2 - 5\,\mu\mathrm{m}$ in distal generations (cited references are [51, 79]).
- According to [58], in the airways the thickness of the surface fluid is thought to average about $5 - 10\,\mu\mathrm{m}$ (cited references are [80, 11, 1]) gradually decreasing distally until the vast expanse of the alveoli is reached which is covered with a very thin layer of fluid that averages about $0.05 - 0.08\,\mu\mathrm{m}$ thick but may be several microns thick in pooled areas and as thin as $15 - 20\,\mathrm{pm}$ (cited reference: [78]).

$\tilde{\phi}$ ($\mu\mathrm{m} \cdot \mathrm{s}^{-1}$)	δ_0 (μm)	[34]	[58]	δ_{16} (μm)	[34]	[58]	
$1.139 \cdot 10^{-4}$	1.63			$\underline{1.00} \cdot 10^{-3}$		☐	
$3.501 \cdot 10^{-4}$	$\underline{5.00}$		■	$3.07 \cdot 10^{-3}$		☐	
$5.694 \cdot 10^{-4}$	8.14		■	$\underline{5.00} \cdot 10^{-3}$		☐	
$6.999 \cdot 10^{-4}$	$\underline{10.00}$	■	■	$6.15 \cdot 10^{-3}$		☐	← see Fig. 2.10
$1.050 \cdot 10^{-3}$	$\underline{15.00}$	■		$9.22 \cdot 10^{-3}$		☐	← see Fig. 2.10
$1.139 \cdot 10^{-3}$	16.28	■		$\underline{1.00} \cdot 10^{-2}$		☐	
$2.097 \cdot 10^{-3}$	$\underline{30.00}$	■		$1.84 \cdot 10^{-2}$		☐	← see Fig. 2.10
$5.694 \cdot 10^{-3}$	81.68			$\underline{5.00} \cdot 10^{-2}$		■	
$9.110 \cdot 10^{-3}$	131.04			$\underline{8.00} \cdot 10^{-2}$		■	
$1.139 \cdot 10^{-2}$	164.10			$\underline{1.00} \cdot 10^{-1}$		☐	
$1.137 \cdot 10^{-1}$	1803.85			$\underline{1.00} \cdot 10^{+0}$		☐	

Table 2.3 – Different values of the secretion rate lead to different mucus thickness distributions. In particular, each value of the secretion rate $\tilde{\phi}$ is associated to a mucus thickness at the trachea (δ_0) and in the deepest generation (δ_{16}).

Results III: Constant mucus secretion rate

In figure 2.10, we observe that mucus thickness depends almost linearly on the associated secretion rate $\tilde{\phi}$. As we impose mucus thickness at the trachea to be $\delta_0 = 5\,\mu\mathrm{m}$, the secretion rate is almost divided by 2 comparing to the secretion rate associated to $\delta_0 = 10\,\mu\mathrm{m}$. Also in Table 2.3, as we impose mucus thickness at the last generation $\delta_{16} = 1\,\mu\mathrm{m}$ which is the same order as in [34], mucus thickness in the trachea will be two orders of magnitude higher than mucus thickness in the trachea mentioned in [34], and the secretion rate obtained is three orders of magnitude higher than the secretion rate associated to mucus thickness $\delta_0 = 10\,\mu\mathrm{m}$ imposed at the trachea.

2.4.2 Variable mucus secretion rate

As numerical results obtained with constant secretion rate $\tilde{\phi}$ lead to an underestimated value of the mucus thickness in the distal regions (see Fig. 2.4 and related comments), we propose to take into

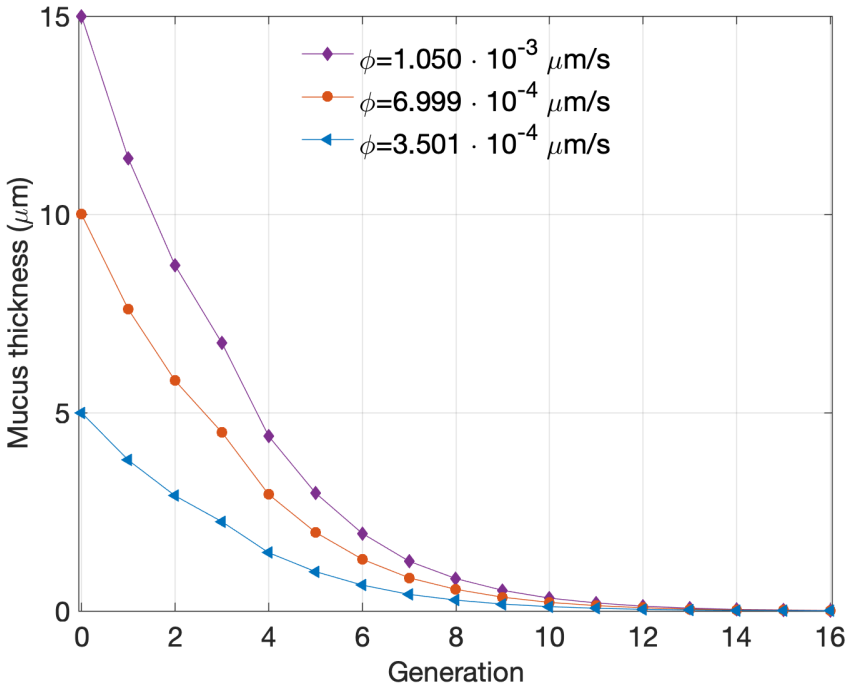

Figure 2.10 – Bronchial distribution of the mucus thickness $\delta_i := r_i^m - r_i^{a\star}$ at equilibrium for different constant values of the secretion rate. All data provided in Table 2.2.

account variable secretion rate in the bronchial tree. In that prospect we relax Assumption 2 and consider that

$$\phi_i = 2\pi\, r_i^b\, \ell_i^b\, \tilde{\phi}_i,$$

where $\tilde{\phi}_i$ has to be defined for each generation. We investigate two possible scenarios:

- *linear case:*

$$\tilde{\phi}_i := \tilde{\phi}_{\text{prox.}} + \frac{i}{16}(\tilde{\phi}_{\text{dist.}} - \tilde{\phi}_{\text{prox.}}), \quad \text{for } i \in \{0, \cdots, 16\}$$

  as we consider that the mucus secretion rate linearly varies from proximal region to the distal region.

- *proximal-distal case:*

$$\tilde{\phi}_i := \begin{cases} \tilde{\phi}_{\text{prox.}}, & \text{for } i \in \{0, \cdots, 8\} \quad \text{(proximal generations)} \\ \tilde{\phi}_{\text{prox.}} + \frac{i-8}{16-8}(\tilde{\phi}_{\text{dist.}} - \tilde{\phi}_{\text{prox.}}), & \text{for } i \in \{8, \cdots, 16\} \quad \text{(distal generations)} \end{cases}$$

  as we consider that the mucus secretion rate is constant in the proximal region whereas it linearly increases in the distal region.

Proposition 2.3.1 readily adapts into:

Proposition 2.4.1 (Stationary states with $f_1 = f_2 = 0$)**.** *Under Assumption 1, stationary states are defined by:*

$$r_i^{a\star} = \sqrt{(r_i^m)^2 - \left(\frac{2}{\overline{u_i}(f_i)} \sum_{J=i}^{N} 2^{J-i} \tilde{\phi}_J r_J^b\, \ell_J^b\right)}, \qquad i \in \{1, ..., N\}, \tag{2.18}$$

Model	$r_0^{a\star} - r_0^m$ (μm)	$r_{16}^{a\star} - r_{16}^m$ (μm)	$\tilde{\phi}_{\text{prox.}}$ ($\mu\text{m}\cdot\text{s}^{-1}$)	$\tilde{\phi}_{\text{dist.}}$ ($\mu\text{m}\cdot\text{s}^{-1}$)	Mucus distribution
linear	$1\cdot10^{+1}$	$2\cdot10^{+0}$	$-1.265\cdot10^{+0}$	$+2.268\cdot10^{-1}$	(A_1), see Fig. 2.11
linear	$1\cdot10^{+1}$	$5\cdot10^{-2}$	$-2.726\cdot10^{-2}$	$+5.694\cdot10^{-3}$	(A_2), see Fig. 2.12
linear	$1\cdot10^{+1}$	$1\cdot10^{-2}$	$-1.757\cdot10^{-3}$	$+1.139\cdot10^{-3}$	(A_3), see Fig. 2.13
linear	$1\cdot10^{+1}$	$5\cdot10^{-3}$	$+1.430\cdot10^{-3}$	$+5.695\cdot10^{-4}$	(A_4), see Fig. 2.14
prox.-dist.	$1\cdot10^{+1}$	$2\cdot10^{+0}$	$-6.085\cdot10^{-1}$	$+2.268\cdot10^{-1}$	(B_1), see Fig. 2.11
prox.-dist.	$1\cdot10^{+1}$	$5\cdot10^{-2}$	$-1.275\cdot10^{-2}$	$+5.694\cdot10^{-3}$	(B_2), see Fig. 2.12
prox.-dist.	$1\cdot10^{+1}$	$1\cdot10^{-2}$	$-4.828\cdot10^{-4}$	$+1.139\cdot10^{-3}$	(B_3), see Fig. 2.13
prox.-dist.	$1\cdot10^{+1}$	$5\cdot10^{-3}$	$+1.051\cdot10^{-3}$	$+5.695\cdot10^{-4}$	(B_4), see Fig. 2.14

Table 2.4 – Different values of mucus thickness at the first and last generation lead to different secretion rates $\tilde{\phi}_{\text{prox.}}$ and $\tilde{\phi}_{\text{dist.}}$.

where $\overline{u_i}(f_i)$ denotes the velocity fluid of the mucus at generation i (which depends on the ciliary beat frequency f_i).

At this stage, the distribution of the ciliary beat frequency $i \mapsto f_i$ is known but the distribution of the mucus secretion $i \mapsto \tilde{\phi}_i$ is not known, as it depends on $\tilde{\phi}_{\text{prox.}}$ and $\tilde{\phi}_{\text{dist.}}$ which have to be evaluated. This can be done in the following way:

- The distal secretion rate $\tilde{\phi}_{\text{dist.}}$ is computed in a straightforward way, as Eq. (2.18)$_{(N)}$ reduces to:

$$r_N^{a\,\star} = \sqrt{(r_N^m)^2 - \left(\frac{2}{\overline{u_N}(f_N)}\tilde{\phi}_N r_N^b\,\ell_N^b\right)}.$$

  As $\overline{u_N}(f_N)$ does not depend on the mucus thickness (this is a consequence of Assumption 1), it can be computed easily. Then as r_N^b, ℓ_N^b and r_N^m are defined as well, $\tilde{\phi}_N$ is deduced from the fact that $r_N^{a\,\star} - r_N^m$ is set to $2\ \mu\text{m}$.

- The proximal secretion rate $\tilde{\phi}_{\text{prox.}}$ can be computed by dichotomy, as a given value of $\tilde{\phi}_{\text{prox.}}$ provides an explicit scenario for the secretion rate, thus allowing to compute the corresponding distribution of mucus thickness $\{r_i^{a\star} - r_i^m\}_{i=0,\cdots,N}$. Then the suitable choice for $\tilde{\phi}_{\text{prox.}}$ leads to a mucus thickness at the trachea $r_0^{a\star} - r_0^m$ corresponding to $10\ \mu\text{m}$.

Numerical results are obtained for the morphometric geometry and data provided in Table 2.2. Note that the mucus secretion rate is not constant anymore (since we investigate two spatial-varying scenarios) and computations lead us to the following values in order to satisfy prescribed values for $r_0^{a\star} - r_0^m$ and $r_{16}^{a\star} - r_{16}^m$:

Results IV: Variable mucus secretion rate

Figure 2.11 shows the distribution of mucus at equilibrium with different secretion rates. At the trachea we imposed mucus thickness to be $\delta_0 = 10\mu m$ and at the last generation $\delta_{16} = 2\mu m$. We observe higher mucus thicknesses at the proximal generations up to one order of magnitude higher at the generation 1 and 2 than mucus thickness at the trachea. This scenario is less significant in the case where we impose $\delta_{16} = 5\cdot10^{-2}\mu m$ (Figure 2.12). The total secretion obtained using the linear case is

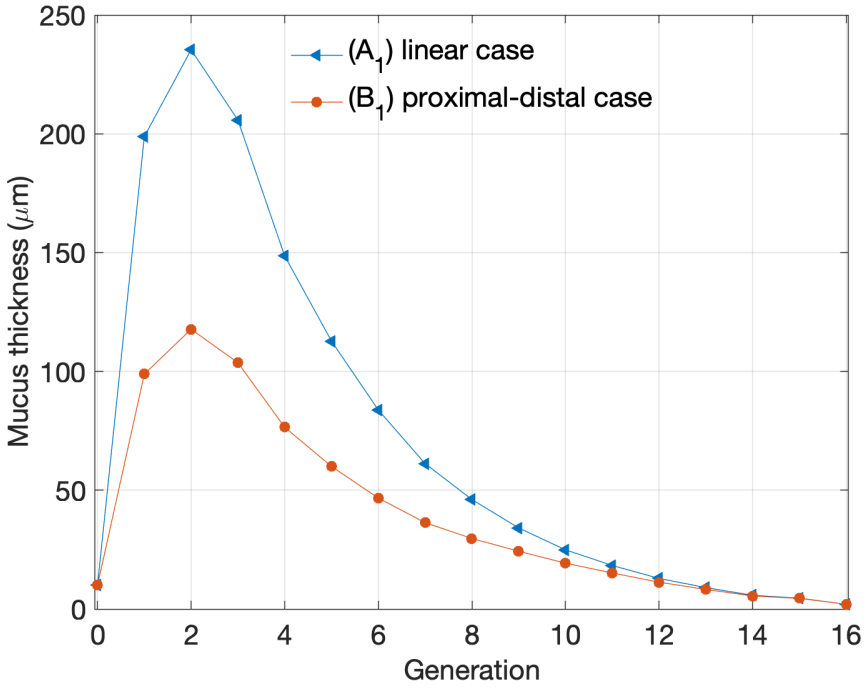

Figure 2.11 – Bronchial distribution of the mucus thickness $\delta_i := r_i^m - r_i^{a\star}$ at equilibrium with varying secretion rate ($\delta_0 = 1 \cdot 10^{+1}\,\mu\text{m}$, $\delta_{16} = 2 \cdot 10^{+0}\,\mu\text{m}$). All data provided in Table 2.2.

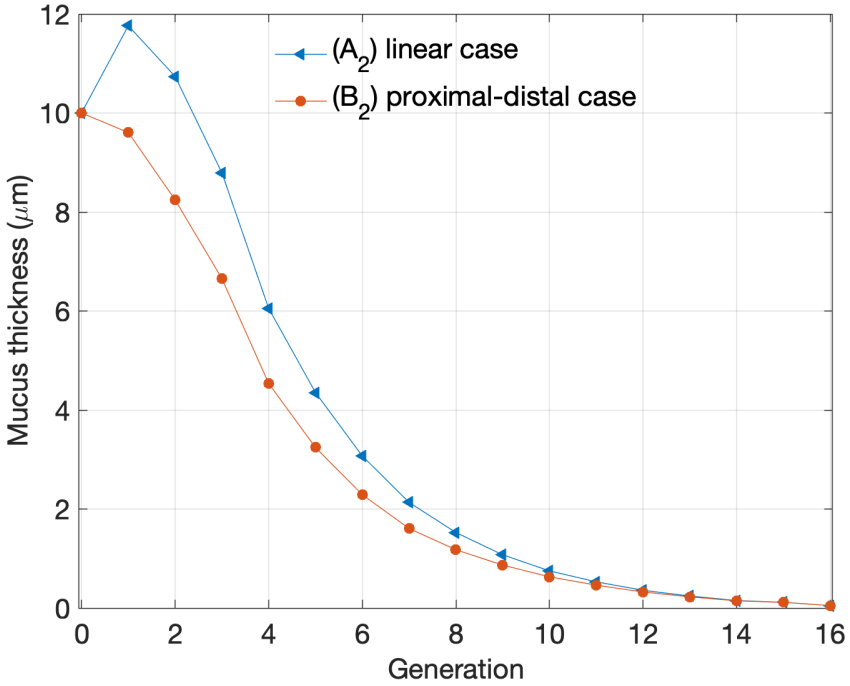

Figure 2.12 – Bronchial distribution of the mucus thickness $\delta_i := r_i^m - r_i^{a\star}$ at equilibrium with varying secretion rate ($\delta_0 = 1 \cdot 10^{+1}\,\mu\text{m}$, $\delta_{16} = 5 \cdot 10^{-2}\,\mu\text{m}$). All data provided in Table 2.2.

higher than the proximal-distal case, so mucus thicknesses are higher with the linear case than the proximal-distal case (2.11 and 2.12). Also in Table 2.4, using (A_1) or (A_2) or (B_1) or (B_2), the proximal secretion rate $\tilde{\phi}_{\text{prox.}}$ obtained is negative. This scenario is of course nonrealistic. In figure 2.13 and 2.14 we observe that there is no significant difference in mucus thicknesses between the linear and the proximal-distal case. Mucus thickness decreases et each generation in the same way as using a constant secretion rate. But as for the (A_1), (A_2), (B_1) and (B_2) the proximal secretion term obtained is negative in the (A_3) and (B_3) cases.

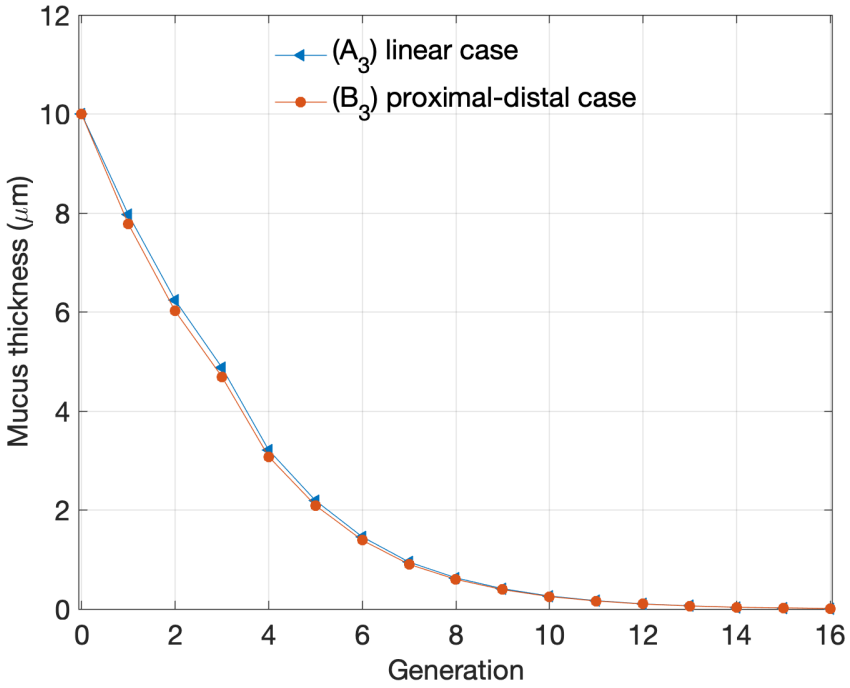

Figure 2.13 – Bronchial distribution of the mucus thickness $\delta_i := r_i^m - r_i^{a\star}$ at equilibrium with varying secretion rate ($\delta_0 = 1 \cdot 10^{+1}\,\mu$m, $\delta_{16} = 1\mu\text{m} \cdot 10^{-2}\,\mu$m). All data provided in Table 2.2.

2.4.3 An inverse problem: identification of the mucus secretion rate distribution

To the best of our knowledge, the *detailed* distribution of the mean mucus thickness is not known: it is identified in the trachea and in distal generations [34, 72, 40, 51, 62, 79]. However we may investigate the following question: *Given the distribution of the mucus thickness at equilibrium, is it possible to determine the associated distribution of mucus secretion rates?*

From Eq. (2.18), iterative straightforward computations lead us to:

- $\tilde{\phi}_N = \dfrac{\overline{u_N}(f_N)\left[\frac{(r_N^m)^2}{2} - \frac{(r_N^{a,\star})^2}{2}\right]}{r_N^b\,\ell_N^b}$.
- $\tilde{\phi}_i = \dfrac{\overline{u_i}(f_i)\left[\frac{(r_i^m)^2}{2} - \frac{(r_i^{a\star})^2}{2}\right] - \sum_{J=i+1}^{N} 2^{J-i}\tilde{\phi}_J r_J^b\,\ell_J^b}{r_i^b\,\ell_i^b}$, for $i \in \{N-1, \cdots, 0\}$.

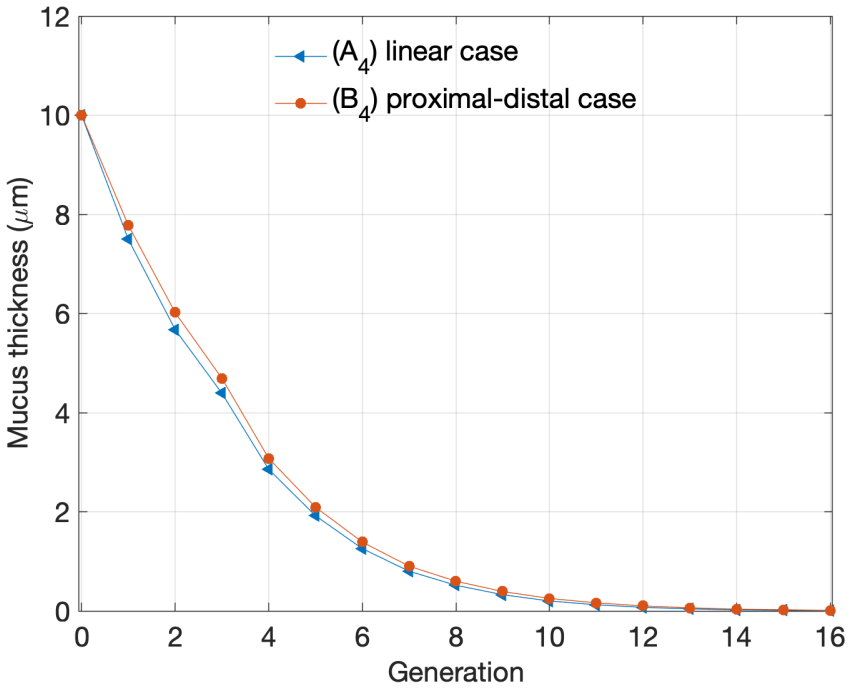

Figure 2.14 – Bronchial distribution of the mucus thickness $\delta_i := r_i^m - r_i^{a\star}$ at equilibrium with varying secretion rate ($\delta_0 = 1 \cdot 10^{+1}\ \mu$m, $\delta_{16} = 5 \cdot 10^{-3}\ \mu$m). All data provided in Table 2.2.

Alternatively we may use the identification from Eq. (2.1):

$$\tilde{\phi}_i = \frac{\overline{u_i}(f_i)\left[\frac{(r_i^m)^2}{2} - \frac{(r_i^{a\star})^2}{2}\right] - 2\overline{u_{i+1}}(f_{i+1})\left[\frac{(r_{i+1}^m)^2}{2} - \frac{(r_{i+1}^{a\star})^2}{2}\right]}{r_i^b\,\ell_i^b}, \qquad i \in \{1, \cdots, N-1\}.$$

Numerical results are obtained for different distributions of mucus thickness (in the case of the morphometric geometrical model with data provided in Table 2.2). Cases A, B, C, D, E, F correspond to distributions varying from δ_0 to δ_{16} with constant thickness in proximal and distal regions and a transition mucus thickness that varies smoothly to sharply:

A) $(\delta_0, \delta_{16}) = (1 \cdot 10^{+0}, 5 \cdot 10^{-3})\ \mu$m;

B) $(\delta_0, \delta_{16}) = (1 \cdot 10^{+0}, 1 \cdot 10^{-2})\ \mu$m;

C) $(\delta_0, \delta_{16}) = (1 \cdot 10^{+0}, 5 \cdot 10^{-2})\ \mu$m;

D) $(\delta_0, \delta_{16}) = (1 \cdot 10^{+0}, 1 \cdot 10^{-1})\ \mu$m;

E) $(\delta_0, \delta_{16}) = (1 \cdot 10^{+0}, 5 \cdot 10^{-1})\ \mu$m;

F) $(\delta_0, \delta_{16}) = (1 \cdot 10^{+0}, 1 \cdot 10^{+0})\ \mu$m.

Other cases investigate particular profiles:

G) *Gaussian* profiles of the mucus thickness, varying from $\delta_0 = 1 \cdot 10^{+0}\ \mu$m to different values of δ_{16} (successively $5 \cdot 10^{-3}$, $1 \cdot 10^{-2}$, $5 \cdot 10^{-2}$, $1 \cdot 10^{-1}$, $5 \cdot 10^{-1}$, $1 \cdot 10^{+0}\ \mu$m);

H) *geometrical* profiles of the mucus thickness, varying from $\delta_0 = 1 \cdot 10^{+0}\ \mu$m to different values of δ_{16} (successively $5 \cdot 10^{-3}$, $1 \cdot 10^{-2}$, $5 \cdot 10^{-2}$, $1 \cdot 10^{-1}$, $5 \cdot 10^{-1}$, $1 \cdot 10^{+0}\ \mu$m).

A)

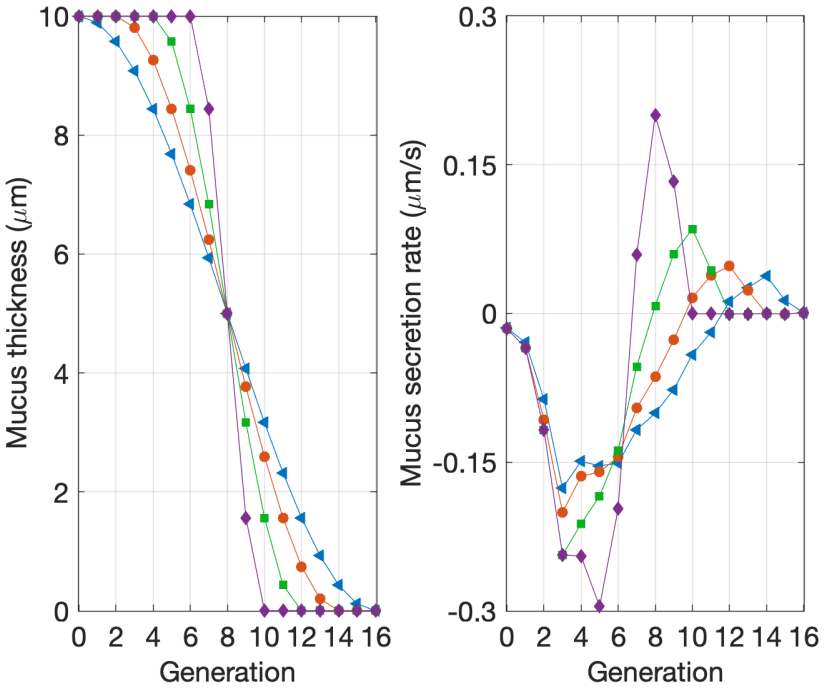

B)

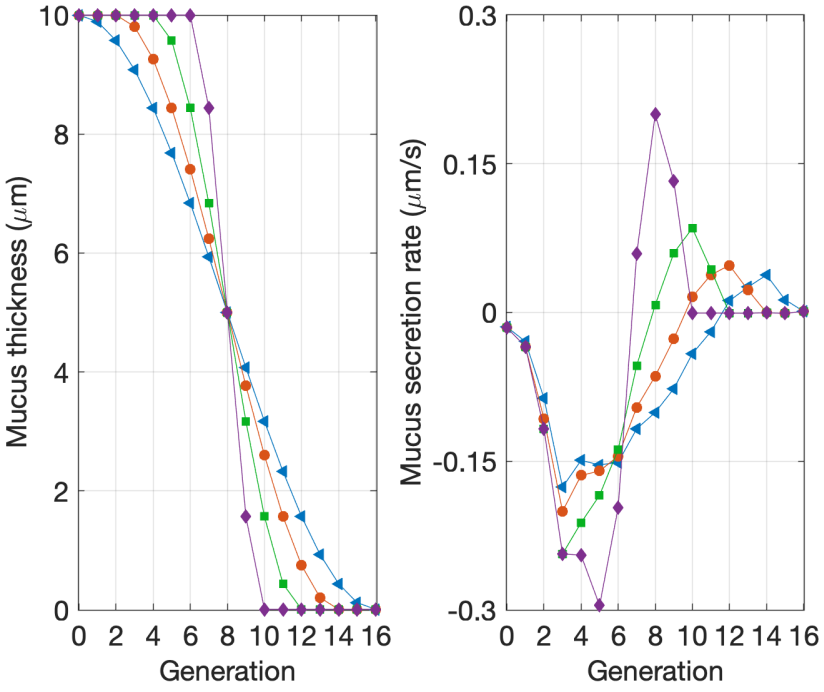

Figure 2.15 – Secretion rate associated to *given* mucus thickness distribution, in case A mucus thickness $\delta_{16} = 5 \cdot 10^{-3}$ μm and $\delta_{16} = 1 \cdot 10^{-2}$ μm in case B. All data provided in Table 2.2.

C)

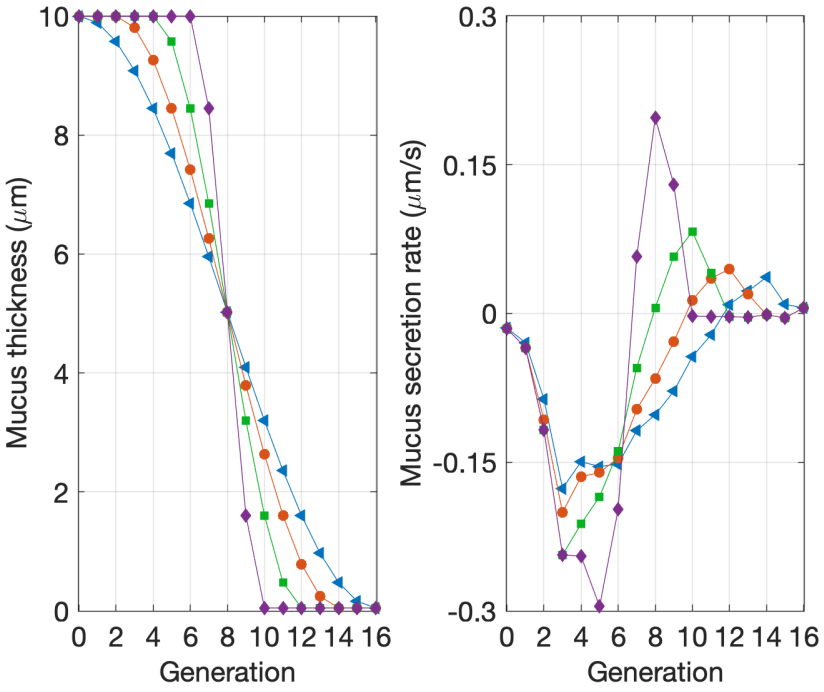

D)

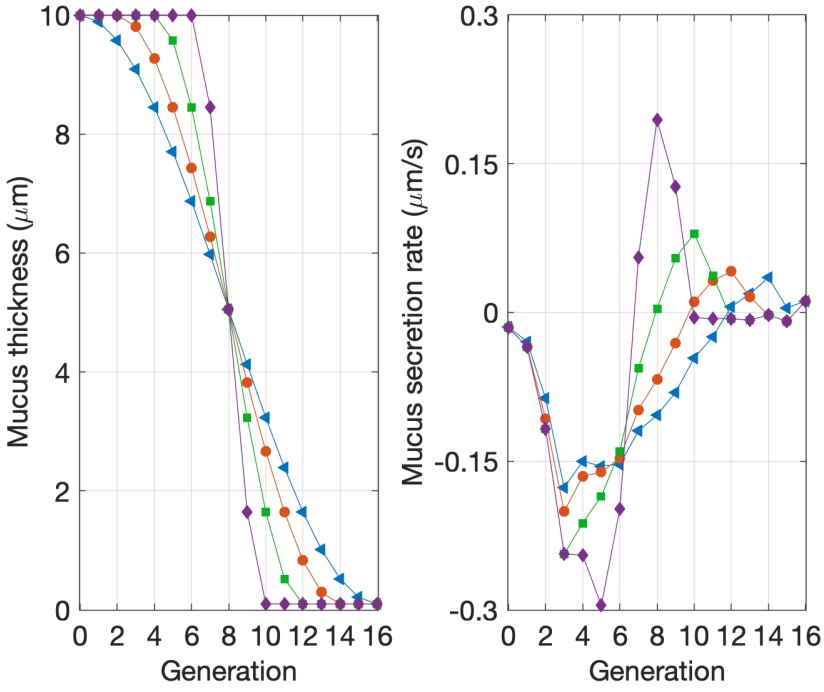

Figure 2.16 – Secretion rate associated to *given* mucus thickness distribution, in case C mucus thickness $\delta_{16} = 5 \cdot 10^{-2}$ μm and $\delta_{16} = 1 \cdot 10^{-1}$ μm in case D. All data provided in Table 2.2.

E)

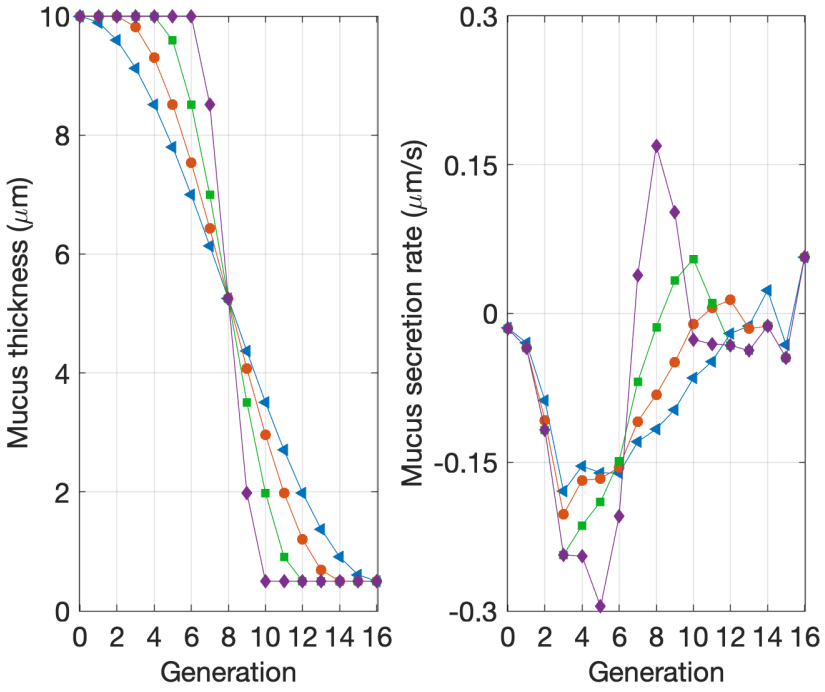

F)

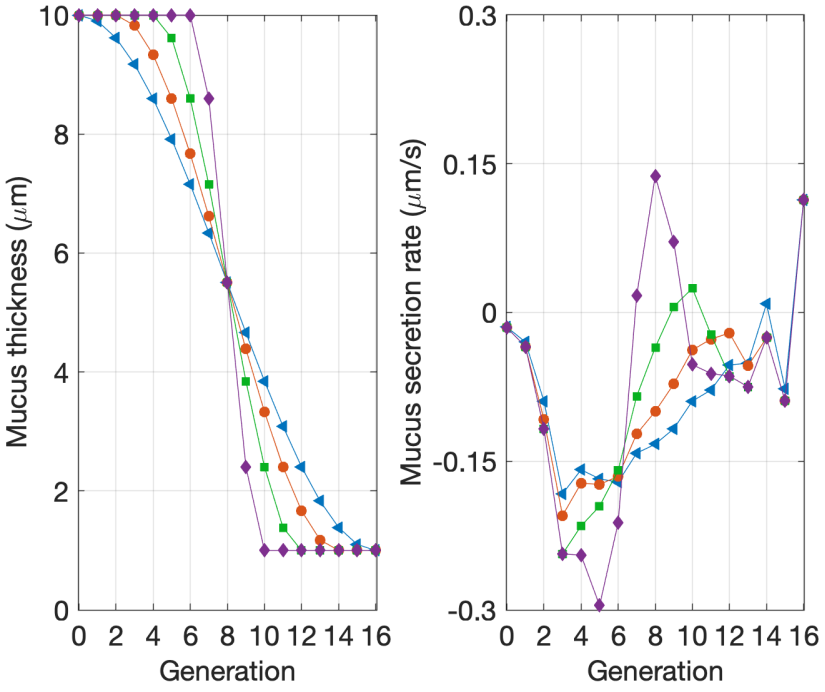

Figure 2.17 – Secretion rate associated to *given* mucus thickness distribution, in case E mucus thickness $\delta_{16} = 5 \cdot 10^{-1}$ μm and $\delta_{16} = 1 \cdot 10^{+0}$ μm in case F. All data provided in Table 2.2.

G)

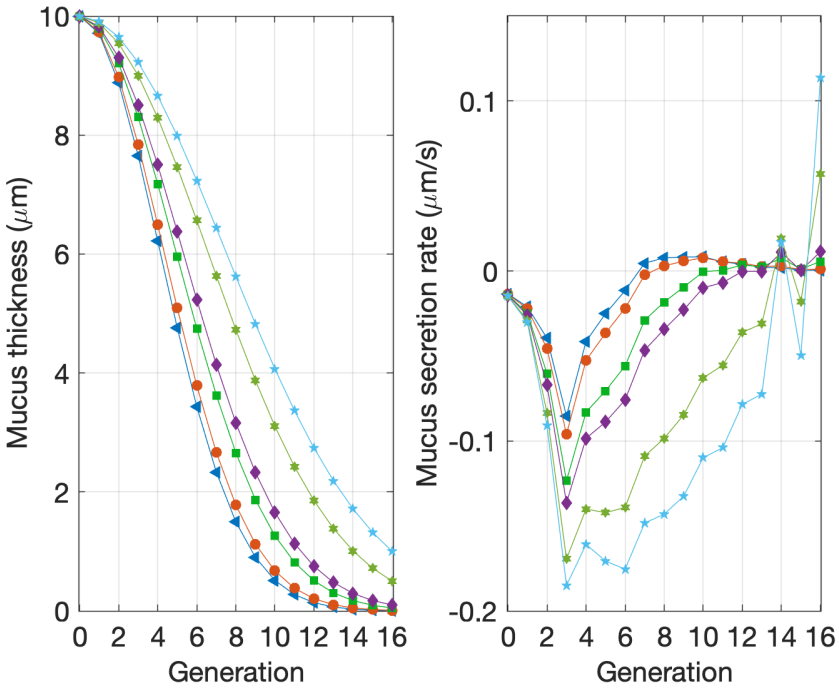

H)

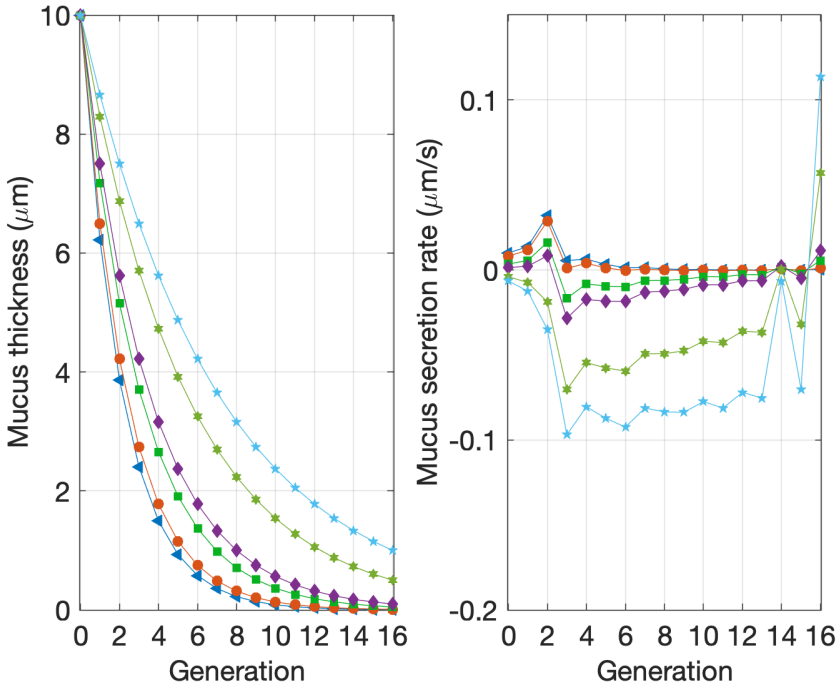

Figure 2.18 – Secretion rate associated to *given* mucus thickness distribution with both gaussian and geometrical profile. All data provided in Table 2.2.

Results V: identification of mucus secretion rate distribution

In figure 2.15 and 2.16 and 2.17, we observe almost the same distribution of the secretion rate of mucus. The secretion rate is negative in the sixth generation, but increases by smoothing the distribution of mucus thickness. The secretion rate reaches its maximal value at the 8-th generation and its minimal value at the 5-th generation. From case A to F, we fix the mucus thickness δ_0 at the trachea and vary δ_{16}. We observe that the higher the mucus thickness δ_{16}, the lower the total secretion rate. This scenario is also observed in figure 2.18 where mucus thickness δ_0 is fixed and δ_{16} varies from $5 \cdot 10^{-3}\mu$m to $1 \cdot 10^{+0}\mu$m. Also in both cases from A to H we obtain a positive secretion rate at the last generation, and positive in every generation in the H case with imposed mucus thickness drawn with the red line marked with a circle and blue line marked with a triangle. Finally in our model, to obtain a positive secretion rate in every generation, mucus thickness distribution should have a geometrical profile with an order of $10^{-3}\mu$m of mucus thickness at the last generation.

2.5 Conclusion

In this work, we developed a new model for estimating mucus thicknesses in a symmetrical bronchial lumen. This model takes into account the characteristic sizes of the cilia, that is to say on the microscopic scale, and the characteristic sizes on the macroscopic scale, namely that of the pulmonary bronchi. By taking into account on the one hand the ciliary activity to evacuate mucus from the bronchi, and on the other hand the secretion of mucus at the level of the epithelium, we compute the equilibrium state of the mucus layer thickness in each generation. Furthermore, the PCL layer is assumed to be constant in time, so there is no transfer of the PCL from one generation to another. Subsequently, estimates of the secretion rate were made by studying different configurations, nevertheless, questions can be raised on this subject, namely: does the secretion rate at the level of a bronchus depend on the generation to which the bronchus belongs? Also, is the secretion rate uniform across the surface of the bronchus? Furthermore, this is one of the hypotheses considered in our model. In the case where the secretion rate depends only on generations, in what way does it depend, increasing according to generations or decreasing?

Also in our model, we assumed that the density of cilia is constant over the entire surface of the bronchi. However, as mentioned in [51], cilia are less and less present through the generations. This constitutes perspectives for enriching our model and therefore obtaining a more realistic version.

Chapter 3

Dynamics of the mucociliary transport in the bronchial tree

3.1 Introduction

In a breathing regime, airflow stress may have a role in the mucus clearance process. The study of the impact of airflow on mucus draining has been one of the works of Mauroy et al [48]. By adopting a Weibel type bronchial tree geometry, and under the influence of air shear due to airflow, the authors studied the dynamic of mucus which is assumed to be a non-Newtonian Bingham fluid. Afterward, for an imposed airflow and a given yield stress, the authors studied the mucus distribution at equilibrium in the tree. Also, physiotherapy is a very powerful tool for mucus draining, in fact in a pathological case, the goal is to optimize the evacuation of mucus through a series of inspirations and then expirations. The study of the impact of physiotherapy on the flow of mucus was one of the works of Mauroy et al [47]. Under the influence of air shear due to a regime of inspiration then expiration, the authors studied the evolution of the mucus layer carried on each generation of bronchi, and the latter can be deformed thanks to external manipulations on a patient's thorax.

In this chapter, we will combine two phenomena, namely, the influence of airflow on mucus, and the constraint linked to ciliary activity on mucus in a bronchial tree geometry. To do this, we will use the model established in Chapter 2, which provides us with the average speed of the flow due to the movement of the cilia in each generation of bronchus. To this constraint, we add others linked to the shear applied by the air on the mucus. The airflow will be considered from Poiseuille, we thus have an explicit expression of the constraints exerted on the fluid.

3.2 Periodic behaviour in breathing scenarios

Let $T > 0$ be the breathing period and $t \mapsto \Phi^{\text{air}}_{\text{mouth}}(t)$ a $T-$periodic function that defines the airflow at the trachea (breathing scenario). Under Assumption 2, evolution of the mucus distribution is governed by:

$$\frac{\mathrm{d}r_i^a(t)}{\mathrm{d}t} = \frac{Q_i(U_i; r_i^a(t)) - 2Q_{i+1}(U_{i+1}; r_{i+1}^a(t))}{2\pi \ell_i^b r_i^a(t)} - \tilde{\phi}\frac{r_i^b}{r_i^a(t)}, \qquad i \in \{0, ..., N\}. \tag{3.1}$$

The periodicity problem writes: for $i = 0, \cdots, N$, find $r^a_{i,0}$ such that the unique solution of the Cauchy problem:

$$(\mathrm{O}_i) \begin{cases} \bullet \quad \dfrac{\mathrm{d}r^a_i(t)}{\mathrm{d}t} = \dfrac{Q_i(U_i; r^a_i(t)) - 2Q_i(U_{i+1}; r^a_{i+1}(t))}{2\pi \ell^b_i r^a_i(t)} - \tilde{\phi}\dfrac{r^b_i}{r^a_i(t)}, \ t \in (0,T), \\ \bullet \quad r^a_i(0) = r^a_{i,0} \end{cases}$$

satisfies $r^a_i(T) = r^a_i(0)$.

We recall that U_i, u_i, v_i denote respectively the solution of the (M+A) problem, (M) problem and (A) problem defined in Chapter 2, and that $U_i = u_i + v_i$.

Mathematical structure of problems $(\mathrm{O}_i)_{i=0,\cdots,N}$

Terminal generation

We first focus on the last generation, since we take advantage of the fact that $Q_{N+1} \equiv 0$. Solving problem (O_N) requires to focus on $Q_N(U_N; r^a_N(t))$, which is modified as

$$Q_N(U_N; r^a_N) = Q_N(u_N; r^a_N) + Q_N(v_N; r^a_N) = 2\pi\overline{u_N}\left[\frac{(r^m_N)^2}{2} - \frac{(r^a_N)^2}{2}\right] + 2\pi \int_{r^a_N}^{r^m_N} r v_N(r)\,\mathrm{d}r.$$

As a consequence, r^a_N satisfies the ODE

$$\frac{\mathrm{d}r^a_N(t)}{\mathrm{d}t} = \frac{2\pi\overline{u_N}\left[\frac{(r^m_N)^2}{2} - \frac{(r^a_N(t))^2}{2}\right] + 2\pi\int_{r^a_N(t)}^{r^m_N} r v_N(r)\,\mathrm{d}r}{2\pi \ell^b_N r^a_N(t)} - \tilde{\phi}\frac{r^b_N}{r^a_N(t)}$$

and defining

$$\tilde{\alpha}_N := \frac{\overline{u_N}(r^m_N)^2}{\ell^b_N} - 2\tilde{\phi} r^b_N, \qquad \tilde{\beta}_N := \frac{\overline{u_N}}{\ell^b_N}, \qquad \tilde{\gamma}_N := \frac{2}{\ell^b_N},$$

it can be rewritten as

$$\frac{\mathrm{d}[r^a_N(t)]^2}{\mathrm{d}t} = \tilde{\alpha}_N - \tilde{\beta}_N[r^a_N(t)]^2 + \tilde{\gamma}_N \int_{r^a_N(t)}^{r^m_N} r v_N(r)\,\mathrm{d}r.$$

Thus problem (O_N) consists in finding $r^a_{N,0}$ such that the unique solution $t \mapsto r^a_N(t)$ of

$$\begin{cases} \dfrac{\mathrm{d}[r^a_N(t)]^2}{\mathrm{d}t} = \tilde{\alpha}_N - \tilde{\beta}_N[r^a_N(t)]^2 + \tilde{\gamma}_N \displaystyle\int_{r^a_N(t)}^{r^m_N} r v_N(r)\,\mathrm{d}r, \quad t \in (0,T), \\ r^a_N(0) = r^a_{N,0} \end{cases} \tag{3.2}$$

satisfies

$$r^a_N(T) = r^a_N(0).$$

Other generations

We assume that (O_{i+1}) is solved, thus providing a (known) periodic function $t \mapsto r^a_{i+1}(t)$ over $(0,T)$. We now focus on generation i: solving problem (O_i) requires to focus on $Q_i(U_i; r^a_i(t))$, which is written as

$$Q_i(U_i; r^a_i) = Q_i(u_i; r^a_i) + Q_i(v_i; r^a_i) = 2\pi\overline{u_i}\left[\frac{(r^m_i)^2}{2} - \frac{(r^a_i)^2}{2}\right] + 2\pi \int_{r^a_i}^{r^m_i} r v_i(r)\,\mathrm{d}r.$$

As a consequence, r_i^a satisfies the ODE

$$\frac{\mathrm{d}r_i^a(t)}{\mathrm{d}t} = \frac{2\pi\overline{u_i}\left[\frac{(r_i^m)^2}{2} - \frac{(r_i^a(t))^2}{2}\right] + 2\pi\int_{r_i^a(t)}^{r_i^m} rv_i(r)\,\mathrm{d}r - 2Q_{i+1}(U_{i+1}; r_{i+1}^a(t))}{2\pi\ell_i^b r_i^a(t)} - \tilde{\phi}\frac{r_i^b}{r_i^a(t)}$$

where the term $Q_{i+1}(U_{i+1}; r_{i+1}^a(t))$ is known. Defining parameters $\tilde{\alpha}_i$, $\tilde{\beta}_i$, $\tilde{\gamma}_i$ and function $t \mapsto \tilde{\delta}_i(t)$

$$\tilde{\alpha}_i := \frac{\overline{u_i}(r_i^m)^2}{\ell_i^b} - 2\tilde{\phi}r_i^b, \qquad \tilde{\beta}_i := \frac{\overline{u_i}}{\ell_i^b}, \qquad \tilde{\gamma}_i := \frac{2}{\ell_i^b}, \qquad \tilde{\delta}_i(t) := \frac{2}{\pi\ell_i^b}Q_{i+1}(U_{i+1}; r_{i+1}^a(t)),$$

it can be rewritten as

$$\frac{\mathrm{d}[r_i^a(t)]^2}{\mathrm{d}t} = \tilde{\alpha}_i - \tilde{\delta}_i(t) - \tilde{\beta}_i[r_i^a(t)]^2 + \tilde{\gamma}_i\int_{r_i^a(t)}^{r_i^m} rv_i(r)\,\mathrm{d}r.$$

Thus problem (O_i), for $i = 0, \cdots, N-1$, consists in finding $r_{i,0}^a$ such that the unique solution $t \mapsto r_i^a(t)$ of

$$\begin{cases} \dfrac{\mathrm{d}[r_i^a(t)]^2}{\mathrm{d}t} = \tilde{\alpha}_i - \tilde{\delta}_i(t) - \tilde{\beta}_i[r_i^a(t)]^2 + \tilde{\gamma}_i\displaystyle\int_{r_i^a(t)}^{r_i^m} rv_i(r)\,\mathrm{d}r, \quad t \in (0,T), \\ r_i^a(0) = r_{i,0}^a \end{cases} \tag{3.3}$$

satisfies

$$r_i^a(T) = r_i^a(0).$$

At this stage it is not possible to easily compute $i = 0, \cdots, N-1$ the value of $r_i^a(0)$ that would guarantee the periodicity of $t \mapsto r_i^a(t)$. Nevertheless a numerical procedure allows us to build the solution, based upon a dichotomy strategy, see Algorithm 2, or a fixed point strategy, see Algorithm 3.

Strategies for solving $(\mathrm{O}_i)_{i=0,\cdots,N}$

Solving (O_N) or $(\mathrm{O}_i)_{i=0,\cdots,N-1}$ follows the same guideline, as Eq. (3.2) and (3.3) have the very same mathematical structure (the problems only differ by the definitions of function $\tilde{\alpha}_i$ and parameters $\tilde{\beta}_i$, $\tilde{\gamma}_i$).

Algorithm 2 (Solving $(\mathrm{O}_i)_{i=0,\cdots,N-1}$ by dichotomy)**.**

- Initialization:

  $a^{(0)} := 0$ *and* $b^{(0)} := r_i^m$.

  Solve Eq. (3.2) *if* $i = N$, *or Eq.* (3.3) *if* $i < N$, *with initial data* $r_i^a(0) = a^{(0)}$. *We get* $r_i^a(T) - r_i^a(0) < 0$.

  Solve Eq. (3.2) *if* $i = N$, *or Eq.* (3.3) *if* $i < N$, *with initial data* $r_i^a(0) = b^{(0)}$. *We get* $r_i^a(T) - r_i^a(0) > 0$.

- Iterations: *for* $k \geq 0$,

  $[r_i^a]^{(k)}(0) := \frac{a^{(k)}+b^{(k)}}{2}$

  Solve Eq. (3.2) *if* $i = N$, *or Eq.* (3.3) *if* $i < N$, *with initial data* $r_i^a(0) = [r_i^a]^{(k)}(0)$. *Then,*

  if $r_i^a(T) - r_N^a(0) < 0$, $a^{k+1} = [r_i^a]^{(k)}(0)$, $b^{(k+1)} = b^{(k)}$,
  if $r_i^a(T) - r_N^a(0) > 0$, $b^{k+1} = [r_i^a]^{(k)}(0)$, $a^{(k+1)} = a^{(k)}$.

- Conclusion: *the initial condition that provides a periodic solution* $t \mapsto r_i^a(t)$ *over* $(0,T)$ *is*

$$r_i^a(0) := \frac{a^{(\infty)} + b^{(\infty)}}{2}.$$

An alternative strategy is based upon a fixed point procedure:

Algorithm 3 (Solving $(\mathrm{O}_i)_{i=0,\cdots,N-1}$ by fixed point procedure)**.**

- Define:

$$\mathcal{F}_i : r_i^a(0) \mapsto r_i^a(T),$$

where $r_i^a(T)$ *is the solution at time* T *of Eq.* (3.2) *if* $i = N$*, or Eq.* (3.3) *if* $i < N$*, with initial data* $r_i^a(0)$*.*

- Initialization:

$[r_i^a]^{(0)}(0)$ *is chosen.*

- Iterations: *for* $k \geq 0$*,*

$[r_i^a]^{(k+1)}(0) := \mathcal{F}_i([r_i^a]^{(k)}(0))$ *(this step requires to solve Eq.* (3.2) *if* $i = N$*, or Eq.* (3.3) *if* $i < N$*, with initial data* $r_i^a(0) = [r_i^a]^{(k)}(0)$*.*

- Conclusion: *the initial condition that provides a periodic solution* $t \mapsto r_i^a(t)$ *over* $(0,T)$ *is*

$$r_i^a(0) := [r_i^a]^{(\infty)}(0).$$

Note that a specific order is required for solving the periodic problem: one should first solve (O_N), then (O_{N-1}), (O_{N-2}), $\cdots$, (O_1).

Discretization and numerical scheme

Terminal generation Let us first discuss the dynamics of mucus in generation N. Solving Eq. (3.2) can be performed in the following way: time interval is divided into K time steps, $T = K\Delta t$. Furthermore, for the sake of clarity, we will use the notations

$$r^n \simeq r_N^a(n\Delta t), \qquad R^n \simeq [r_N^a]^2(n\Delta t), \qquad n = 0, \cdots, K.$$

Using a discretization process leading to the computation of the sequence $\{r^n\}_{n=0,\cdots,K}$, the numerical approximation of $r_N^a(T)$ (required in Algorithm 2 or 3) is identified to r^K. Solving Eq. (3.2) consists in solving (D_N) :

$$(\mathrm{D}_N) \quad : \quad \frac{\mathrm{d}[r_N^a(t)]^2}{\mathrm{d}t} = \frac{Q_N(U_N; r_N^a(t))}{\pi \ell_N^b} - 2\tilde{\phi} r_N^b, \quad t \in (0,T),$$

wich can be rewritten as

$$(\mathrm{E}_N) \quad : \quad \frac{\mathrm{d}[r_N^a(t)]^2}{\mathrm{d}t} = \frac{Q_N(u_N; r_N^a(t)) + Q_N(v_N; r_N^a(t))}{\pi \ell_N^b} - 2\tilde{\phi} r_N^b, \quad t \in (0,T),$$

with a given initial condition $r_N^a(0)$. Let us now discuss how (D_N) or (E_N) can be solved numerically.

Explicit scheme The most simple strategy, perhaps, is based upon a full explicit scheme: it is straightforward but it may lead to impose small time steps in order to ensure stability of the computations.

- *Version 1 based upon (M+A).* We define

$$\frac{R^{n+1}-R^n}{\Delta t} = \frac{Q_N(U_N;r^n)}{\pi \ell_N^b} - 2\tilde{\phi} r_N^b, \qquad r^{n+1} = \sqrt{R^{n+1}}.$$

  As a consequence, the scheme is only based upon the computation of $Q_N(U_N;r^n) = 2\pi \int_{r^n}^{r_i^m} rU_N(r)\,\mathrm{d}r$, which requires at each time step to solve a (M+A) problem on (r^n, r_N^b) and store the value of $Q_N(U_N;r^n)$.

- *Version 2 based upon (A) (and (M) offline).* We define

$$\frac{R^{n+1}-R^n}{\Delta t} = \frac{Q_N(u_N;r^n)+Q_N(v_N;r^n)}{\pi \ell_N^b} - 2\tilde{\phi} r_N^b, \qquad r^{n+1} = \sqrt{R^{n+1}}.$$

  The scheme actually writes, after simple computations:

$$\frac{R^{n+1}-R^n}{\Delta t} = \tilde{\alpha}_N - \tilde{\beta}_N R^n + \tilde{\gamma}_N \int_{r^n}^{r_N^m} r v_N(r)\,\mathrm{d}r, \qquad r^{n+1} = \sqrt{R^{n+1}}. \tag{3.4}$$

  As a consequence, the scheme is only based upon the computation of two contributions: the first one, $Q_N(u_N;r^n) = 2\pi\overline{u_N}\left[(r_i^m)^2 - (r^n)^2\right]$, is straightforward, provided that $\overline{u}_N$ is known (this can be done offline once for all); the second one $Q_N(v_N;r^n) = 2\pi \int_{r^n}^{r_i^m} r v_N(r)\,\mathrm{d}r$ requires at each time step to solve an (A) problem on (r^n, r_N^b) and store the value of $Q_N(v_N;r^n)$.

Implicit-explicit scheme Using (E_N), the implicit-explicit scheme is defined by:

$$\begin{aligned} \frac{R^{n+1}-R^n}{\Delta t} &= \frac{Q_N(u_N;r^{n+1})+Q_N(v_N;r^n)}{\pi \ell_N^b} - 2\tilde{\phi} r_N^b, \\ r^{n+1} &= \sqrt{R^{n+1}}. \end{aligned}$$

The scheme actually states, after simple computations:

$$\frac{R^{n+1}-R^n}{\Delta t} = \tilde{\alpha}_N - \tilde{\beta}_N R^{n+1} + \tilde{\gamma}_N \int_{r^n}^{r_N^m} r v_N(r)\,\mathrm{d}r, \qquad r^{n+1} = \sqrt{R^{n+1}}. \tag{3.5}$$

A simple computation on Eq. (3.5) leads us to the following sequence:

$$r^{n+1} = \sqrt{\frac{(r^n)^2 + \Delta t\tilde{\alpha}_N + \Delta t\tilde{\gamma}_N \displaystyle\int_{r^n}^{r_N^m} r v_N(r)\,\mathrm{d}r}{1+\Delta t\tilde{\beta}_N}}.$$

Note that, at each time step, the computation of (R^{n+1}, r^{n+1}) requires to solve an (A) problem on (r^n, r_N^b). It also requires to solve a (M) problem in order to compute $\overline{u_N}$ (that is required in parameters α_N and β_N) but, as already outlined, this computation can be done once for all (as $\overline{u_N}$ does not depend on r^n, provided $r^n < r_N^m$).

Remark 21. *Eq.* (3.5) *takes advantage of an implicit/explicit discretization:*

- *the implicit treatment of the motility contribution* $-\tilde{\beta}_N R^{n+1}$ *provides stability of the numerical scheme;*
- *the explicit treatment of the airflow contribution* $\tilde{\gamma}_N \displaystyle\int_{r^n}^{r_N^m} r v_N(r)\,\mathrm{d}r$ *skips the main computational difficulty.*
- *as a conclusion the implicit/explicit and the explicit schemes share a similar computational cost; but the implicit-explicit scheme is numerically more stable than the explicit scheme: the stability could be unconditional in practice, as the influence of the explicit term is perturbative (see (a) in Figure 2.8).*

Remark 22. *It is possible to define a fully implicit scheme, defining subiterations based upon Eq.* (3.5)*:*

- Initialization:

  $R^{(0)} := R^n$ *and* $r^{(0)} := r^n$.

- Iterations: *for* $k \geq 0$,

$$\frac{R^{(k+1)} - R^n}{\Delta t} = \tilde{\alpha}_N - \tilde{\beta}_N R^{(k+1)} + \tilde{\gamma}_N \int_{r^{(k)}}^{r_N^m} r v_N(r)\,\mathrm{d}r, \qquad r^{(k+1)} = \sqrt{R^{(k+1)}}.$$

- Conclusion: $(R^{n+1}, r^{n+1}) = (R^{(\infty)}, r^{(\infty)})$.

However the implicit scheme requires many resolutions of (A) problems (defined on $(r^{(k)}, r_N^b)$*), leading to a high computational cost for little quality increase as the considered term is presumably perturbative.*

Discretization for other generations

The implicit-explicit scheme defined for generation N readily adapts, up to the fact that $\tilde{\delta}_i$ depends on time and should be approached by its approximated value at time $t^{n+1}\Delta t$. For the sake of clarity, we use the notations

$$r^n \simeq r_i^a(n\Delta t), \qquad R^n \simeq [r_i^a]^2(n\Delta t), \qquad n = 0, \cdots, K.$$

Using a discretization process leading to the computation of the sequence $\{r^n\}_{n=0,\cdots,K}$, the numerical approximation of $r_i^a(T)$ (required in Algorithm 2 or 3) is identified to r^K. Solving Eq. (3.3) numerically relies on the implicit-explicit scheme:

$$\frac{R^{n+1} - R^n}{\Delta t} = \tilde{\alpha}_i - \tilde{\delta}_i^{n+1} - \tilde{\beta}_i R^{n+1} + \tilde{\gamma}_i \int_{r^n}^{r_N^m} r v(r)\,\mathrm{d}r, \qquad r^{n+1} = \sqrt{R^{n+1}}, \tag{3.6}$$

where $\tilde{\delta}_i^{n+1}$ approximates $\tilde{\delta}_i(t^{n+1})$ in the following way:

$$\tilde{\delta}_i^{n+1} = \frac{2Q_{i+1}(U_{i+1}; [r_{i+1}^a]^{n+1})}{\pi \ell_i^b} = \frac{2\left\{2\pi\overline{u_{i+1}}\left[\frac{(r_{i+1}^m)^2}{2} - \frac{([r_{i+1}^a]^{n+1})^2}{2}\right] + Q_{i+1}(v_{i+1}; [r_{i+1}^a]^{n+1})\right\}}{\pi \ell_i^b},$$

where $\{r_{i+1}^a]^n\}_{n=0,\cdots,K}$ denotes the numerical approximation of $t \mapsto r_{i+1}^a(t)$ (which is known). This does not require to solve additional 1D problem but to store the numerical approximations related to generation $i+1$, in particular the numerical approximations at time t^{n+1} of

- either $t \mapsto Q_{i+1}(U_{i+1}; r_{i+1}^a(t))$,

- or $t \mapsto r_{i+1}^a(t)$ and $t \mapsto Q_{i+1}(v_{i+1}; r_{i+1}^a(t))$).

Note that a simple computation on Eq. (3.6) leads us to the following sequence:

$$r^{n+1} = \sqrt{\frac{(r^n)^2 + \Delta t(\tilde{\alpha}_i - \tilde{\delta}_i^{n+1}) + \Delta t \tilde{\gamma}_i \displaystyle\int_{r^n}^{r_i^m} r v_i(r)\,\mathrm{d}r}{1 + \Delta t \tilde{\beta}_i}}.$$

Remark 23. *Let N be the number of generations of the bronchial tree, K the number of time steps for the discretization of time interval $(0, T)$ and n_D the number of dichotomy iterations in Algorithm 2 or 3. Solving $(\mathrm{O}_i)_{i=0,\cdots,N-1}$ requires $\mathcal{C} = N \times K \times n_D$ resolutions of 1D problems (M+A or A). In practice, for $N = 17$, $K = 100$, $\mathcal{C} = 1700 \times n_D$.*

3.3 Numerical results

3.3.1 Sinusoidal airflow

We consider the following data:

- the geometrical bronchial tree is based upon the morphometric model, see Table 2.1;
- ciliary activity is taken from Table 2.2 with a variable frequency beat;
- the air flux at mouth is idealized:

$$\Phi_{\mathrm{mouth}}^{\mathrm{air}}(t) = \Phi_{\mathrm{max}}^{\mathrm{air}} \sin\left(2\pi \frac{t}{T}\right)$$

  where the breathing period T is fixed to 4 s. The value assigned to $\Phi_{\mathrm{max}}^{\mathrm{air}}$ allows us to mimic the different respiratory regimes:

  - normal breathing: $\Phi_{\mathrm{max}}^{\mathrm{air}} = 0.25\,\mathrm{L}\cdot\mathrm{s}^{-1}$;
  - forced breathing: $\Phi_{\mathrm{max}}^{\mathrm{air}} = 2.50\,\mathrm{L}\cdot\mathrm{s}^{-1}$;
  - extreme breathing: $\Phi_{\mathrm{max}}^{\mathrm{air}} = 25.0\,\mathrm{L}\cdot\mathrm{s}^{-1}$.

- numerical parameters are $\Delta t = 0.05$ s (20 approximation nodes per second) and tolerance for the fixed-point iterative process is set to 10^{-5} for the relative error (for any generation).

Figures 3.1 to 3.3 describe the evolution of the mucus thickness in different respiration regimes: normal, forced and extreme. Figure 3.4 focuses on the very last generation (the most distal one) and compares the evolution of the mucus thickness in the three regimes: noteworthily the evolution of mucus thickness is little affected in normal conditions whereas it may reach nearly 10% in variation in extreme conditions.

Computations have been performed with a very simple sinusoidal respiration pattern. However in next subsections we aim to deal with more realistic flow patterns.

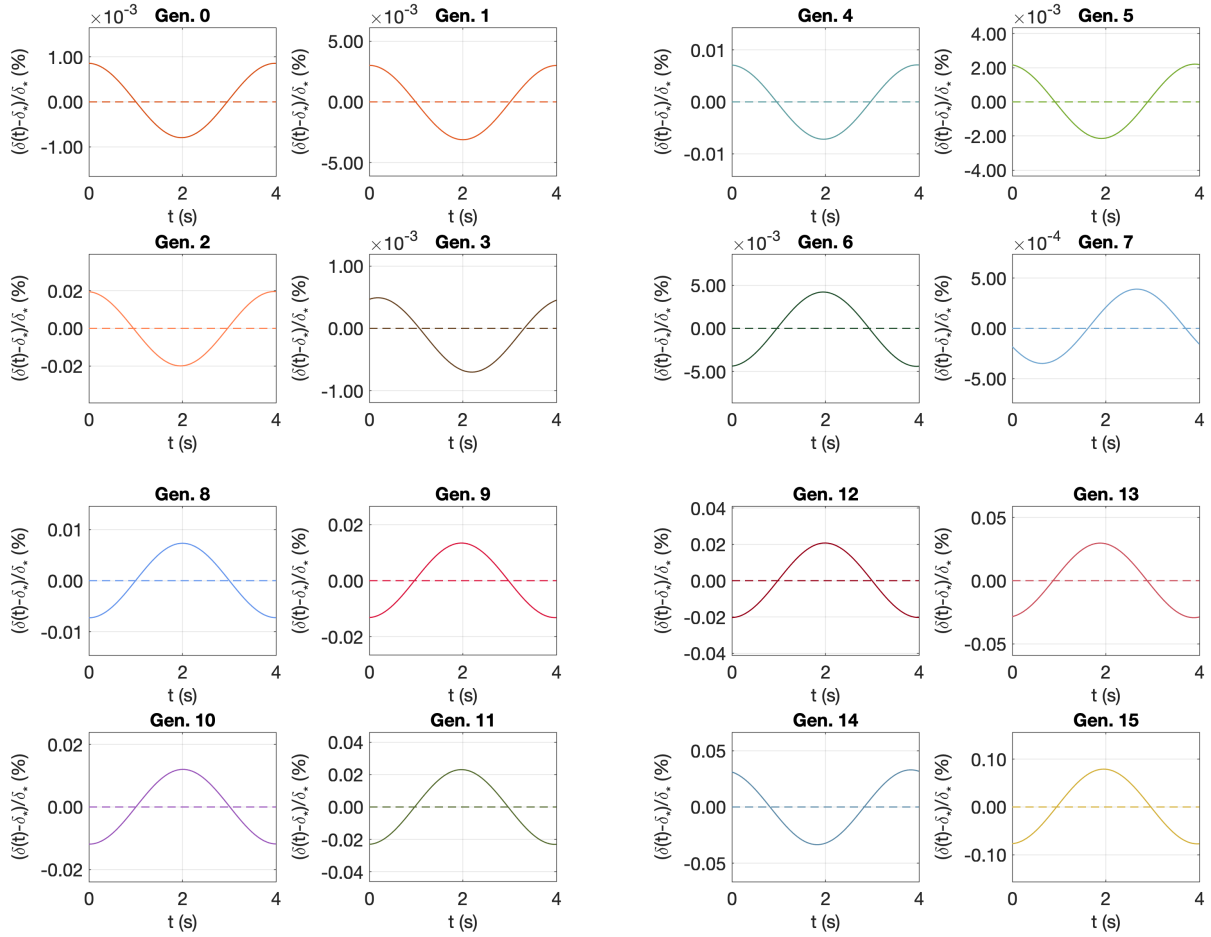

Figure 3.1 – *Normal* breathing ($\Phi^{\text{air}}_{\max} = 0.25\,\text{L}\cdot\text{s}^{-1}$): evolution of the mucus thickness $t \mapsto \delta(t) = r_i^m - r_i^a(t)$. The notation δ_* corresponds to the equilibrium mucus thickness of the considered generation. All data provided in Tables 2.1 and 2.2.

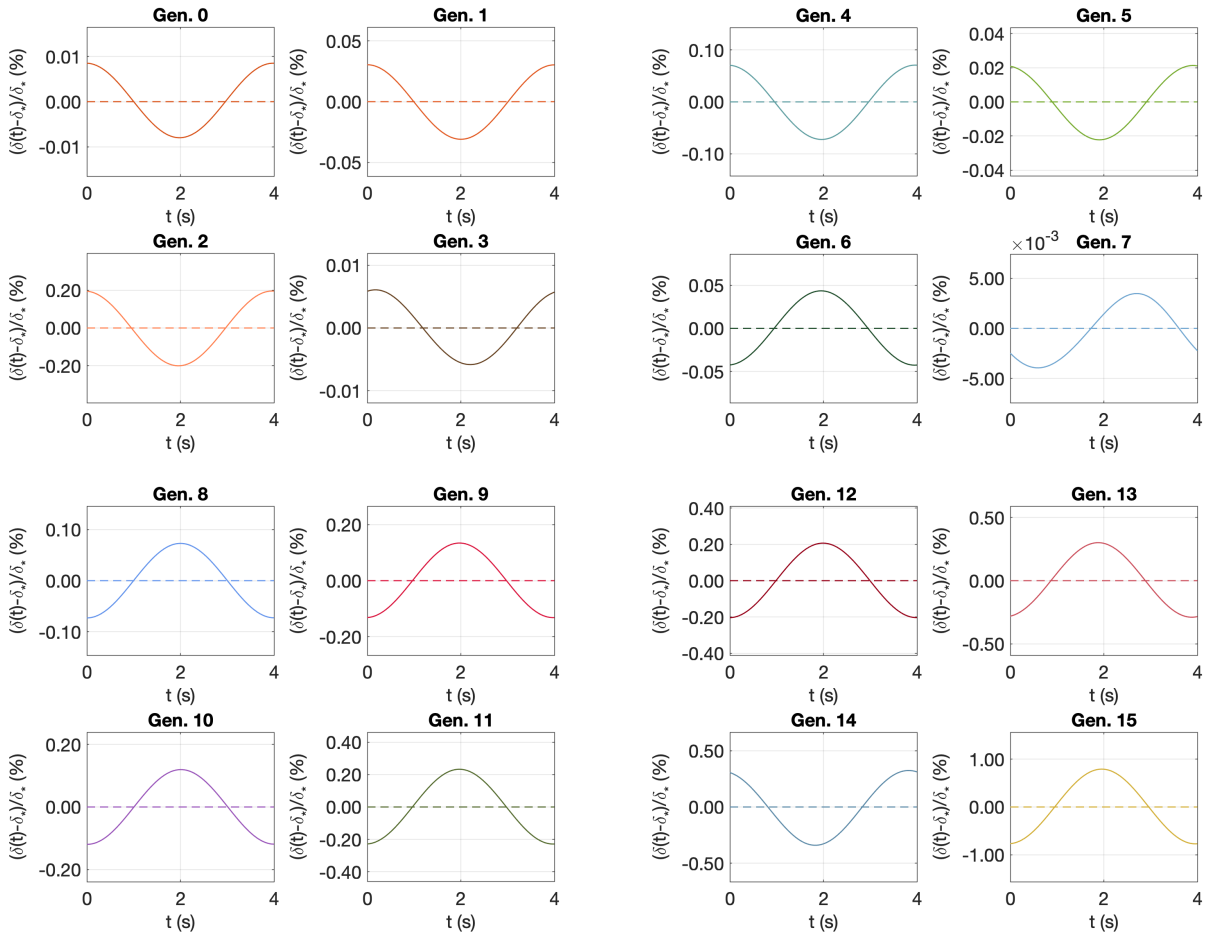

Figure 3.2 – *Forced* breathing ($\Phi^{\text{air}}_{\max} = 2.50\,\text{L}\cdot\text{s}^{-1}$): evolution of the mucus thickness $t \mapsto \delta(t) = r_i^m - r_i^a(t)$. The notation δ_* corresponds to the equilibrium mucus thickness of the considered generation. All data provided in Tables 2.1 and 2.2.

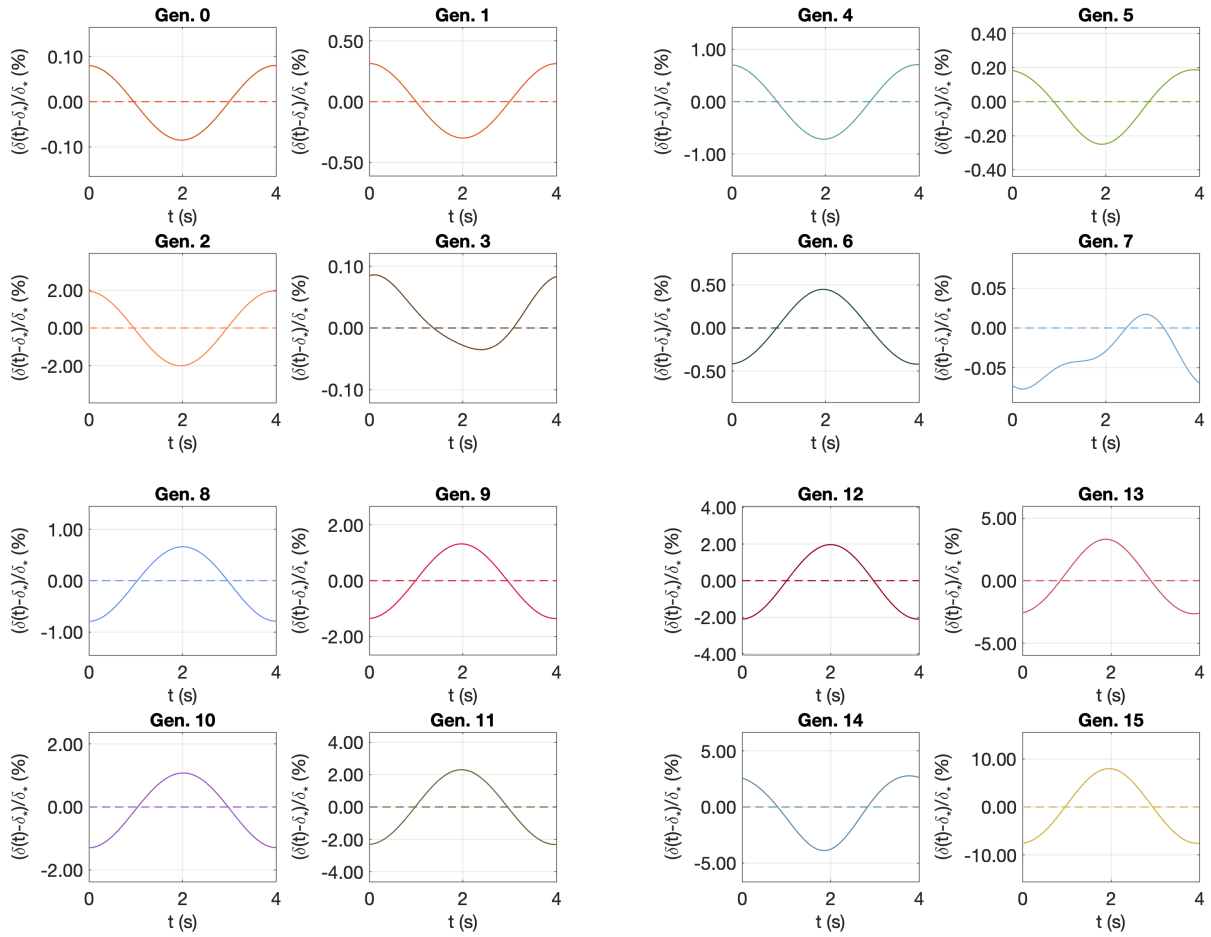

Figure 3.3 – *Extreme* breathing ($\Phi^{\text{air}}_{\max} = 25.0\,\text{L}\cdot\text{s}^{-1}$): evolution of the mucus thickness $t \mapsto \delta(t) = r_i^m - r_i^a(t)$. The notation δ_* corresponds to the equilibrium mucus thickness of the considered generation. All data provided in Tables 2.1 and 2.2.

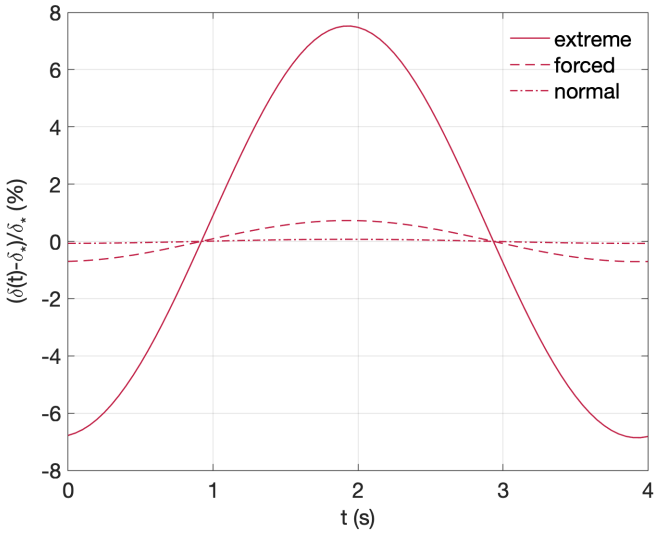

Figure 3.4 – Evolution of the mucus thickness $t \mapsto \delta(t) = r_i^m - r_i^a(t)$ in generation 16 (terminal generation, located before the entrance of the acinus) for different respiratory regimes: *normal* breathing ($\Phi_{\max}^{\text{air}} = 0.25\,\text{L}\cdot\text{s}^{-1}$), *forced* breathing ($\Phi_{\max}^{\text{air}} = 2.50\,\text{L}\cdot\text{s}^{-1}$) and *extreme* breathing ($\Phi_{\max}^{\text{air}} = 25.0\,\text{L}\cdot\text{s}^{-1}$). The notation δ_* corresponds to the equilibrium mucus thickness. All data provided in Tables 2.1 and 2.2.

3.3.2 Realistic airflow

In order to address more realistic flows, we consider the simplest linear mechanical model for the pulmonary dynamics: the pulmonary volume $t \mapsto V(t)$ satisfies a simple ODE:

$$R\dot{V}(t) + E(V(t) - V_{\text{FRC}}) = -P_{\text{ext}}(t), \tag{3.7}$$

The ODE involves the resistance R of the branches connecting alveoli to the outside air, the elastic properties of the surrounding medium measured by the elastance E, the functional residual volume V_{FRC} (volume at rest) for a healthy patient. The dynamics is ruled by $P_{\text{ext}}(t)$, which is the muscular pressure leading to the deformation of the lung parenchyma, which induces inspiration (and possibly forced expiration) at time t. This last quantity, often referred to as the airway opening or transpulmonary pressure, is chosen here as a periodic function: note that the pressure accounts for the effort of the diaphragm ($P_{\text{ext}}(t) < 0$ for inspiration), and possibly of the abdomen muscles during a forced expiration ($P_{\text{ext}}(t) = 0$ for passive expiration and $P_{\text{ext}}(t) > 0$ for forced expiration). We use a very simple respiratory command, which is assumed to be piecewise constant:

$$P_{\text{ext}}(t) = \begin{cases} -P_{\text{in}}, & \text{for } 0 < t \leq \alpha T \quad \text{i.e. at inspiration,} \\ +P_{\text{out}}, & \text{for } \alpha T < t \leq T \quad \text{i.e. at expiration,} \end{cases}$$

where P_{in} (resp. P_{out}) corresponds to the inspiratory (resp. expiratory) pressure controlled by the respiratory muscles.

Eq. (3.7) must be supplemented by an initial condition

$$V(0) = V_0 \tag{3.8}$$

and in order to have a $T-$periodic evolution of the volume, the value of V_0 is set to

$$V_0 = \frac{P_{\text{in}}\left(1 - e^{-\alpha T/\tau}\right) - P_{\text{out}}\left(e^{(1-\alpha)T/\tau} - 1\right)}{E\left(e^{(1-\alpha)T/\tau} - e^{-\alpha T/\tau}\right)} \tag{3.9}$$

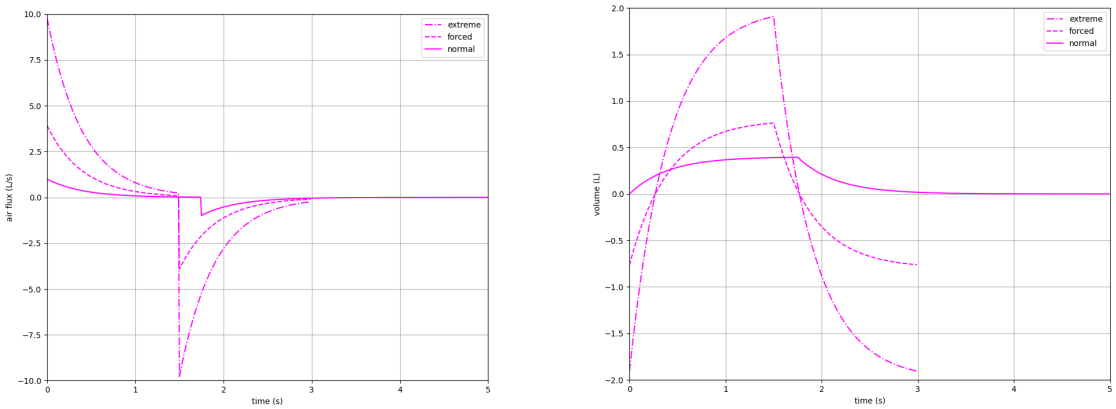

Figure 3.5 – Representation of air flux (left) and the associated lung volume (right) corresponding to different breathing scenarios.

where $\tau = (E/R)^{-1}$ is the characteristic relaxation time of the system.

Using Eq. (3.9) as the initial condition, the solution of Eq. (3.7)-(3.8) is periodic and writes:

$$V(t) = \begin{cases} V_0 e^{-t/\tau} + \frac{P_{\text{in}}}{E}\left(1 - e^{-t/\tau}\right), & \text{for } 0 < t \leq \alpha T \quad \text{i.e. at inspiration,} \\ V_0 e^{-t/\tau} + \frac{P_{\text{in}}}{E} e^{-t/\tau}\left(e^{+\alpha T/\tau} - 1\right) - \frac{P_{\text{out}}}{E}\left(1 - e^{-(t-\alpha T)/\tau}\right), & \text{for } \alpha T < t \leq T \quad \text{i.e. at expiration.} \end{cases}$$

As a consequence, the instantaneous air flux that enters the bronchial tree is derived from the volume and writes

$$Q(t) = \begin{cases} -\frac{V_0}{\tau} e^{-t/\tau} + \frac{P_{\text{in}}}{R} e^{-t/\tau}, & \text{for } 0 < t \leq \alpha T, \\ -\frac{V_0}{\tau} e^{-t/\tau} - \frac{P_{\text{in}}}{R} e^{-t/\tau}\left(e^{+\alpha T/\tau} - 1\right) - \frac{P_{\text{out}}}{R} e^{-(t-\alpha T)/\tau}, & \text{for } \alpha T < t \leq T. \end{cases} \tag{3.10}$$

Therefore Eq. (3.10) may be used for the modelling of air flux at mouth during a respiratory cycle.

For healthy patients, we use classical values available in the literature: $E = 3.5\,\text{cmH}_2\text{O} \cdot \text{L}^{-1}$ [32, 5, 6], $R = 2\,\text{cmH}_2\text{O} \cdot \text{s} \cdot \text{L}^{-1}$ [32, 6], $V_{\text{FRC}} = 3\,\text{L}$ [32, 74, 35]. The values assigned to P_{in} and P_{out} allow us to mimic the different respiratory regimes:

- normal breathing: $P_{\text{in}} = 2\,\text{cmH}_2\text{O}$, $P_{\text{out}} = 0\,\text{cmH}_2\text{O}$ (passive expiration); moreover we choose $T = 5\,\text{s}$ and $\alpha = 0.35$, which means that expiration is longer than inspiration;
- forced breathing: $P_{\text{in}} = 4\,\text{cmH}_2\text{O}$, $P_{\text{out}} = 4\,\text{cmH}_2\text{O}$ (active expiration); moreover we choose $T = 3\,\text{s}$ and $\alpha = 0.5$, which allows us to mimic forced maneuvers;
- extreme breathing: $P_{\text{in}} = 10\,\text{cmH}_2\text{O}$, $P_{\text{out}} = 10\,\text{cmH}_2\text{O}$; moreover we choose $T = 3\,\text{s}$ and $\alpha = 0.5$, as in the forced breathing scenario.

Remark 24. *In Figure 3.9, using a morphometric model and at the 16-th genration, we observe that mucus thickness oscillates around mucus thickness at equilibrium in a period of time. The inspiration tends to increase mucus thickness and expiration tends to decrease mucus thickness. Also, the higher imposed air flow $\Phi_{\text{max}}^{\text{air}}$ is, the higher is the amplitude of mucus thickness. We observe the same variation of mucus thickness with the Weibel model (Figure 3.4). This phenomenon is observed in every generation (Figure 3.6, 3.7 and 3.8) expect in generation 0, 1, 2, 3 and 14 where inspiration tends to decrease mucus thickness and expiration tends to increase mucus thickness. The reason is the geometry of the bronchus tree, more*

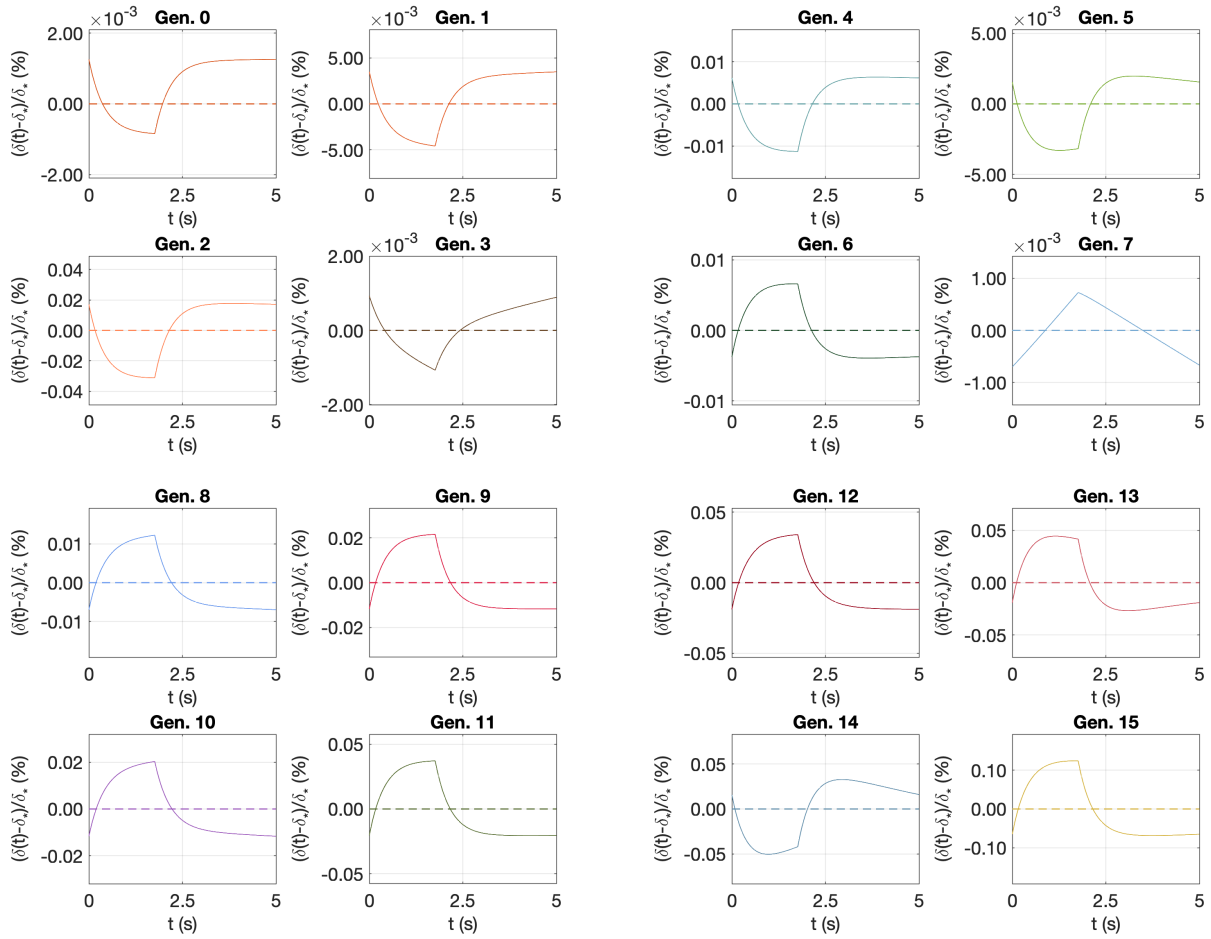

Figure 3.6 – *Normal* breathing ($\Phi^{\text{air}}_{\max} \sim 1.00\,\mathrm{L}\cdot\mathrm{s}^{-1}$): evolution of the mucus thickness $t \mapsto \delta(t) = r_i^m - r_i^a(t)$. The notation δ_* corresponds to the equilibrium mucus thickness of the considered generation. All data provided in Tables 2.1 and 2.2.

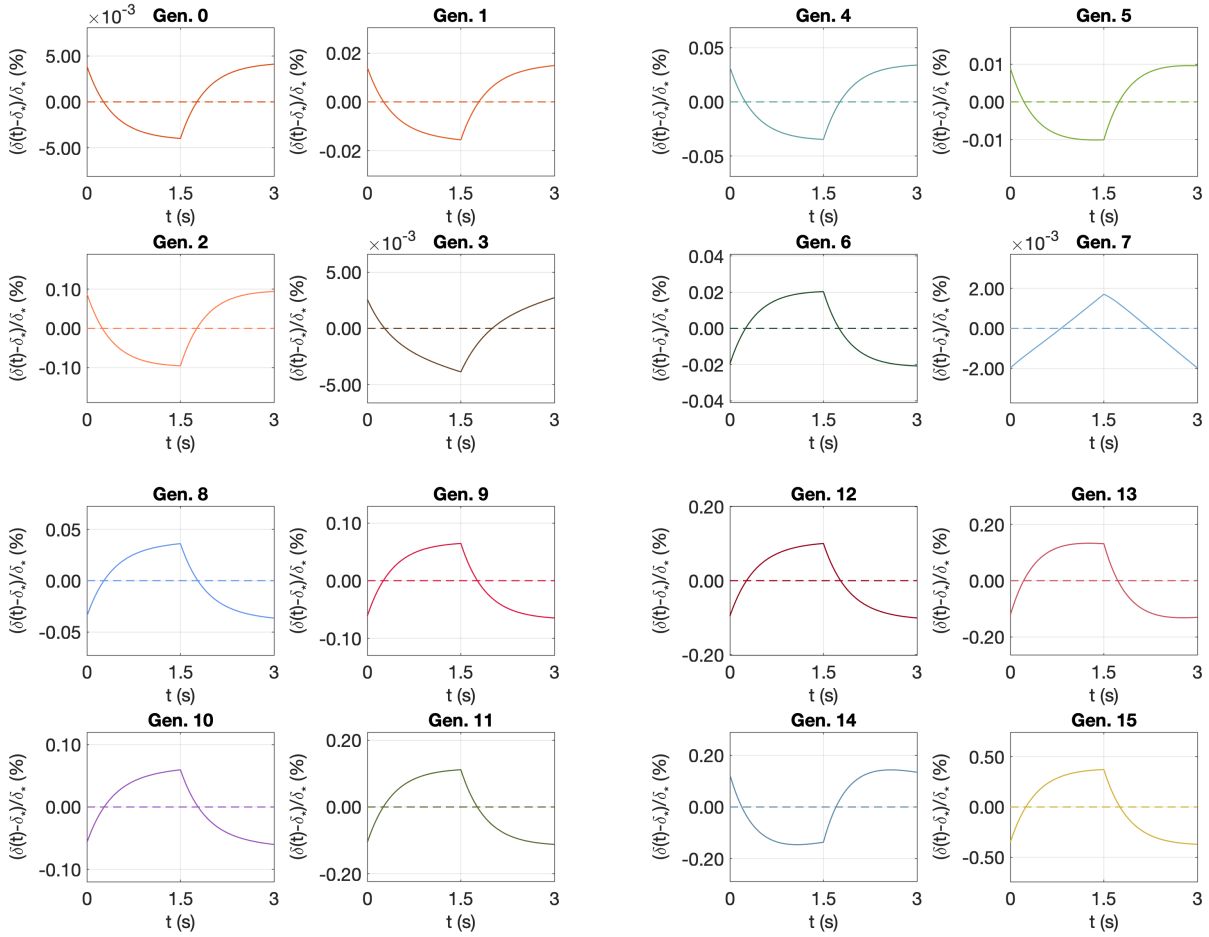

Figure 3.7 – *Forced* breathing ($\Phi^{\text{air}}_{\max} \sim 4.00\,\text{L}\cdot\text{s}^{-1}$): evolution of the mucus thickness $t \mapsto \delta(t) = r_i^m - r_i^a(t)$. The notation δ_* corresponds to the equilibrium mucus thickness of the considered generation. All data provided in Tables 2.1 and 2.2.

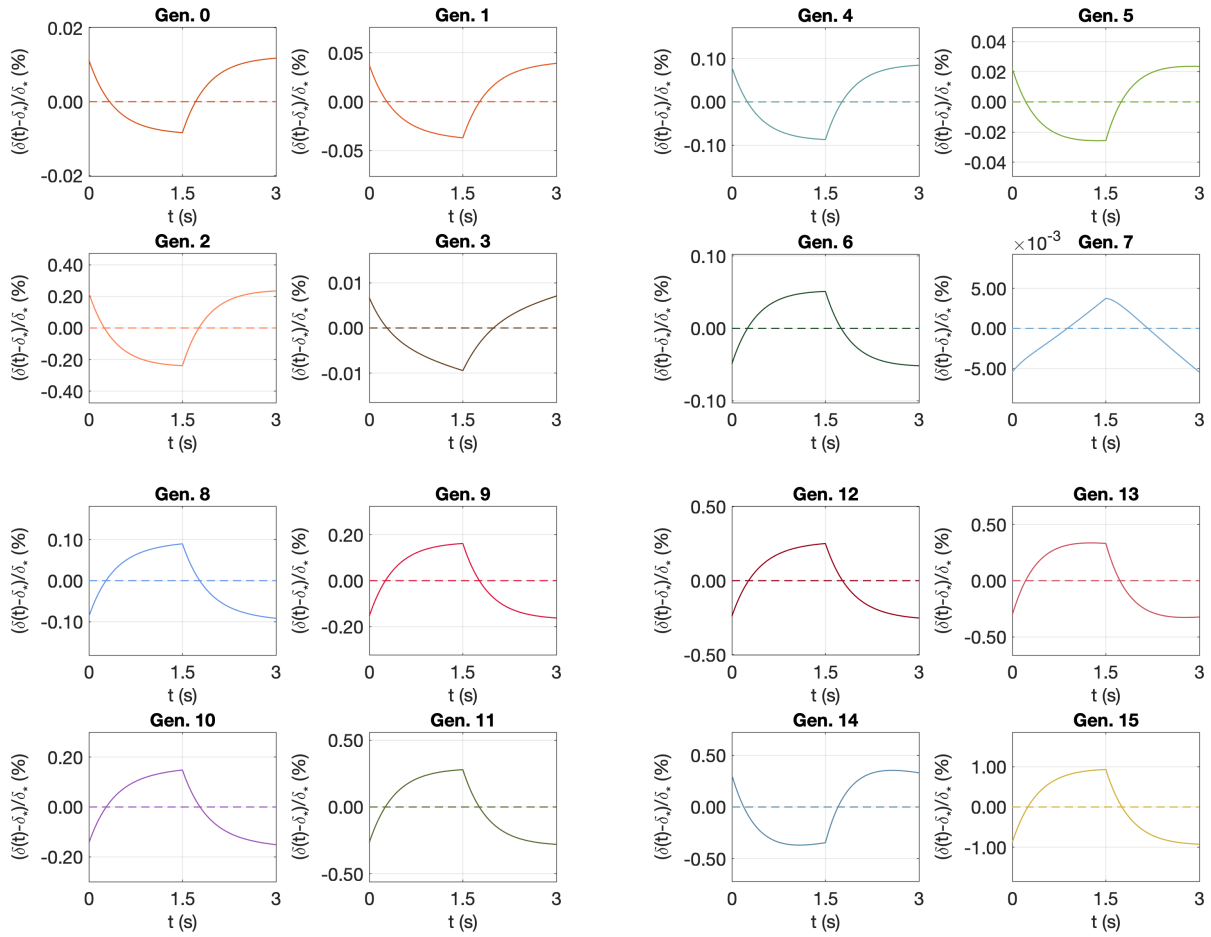

Figure 3.8 – *Extreme* breathing ($\Phi^{\text{air}}_{\max} \sim 10.00\,\mathrm{L}\cdot\mathrm{s}^{-1}$): evolution of the mucus thickness $t \mapsto \delta(t) = r_i^m - r_i^a(t)$. The notation δ_* corresponds to the equilibrium mucus thickness of the considered generation. All data provided in Tables 2.1 and 2.2.

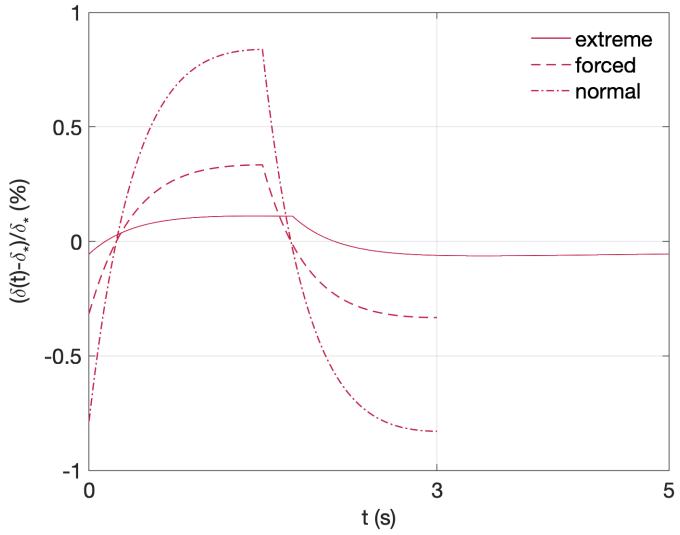

Figure 3.9 – Evolution of the mucus thickness $t \mapsto \delta(t) = r_i^m - r_i^a(t)$ in generation 16 (terminal generation, located before the entrance of the acinus) for different respiratory regimes: *normal* breathing ($\Phi_{\max}^{\text{air}} \sim 1.00\,\text{L}\cdot\text{s}^{-1}$), *forced* breathing ($\Phi_{\max}^{\text{air}} \sim 4.00\,\text{L}\cdot\text{s}^{-1}$) and *extreme* breathing ($\Phi_{\max}^{\text{air}} \sim 10.00\,\text{L}\cdot\text{s}^{-1}$). The notation δ_* corresponds to the equilibrium mucus thickness. All data provided in Tables 2.1 and 2.2.

precisely because of the bifurcations. To make mucus thickness decrease in a i-th generation (at inspiration or expiration), mucus flow in this generation has to be greater than 2 times mucus flow at generation $i+1$. So at generation 0, 1, 2, 3 and 14, at inspiration mucus flow is greater than 2 times mucus flow at generation 1, 2, 3 and 15 respectively.

3.3.3 Towards pathological situations

Spontaneous excess of mucus I

We investigate the elimination of the excess of mucus observed at initial time (all other parameters corresponding to the healthy situation). The initial configuration corresponds to a near-equilibrium mucus distribution of the mucus-air interface r_i^a

$$r_i^a(0) := r_i^{a\star} - \varepsilon_i,$$

or, equivalently, to a near-equilibrium mucus distribution of the mucus thickness $\delta_i = r_i^m - r_i^a$

$$\delta_i(0) := r_i^m - r_i^{a\star} + \varepsilon_i,$$

meaning that the the mucus thickness at generation i is increased by ε_i in comparison the the equilibrium value.

In numerical simulations, we studied the following cases:

- Test A: $\varepsilon_i = 0$ for $i \in \{0, \cdots, 16\} \setminus \{3\}$ and

  $$\varepsilon_3 := r_3^m - r_3^a,$$

  corresponding to an initial 100% overload of the mucus thickness in this proximal generation. Results are shown on Fig. 3.10.

- Test B: $\varepsilon_i = 0$ for $i \in \{0, \cdots, 16\} \setminus \{7\}$ and

$$\varepsilon_7 := r_7^m - r_7^a,$$

corresponding to an initial 100% overload of the mucus thickness in this intermediate generation. Results are shown on Fig. 3.11.

- Test C: $\varepsilon_i = 0$ for $i \in \{0, \cdots, 16\} \setminus \{11\}$ and

$$\varepsilon_{11} := r_{11}^m - r_{11}^a,$$

corresponding to an initial 100% overload of the mucus thickness in this intermediate generation. Results are shown on Fig. 3.12.

- Test D: $\varepsilon_i = 0$ for $i \in \{0, \cdots, 16\} \setminus \{15\}$ and

$$\varepsilon_{15} := r_{15}^m - r_{15}^a,$$

corresponding to an initial 100% overload of the mucus thickness in this distal generation. Results are shown on Fig. 3.13.

Numerical results highlight the fact that generations below the position of the excess of mucus are not affected by the strong initial state perturbation, as the mucociliairy clearance prevents mucus to go deeper in the distal direction. In the context of a healthy situation (as modelled by healthy parameters), the excess of mucus is expelled towards the trachea with a diffusion-like effect in the proximal generations that is described by a damped profile of mucus thickness distribution.

Spontaneous excess of mucus II

Critical secretion production $\tilde{\phi}^{(i)}_{\text{crit.}}$ can be defined at each generation i as the value corresponding to a complete filling of the bronchus with mucus, at equilibrium, namely

$$r_i^{a\star} = 0 = \sqrt{(r_i^m)^2 - \tilde{\phi}^{(i)}_{\text{crit.}} \left(\frac{2}{\overline{u_i}} \sum_{J=i}^{N-1} 2^{J-i} r_J^b \, \ell_J^b \right)}, \qquad i \in \{0, ..., N-1\},$$

where $\overline{u_i}$ denotes the velocity fluid of the mucus at each generation. We thus define:

$$\tilde{\phi}^{(i)}_{\text{crit.}} := \frac{(r_i^m)^2}{\dfrac{2}{\overline{u_i}} \displaystyle\sum_{J=i}^{N-1} 2^{J-i} r_J^b \, \ell_J^b}, \qquad i \in \{0, ..., N-1\},$$

and we define the *global critical secretion production* as

$$\tilde{\phi}_{\text{crit.}} := \min_i \{\tilde{\phi}^{(i)}_{\text{crit.}}\},$$

which defines the minimal secretion production for which a bronchus is completely filled at equilibrium. When considering morphometric data, the global critical secretion production has a magnitude of $2.173 \cdot 10^{-1}\ \mu\text{m} \cdot \text{s}^{-1}$ (it is attained in Generation 3), which is approximatively 500 times higher than the classical value ($4.772 \cdot 10^{-3}\ \mu\text{m} \cdot \text{s}^{-1}$), see Fig. 3.14.

Now the choice of a secretion production term determines an equilibrium state for each generation. In Fig. 3.15–3.16 we start from an initial condition that corresponds to a particular high value of the secretion term (it is thus associated to an important thickness of the mucus) and, under standard conditions of mucus production, we let evolve the mucus distribution back to the periodic healthy trajectory.

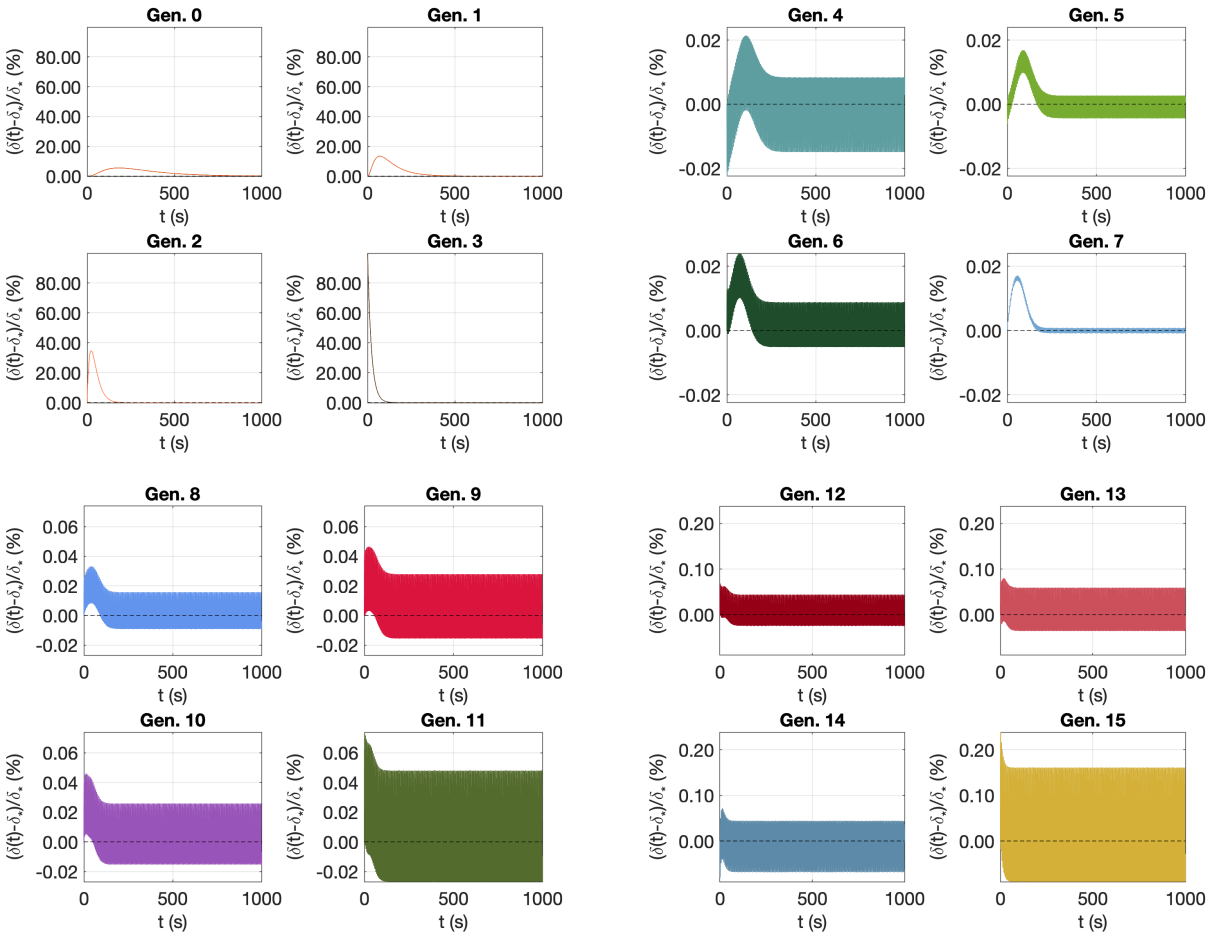

Figure 3.10 – Evolution of the mucus thickness $t \mapsto \delta(t) = r_i^m - r_i^a(t)$ due to an initial 100% overload of mucus thickness in generation 3. The notation δ_* corresponds to the equilibrium mucus thickness of the considered generation. All data provided in Tables 2.1 and 2.2.

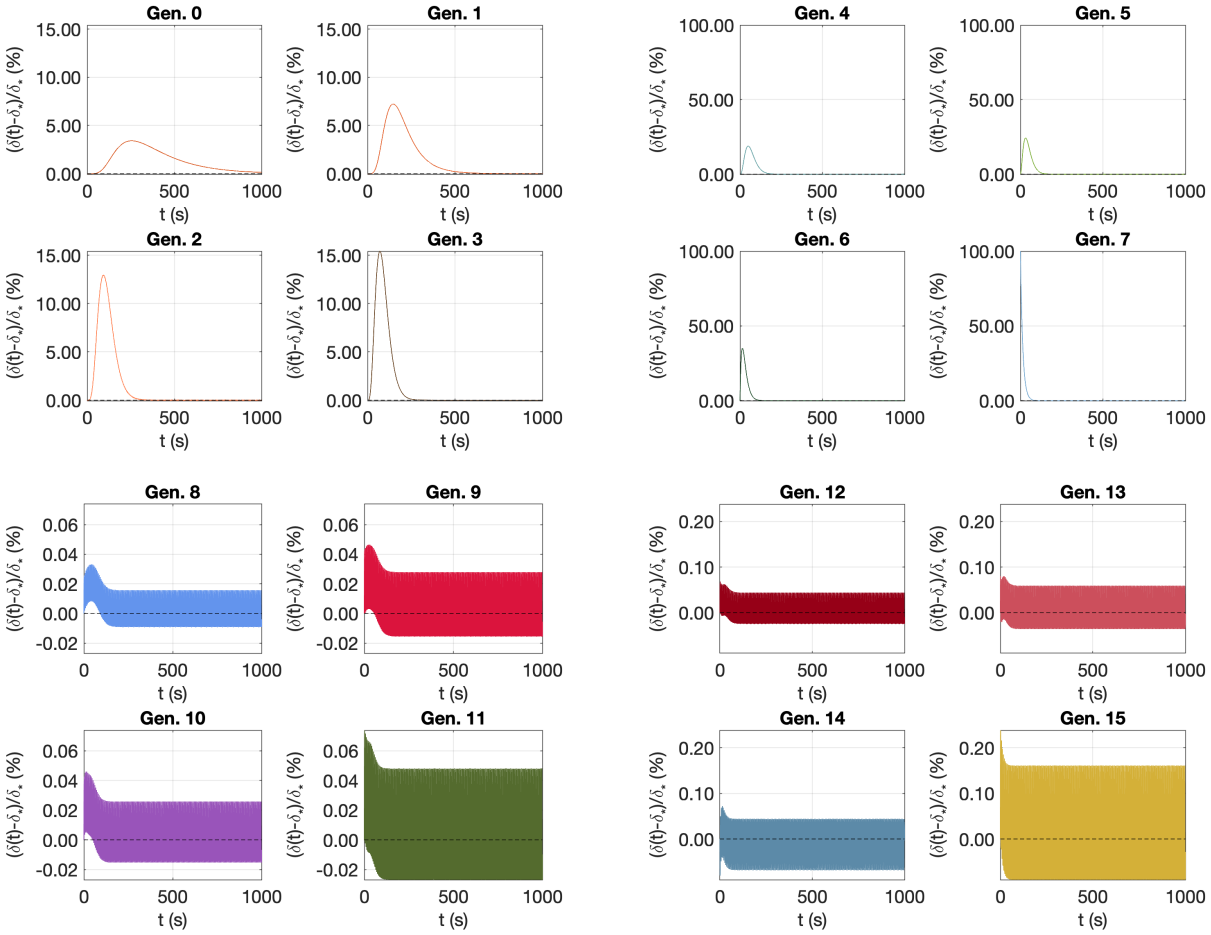

Figure 3.11 – Evolution of the mucus thickness $t \mapsto \delta(t) = r_i^m - r_i^a(t)$ due to an initial 100% overload of mucus thickness in generation 7. The notation δ_* corresponds to the equilibrium mucus thickness of the considered generation. All data provided in Tables 2.1 and 2.2.

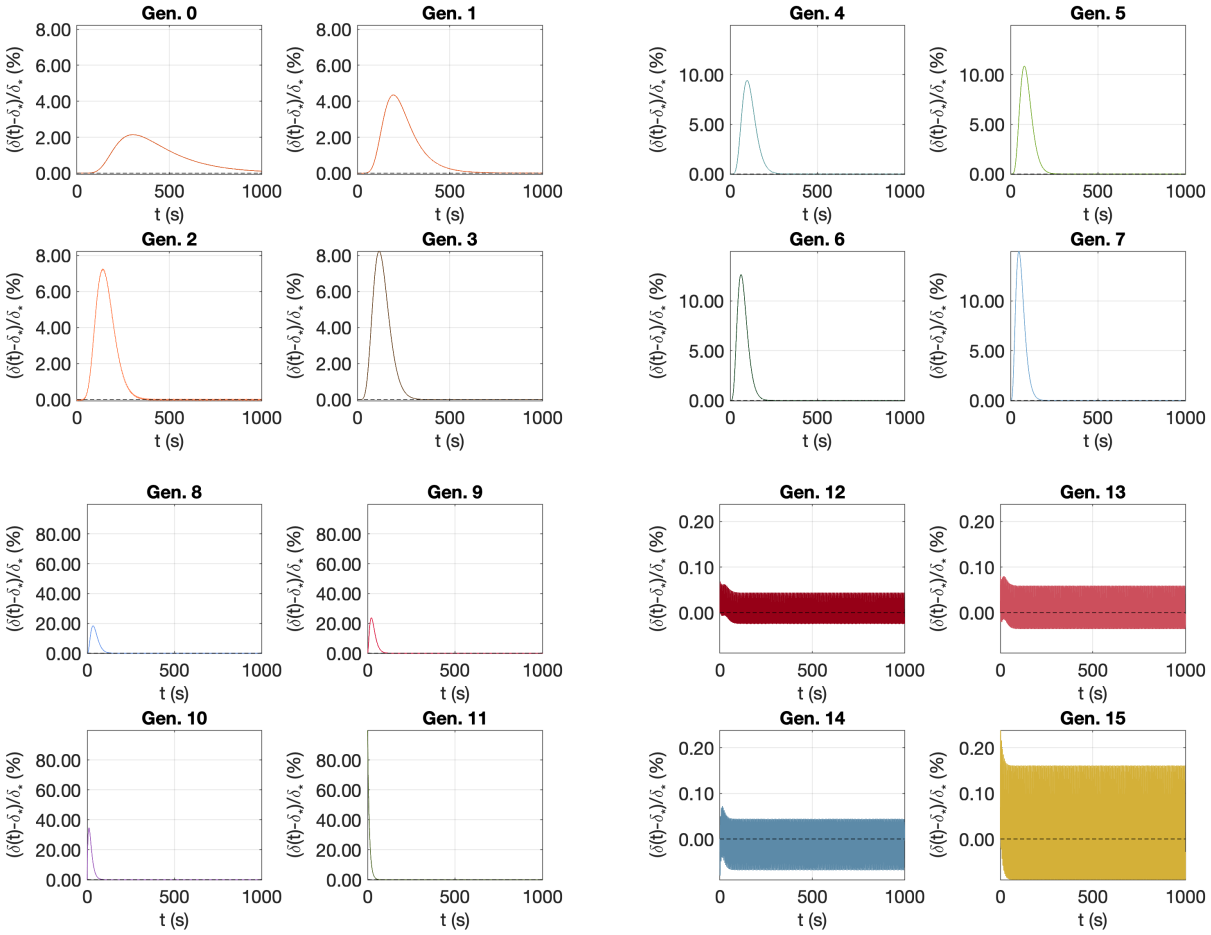

Figure 3.12 – Evolution of the mucus thickness $t \mapsto \delta(t) = r_i^m - r_i^a(t)$ due to an initial 100% overload of mucus thickness in generation 11. The notation δ_* corresponds to the equilibrium mucus thickness of the considered generation. All data provided in Tables 2.1 and 2.2.

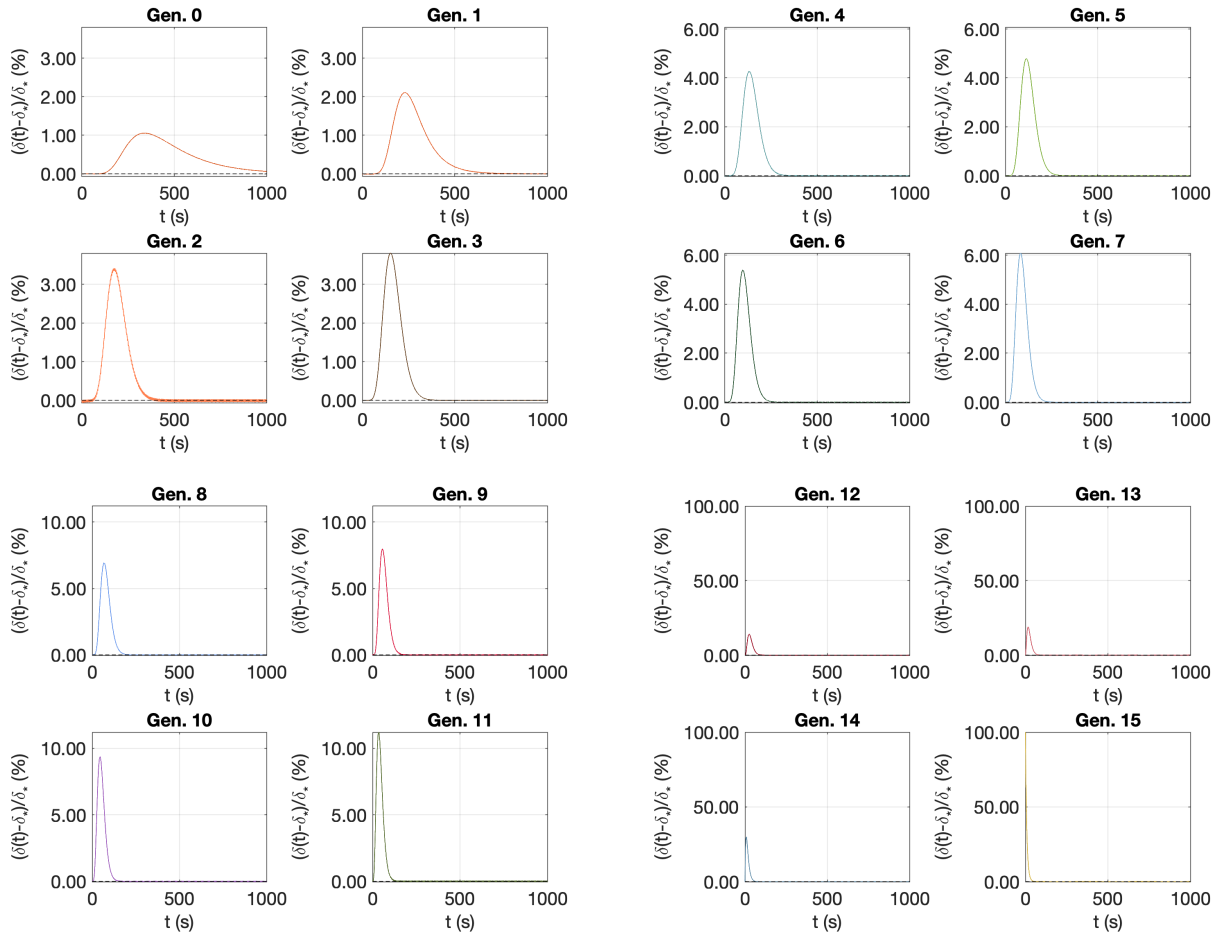

Figure 3.13 – Evolution of the mucus thickness $t \mapsto \delta(t) = r_i^m - r_i^a(t)$ due to an initial 100% overload of mucus thickness in generation 15. The notation δ_* corresponds to the equilibrium mucus thickness of the considered generation. All data provided in Tables 2.1 and 2.2.

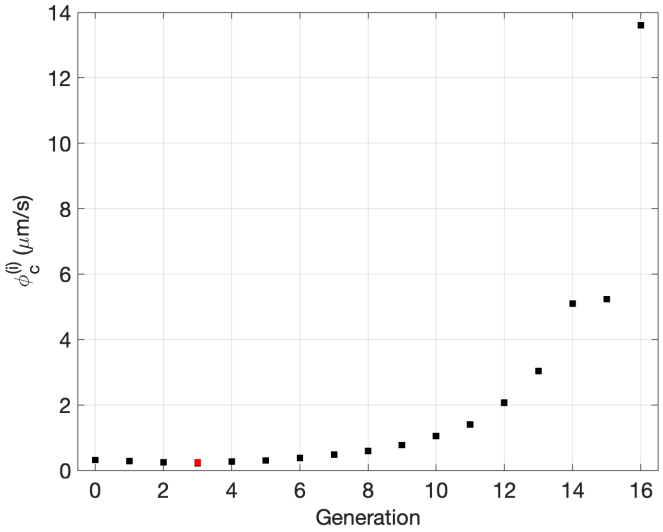

Figure 3.14 – Distribution of the critical secretion mucus secretion rates $\tilde{\phi}^{(i)}_{\text{crit.}}$ for the morphometric data. The global critical secretion production is reached at Generation 3, corresponding to $2.173 \cdot 10^{-1}\,\mu\text{m} \cdot \text{s}^{-1}$.

- In Fig. 3.15, the initial state corresponds to the equilibrium state obtained with $\tilde{\phi} = 50\%\,\tilde{\phi}_{\text{crit.}}$.
- In Fig. 3.16, the initial state corresponds to the equilibrium state obtained with $\tilde{\phi} = 10\%\,\tilde{\phi}_{\text{crit.}}$.
- In Fig. 3.17, the initial state corresponds to the equilibrium state obtained with $\tilde{\phi} = 1\%\,\tilde{\phi}_{\text{crit.}}$.

The results highlight the fact that, despite sharp initial overload of mucus, the mucociliary clearance is able to drag the mucus out of the bronchial tree, under healthy conditions of mucus secretion. The return to balanced dynamics around the healthy equilibrium mucus thickness depends on the generations: it is faster in distal generations than in proximal generations, as the ciliary activity drags the excess of mucus from bottom to top.

Excess of mucus secretion

The definition of a global critical secretion production can be associated to some degree of pathology: starting from the standard secretion rate ($\tilde{\phi} = 4.772 \cdot 10^{-3}\,\mu\text{m} \cdot \text{s}^{-1}$), we may increase the secretion term and observe how the equilibrium states and periodic evolution of the mucus thickness $t \mapsto \delta(t) = r_i^b - r_i^a(t)$ under the action. of normal respiration are affected by increasing values of $\tilde{\phi}$:

- $\tilde{\phi} = 50\%\,\tilde{\phi}_{\text{crit.}}$ corresponds to a heavy pathological situation.
- $\tilde{\phi} = 10\%\,\tilde{\phi}_{\text{crit.}}$ corresponds to an intermediate pathological situation.
- $\tilde{\phi} = 1\%\,\tilde{\phi}_{\text{crit.}}$ corresponds to a light pathological situation (the secretion rate is approximatively 5 times higher than the standard one).

We simulate the dynamics of the mucus thickness, which is analyzed through the filling rate of generation i, defined as the ratio between the space occupied by mucus ($r_i^m - r_i^a(t)$) and the maximal available space (r_i^m):

$$\tau_i(t) = \frac{r_i^m - r_i^a(t)}{r_i^m} \in [0, 1].$$

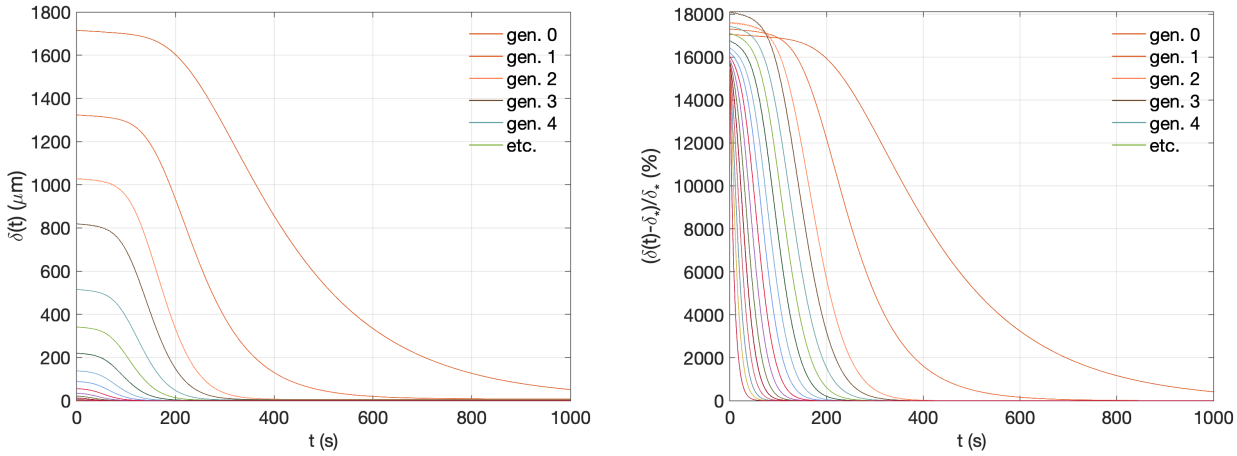

Figure 3.15 – Evolution of the mucus thickness $t \mapsto \delta(t) = r_i^m - r_i^a(t)$ due to an initial overload of mucus thickness: the initial state corresponds to the equilibrium state obtained with $\tilde{\phi} = 50\%\,\tilde{\phi}_{\text{crit.}}$. The notation δ_* corresponds to the equilibrium mucus thickness of the considered generation. All data provided in Tables 2.1 and 2.2.

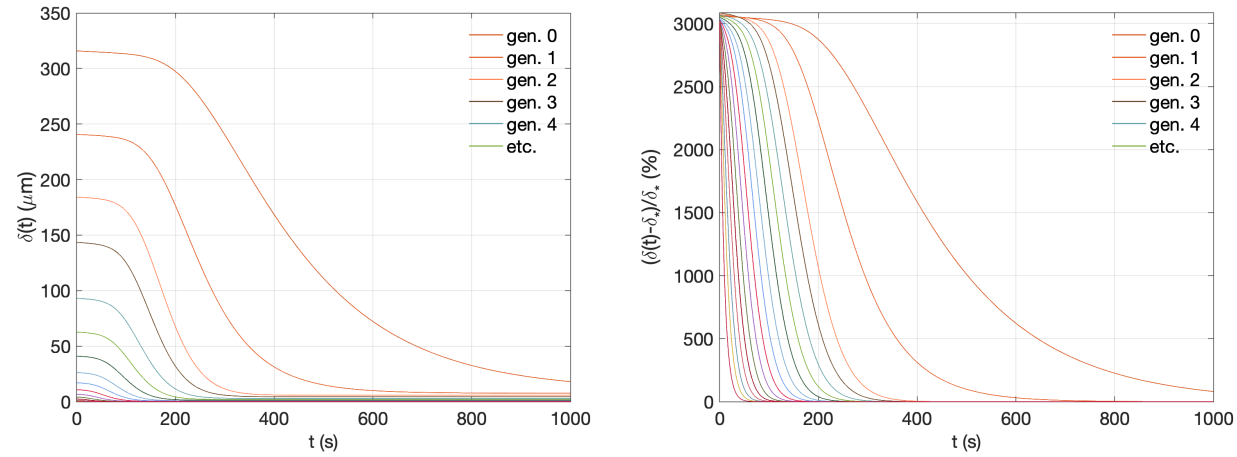

Figure 3.16 – Evolution of the mucus thickness $t \mapsto \delta(t) = r_i^m - r_i^a(t)$ due to an initial overload of mucus thickness: the initial state corresponds to the equilibrium state obtained with $\tilde{\phi} = 10\%\,\tilde{\phi}_{\text{crit.}}$. All data provided in Tables 2.1 and 2.2.

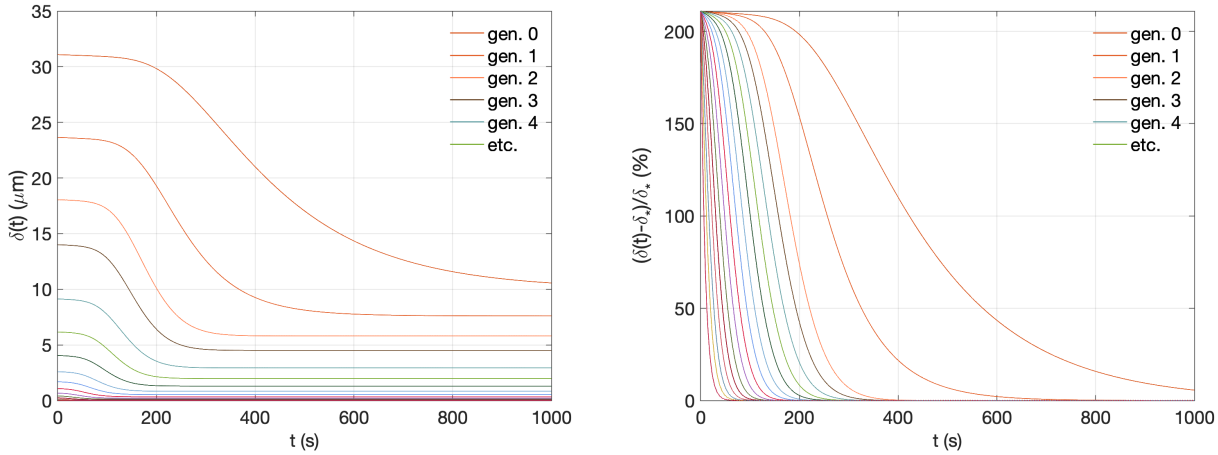

Figure 3.17 – Evolution of the mucus thickness $t \mapsto \delta(t) = r_i^m - r_i^a(t)$ due to an initial overload of mucus thickness: the initial state corresponds to the equilibrium state obtained with $\tilde{\phi} = 1\%\, \tilde{\phi}_{\text{crit.}}$. All data provided in Tables 2.1 and 2.2.

It means in particular that

- when $\tau_i = 1$, the bronchi at generation i are completely filled with mucus: no air can flow through the bronchial lumen;
- when $\tau_i = 0$, the bronchi at generation i have no mucus.

Fig. 3.18 provides the evolution of the mucus filling rate for a secretion rate which is $\tilde{\phi} = 50\%\, \tilde{\phi}_{\text{crit.}}$ (heavy pathological situation) in a respiratory normal regime. In the periodic regime, the proximal generations are heavily affected by the excess of mucus secretion: in particular, the maximal filling rate is attained in generation 3, with nearly 30% bronchial obstruction. Noteworthily the distal generations are less affected by the excess of mucus secretion, as less than 5% bronchial obstruction is observed from generation 11 to the terminal generations.

Fig. 3.19 and Fig. 3.20 provide the evolution of the mucus filling rate for secretion rates $\tilde{\phi} = 10\%\, \tilde{\phi}_{\text{crit.}}$ (intermediate pathological situation) and $\tilde{\phi} = 1\%\, \tilde{\phi}_{\text{crit.}}$ (light pathological situation) in a respiratory normal regime. Unsurprisingly the bronchial obstruction becomes less and less severe as the excess of mucus secretion decreases. We emphasize that the model is able to quantify the excess of mucus in severe pathological situations, *provided that the rate of mucus secretion is known* (which currently remains an information that is difficult to observe in the bronchial tree).

3.4 Conclusion

To our knowledge, this work was the first to study a model of mucus clearance which takes into account both the influence of airflow and ciliary activity on the distribution of layer thicknesses of mucus in a bronchial tree. We explored the role of the airflow in a periodic breathing regime (inspiration than expiration), on the evolution of the mucus inside the bronchial tree. Starting from a distribution of the initial mucus layer, we compute a transient regime but also a periodic regime of the distribution of the mucus layer in each generation of bronchus. Our model gives us a prediction of the evolution over time of the thicknesses of the mucus layer. We are then able to compute the time needed to reach a periodic state of the mucus layer distribution. This duration strongly depends on the viscosity

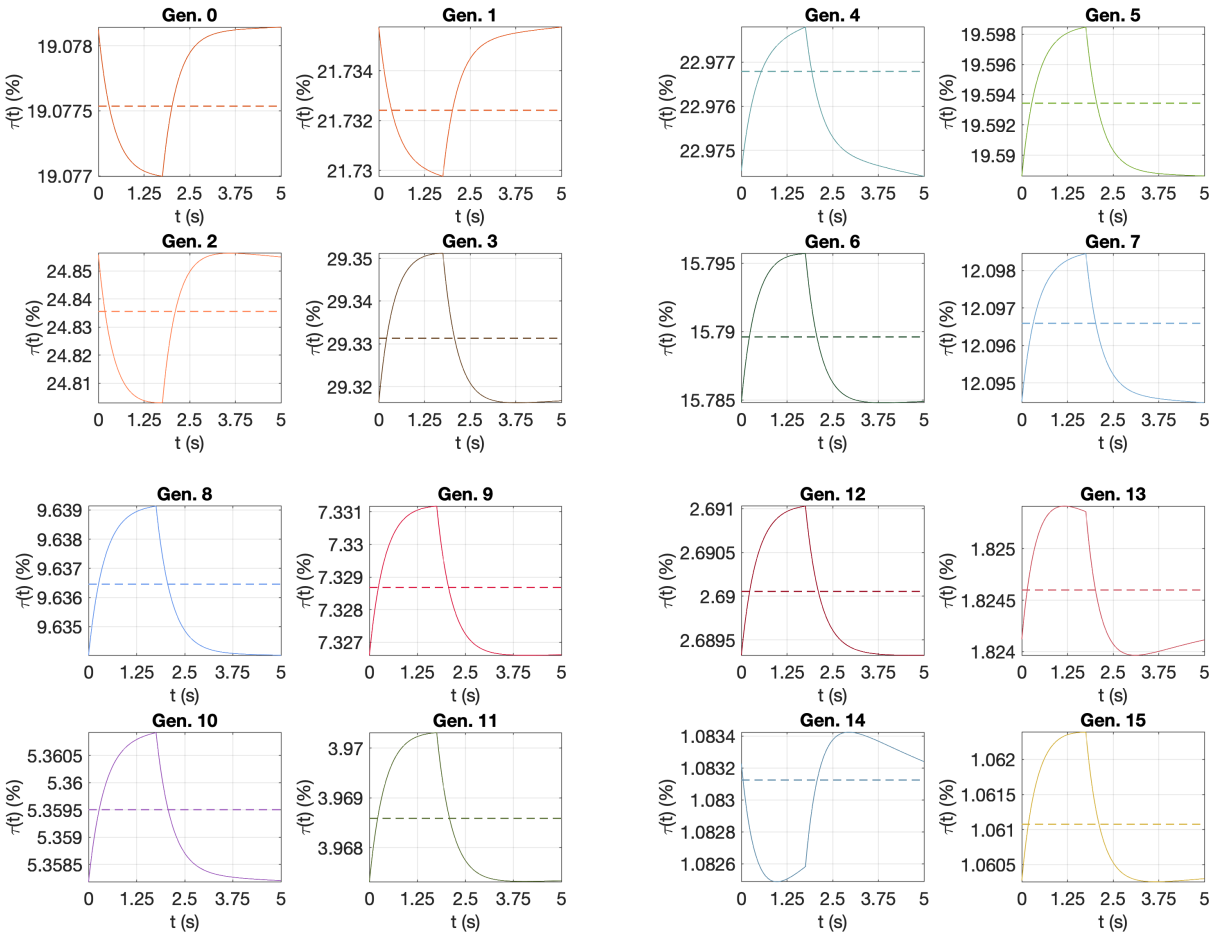

Figure 3.18 – Evolution of the mucus filling rate $t \mapsto \tau_i(t)$ for each generation, due to a secretion rate $\tilde{\phi} = 50\% \, \tilde{\phi}_{\text{crit.}}$ (heavy pathological situation).

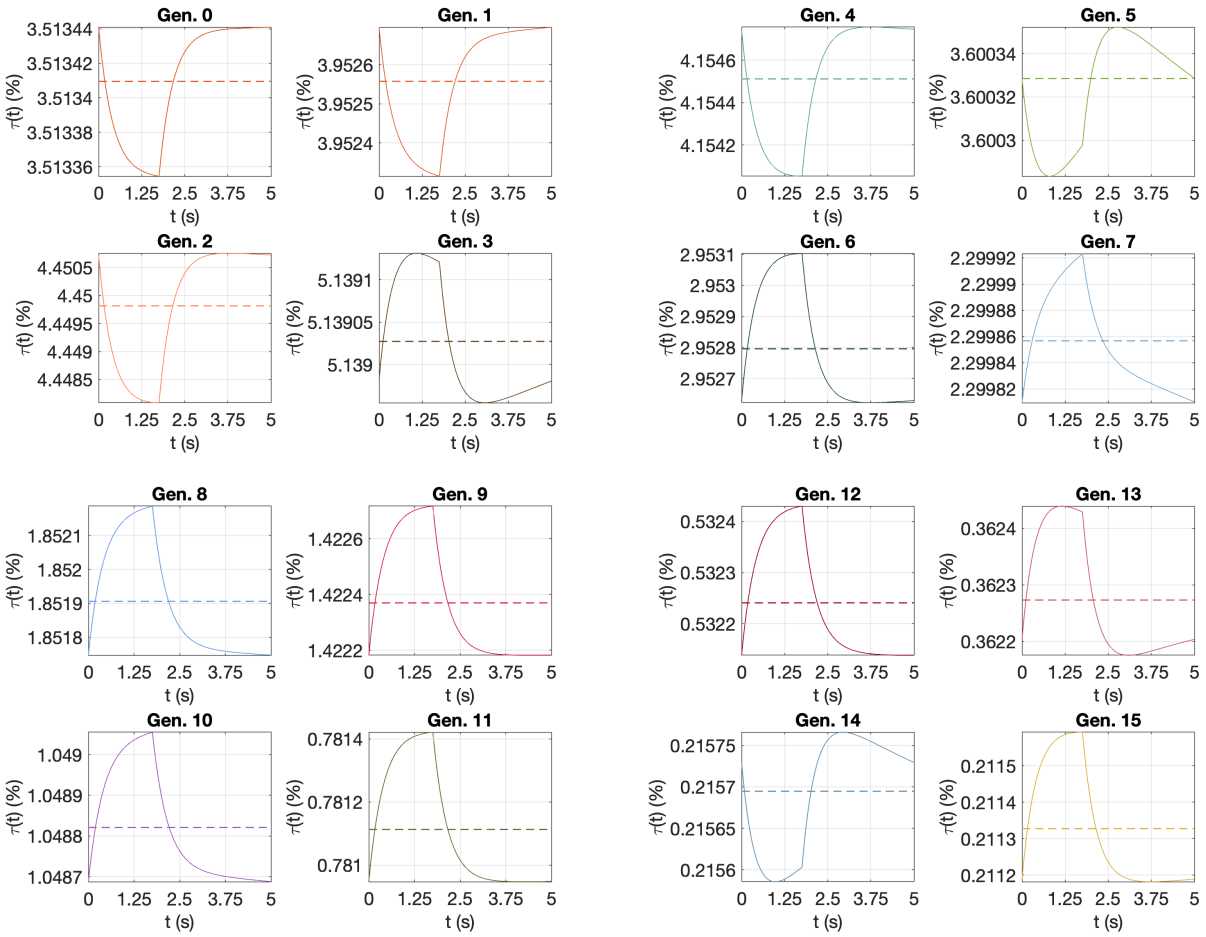

Figure 3.19 – Evolution of the mucus filling rate $t \mapsto \tau_i(t)$ for each generation, due to a secretion rate $\tilde{\phi} = 10\% \, \tilde{\phi}_{\text{crit.}}$ (intermediate pathological situation).

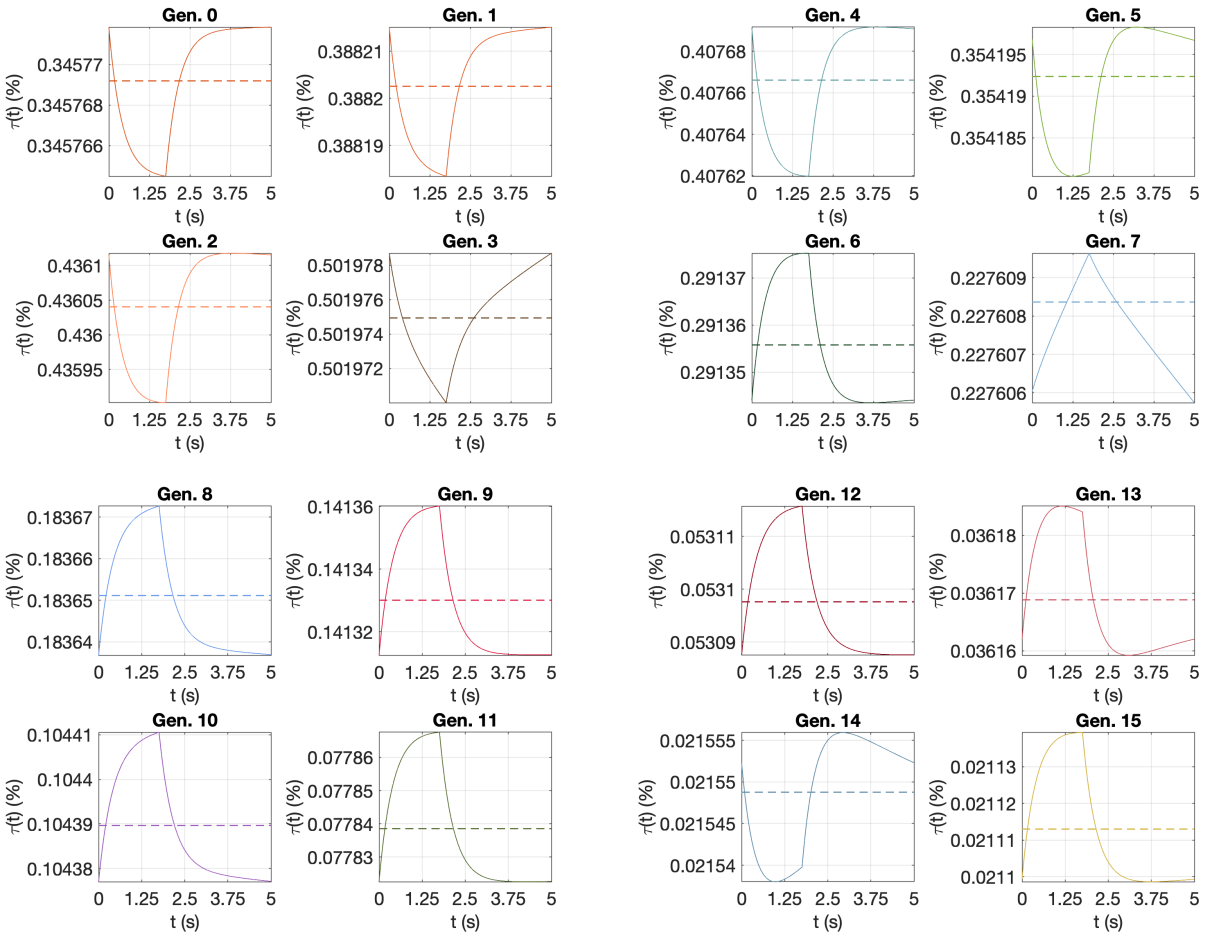

Figure 3.20 – Evolution of the mucus filling rate $t \mapsto \tau_i(t)$ for each generation, due to a secretion rate $\tilde{\phi} = 1\% \, \tilde{\phi}_{\text{crit.}}$ (light pathological situation).

of the mucus, the frequency of beating of the cilia as well as the airflow to the trachea. The lower the viscosity of the mucus, the greater the shear stress due to the airflow applied to the fluid, and therefore the more quickly the mucus moves in the tree.

Conclusion et perspectives

L'objectif de la thèse est de modéliser et de simuler l'écoulement du mucus engendré par l'activité des cils, en développant une hiérarchie de modèles permettant : 1) une description 3D de l'écoulement à l'échelle d'une onde méthachronale 2) une description 1D à l'échelle de l'arbre bronchique. Aussi, il s'agit de la prise en compte de l'influence de l'air sur le mucus. Par ailleurs, la description du mouvement d'un cil renseigné dans la littérature [9] nous permet une étude précise de l'action des cils sur l'écoulement du mucus. En utilisant certaines données déjà existantes, on a pu développer un modèle riche capable de simuler un grand nombre de cils en mouvement dans un fluide visqueux, cela afin de mieux comprendre le processus du transport mucociliaire et les pathologies associées.

Un des points cruciaux dans le chapitre 1 est la façon dont nous avons pris en compte les effets de la tension superficielle agissant au niveau de l'interface mucus/PCL. Le résultat est que au niveau de la couche de mucus on observe un écoulement homogène, de vitesse quasiment constante en espace tel un tapis qui se déplace. C'est aussi ce qui est observé dans les images obtenues par Sanderson et Sleigh [64] grâce au microscope électronique. Aussi, nous avons modélisé la contribution du cil par une distribution de forces le long de la ligne centrale du cil, dont l'intensité est calculée en utilisant l'asymptotique où le rapport entre l'épaisseur et la longueur du cil est très petite. Par ailleurs, nous avons aussi tenu compte de la vitesse du fluide "background" (terme modélisant la contribution collective de la forêt de cils). Ces modélisations conduisent à un problème à la fois singulier mais aussi non-local nécessitant (pour des raisons liées au coûts numériques) l'élaboration d'une méthode numérique basée sur la méthode des éléments finis.

Dans le chapitre 2, en se basant sur les équations de la conservation de la masse, on a étudié la dynamique de l'épaisseur de la couche de mucus pour différentes générations d'un arbre bronchique symétrique, en supposant que l'épaisseur de la couche de mucus est constante par génération. Ceci nous a permis de simplifier notre modèle en se ramenant à l'étude au niveau des générations et non pas des bronches individuellement. Par la suite, on a étudié les états d'équilibre de notre système. En effet, le mucus est un fluide qui est à la fois évacué des bronches pulmonaires grâce au mouvement synchronisé des cils, mais aussi sécrété par des glandes submucosales au niveau de l'épithélium vers les bronches. Ces deux phénomènes font naître une épaisseur de la couche de mucus stable au cours du temps. Ces épaisseurs dépendent fortement du taux de sécrétion, qui est un paramètre mal connu et difficile à estimer, mais essentiel pour comprendre la dynamique de la couche de mucus sur tout l'arbre bronchique. Par ailleurs, une question se pose à propos de ce taux, à savoir :

- le taux de sécrétion est-il uniforme sur tout l'arbre bronchique ? C'est une de nos hypothèses considérées dans notre modèle.

Comme précisé plus tôt, notre système donne une expression explicite des épaisseurs de la couche de mucus à l'équilibre en chaque génération en fonction du taux de sécrétion. En connaissant les épaisseurs de la couche de mucus, on peut alors évaluer le taux de sécrétion de mucus. Par ailleurs, quelques questions sur les épaisseurs peuvent être soulevées, à savoir :

- Quelle est la distribution des épaisseurs de la couche de mucus en chaque bronche? Est elle constante par génération? Des valeurs des épaisseurs de la couche de mucus ont été renseignées dans la littérature (voir chapitre 2) mais restent peu précises.

Enfin dans le Chapitre 3, nous avons enrichi notre modèle 1D permettant de calculer les vitesses moyennes en une bronche d'une certaine génération en ajoutant l'influence de l'air, à travers un débit d'air à la trachée périodique modélisant le régime respiratoire (inspiration puis expiration). À l'aide d'un l'algorithme de type point fixe, on peut calculer la dynamique périodique.

Nous terminons ce manuscrit en donnant des perspectives de recherche à explorer pour enrichir ce travail.

Force appliquée le long du cil

Dans le chapitre 1 on a approché la distribution de la force exercée le long du cil grâce à une formule définie dans Cox [20] qu'on rappelle ici:

$$\mathbf{f}(s,t) = \frac{2\pi\mu}{\ln(\frac{L}{r})}\left(2\mathbb{I}_3 \frac{\partial_s\boldsymbol{\xi}(s,t)\otimes\partial_s\boldsymbol{\xi}(s,t)}{|\partial_s\boldsymbol{\xi}(s,t)|^2}\right)(\partial_t\boldsymbol{\xi}(s,t) - \mathbf{u}_{bg}\boldsymbol{\xi}(s,t)). \tag{3.11}$$

Cette expression a été obtenue en utilisant un développement asymptotique de la vitesse $\mathbf{u}$ solution du problème de Stokes :

$$-\mu\Delta\mathbf{u} + \nabla p = 0, \;\; \mathrm{div}(\mathbf{u}) = 0, \;\; \text{in } \mathbb{R}^3,$$

avec la condition au bord $\mathbf{u} = \mathbf{U}^*(s)$ à la surface du corps fin. $\mathbf{U}^*(s)$ représente la vitesse au point de la ligne centrale du corps fin paramétrisée par l'abscisse curviligne s. Un moyen de s'affranchir de cette approximation est d'étudier un problème inverse. Comme dans Ohm et al [2], pour une forêt à N cils on cherchera à trouver les forces $(\mathbf{f}_i)_{i\in\{1,..,N\}}$ telles que la vitesse $\mathbf{u}$ solution du système de Stokes singulier :

$$\begin{cases} -\mu\Delta\mathbf{u} + \nabla p &= \sum_i \mathbf{f}_i\,\delta_{\Gamma_i} & \text{dans } \mathbb{R}^3, \\ \mathrm{div}(\mathbf{u}) &= 0 & \text{dans } \mathbb{R}^3, \\ |\mathbf{u}| &\longrightarrow 0 & \text{quand } |\mathbf{x}| \longrightarrow +\infty \end{cases} \tag{3.12}$$

vérifie la condition $\mathbf{u}|_{\partial\Sigma} = \mathbf{u}_{cil}$, où $\partial\Sigma_j$ est la surface du j-ème cil et $\mathbf{u}_{cil}$ est la vitesse du mouvement du cil. Dans cette configuration, on peut définir explicitement la vitesse solution fondamentale de (3.12) par

$$8\pi\mu\mathbf{u}(\mathbf{x}) = \sum_i \int_0^L [\mathcal{S}(\mathbf{x}-\boldsymbol{\xi}_i(s,t)) + \frac{\epsilon^2}{2}\mathcal{D}(\mathbf{x}-\boldsymbol{\xi}_i(s,t))]\mathbf{f}_i(s,t)ds, \tag{3.13}$$

où $\epsilon = 2r$ est l'épaisseur du cil, $\mathcal{S}$ et $\mathcal{D}$ représentent respectivement la stokeslet et la doublet:

$$\mathcal{S}(\mathbf{x}) = \frac{\mathbb{I}_3}{|\mathbf{x}|} + \frac{\mathbf{x}\mathbf{x}^T}{|\mathbf{x}|^3}, \; \mathcal{D}(\mathbf{x}) = \frac{\mathbb{I}_3}{|\mathbf{x}|^3} - 3\frac{\mathbf{x}\mathbf{x}^T}{|\mathbf{x}|^5}, \;\; \mathbf{x}\in\mathbb{R}^3$$

$\mathbb{I}_3$ est la matrice identité et $|\mathbf{x}| = \sqrt{x^2+y^2+z^2}$. En procédant aux mêmes démarches que dans Ohm et al [2] a savoir: on évalue l'expression (3.13) à la surface du j-ème cil $\partial\Sigma_j$, et en éliminant les termes

en $\mathcal{O}(\epsilon \log(\epsilon))$ on obtient:

$$8\pi\mu \frac{\partial \boldsymbol{\xi}_j}{\partial t}(s',t) = \sum_i \int_0^L [\mathcal{S}_{ij}^\epsilon(s,s',t) + \frac{\epsilon^2}{2}\mathcal{D}_{ij}^\epsilon(s,s',t)]\mathbf{f}_i(s,t)ds, \tag{3.14}$$

$$\mathcal{S}_{ij}^\epsilon(s,s',t) = \frac{\mathbb{I}_3}{(\Delta\boldsymbol{\xi}_{ij}+\epsilon^2)^{1/2}} + \frac{\Delta\boldsymbol{\xi}_{ij}\Delta\boldsymbol{\xi}_{ij}^T}{(\Delta\boldsymbol{\xi}_{ij}+\epsilon^2)^{3/2}}, \tag{3.15}$$

$$\mathcal{D}_{ij}^\epsilon(s,s',t) = \frac{\mathbb{I}_3}{(\Delta\boldsymbol{\xi}_{ij}+\epsilon^2)^{3/2}} - 3\frac{\Delta\boldsymbol{\xi}_{ij}\Delta\boldsymbol{\xi}_{ij}^T}{(\Delta\boldsymbol{\xi}_{ij}+\epsilon^2)^{5/2}}. \tag{3.16}$$

Par la suite à l'aide d'une méthode d'interpolation, on discrétise en M points l'intégrale définie dans (3.14) pour se ramener à un système de type $\mathcal{A}\mathbf{F} = \mathbf{b}$ de taille $3N \times M$ à inverser. Une fois qu'on a trouvé nos forces inconnues au départ en chaque point de chaque cil, on les injecte dans notre système de Stokes (1.2) de départ défini dans le chapitre 1 pour le résoudre.

Travail à mouvement imposé

Des choix de modélisation ont été établis dans le chapitre 1, et les résultats numériques montrent que notre modèle est limité. Son principal défaut est que les cils battent suivant un mouvement imposé, ainsi la force exercée par le cil s'adapte à la viscosité du fluide environnant. Un modèle plus réaliste et qui puisse tenir compte de la rétroaction du fluide, serait de non pas imposer le mouvement du cil, mais de résoudre un problème d'interaction fluide-structure 3D-1D complet, tenant compte de l'activité interne des cils. Une des difficultés de ce problème réside au niveau du couplage des vitesses. En effet, pour une structure 1D plongée dans un fluide 3D, la vitesse du fluide est singulière le long de la structure. Une idée pour s'affranchir de cette difficulté est de définir une surface qu'on note $\partial\Sigma$ représentant la frontière du cil, d'écrire la condition de continuité des vitesses sur $\partial\Sigma$. Pour ce qui est du modèle 1D pour la déformation de la structure, a partir d'un modèle 3D développé par Vergnet et al [22], on pourrait dériver un modèle 1D via un développement asymptotique suivant l'épaisseur de la structure.

Modèle d'arbre bronchique

Dans le chapitre 2, on a étudié les épaisseurs de la couche de mucus à l'équilibre en considérant deux types d'arbres bronchiques idéalisés, celui de Weibel, et un autre modèle dit morphométrique. Mais dans le chapitre 3 on a considéré uniquement le modèle morphométrique puisqu'il offre les mêmes grandeurs des bronches que celles qu'on retrouve dans le poumon humain. Comme précisé précédemment, on a associé chaque génération à une épaisseur de la couche de mucus, de la première génération (trachée) à la 17-ème et dernière génération. Toutefois on peut relaxer cette hypothèse en considérant un modèle d'arbre bronchique à plusieurs sous-arbres, chaque sous-arbre étant symétrique en la morphométrie et la couche de mucus, et indépendant de l'autre. Pour un arbre symétrique à 17 générations à 2^N sous arbre, le nombre d'équations constituant notre système dynamique serait ainsi égale à $2^N(17-N)+N$, notre modèle est en général plus coûteux pour l'étude que le modèle d'arbre bronchique de départ à 17 générations. Mais pour autant, ce choix de modélisation serait utile pour étudier des cas où on a un surencombrement très local dans l'arbre bronchique (au niveau d'un seul sous arbre), puisqu'on réduit notre étude (et donc le coût de calcule) uniquement au sous arbre considéré.

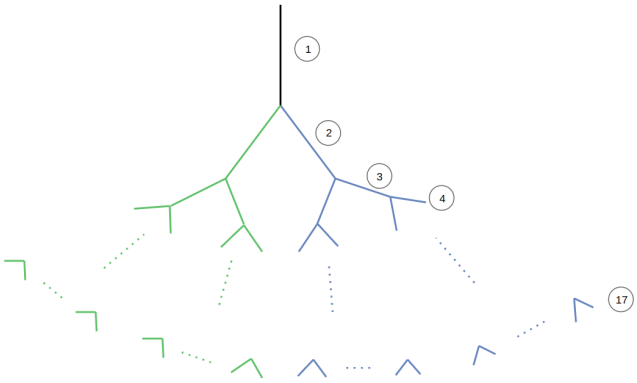

Figure 3.21 – Exemple d'arbre symétrique à 17 générations et à 2^1 sous arbres (en vert et bleu), le nombre d'équations constituant notre système dynamique est de $2^1(17-1)+1=33$.

Bibliography

[1] S.D. Anderson. Asthma provoked by exercise, hyperventilation, and the inhalation of non-isotonic aerosols. In Peter J. Barnes, Ian W. Rodger, and Neil C. Thomson, editors, *Asthma: Basic Mechanisms and Clinical Management*, pages 569–587. Academic Press, London, third edition edition, 1998.

[2] Celledoni E. Ohm L. Owren B. Andersson, H. I. and B. K. Tapley. An integral model based on slender body theory, with applications to curved rigid fibers. *Comm. Pure Appl. Math.*, 73, 2020.

[3] C. Barton and S. Raynor. Analytical investigation of cilia induced mucous flow. *Bull. of Math. Biophys.*, 29(3):419–428, 1967.

[4] P. J. Basser, T. A. Mcmahon, and P. Griffith. The mechanism of mucus clearance in cough. *Trans. ASME, J. Biomech. Eng.*, 111:288–97, 1989.

[5] R. Begin, A. D. Renzetti, A. H. Bigler, and S. Watanabe. Flow and age dependence of airway closure and dynamic compliance. *J. Appl. Physiol.*, 38(2):199–207, 1975.

[6] A. Ben-Tal. Simplified models for gas exchange in the human lungs. *J. Theor. Biol.*, 238(2):474–495, 2006.

[7] S. Bertoluzza, A. Decoene, L. Lacouture, and S. Martin. Local error analysis for the Stokes equations with a punctual source term. *Numer. Math.*, 140(3):677–701, 2018.

[8] N. Bessonov and V. Volpert. Airway obstruction in respiratory viral infections due to impaired mucociliary clearance. *International Journal for Numerical Methods in Biomedical Engineering*, pages 1–11, 2023.

[9] J. R. Blake. A model for the micro-structure in ciliated organisms. *J. Fluid Mech.*, 55:1–23, 1972.

[10] M. Bottier, M. Peña Fernández, G. Pelle, D. Isabey, B. Louis, J.B. Grotberg, and M. Filoche. A new index for characterizing micro-bead motion in a flow induced by ciliary beating: Part II, modeling. *PLOS Comput. Biol.*, 13(7):1–21, 07 2017.

[11] R.C. Boucher. Human airway ion transport. part I. *Am. J. Respir. Crit. Care*, 150:271–281, 1994.

[12] D.R. Brumley, K.Y. Wan, M. Polin, and R.E. Goldstein. Flagellar synchronization through direct hydrodynamic interactions. *eLife*, 3:e02750, jul 2014.

[13] B. Button and R. C. Boucher. Role of mechanical stress in regulating airway surface hydration and mucus clearance rates. *Respir. Physiol. Neurobiol.*, 163:189–201, 2008.

[14] B. Chakrabarti, , and D. Saintillan. Hydrodynamic synchronization of spontaneously beating filaments. *Phys. Rev. Lett.*, 123:208101, Nov 2019.

[15] B. Chakrabarti, S. Fürthauer, and M.J. Shelley. A multiscale biophysical model gives quantized metachronal waves in a lattice of beating cilia. *Proc. Natl. Acad. Sci. U.S.A.*, 119(4):e2113539119, 2022.

[16] S. Chateau, J. Favier, U. D'Ortona, and S. Poncet. Transport efficiency of metachronal waves in 3d cilium arrays immersed in a two-phase flow. *J. Fluid Mech.*, 824:931–961, 2017.

[17] R. Chatelin. Méthodes numériques pour l'écoulement de Stokes 3d : fluides à viscosité variable en géométrie complexe mobile ; application aux fluides biologiques. *Thèse de doctorat de l'université Paul Sabatier, 197 pp.*, 2013.

[18] R. Chatelin and P. Poncet. A hybrid grid-particle method for moving bodies in 3D Stokes flow with variable viscosity. *SIAM J. Sci. Comput.*, 35(4):925–949, 2013.

[19] A. Choudhury, M. Filoche, N.M. Ribe, N. Grenier, and G.F. Dietze. On the role of viscoelasticity in mucociliary clearance: a hydrodynamic continuum approach. *J. Fluid Mech.*, 971:A33, 2023.

[20] R. G. Cox. The motion of long slender bodies in a viscous fluid. Part 1. General theory. *J. Fluid Mech.*, 44:791–810, 1970.

[21] A. Decoene, S. Martin, and B. Maury. Direct simulation of rigid particles in a viscoelastic fluid. *J. Non-Newton. Fluid Mech.*, 260:1–25, 2018.

[22] A. Decoene, S. Martin, and F. Vergnet. A continuum active structure model for the interaction of cilia with a viscous fluid. *Z. Angew. Math. Mech.*, accepted for publication (29 p.), 2023.

[23] R. H. Dillon, L. J. Fauci, C. Omoto, and X. Yang. Fluid dynamic models of flagellar and ciliary beating. *Ann. N. Y. Acad. Sci.*, 1101(1):494–505, 2007.

[24] S. Enault, D. Lombardi, P. Poncet, and M. Thiriet. Mucus dynamics subject to air and wall motion. *ESAIM: Proc.*, 30:125–141, 2010.

[25] G. R. Fulford and J. R. Blake. Force distribution along a slender body straddling an interface. *J. Austral. Math. Soc. Ser. B*, 27(3):295–315, 1986.

[26] G. R. Fulford and J. R. Blake. Muco-ciliary transport in the lung. *J. Theor. Biol.*, 121(4):381–402, 1986.

[27] L. Gheber, A. Korngreen, and Z. Priel. Effect of viscosity on metachrony in mucus propelling cilia. *Cell Motil. Cytoskel.*, 39(1):9–20, 1998.

[28] I. R. Gibbons. Cilia and flagella of eukaryotes. *J. Cell. Biol.*, 91(3):107–124, 1981.

[29] S. Gueron and K. Levit-Gurevich. A three-dimensional model for ciliary motion based on the internal 9 + 2 structure. *Proc. Biol. Sci.*, 268(1467):599–607, 2001.

[30] S. Gueron and N. Liron. Ciliary motion modeling, and dynamic multicilia interactions. *Biophys. J.*, 63:1045–1058, 1992.

[31] S. Gueron and N. Liron. Simulations of three-dimensional ciliary beats and cilia interactions. *Biophys. J.*, 65:499–507., 1993.

[32] J. E. Guyton and M. E. Hall. *Textbook of medical physiology*. Elsevier, 13th edition, 2016.

[33] T. L. Hayden. Representation theorems in reflexive Banach spaces. *Math. Z.*, 104:405–406, 1968.

[34] C. Karamaoun, B. Sobac, B. Mauroy, A. Van Muylem, and B. Haut. New insights into the mechanisms controlling the bronchial mucus balance. *PLoS One*, 13(6):e0199319, 2018.

[35] J. Kibble and C. Halsey. *Medical Physiology: The Big Picture*. McGraw Hill, 2016.

[36] M. R. Knowles and R. C. Boucher. Mucus clearance as a primary innate defense mechanism for mammalian airways. *J. Clin. Invest.*, 109(5):571–577, 2002.

[37] P. Kurbatova, N. Bessonov, V. Volpert, H.A.W.M. Tiddens, C. Cornu, P. Nony, and D. Caudri. Model of mucociliary clearance in cystic fibrosis lungs. *J. Theor. Biol.*, 372:81–88, 2015.

[38] L. Lacouture. Modélisation et simulation du mouvement de structures fines dans un fluide visqueux : application au transport mucociliaire. *Thèse de doctorat de l'université Paris-Sud*, 2016.

[39] S. K. Lai, Y. Y. Wang, D. Wirtz, and J. Hanes. Micro- and macrorheology of mucus. *Adv. Drug Deliv. Rev.*, 61:86–100, 2009.

[40] J. Leal, H.D.C. Smyth, and D. Ghosh. Physicochemical properties of mucus and their impact on transmucosal drug delivery. *Int. J. Pharm.*, 532(1):555–572, 2017.

[41] W. L. Lee, P. G. Jayathilake, Zhijun Tan, D. V. Le, H. P. Lee, and B. C. Khoo. Muco-ciliary transport: effect of mucus viscosity, cilia beat frequency and cilia density. *Comput. & Fluids*, 49:214–221, 2011.

[42] N. Liron and S. Mochon. The discrete-cilia approach to propulsion of ciliated micro-organisms. *J. Fluid Mech.*, 75:593–607, 1976.

[43] A. M. Lucas and L. C. Douglas. Principles underlying ciliary activity in the respiratory tract: II. A comparison of nasal clearance in man, monkey and other mammals. *Arch. Otolaryngol.*, 20(4):518–541, 1934.

[44] Y Man, F. Ling, and E. Kanso. Cilia oscillations. *Phil. Trans. R. Soc. B*, 375:20190157, 2019.

[45] S. Martin and B. Maury. Notion de résistance de l'arbre pulmonaire bronchique dans la ventilation respiratoire humaine. *Modéliser et simuler. Épistémologies et pratiques de la modélisation et de la simulation*, page 493–524, 2014.

[46] O. K. Matar and P. D. M. Spelt. Dynamics of thin free films with reaction-driven density and viscosity variations. *Phys. Fluids*, 17(12):122102, 15, 2005.

[47] B. Mauroy, Patrice F., Dominique P., Christian F., Jacques M., and Barrett R. M. Toward the modeling of mucus draining from the human lung: role of airways deformation on air-mucus interaction. *Frontiers in Physiology*, 6:15, 2015.

[48] B. Mauroy, C. Fausser, D. Pelca, J. Merckx, and P. Flaud. Toward the modeling of mucus draining from the human lung: role of the geometry of the airway tree. *Phys. Biol.*, 8(5):056006, 12, 2011.

[49] B. Mauroy, M. Filoche, E. Weibel, and B. Sapoval. An optimal bronchial tree may be dangerous. *Nature*, 427:633–636, 2004.

[50] B. Mauroy and Bokov P. The influence of variability on the optimal shape of an airway tree branching asymmetrically. *Phys. Biol.*, 7(1):16007, 2010.

[51] R.R. Mercer, M.L. Russell, and J.D. Crapo. Mucous lining layers in human and rat airways. *Am. Rev. Respir. Dis.*, 145:A355, 1992.

[52] D.R. Mitchell. *The Evolution of Eukaryotic Cilia and Flagella as Motile and Sensory Organelles*, chapter 11, pages 130–140. Eukaryotic Membranes and Cytoskeleton: Origins and Evolution. Advances in Experimental Medicine and Biology, vol 607. Springer New York, 2007.

[53] S. Mitran. Metachronal wave formation in a model of pulmonary cilia. *Comput. Struct.*, 85(11-14):763–774, 2007.

[54] S. Mitran. Continuum-kinetic-microscopic model of lung clearance due to core-annular fluid entrainment. *J. Comput. Phys.*, 244:193–211, 2013.

[55] N. Mizuno, M. Taschner, B.D. Engel, and E. Lorentzen. Structural studies of ciliary components. *J. Mol. Biol.*, 422(2):163–180, 2012.

[56] Y. Mori, L. Ohm, and D. Spirn. Theoretical justification and error analysis for slender body theory. *Comm. Pure Appl. Math.*, 73(6):1245–1314, 2020.

[57] D. Oriola, H. Gadêlha, and J. Casademunt. Nonlinear amplitude dynamics in flagellar beating. *R. Soc. open sci.*, 4(3):160698, 2017.

[58] J.S. Patton. Mechanisms of macromolecule absorption by the lungs. *Adv. Drug Deliv. Rev.*, 19(1):3–36, 1996. Pulmonary Polypeptide and Polynucleic Acid Delivery.

[59] B. Prevon, J.M. Scholey, and E.J.G. Peterman. Intraflagellar transport: mechanisms of motor action, cooperation, and cargo delivery. *FEBS J.*, 284(18):2905–2931, 2017.

[60] E. M. Purcell. Life at low Reynolds number. *Am. J. Phys.*, 45:3–11, 1977.

[61] S. M. Ross. A wavy wall analytical model of mucociliary pumping. *(Ph.D. thesis). John Hopkins University.*, 1971.

[62] N. Sanders, C. Rudolph, K. Braeckmans, S.C. De Smedt, and J. Demeester. Extracellular barriers in respiratory gene therapy. *Adv. Drug Deliv. Rev.*, 61(2):115–127, 2009.

[63] M. J. Sanderson and E. R. Dirksen. A versatile and quantitative computer-assisted photoelectronic technique used for the analysis of ciliary beat cycles. *Cell Motil.*, 5:267–292, 1985.

[64] M. J. Sanderson and M. A. Sleigh. Ciliary activity of cultured rabbit tracheal epithelium: beat pattern and metachrony. *J. Cell Sci.*, 47(1):331–347, 1981.

[65] M.J. Sanderson and M.A. Sleigh. Ciliary activity of cultured rabbit tracheal epithelium: beat pattern and metachrony. *J. Cell Sci.*, 47(1):331–347, 1981.

[66] M.H. Sedaghat, S. Sadrizadeh, and O. Abouali. Three-dimensional simulation of mucociliary clearance under the ciliary abnormalities. *J. Non-Newton. Fluid Mech.*, 316:105029, 2023.

[67] M.H. Sedaghat, M.M. Shahmardan, M. Norouzi, and M. Heydari. Effect of cilia beat frequency on muco-ciliary clearance. *J. Biomed. Phys. Eng.*, 6(4):265–278, 2016.

[68] C. G. Simader. *On Dirichlet's Boundary value Problem. An L^p-theory based on a generalization of Garding's inequality.*, volume 268 of *Lecture Notes in Mathematics*. Springer-Verlag, Berlin-Heidelberg-New York, 1972.

[69] M.A. Sleigh. The nature and action of respiratory tract cilia. In J. D. Brain, D. F. Proctor, and L. M. Reid, editors, *Respiratory defense mechanisms. Part I*, pages 247––288. New York: Marcel Dekker, 1977.

[70] D. J. Smith, E. A. Gaffney, and J. R. Blake. Discrete cilia modelling with singularity distributions: application to the embryonic node and the airway surface liquid. *Bull. Math. Biol.*, 69(5):1477–1510, 2007.

[71] D. J. Smith, E. A. Gaffney, and J. R. Blake. A viscoelastic traction layer model of muco-ciliary transport. *Bull. Math. Biol.*, 69(1):289–327, 2007.

[72] D.J. Smith, E.A. Gaffney, and J.R. Blake. Modelling mucociliary clearance. *Respir. Physiol. Neurobiol.*, 163(1):178–188, 2008. Respiratory Biomechanics.

[73] T.T. Soong, P. Nicolaides, C.P. Yu, and S.C. Soong. A statistical description of the human tracheobronchial tree geometry. *Respir Physiol.*, 37(2):161–172, 1979.

[74] J. Sznitman. Convective gas transport in the pulmonary acinus: comparing roles of convective and diffusive lengths. *J. Biomech.*, 42:789–792, 2009.

[75] M. H. Tawhai, P. Hunter, J. Tschirren, J. Reinhardt, G. McLennan, , and A. E. Hoffman. Ct-based geometry analysis and finite element models of the human and ovine bronchial tree. *J. Appl. Physiol.*, 97:231021, 2004.

[76] ; Mirko Tos ; Niels Mygind Vildana Cerkez. Quantitative study of goblet cells in the upper lobe of the normal human lung. *Arch Otolaryngol Head neck surg*, 112:316–320, 1986.

[77] J. Waldron. *Asthma Care in the Community*. John Wiley and Sons, 2007.

[78] E. R. Weibel. *Morphometry of the human lung*. Academic Press, 1963.

[79] D. Yager, T. Cloutier, H. Feldman, J. Bastacky, J.M. Drazen, and R.D. Kamm. Airway surface liquid thickness as a function of lung volume in small airways of the guinea pig. *J. Appl. Physiol.*, 77(5):2333–2340, 1994.

[80] K. Yoneda. Mucous blanket of rat bronchus. *Am. Rev. Respir. Dis.*, 114:837–842, 1976.